

Alma Mater Studiorum - Università di Bologna

DOTTORATO DI RICERCA IN  
SCIENZE DELLA TERRA, DELLA VITA E DELL'AMBIENTE

Ciclo 36

**Settore Concorsuale:** 04/A2 - GEOLOGIA STRUTTURALE, GEOLOGIA STRATIGRAFICA,  
SEDIMENTOLOGIA E PALEONTOLOGIA

**Settore Scientifico Disciplinare:** GEO/02 - GEOLOGIA STRATIGRAFICA E SEDIMENTOLOGICA

HIGH-RESOLUTION STRATIGRAPHY AND SEISMIC SITE CHARACTERIZATION  
OF LATE QUATERNARY PALEOVALLEY SYSTEMS (ADRIATIC COASTAL  
PLAIN, ITALY)

**Presentata da:** Andrea Di Martino

**Coordinatore Dottorato**

Maria Giovanna Belcastro

**Supervisore**

Alessandro Amorosi

**Esame finale anno 2024**

## Table of Contents

Abstract	1
1. Introduction	4
1.1 Organization of Dissertation	9
2. Paleovalley systems: Formation, evolution, and facies architecture	11
2.1 Late Quaternary paleovalley systems in the Italian geological record	15
3. Methods	35
4. Late Quaternary sedimentary record of estuarine incised-valley filling and interfluvial flooding: the Manfredonia paleovalley system (southern Italy)	49
Abstract	50
Keywords	50
4.1 Introduction	51
4.2 Geological setting	53
4.3 Methods	55
4.4 Offshore seismic stratigraphy	57
4.5 Onshore sedimentary facies associations	61
4.6 Geochemical signature of valley-fill deposits	70
4.7 Stratigraphic architecture of Apulian paleovalleys	72
4.8 Conclusions	76
5. Late Pleistocene to Holocene glacio-eustatic history as recorded in the Pescara paleovalley system (Central Italy, Adriatic basin)	78
Abstract	79
Keywords	79
5.1 Introduction	80
5.2 Geological and geomorphological setting	83
5.3 Methods	85
5.4 Substrate and Facies associations	90
5.5 Paleovalley fill architecture and sequence-stratigraphic interpretation	99
5.6 Millennial-scale architecture and sediment accumulation rates	104
5.7 Holocene paleoenvironmental evolution and glacio-eustatic control at parasequence scale	106
5.8 Conclusions	113
6. Reconstructing late Quaternary paleovalley systems of Italy through mHVSr: A tool for seismic hazard assessment in modern coastal lowlands	117
Abstract	118
Plain Language Summary	118
Key Points	119
Index Term	119
Keywords	119

6.1 Introduction	120
6.2 Geological background	124
6.3 Materials and Methods	131
6.4 Results	143
6.5 Discussion and Conclusion	147
<b>7. Seismic Amplification of Late Quaternary Paleovalley Systems: 2D-1D Seismic Response Analysis of the Pescara Paleovalley (Central Italy)</b>	<b>151</b>
Abstract	152
Keywords	152
7.1 Introduction	153
7.2 Geological setting: The Pescara paleovalley system	157
7.3 Resonance frequencies of the Pescara paleovalley	159
7.4 Geophysical 3D modeling of the paleovalley system	163
7.5 shear wave velocity of the paleovalley fill	167
7.6 Seismic Response Analysis	171
7.7 Discussion and Conclusions	183
<b>8. Sediment core analysis using artificial intelligence</b>	<b>187</b>
Abstract:	188
8.1 Introduction	188
8.2 Results	190
8.3 Discussion	198
8.4 Materials and Methods	201
<b>9. Conclusions</b>	<b>207</b>
<b>Reference</b>	<b>212</b>
<b>Supplementary Material</b>	<b>256</b>

## Abstract

In highly urbanized coastal lowlands, effective site characterization is crucial for accurately assessing seismic risk; it requires comprehensive stratigraphic analysis of the shallow subsurface coupled with the precise assessment of the engineering and geophysical properties of buried deposits. The lateral variability of 3D subsurface architecture can play a fundamental role in model prediction. In this context, late Quaternary paleovalley systems, shallowly buried fluvial incisions formed in response to the Late Pleistocene sea-level fall and filled with sediment during the subsequent Holocene sea-level rise, can represent an underestimated geological hazard for large cities and urban areas of the coastal plain. In these areas, the soft sediment infill of paleovalleys, alongside the sharp lithologic contrasts with the adjacent substrate, can lead to significant seismic amplification.

In this research, we conducted a high-resolution stratigraphic analysis of two distinct regions, the Pescara and Manfredonia areas along the Adriatic coastline of Italy, to delineate the geometries and facies architecture of two paleovalley systems. Geophysical investigations were carried out to characterize the study areas comprehensively and perform a seismic response analysis of both paleovalley systems. In this work, we also explored the applicability of artificial intelligence in performing facies analysis directly from borehole images, making facies classification fast and accessible.

The depositional architecture of the paleovalleys in the Pescara and Manfredonia areas shows strong similarity. Above a prominent erosional surface (Sequence Boundary, SB), the base of the paleovalleys is characterized by the presence of fluvial-channel gravels and sands (lowstand systems tract, LST). These are overlain by a deepening-upward, valley-fill succession of soft estuarine clay (transgressive systems tract – TST). The topmost portion of the paleovalley fill is capped by a progradational succession that reflects normal regression under highstand conditions (highstand systems tract, HST).

In the Manfredonia area, three contiguous onshore paleovalley systems (Candelaro, Cervaro, and Carapelle rivers) were documented. The stratigraphic architecture and their sedimentary response to Late Pleistocene valley excavation and Holocene filling were reconstructed through the integration of sedimentary, paleoecological (mollusks, benthic foraminifers, ostracods), and geochemical analyses from three 30-50 m-long onshore cores and a sequence-stratigraphic framework chronologically constrained by 25 radiocarbon data. In this area, the transgressive

portion of the paleovalley fill is characterized by inner-estuarine to outer-estuarine muds overlain by laterally extensive bay deposits (upper TST). Prodelta/delta front and offshore/shoreface deposits characterize the uppermost portion of the valley fill (HST).

In the Pescara area, we reconstructed a buried paleovalley system about 50 m deep and 2 km wide. The paleovalley profile and 3D facies architecture were reconstructed based on stratigraphic, sedimentological, paleontological, and geotechnical data collected on a reference core recovered in the paleovalley depocenter. The chronological framework was based on 17 radiocarbon dates. The lowermost portion of the paleovalley (LST) is marked by a laterally extensive fluvial gravel body, up to 13 m thick, overlain by a 21 m thick deepening-upward succession of freshwater (inner-estuarine) to brackish (outer-estuarine) facies associations (TST). The upper part of the succession (HST) shows a shallowing-upward tendency from paludal to fluvio-deltaic deposits.

Mapping the buried geometry of paleovalley systems can be very expensive and time-consuming if conducted only with the aid of core data or geotechnical investigations. To overcome this limitation, we tested the microtremor-based horizontal-to-vertical spectral ratio as a mapping tool to reconstruct the buried paleovalley geometries. We performed mHVSR measurements in the Pescara and Manfredonia study areas, detecting rapid lateral variations in resonance frequencies highlighted by laterally continuous impedance contrast surfaces.

Relying on the robust stratigraphic frameworks from both study areas, we carefully evaluated the relation between geological and geophysical data and identified the stratigraphic surfaces responsible for the observed resonances. By means of two distinct frequency-depth models, we reconstructed the geometry of the two buried paleovalley, even in the absence of geological data, and compared the geophysical subsurface models with the stratigraphic cross-sections.

An effective site characterization necessitates the meticulous reconstruction of subsurface features: geometry, sedimentary facies, and variations in the geophysical properties of rocks and sediments must be considered, as their spatial variability can significantly influence site effect, modifying the frequency content, intensity, and duration of ground shaking.

To perform seismic response analysis of the Pescara paleovalley system, which is the biggest city of the seismically active Abruzzo region in Central Italy, we conducted a geological and seismic characterization based on an accurate stratigraphic framework and through the acquisition of microtremor and shear wave velocity measurements.

In the study area, abrupt resonance frequency variations occur, ranging between 12 Hz at the valley margins and 0.9 Hz in the depocenter, within a distance of only 2.5 km. Down-hole tests

revealed an overall low shear wave velocity ( $V_s$ ) of the valley fill and showed distinct seismic/stratigraphic layers.

The seismic response analysis highlighted strong seismic amplifications in frequency ranges that can interact with a wide variety of building types. Furthermore, the response spectra derived from the 2D modeling with those proposed by Eurocode 8 document a strong underestimation of spectral accelerations and the inadequacy of using only  $V_{s30}$  to classify soil categories.

Despite the acknowledged relevance of subsurface stratigraphic modeling for a variety of environmental, societal, and economic challenges, the need for specific sedimentological skills in sediment core analysis may constitute a limitation. In this work, we used a robust dataset of high-resolution digital images from continuous sediment cores of Holocene age to outline a novel deep-learning-based approach to perform automatic semantic segmentation directly on core images, leveraging the power of convolutional neural networks. To optimize the interpretation process and maximize scientific value, we used six sedimentary facies associations as target classes *in lieu* of ineffective classification methods based uniquely on lithology. We propose an automated model that could rapidly characterize sediment cores reproducing the sedimentologist interpretation and allowing immediate guidance for stratigraphic correlation and subsurface reconstructions.

## 1. Introduction

Incised valleys (Van Wagoner et al., 1990) or paleovalley systems (Blum and Törnqvist, 2000; Blum et al., 2013) are important features in the stratigraphic record. Late Quaternary paleovalley systems are shallow subsurface incisions formed during the Late Pleistocene episode of global sea-level fall and filled with sediment during the subsequent, Holocene sea-level rise (Posamentier and Vail, 1988; Posamentier et al., 1988; Wright and Marriott, 1993). Typically, they are buried beneath modern coastal plains and have no geomorphic expression, as the progressive filling of the valley, followed by sedimentation above the interfluvial areas, led to complete obliteration of the original erosional features. Paleovalley systems are best recognized in coastal areas, where high-magnitude glacio-eustatic fluctuations create a predictable systems tracts architecture, with highly contrasting lithologies between valley fills and the adjacent substrate (Boyd et al., 2006; Gibling et al., 2011; Blum et al., 2013).

Paleovalley systems have been widely investigated worldwide due to their economic value, as they might contain abundant hydrocarbon and water reserves (Harms, 1966; Jennette et al., 1991; Dalrymple et al., 1994; Salem et al., 2005). Furthermore, following the first sequence stratigraphic studies, several authors analyzed ancient paleovalley system to refine the sequence stratigraphy concept and model (Shanley and McCabe, 1992; Allen and Posamentier, 1993; Wright and Marriott, 1993; Lagarreta and Uliana, 1998).

Paleovalley fills are stratigraphically expanded sedimentary successions where early transgressive deposits, generally poorly documented in the stratigraphic record, can be widely preserved, thus shedding new light on paleoclimate variations at glacial-interglacial transitions (Thomas and Anderson, 1994; Blum et al., 1995; Blum and Price, 1998; Blum and Aslan, 2006; Drago et al., 2006; Payenberg et al., 2006; Busschers et al., 2007; Rittenour et al., 2007; Simms et al., 2010; Peeters et al., 2015; Ishihara and Sugai, 2017). Late Quaternary paleovalleys are considered important geological archives for understanding ancient systems and environmental changes driven by allogenic/autogenic forcings (Boyd et al., 1989; Blum and Törnqvist, 2000; Amorosi et al., 2009; Durand et al., 2018; Horozal et al., 2021; McGhee et al., 2022).

In Italy, late Quaternary paleovalley systems have been widely documented along the Tyrrhenian Sea (Amorosi et al., 2009, 2012, 2013; Breda et al., 2016; Girotti and Mancini, 2003; Milli et al., 2013, 2016; Rossi et al., 2012, 2017) and Ionian Sea (Tropeano et al., 2013) coastal plains. In the Adriatic area, onshore paleovalley systems have been identified only in the Venetian-Friulian plain (Ronchi

et al., 2021) and in the Biferno coastal plain (Amorosi et al., 2016b). On the other hand, paleovalley systems have been recognized in the Adriatic Sea offshore (Maselli and Trincardi, 2013; Maselli et al., 2014; De Santis and Caldara, 2016; De Santis et al., 2020a).

Within this framework, as part of PRIN 2017 Project “*The Po-Adriatic Source-to-Sink system (PASS): from modern sedimentary processes to millennial-scale stratigraphic architecture*” (PI: Alessandro Amorosi), we investigated the onshore segments of two paleovalley systems along the Adriatic coastline of Italy: the Pescara paleovalley system and the Manfredonia paleovalley system, this latter being composed of the Candelaro River, Cervaro River, and Carapelle River paleovalleys.

Relying on an integrated approach, through the combined sedimentological, paleontological, geochronological, and geochemical analysis of two reference cores, about 50 m thick, acquired in the depocenter of the Pescara and Manfredonia paleovalley systems, specific aims of the first part of the dissertation are: to i) achieve high-resolution (millennial-scale) stratigraphic analysis of both paleovalley fills, ii) reconstruct facies architecture along stratigraphic cross-sections, iii) accomplish the sequence stratigraphic interpretation of the investigated succession, iv) and assess the influence of glacio-eustatic changes on sediment accumulation and facies architecture over the past 30 ky.

Reconstructing paleovalley geometries is also fundamental for better understanding seismic site effects. Paleovalley systems are being increasingly studied, as these features are known to have the potential to modify earthquake motions due to their complex geometry and the sharp contrast between the soft sediment fill and the adjacent overconsolidated substrate. Recently, the Geological Survey of Japan investigated the Quaternary paleovalley fills beneath Tokyo and Nakagawa lowlands in the Kanto Basin to mitigate earthquake damage. Paleovalley fills here mainly consist of soft clays that can amplify seismic waves, leading to longer higher ground shaking. Relying on data from the 1923 earthquake disaster, Tanabe et al. (2021) established a link between the spatial distribution of a buried paleovalley fill and structural damage to buildings. These studies, however, predominantly compared stratigraphic data with structural damages, without building a comprehensive modeling of the seismic behavior. An effective site characterization requires the accurate reconstruction of subsurface features, including variations in the geophysical properties of rocks and sediments; critical parameters such as shear wave velocities ( $V_s$ ) and resonance frequencies ( $f$ ) represent essential elements to be considered.

In this context, seismic microtremor surveys, first introduced by Aki (1957) and later developed by Okada and Ling (1994) and Okada (2003), can be an effective tool for exploration. Microtremor measurements are considered a fundamental geophysical source of information. Shear wave

velocity can be inferred using several microtremor-based seismic analyses, and with microtremor records, the microtremor-based horizontal-to-vertical spectral ratio (mHVSR) can be performed.

The mHVSR method, or simply H/V, was introduced in Japan by Nogoshi and Igarashi (1971) and then popularized by Nakamura (1989, 2000). This geophysical technique is widely used due to its simplicity and capability to provide a large amount of information. Additionally, the H/V technique is recognized for its reliable estimates of the resonance frequency, which is strongly related to sediment thickness, making it a fast and powerful stratigraphic tool. (e.g., Ibs-Von Seht and Wohlenberg, 1999; Parolai et al., 2001, 2002; Castellaro and Mulargia, 2009; Grippa et al., 2011; Tropeano et al., 2011; Francesco et al., 2013; Sgattoni and Castellaro, 2020; 2021).

In the second part of the dissertation, we performed a series of microtremor measurements across the Pescara and Manfredonia Paleovalley systems, aiming to evaluate the potential of the mHVSR technique as a stratigraphic exploration tool for mapping late Quaternary paleovalleys systems. Using the robust stratigraphic framework around these sites as a reference and through the acquisition of microtremor measurements along two transects perpendicular to the paleovalley axes, we aimed to: (i) identify variations in resonance frequencies along the transects highlighting laterally-continuous impedance contrasts, (ii) evaluate the relation between geological and geophysical data and identify the stratigraphic surfaces responsible for the observed resonances, (iii) derive  $V_s$  models for the sediment fill in the two paleovalleys, and (iv) estimate the thickness of the soft Holocene valley fills, reconstructing the buried paleovalley geometries even in the absence of geological data.

Late Quaternary paleovalley systems represent an underestimated seismic hazard for large cities and rapidly expanding urban areas of modern coastal lowlands; their local seismic response should be extensively studied to mitigate potential earthquake-induced damages.

Several studies have attempted to model seismic site effects by focusing on simple one-dimensional (1D) simulations, assuming lateral subsurface homogeneity (Hallal and Cox., 2022) and oversimplifying sediment body geometry and facies architecture. Two-dimensional ground motion simulations are expected to provide more realistic results, as the subsurface stratigraphy can rarely be assumed as 1D.

In complex geological contexts, such as paleovalley systems, numerous non-1D factors must be considered. These include significant heterogeneities in the stratigraphic layering and variable geometries of the substrate (Bard and Gariel., 2009; Semblat et al., 2005), resulting in the remarkable deviation from the assumption of shear waves propagating vertically in a homogeneous

medium. However, a common limitation of 2D simulations lies in the difficulty of obtaining accurate site characterization, including velocity profiles, stratigraphic layering, and soil properties, through reliable subsurface models over large areas. On the other hand, 1D simulations remain a reasonable approximation wherever the stratigraphic framework is simple and relatively homogeneous (Macerola et al., 2019; Hallal et al., 2022c).

The central part of the Italian peninsula is well-known for being a high-risk seismic area. In recent years, numerous earthquakes have struck the regions of Marche and Abruzzo. In 2009, an earthquake of  $M_w = 6.3$  struck L'Aquila, resulting in many losses and structural damage to buildings and infrastructures (Lagomarsino, 2012; Di Ludovico et al., 2017a 2017b). In August 2016, a  $M_w=6$  earthquake hit Amatrice, causing significant loss of lives and damage to historical and cultural heritage (Fiorentino et al., 2018; Saganetti et al., 2020; Karimzadeh and Mastuoka, 2017).

Given the high seismic risk in central Italy, seismic microzonation of urban areas is needed, and high-resolution seismic site response studies should be performed to mitigate earthquake-induced damages (Iyengar and Ghosh, 2004; Cox et al., 2011; Moscatelli et al., 2020; Pergalani et al., 2020).

Leveraging a large amount of geological, geophysical, and geotechnical data from Pescara, we aim to perform a complete seismic site response analysis of the paleovalley system and comprehensively characterize geometries, velocity profiles, and soil properties.

With this aim, we: i) mapped the main resonance frequencies based on 85 microtremor measurements; ii) estimated an average  $V_s$  model for the valley, correlating the measured resonance frequencies with borehole stratigraphy, enabling the reconstruction of the 3D substrate geometry; iii) compared the microtremor-based  $V_s$  model with  $V_s$  data from 6 Down Hole measurements to refine the valley fill  $V_s$  model, building a layering that integrates  $V_s$  and subsurface stratigraphy; and iv) conducted 2D seismic response simulations along a cross-section in the paleovalley depocenter, comparing the results with 1D simulations and v) compared the response spectra based on the (EUROPEAN COMMITTEE FOR STANDARDIZATION, 2004) Eurocode 8 (EC8) soil classification guidelines with the model-based response spectra, to achieve a robust soil classification.

To reconstruct an accurate subsurface model, a precise distinction between sedimentary facies is necessary; traditional classification methods based uniquely on lithology are ineffective. However, the need for specific sedimentological skills in sediment core analysis may constitute a limitation.

Recent advances in Artificial Intelligence research are setting new standards for many research fields, with automated methods based on Machine Learning (ML) and Deep Learning (DL) achieving state-of-the-art performance in solving complex problems (Devlin et al., 2019; Redmon et al.,

2016). Artificial intelligence methods have been increasingly applied in Earth and environmental science in the last few years (Boland et al., 2017; Kuwatani et al., 2014; Kadow et al., 2020) . However, without fully exploiting the potential of ML and DL systems, the usage of AI in geoscience remains limited.

In the last part of the dissertation, we propose a novel approach leveraging DL to perform automatic semantic segmentation of digital images from sediment cores directly acquired in the field. Semantic segmentation is a computer vision technique used to analyze digital images by classifying each pixel in a specific category; Convolutional Neural Networks (CNNs) usually achieve state-of-the-art performance in this task (Guo et al., 2018; li et al., 2022).

We considered six target Holocene sedimentary classes from the Po Plain and the Adriatic coastal plain of Marche, Abruzzo, and Apulia regions (Italy) including Well-drained floodplain (WDF), Poorly-drained floodplain (PDF), Prodelta (P), Peat layer (PL), Fluvial sand (FS), and Swamp (Sw) deposits, with an additional background class.

Each core image was annotated in conjunction with the associated segmentation masks (i.e. Facies interpretation), producing a final dataset of 82 non-overlapping, high-resolution digital images acquired from 32 continuous sediment cores. The dataset was divided into three mutually exclusive subsets: training, validation, and test, containing 77%, 11%, and 12% of the data, respectively.

Our model aims to reproduce the sedimentologist interpretation of sedimentary facies. To verify the quality of the results, we tested the model prediction according to the most used segmentation metrics: mean Intersection over Union IoU, F1 score, and balanced accuracy.

One of the most common problems of Deep Learning methods is their limited interpretability. To better understand our results, we visualized the regions of higher segmentation error and modeled prediction confidence, improving the model reliability.

## 1.1 Organization of Dissertation

Following **Chapter 1 (Introduction)**, **Chapter 2 (Paleovalley systems: Formation, evolution, and facies architecture)**, and **Chapter 3 (Materials and Methods)**, the results of this dissertation are organized into five major chapters (**Chapters 4 to 8**): each chapter is a self-contained journal article that includes an introduction, geological framework, methodology, results, discussion, figures and a literature review. In the end, **Chapter 9** provides the final conclusion. The five main chapters follow a logical progression as delineated below.

- **Chapter 4: Late Quaternary sedimentary record of estuarine incised-valley filling and interfluvial flooding: the Manfredonia paleovalley system (southern Italy).** This research explores the stratigraphic architecture and sedimentary evolution of a multiple late Quaternary paleovalley system from the Manfredonia area, including the Candelaro, Cervaro, and Carapelle paleovalleys. The stratigraphic reconstruction was conducted leveraging an integrated approach based on sedimentary, paleoecological, and geochemical analyses across three 30-50 m-long onshore reference cores and a high-resolution stratigraphic framework constrained by 25 radiocarbon data. This study shows the sedimentary response to Late Pleistocene valley formation and consequent Holocene filling. In this work, we document a shift in sediment provenance from Southern Apennine source rocks to a mixed composition, indicative of an increased alongshore sediment contribution from northern sources.
- **Chapter 5: Late Pleistocene to Holocene glacio-eustatic history as recorded in the Pescara paleovalley system (Central Italy, Adriatic basin).** This chapter unveils the high-resolution stratigraphic reconstruction of the Pescara Paleovalley system. Using stratigraphic, sedimentological, paleontological, chronological, and geotechnical data, we meticulously reconstructed the paleovalley profile and 2D facies architecture of the paleovalley fill. Moreover, in this study, we highlight how the sedimentary environments responded to distinct early Holocene sea-level rise events, potentially associated with Melt-Water Pulses (MWP) 1B, 1C, and 1D.

- **Chapter 6: Reconstructing late Quaternary paleovalley systems of Italy through mHVSr: A tool for seismic hazard assessment in modern coastal lowlands.** In this study, we use the microtremor-based horizontal-to-vertical spectral ratio (mHVSr) methodology to map the buried geometry of the Pescara and Manfredonia paleovalley systems along the Adriatic coastal plain of Italy. We employed mHVSr measurements to discern rapid lateral variations in resonance frequencies and identified laterally continuous impedance contrasts surface. Furthermore, we evaluate the strong relation between the local stratigraphy and the observer resonance frequency and build a frequency-depth model, enabling the reconstruction of the buried geometries of the Pescara and Manfredonia paleovalley systems.
- **Chapter 7: Seismic Amplification of Late Quaternary Paleovalley System: 2D-1D Seismic Response Analysis of the Pescara Paleovalley (Central Italy).** This chapter underscores the central role of meticulous subsurface reconstructions for effective site characterization in seismically active regions. It highlights how paleovalley systems are an often-underestimated seismic hazard buried beneath large cities and urban areas. Through the detailed geological and geophysical characterization of the Pescara paleovalley system, the study provides a comparative analysis of 2D and 1D seismic response models. The research shows pronounced seismic amplification in frequency ranges that can interact with various building types. Moreover, a critical evaluation of response spectra, drawn from 2D modeling against those proposed by Eurocode 8, unveils a notable underestimation of spectral accelerations and challenges the adequacy of utilizing only the  $V_{s30}$  value for soil category classification.
- **Chapter 8: Sediment Core Analysis Using Artificial Intelligence.** Given the importance of recognizing the sedimentary facies for a variety of environmental applications, this research proposes a novel deep-learning-based approach to perform automatic semantic segmentation directly on core images from continuous sediment cores of Holocene age. Utilizing a robust dataset of high-resolution digital images and employing state-of-the-art convolutional neural networks, we classified six targets sedimentary facies. Moreover, to overcome the “black-box” problem of neural networks, we visualize the regions of higher segmentation error to improve the model’s reliability. The developed automated model

can rapidly characterize sedimentary facies, providing immediate guidance for stratigraphic correlation and subsurface reconstructions without the need for specific sedimentological skills in sediment core analysis.

## 2. Paleovalley systems: Formation, evolution, and facies architecture

Fluvial valley systems are known to be fundamental geological features of the stratigraphic record; however, a specific focus on ancient valley systems only emerged after the publication of the first sequence stratigraphic models (Wilgus et al., 1988). Paleovalley systems (Blum and Törnqvist, 2000), also known as incised valleys (Van Wagoner et al., 1990), formed under prolonged periods of fluvial incision due to base-level fall, followed by valley filling. Paleovalley systems were initially defined to include erosional relief with truncation of older strata, juxtaposition of fluvial or estuarine strata onto marine deposits, and demarcation of a significant basinward shift in facies, with subaerial exposure on the interfluvies (Blum et al., 2013). They typically have economic value and play a crucial role in identifying sequence-bounding unconformities (Dalrymple et al., 1994; Posamentier and Vail, 1988).

Global climate changes, including cyclic variations in ice volume and sea level, controlled the origin and affected the evolution of paleovalley systems during the Quaternary. Middle to Late Pleistocene paleovalley systems, in particular, display characteristic cycles of erosion and sedimentation (Anderson et al., 2004; Busschers et al., 2007) that reflect glacial-interglacial cycles with a periodicity of ~100 kyr, following the eccentricity of the Earth's orbit. Higher-frequency rhythms predicted by the Milankovitch theory of orbital forcing, including ~43 kyr cyclic changes in axial tilt (Shackleton and Opdyke, 1973; Imbrie and Imbrie, 1979; Martinsen et al., 1987; Lisiecki and Raymo, 2005) and ~20 kyr precessional cycles (Prell and Kutzbach, 1992), played a major role in modulating facies architecture of glacial-interglacial cycles. In particular, Late Pleistocene paleovalley systems buried under modern coastal lowlands reflect fluvial incision that took place due to a significant sea-level drop associated with the transition from the Marine Isotope Stages MIS 3 to MIS 2 (Amorosi et al., 2017).

Paleovalley formation and filling reflect a complete cycle of base-level fall and rise. In a sequence stratigraphy framework, this cycle can be described as the succession of systems tracts initially

defined by Posamentier et al. (1988) to include genetically associated stratigraphic units that were deposited during specific phases of the relative sea-level cycle.

There are four primary types of systems tracts: the Falling Stage Systems Tract (FSST) is formed during a phase of relative sea-level fall. The Lowstand Systems Tract (LST) is formed under low, stable sea-level conditions. The Transgressive Systems Tract (TST) is characteristic of relative sea-level rise. The Highstand Systems Tract (HST) occurs during a period of relatively stable high sea level.

Paleovalley systems can be subdivided into mixed bedrock–alluvial, coastal-plain, and cross-shelf segments (Blum et al., 2013). Mixed bedrock–alluvial segments are cut across bedrock of significantly older age and have an overall degradational architecture. On the other hand, coastal-plain and cross-shelf paleovalley segments respond to relative sea-level fall as river systems cut through the coastal plain and inner shelf clinothems, respectively. Early facies models from the '90s (Dalrymple et al., 1994; Zaitlin et al., 1994; Boyd et al., 2006) identified paleovalley fills as predominantly made of estuarine facies successions associated with relative sea-level rise. The drowned-valley estuarine facies model can be effectively applied to late Quaternary coastal-plain valley systems, such as those investigated in this work.

Paleovalley evolution can be summarized as follow (Fig.1):

1. Rivers cut into the substrate in response to relative sea-level fall (FST), and the valley system shows an overall degradational pattern with a characteristic step-wise incision (Blum, 2007; Rittenour et al., 2007; Blum et al., 2008). Significant sediment by-pass characterizes the valley during this stage, though fluvial deposits may be preserved locally as fluvial terraces against the valley flanks. The basal valley unconformity is the sequence boundary (SB). In the adjacent interfluves, SB is expressed as a paleosol, i.e., a soil formed on a past landscape in response to subaerial exposure, that was buried subsequently with valley evolution (interfluvial sequence boundary of Van Wagoner et al., 1990; Aitkin and Flint, 1996). Recent work from Quaternary systems has shown that overbank packages bounded by immature paleosols may represent a likely alternative to the highly-weathered interfluvial paleosol predicted by classic sequence stratigraphic models (Amorosi et al., 2017).

2. Under lowstand sea-level conditions (LST), fluvial sedimentation occurs within the valley, forming a characteristic amalgamated gravel or sand body at the valley bottom. This lower valley fill (Blum et al., 2013) is composed of fluvial channel and levee facies

representing deposits of migrating and confined channels that cannot avulse outside the paleovalley boundaries (Gibling et al., 2011) and are not subjected to backwater effects.

3. Estuarine facies are deposited into the valley in response to relative sea-level rise (TST). This mud-dominated upper valley fill, with non-amalgamated channels, is separated from the underlying gravel or sand fluvial channel-belt by the transgressive surface (TS), which marks the first significant flooding event (Posamentier and Vail, 1988; Posamentier et al., 1988; Van Wagoner et al., 1990; Zaitlin et al., 1994). Generally, transgressive deposits include a vertical succession of freshwater to brackish estuarine facies formed within the zone of backwater effect during relative sea-level rise as a landward-tapering wedge that scales to backwater length and onlaps the amalgamated valley fill (Blum et al., 2013).

4. With continuing relative sea-level rise, the valley is filled, the interfluves are drowned, and coastal to shallow-marine environments develop above the paleovalley fill. Above the maximum flooding surface (MFS), which records the maximum marine ingressions, prograding coastal and deltaic facies cap the succession (HST).

Late Quaternary paleovalley systems buried beneath modern coastal lowland and delta plains do not have any geomorphological expression; their thickness, typically tens of meters, may exceed 50 m, while their width can vary from 2 km to over 15 km. Paleovalley size, geometry, and sedimentary fill may vary as a function of several boundary conditions and forcing mechanisms, such as the amplitude of relative sea-level change, water supply, and the local geology; thus, valley profiles and facies architectures may differ from valley to valley.

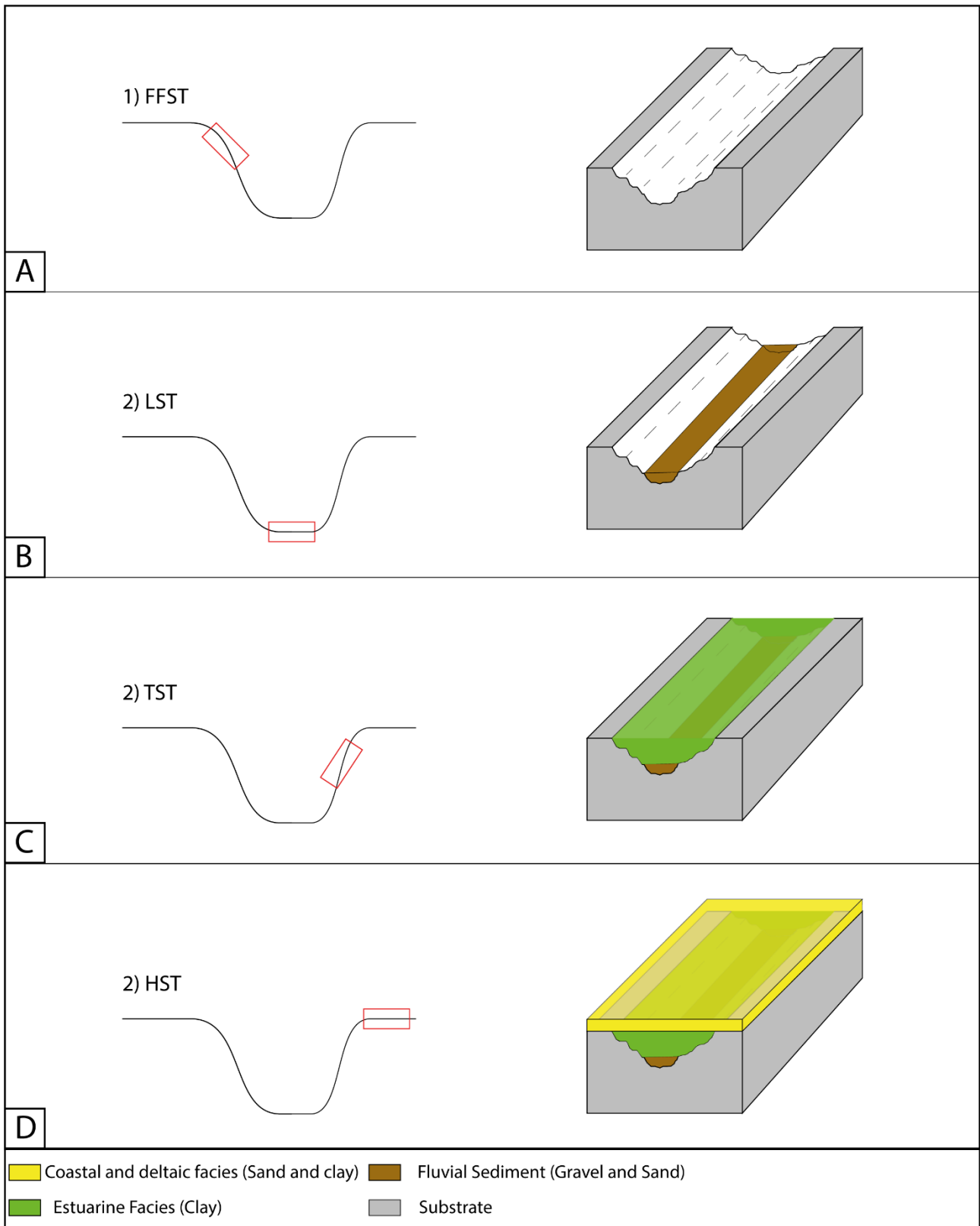


Fig. 1. Conceptual model of the formation and evolution of paleovalley systems. A) During sea-level fall (FSST), fluvial incision occurs. B) During sea-level lowstand (LST), fluvial sediment deposition occurs. C) During sea-level rise (TST), deposition of estuarine clayey sediments occurs. D) During sea-level highstand (HST), complete obliteration of the first incision occurs through coastal and deltaic facies deposition.

## 2.1 Late Quaternary paleovalley systems in the Italian geological record

Several paleovalley systems have been identified in the geological record worldwide (Shanley and McCabe, 1993; Legarreta and Uliana, 1998; Blum and Törnqvist, 2000; Browne and Naish, 2003; Tanabe et al., 2005; Catuneanu et al., 2009; Gibling et al., 2011; Holbrook and Bhattacharya, 2012; Neal et al., 2016; Wang et al., 2019, 2020; McGhee et al., 2022). Late quaternary paleovalley systems in Italy are typically buried beneath the Tyrrhenian, Ionian, and Adriatic sea coasts. Several studies have documented the stratigraphic architecture of paleovalley systems from the Tyrrhenian Sea (Amorosi et al., 2009, 2012, 2013; Breda et al., 2016; Girotti and Mancini, 2003; Milli et al., 2013, 2016; Tropeano et al., 2013; Rossi et al., 2012, 2017), Ionian Sea (Tropeano et al., 2013) and Adriatic sea coastal plains (Fontana et al., 2008; Maselli and Trincardi, 2013; Mozzi et al., 2013; Maselli et al., 2014; De Santis and Caldara, 2014; Amorosi et al., 2016, 2017; Morelli et al., 2017; Ronchi et al., 2018, 2021).

### 2.1.1 The Arno Paleovalley System

On the Tyrrhenian Sea coast, the northern coastal plain of Tuscany covers an area of approximately 550 square kilometers, from Pisa to Viareggio. Three prominent Late quaternary paleovalley systems, made by the Arno, Serchio, and Camaiore–Stiava rivers, have been described from this area (Amorosi et al., 2013; Rossi et al., 2012, 2017).

Detailed stratigraphic studies of the late Quaternary succession, which consists predominantly of alternating continental to shallow-marine deposits, have been concentrated around the city of Pisa during the last decade. These studies identified two transgressive–regressive sequences formed in response to the last two interglacial–glacial cycles (base of MIS 1 and 5e, respectively – Aguzzi et al., 2005). Within the youngest sequence, a paleovalley fill was identified, consisting primarily of estuarine deposits related to the Arno River. This paleovalley fill accumulated during the dramatic Lateglacial–early Holocene eustatic sea-level rise that occurred worldwide in response to the generalized phase of climate amelioration (Fairbanks, 1989, Bard et al., 1996).

The Arno paleovalley body (Fig. 2) is roughly in line with the current course of the Arno River and has a thickness of 40 to 45 meters and a width of 5-8 kilometers. In the depocenter, above a prominent erosional surface (SB) that cuts into the underlying finer-grained alluvial deposits, the lower valley fill is dominated by a lowstand fluvial gravel body abruptly overlain by a thick succession

of Lateglacial–Holocene (ca. 13,000–7800 cal BP) coastal plain to estuarine facies. The boundary between the lowstand gravel body and the overlying clayey sediment is marked by the transgressive surface (TS).

The transgressive surface, which represents the base of the transgressive systems tract (TST), is the most identifiable stratigraphic surface in the area, marking an abrupt facies change from fluvial to organic-rich clay deposits. The TS marks the evolution of the incised-valley systems into wave-dominated estuaries. The TST, dated between ca. 13,000–7800 cal BP, records the progressive infilling and drowning of the Tuscan paleovalleys in response to the rapid post-glacial sea-level rise.

More in detail, TST can be described as a composite succession of very soft organic-rich clay formed in a coastal plain or inner-estuarine environment, showing an upper transition to central- and outer-estuarine clays.

Multy proxy analysis conducted on a reference core in the depocenter shows a high-frequency, millennial-scale cyclicity; changes in palaeosalinity, detected through benthic meiofauna indicators, reveal alternating freshwater and brackish sub-environments during the valley filling process.

Stratigraphic correlations across the Arno River show that approximately 10 meters thick, small-scale cycles are separated by flooding surfaces and exhibit similar facies architecture. This includes central and outer estuarine clays with sharp transition into inner estuary and coastal plain deposits. Facies architecture highlights an aggradational to retrogradational stacking pattern of facies within the valley body.

Furthermore, a laterally extensive sediment body comprising soft clays with abundant brackish fossils correlates above the interfluves, documenting generalized flooding after valley filling. The interfluves can be easily distinguished from the post-LGM succession due to their overconsolidated state and are situated 15–20 meters below sea level on either side of the valley.

The maximum flooding surface (MFS) separates the TST from the overlying HST deposits. Its age is well constrained, around 7800 years BP by radiocarbon dates, and represents the Holocene peak of transgression. This surface has no obvious physical expression, but can be identified from sedimentary core data at the turnaround from deepening-upward to shallowing-upward facies successions on the basis of paleoecological data. The HST constitutes a single "regressive" succession, 15–30 m thick, of deltaic and alluvial plain deposits, which is interpreted to reflect deltaic and coastal plain progradation during the late Holocene phase of deceleration in sea-level rise.

Sedimentological, stratigraphic, and paleontological analyses conducted on sedimentary cores in the Arno, Serchio and Camaiore–Stiava coastal plains show remarkably similar facies architecture

and geometry between the three valleys (Fig. 3). The vertical facies successions suggest that the three valleys underwent a similar process of formation and filling. The valley fills contain evidence of high sedimentation rates; the sediment accumulation in the Tuscan valleys kept up with the early stages of transgression and led to a predominantly aggradational facies architecture within the valley bodies.

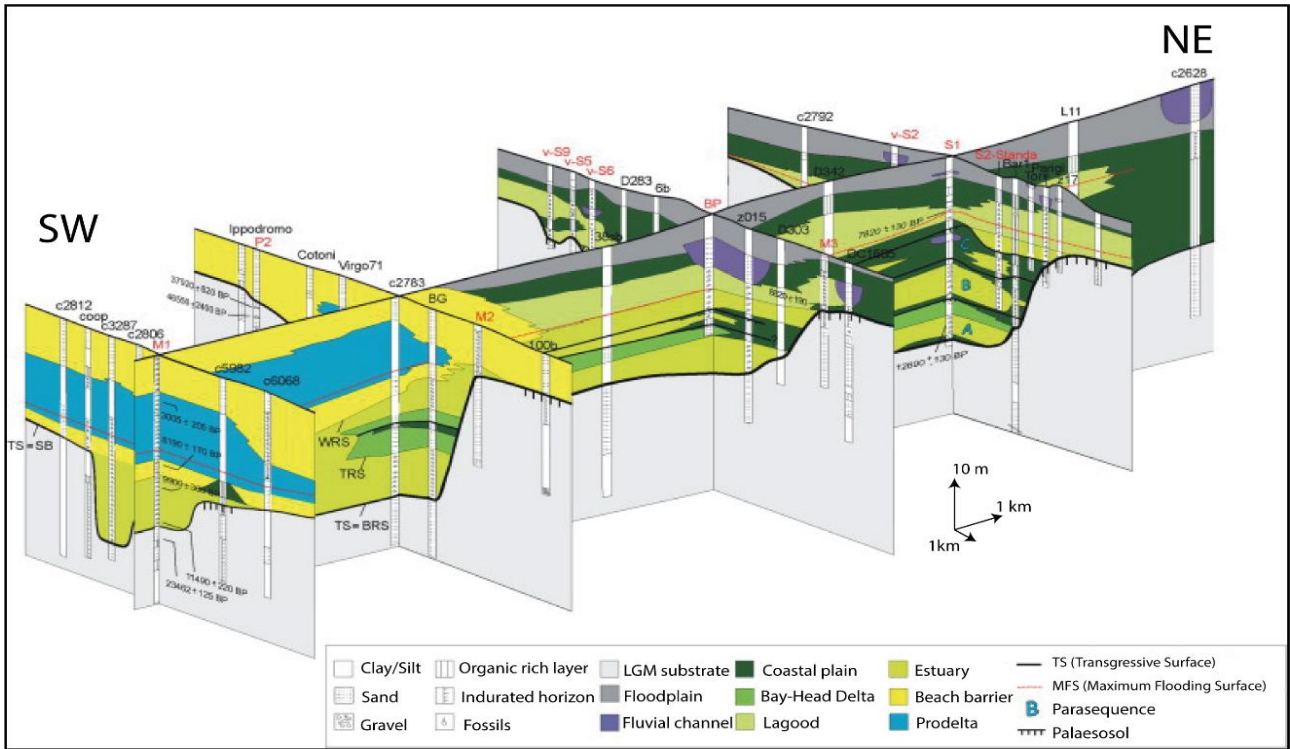


Fig. 3. Three-dimensional architecture of the post-LGM Arno Valley fill, showing distinctive along-dip variability in facies architecture (from Amorosi et al., 2013).

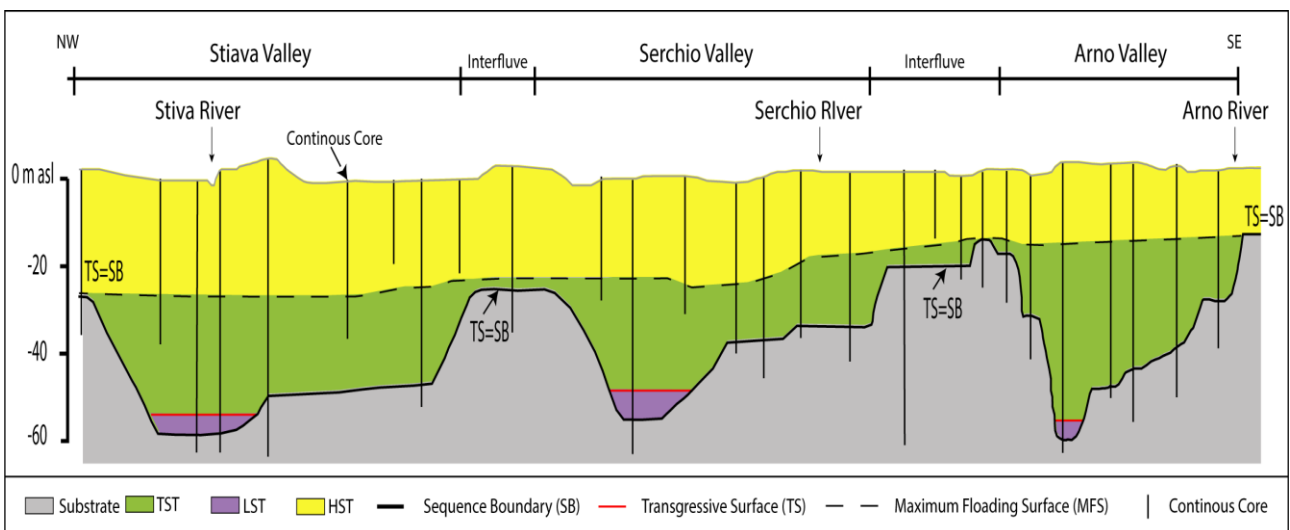


Fig. 2. Representative cross-section of the post-LGM coalescent valleys of Stiva, Serchio, and Arno rivers and their sequence-stratigraphic interpretation (from Amorosi et al., 2013).

### 2.1.2 The Tiber Paleovalley System

Remaining on the Tyrrhenian coastal plain, approximately 250 km south from the modern Arno River, the Tiber paleovalley has been accurately described by Milli et al. (2013, 2016). Through the use of large amounts of data from sedimentary cores, the stratigraphic architecture of the Late Pleistocene/Holocene Tiber delta succession was reconstructed, recording the transition from a wave-dominated estuary to a wave-dominated delta in the context of Late Quaternary sea-level fluctuations. The Tiber delta paleovalley succession (Fig. 4) constitutes a sequence-stratigraphic unit, also known as the Tiber Depositional Sequence (TDS), which was deposited during the last glacial-interglacial cycle.

The subsurface stratigraphy under the modern Tiber coastal plain can be summarised into three units bounded by unconformity surfaces. While the lowermost and middle stratigraphic units reflect Lower to Middle Pleistocene sedimentation, the uppermost unit, assigned to the Late Pleistocene, refers to the TDS and constitutes a fourth-order depositional sequence. The lower boundary of this unit is marked by an erosional surface that cuts into the underlying Lower and Middle Pleistocene deposits and represents the Sequence Boundary (SB).

Above the SB, deposits formed during lowstand (LST) and initial sea level rise are largely preserved, while the preservation of sea-level fall (FST) deposits is negligible.

The LST (age between 30,000–26,000 yr and 14,000 yr BP) mainly occurs in the northernmost and southernmost parts of TDS and is typically represented by fluvial deposits. Sand and gravel lithofacies to mud fluvial deposits characterize the LST. Such deposits show a fining-upward trend and have been interpreted by Milli et al. (2013) as the filling of low-sinuosity channels of a braided fluvial depositional system. Sands and gravels may have constituted bar bodies that filled the channels, while the mud is interpreted as a floodplain deposit. These fluvial deposits form a sedimentary body with a tabular geometry extending over 3–5 km. The LST occupies the most topographically depressed area of the Tiber paleovalley, implying that during LST, the TDS sequence boundary was under subaerial conditions.

The transgressive surface separates LST from TST. TST is constituted by sediments accumulated between 14 and 5–6 kyr BP in response to the rapid post-glacial sea level rise. These deposits are characterized by a retrogradational stacking pattern of the depositional systems, including in a seaward direction: a fluvial-bay-head delta system, a coastal barrier-lagoon system, and a transition-

to-shelf system. The interfingering between these depositional systems occurred in response to the sea-level rise, which led to the evolution of the Tiber fluvial valley into a wave-dominated estuary.

Based on the reference core “Pesce Luna” (Milli et al., 2013), TST is dominated by a soft clay formed in brackish, lagoon–marsh, and marine environments. The local development of marshes and swamps marks the onset of transgressive sedimentation.

More in detail, the TST consists of small-scale, a few meters thick, parasequences with a shallowing-upward trend, similar to the Arno paleovalley system (see sub-section 2.1.1). The transgressive cycles that characterize the TST are believed to have formed in response to discontinuous sea-level rise. These short-lived transgressive phases were followed by phases of relative sea-level stillstand, during which depositional systems experienced brief periods of progradation. These parasequences exhibit distinct facies trends that reflect their relative location within the paleoestuary. Transgressive sedimentation was affected by decelerations and accelerations of sea-level rise from 13 to 8.2 kyBP (e.g., the cold period of the Younger Dryas from 13 to 11.5 kyr BP and the cold climate event of 8.2 kyr BP), producing landward and seaward facies migrations along the Tiber paleovalley.

Landward, the uppermost TST is marked by a thick and continuous peat layer, dated between 6000 and 5000 cal BP, that correlates laterally with lagoon sediments. This thick peat layer was formed under low sediment supply conditions, which allowed the available accommodation space to be filled by peat (Milli et al., 2013). The top of this peat layer marks the maximum transgression and includes the Maximum Flooding Surface (MFS).

Seaward, the MFS is located within a condensed section representing the maximum flooding time on the shelf. Near the Tiber River, high-resolution seismic profiles have identified condensed deposits as an acoustically transparent layer overlying the TDS sequence boundary.

The MFS occurs at distinct stratigraphic levels in different portions of a sedimentary basin (Fig 4). This is related to the fact that the time of maximum transgression is also a function of the local sediment supply (Wehr, 1993, Allen and Posamentier, 1994, Martinsen and Helland Hansen, 1994, Posamentier and Allen, 1999).

Above the MFS, from 6000 yr BP onwards, the HST developed as sea-level rise gradually decreased, approaching a more stable position. In this phase, the filling of the transgressive lagoon and the formations of a cusped delta were the dominant features. Within this lagoon, the Tiber bay-head delta started its rapid progradation in response to increasing sediment supply.

Detailed facies analysis of sedimentary cores shows cyclic gran-size variations and alternating beach and lagoon deposits in highstand parasequences. Milli et al. (2013) interpreted this feature as the expression of the lateral variability of coastal plain sub-environments. In the final stage of HST, the deltaic progradation led to the development of amalgamated sand bodies, about 20 m thick, with a clear coarsening-upward trend, interpreted as beach-ridge deposits. The step-by-step evolution of the Tiber delta from the late LST to the Present is summarized in Figure 5.

The stratigraphic architecture of TDS is the result of the interaction between global sea-level variations and sediment supply, both processes being under the control of climatic changes. Land subsidence, although present, has been considered negligible.

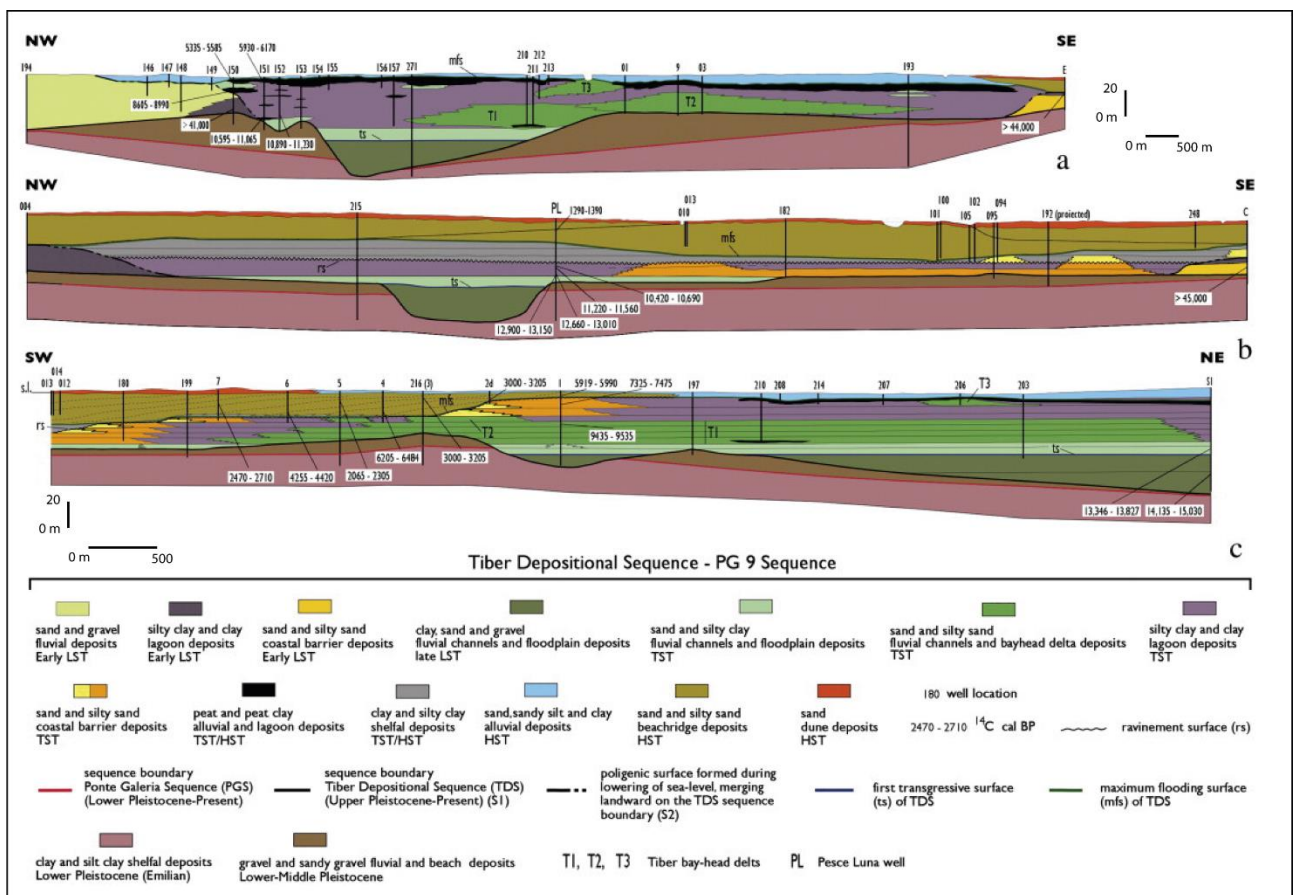


Fig. 4. Stratigraphic cross-sections of the Tiber Depositional Sequence (Milli et al., 2013).

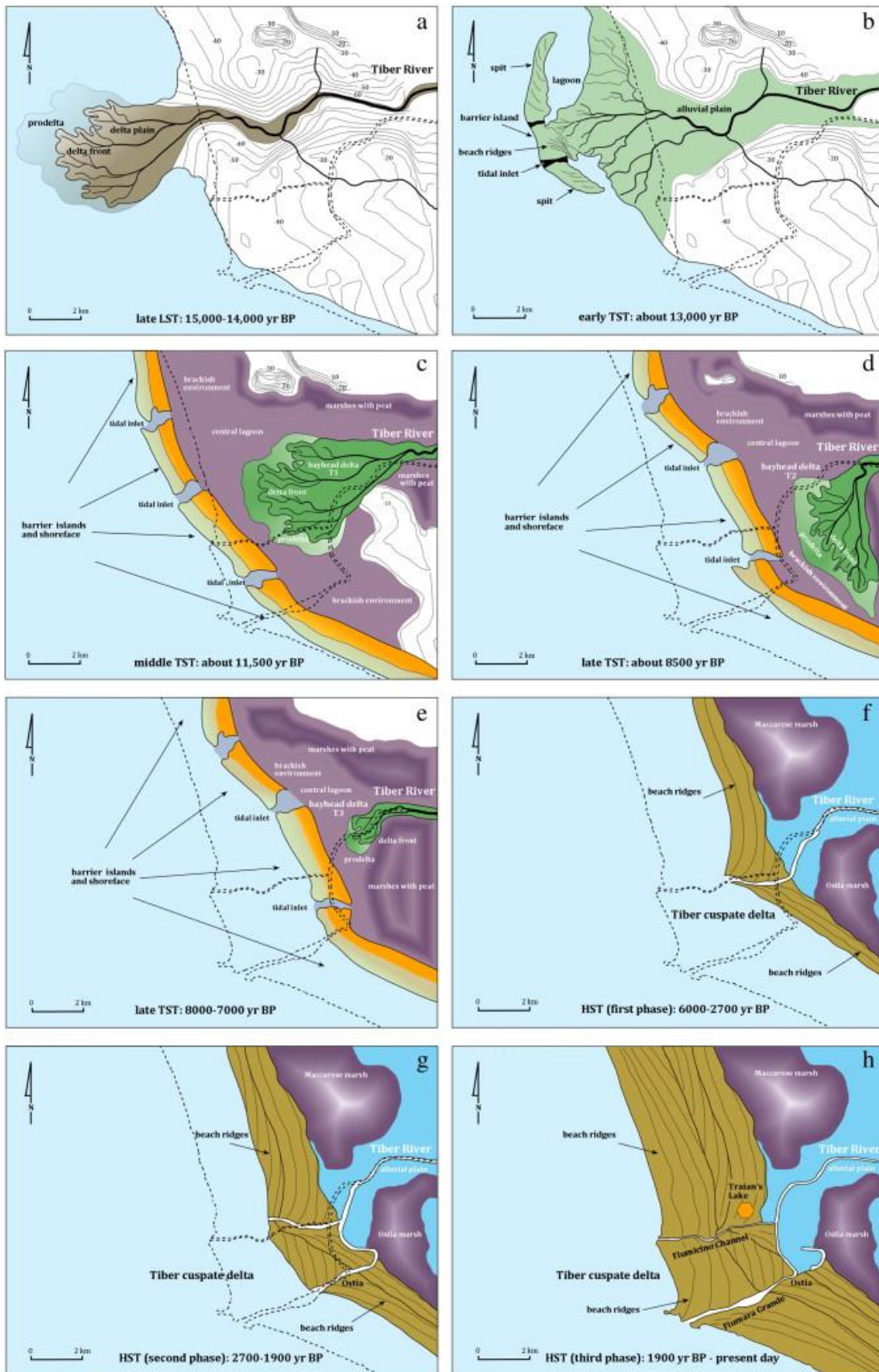


Fig. 5. Paleogeographic map showing the evolution of the Tiber River during the last 18,000 yr BP. a) late lowstand systems tract; b, c, d, e) transgressive systems tract; f, g, h) highstand systems tract. The colors in the figure identify the different depositional environments (Milli et al., 2013).

### 2.1.3 The Ombrone Paleovalley System

In southern Tuscany, the Grosseto Plain was formed by the Ombrone River and the smaller Bruna River. During the Last Glacial Maximum, these two rivers deeply cut into the substrate, mainly composed of Oligo-Miocene arenaceous flysch, Triassic-Jurassic limestones, and metamorphic rocks (Carmignani et al., 2012).

To reconstruct the stratigraphic architecture of the Ombrone paleovalley (Breda et al., 2016) (Fig. 6), a detailed multi-proxy analysis was conducted on two reference cores (OM1 - OM2), 70 m long, acquired along the paleovalley axis. The two reference cores were analyzed in terms of sedimentology, micropaleontological and palynological content, and radiometric ages. The multidisciplinary study of these two reference cores enabled the reconstruction of the late-glacial to Holocene stratigraphic architecture of the Ombrone Paleovalley system.

The valley floor is encountered at 60 m depth below sea level, and the basal erosional surface is interpreted as SB.

A deepening-upward succession from alluvial to coastal facies is observed above the paleovalley floor. The basal fluvial gravel deposits and the overlying succession of floodplain muds constitute the lowstand systems tract (LST) to the early transgressive systems tract (early TST) of the valley-fill sequence. The first marine flooding, marked by the surface FS1 in Figure 6, is encountered at about 40 to 44 meters in the reference cores. Above FS1, which can be tentatively related to the well-known melt water pulse 1B, a variety of inner estuary sub-environments, including swamps and bay-head deltas, developed during late TST within the Ombrone Paleovalley (Breda et al., 2016).

After the first establishment of the estuarine environment, the two cores record different infill histories. In core OM1, as shown in Figure 6, the deepening-upward trend is marked by the transition from inner estuarine to outer estuarine environments. In this core, after a second marine flooding (FS2) at about 28 m depth, a monotonous succession of shell-rich clays suggests the development of more open conditions. The Maximum Flooding Surface (MFS) is placed around the 17m depth, where the sand and shell debris are most abundant.

In contrast, at core OM2, which is located in a more proximal position, the estuarine conditions are interrupted by the presence of continental environments; a thick succession of freshwater swamp clays is present, onto which coastal plain progradation took place during the sea-level highstand (Fig. 6).

The different stratigraphic architecture reconstructed at the two sites is due to their relative location, which is between the middle and inner segments of the paleovalley. The Ombrone paleovalley shows strong variations in the sedimentary infill; the two cores show different facies profiles, including a typical middle segment record at OM1, where sea level was the primary controlling factor, while at core OM2, fluvial sediment input is dominant.

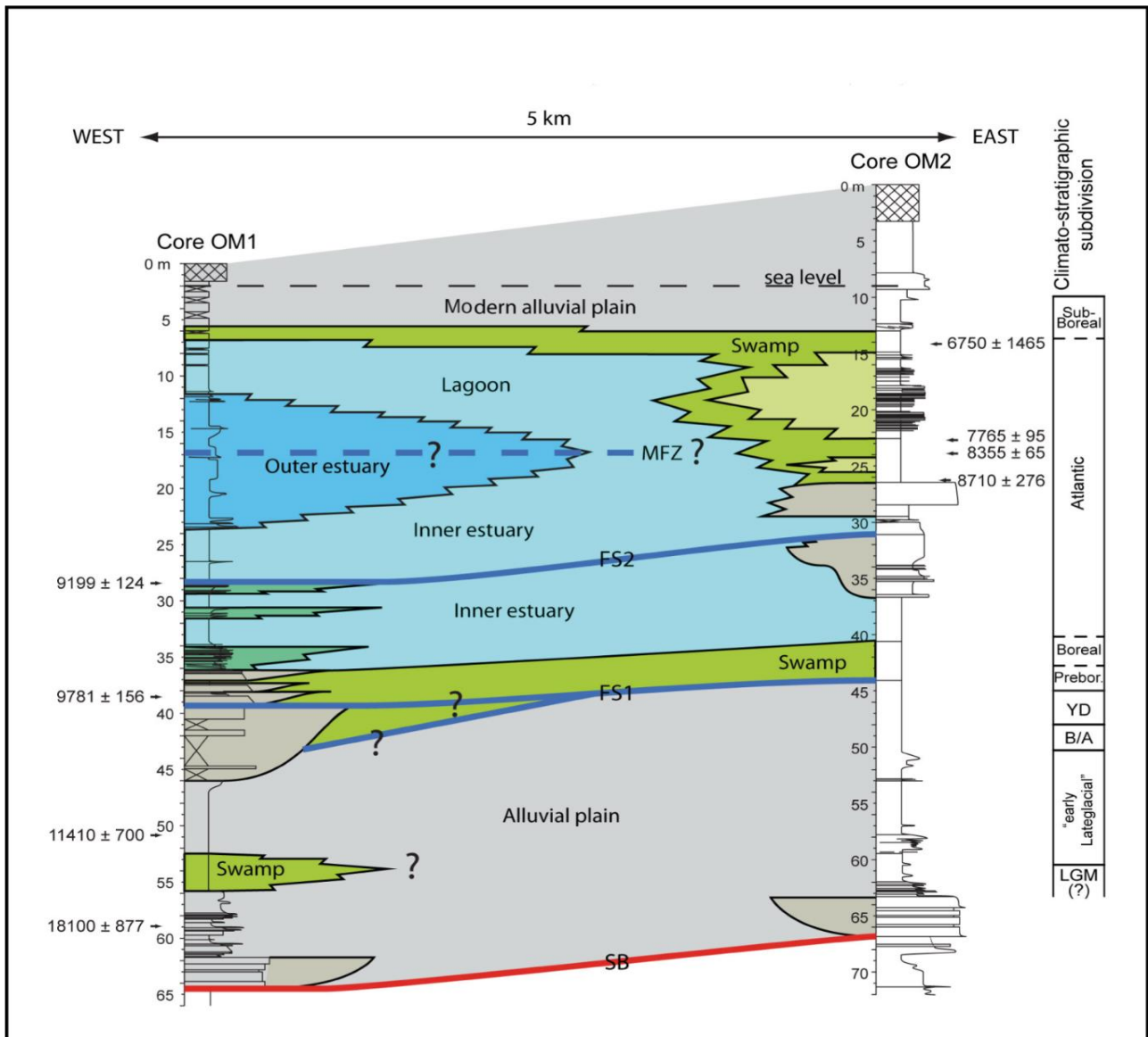


Fig. 6. Longitudinal cross-section of the Ombrone paleovalley showing the seaward-landward correlation between the two cores. SB = Sequence Boundary. FS = Flooding surfaces. MFZ = Maximum flooding zone (tentatively placed in core OM1 in correspondence with the richest level in sand and shell debris) (Breda et al., 2016).

#### 2.1.4 The Volturno Paleovalley System

The Volturno Paleovalley system (Amorosi et al., 2012) is located beneath the homonymous coastal plain, which is part of the "Domitia" coastal zone that extends 50 km along the Tyrrhenian Sea shore, from the Garigliano River delta to Monte di Procida promontory.

In this area, a huge amount of volcanic materials called Campania Grey Tuff (CGT), emplaced by the 39 ky BP eruption, is present (De Vivo et al., 2001, Rolandi et al., 2003). The CGT represents a laterally continuous ignimbritic unit easily identified in core successions due to its peculiar thickness and lithologic attributes. CGT is exposed at the study area's southern and northern flanks, while the top of the ignimbritic unit is observed at progressively higher depths beneath the modern Volturno coastal plain. Thus, stratigraphic correlations make it possible to trace the shape of the paleovalley system cut into CGT.

A multidisciplinary study conducted on core data acquired at the depocenter of the paleovalley allowed the identification of the facies architecture and the reconstruction of the paleovalley geometry (Fig. 7).

The radiocarbon dating of fluvial terrace deposits shows that the valley incision took place immediately after the CGT deposition. This phase of deep incision is interpreted to reflect the fluvial response to intense volcanic activity (Lucchitta et al., 2000, Manville et al., 2005). The incision was likely promoted by the emplacement of CGT and amplified by the soft, unconsolidated nature of this thick ignimbritic unit (Amorosi et al., 2012). A secondary phase of fluvial incision took place in later times; fluvial downcutting, although not well constrained chronologically, is tentatively related to the sea-level fall at the onset of the Last Glacial Maximum.

With the post-LGM sea-level rise, the Volturno paleovalley was rapidly drowned and filled with Holocene deposits. Directly in contact with CGT, a succession of swamp sediments is present (fig. 7). These paludal environments represent the response to the rapid sea-level rise and testify the transition to warmer and milder climate conditions.

With continuing sea-level rise, around 9.5–9 ky cal BP, freshwater environments were replaced by brackish basin areas, interpreted as formed in a backstepping wave-dominated estuary. The end of the transgression is indicated by transgressive barrier sand deposits, which testify the rapid inland migration of the beach-barrier system and that are marked by a well-developed ravinement surface.

At the maximum marine ingression, a continuous beach-ridge system developed throughout the study area. The topmost transgressive sand portions are characterized by the most open-marine

meiofauna of the entire Holocene succession, which can thus lead to the identification of the maximum flooding surface (MFS). The MFS, constrained to about 7 ky cal BP, is overlain by a shallowing-upward highstand succession.

Above MFS, at core CV001 (Fig. 7), which is placed in a distal position, lower prodelta facies are overlain by upper prodelta deposits, mainly composed of sand-and-mud couplets that show an increase in fluvial influence. These, in turn, are overlain by thick, elongated sand bodies corresponding to delta front facies of the wave-dominated delta.

In more internal positions, a similar regression pattern is observed through the vertical layering of brackish, swamp, and alluvial sediments (Core CV002-CV010 in Fig. 7).

Around 2 ky cal BP, beach and lagoonal environments persisted along the modern coastal area. The recent evolution of the Volturno coastal plain was characterized by coastal progradation and alluvial aggradation, with the progressive infilling of swamp areas.

The Volturno coastal plain, located in an active volcanic region, offers a unique chance to study the sedimentary evolution of a coastal system from the latest Pleistocene to the Holocene period in a context that combines siliciclastic and pyroclastic elements. The work of Amorosi et al. (2012) emphasizes the significance of pyroclastic layers as potential markers in siliciclastic successions. It stands out from other incised valley models in published literature by providing a detailed example of an incised valley entirely cut into pyroclastic material.

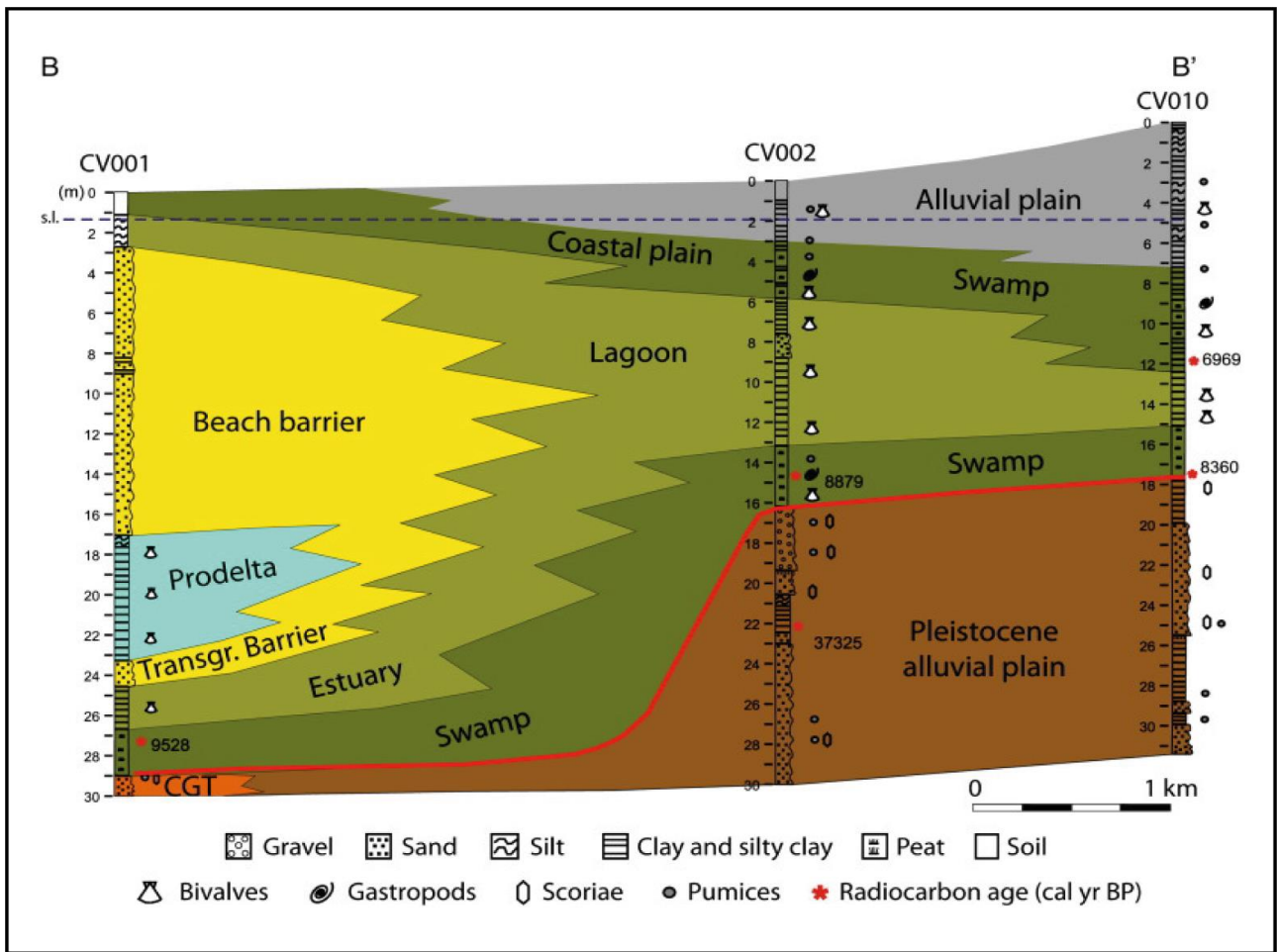


Fig. 7. facies architecture of Voltorno valley fill in a stratigraphic cross-section transverse to the palaeoshoreline. The red line denotes the transgressive surface. CGT: Campania Grey Tuff. (Amorosi et al., 2012).

### 2.1.5 The Tagliamento Paleovalley System

On the northern Adriatic coastal plain, the Tagliamento paleovalley system was studied by Fontana et al. (2008) and Ronchi et al. (2018; 2021).

This area corresponds to the distal portion of the Tagliamento River alluvial megafan. The Tagliamento is one of the major rivers in the Alps. Its catchment area, approximately 2700 km<sup>2</sup> wide, comprises over 70% of limestones and dolostones. In the region, 20 to 35 m of Holocene fluvial and fluvio-glacial deposits aggraded during the Last Glacial Maximum.

A detailed paleoenvironment reconstruction (Fig. 8) of the Tagliamento paleovalley system was conducted through the analysis of a mechanical and hand-made cores dataset. Such paleovalley is up to 1.2 km wide, with a depth of 20 m, and can be traced for a length of 25 km.

The formation of the Tagliamento paleovalley system, in contrast with the classic late Quaternary paleovalley systems, was driven by a climatic response rather than a base-level response. The downcutting only began after the LGM, owing to a decrease in sediment supply that followed the withdrawal of the mountain glaciers from lower Alpine valleys (Arnaud-Fassetta, 2003; Carton et al., 2009; Mozzi et al., 2013; Fontana, 2006, 2008, 2012).

The timing of the paleovalley incision can be estimated by the age of the top of the LGM unit eroded by the fluvial process and the age of the sediments that filled the bottom of the valley. The last phase of LGM aggradation is dated between 19 and 18 ka cal BP, providing a date after which the erosive phase began.

After the erosion, the sedimentations of thick, up to 12 meters, sandy gravels and gravelly sands units, capped by a thick and stiff silty layer, took place. These deposits that occupy the lower portion of the incised valley, represent the Tagliamento River sedimentation (Fig. 8 A).

In the early Holocene, the Tagliamento River stopped using the paleovalley; this is recorded by modest soil formation at the top of the sandy gravel basal unit, which is buried by a peat layer, dated between 9.6 and 8.4 ka cal BP (Fig 8 B).

With the progressive middle Holocene sea-level rise (8.0 ka cal BP), the Tagliamento paleovalley and its southern shoulders were progressively drowned. This process led to the deposition of soft, silty and clayey deposits, characterized by a homogeneous light grey to greenish color. This sediment body has a wedge shape in the longitudinal direction; its thickness decreases from 17 m in the southern sector to zero in the northmost and proximal part of the study area. The analysis conducted on macro and microfossils shows the presence of a brackish fauna. These deposits are interpreted to reflect an extensive lagoon environment that occupied the incised valley system for a considerable

distance inland and that lasted for several millennia within the valley (by around 6.5 ka cal BP) (Fig. 8 C).

Several peat layers are identified within and on top of the lagoonal deposits. Although many of these are lens-shaped, two major peat layers, dated 4.5 ka BP and 1.9 ka BP, respectively, can be followed for almost the entire length of the paleovalley. The deposition of this peat layer likely occurred in response to the progressive silting up and slowdown of the sea-level rise, notably at 4.5 ka cal BP, and between the 1st millennium BCE and the 6th century CE, that caused the alternation of freshwater swamp and lagoonal environments (Fig. 8. D-E).

The topmost portions of the Holocene succession are marked by the presence of greyish-yellowish silty and sandy units characterized by weakly developed soil. The thickness of this unit is up to 5 meters where it covers the paleovalley fill. As it spreads outwards from the paleovalley, it becomes less than 1 meter thick, overlapping the LGM alluvial plain. Based on its stratigraphy and morphology, this deposit indicates a fluvial unit formed in the early Medieval period (Fig 8 F).

The stratigraphic reconstruction led to mapping the geometry and infill of the paleovalley generated by the Tagliamento River in the distal Friulian Plain over 25 km. Chronologic, sedimentological, and paleoenvironmental information allowed the reconstruction of the phases of incision and the Holocene paleoenvironmental evolution of the whole system.

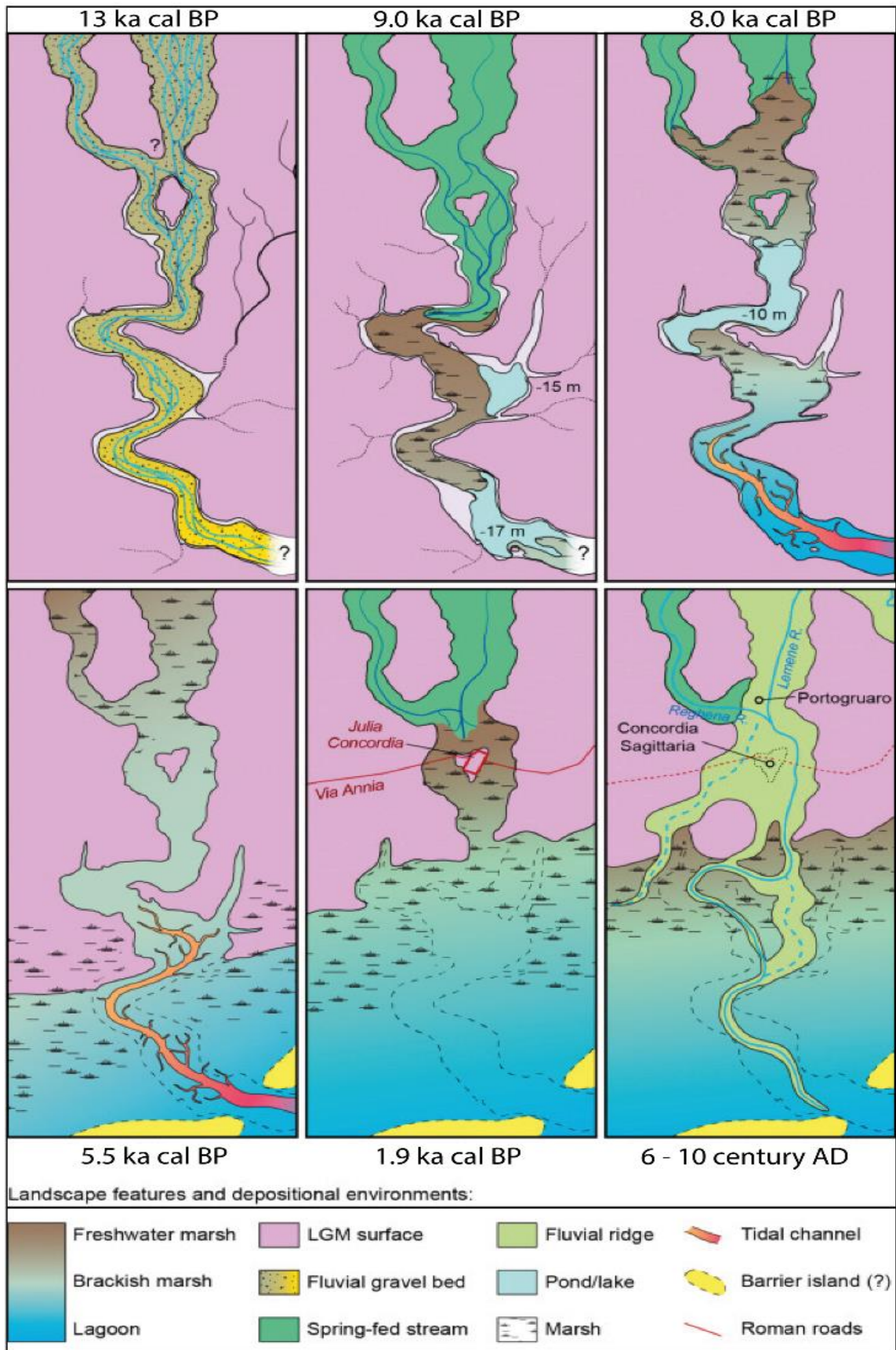


Fig. 8. Paleogeographic evolution of the Tagliamento Paleovalley (Ronchi et al., 2021).

### 2.1.6 The Biferno Paleovalley System

In the Molise region, on the Adriatic coastal plain, the Biferno paleovalley system was studied by Amorosi et al. (2016 - Fig.9). The Biferno River catchment, situated in the Southern Apennines, covers an area of 1300 km<sup>2</sup>. The river runs for 93 km, from the Matese Mounts to the Adriatic Sea.

The stratigraphic architecture of the Biferno coastal plain was reconstructed by analyzing data from 19 boreholes (depth range 20-60 m) and 8 cone penetration tests along a shore-parallel, NW-SE oriented line that crosses the Biferno valley, about 1.5 km landward of the modern coastline.

The late Quaternary stratigraphic architecture of the Biferno coastal plain reveals numerous valley incisions caused by the interaction of pre-existing topography, tectonic activity, and sea-level fluctuations that lasted for over 350,000 years.

Abrupt changes in stratigraphy at the paleovalley margins reveal sharply bounded valley walls. These walls are cut into the Lower Pleistocene bedrock consisting of Montesecco Clays and Serracapriola Sands (as seen in Fig. 9).

Above the basal erosional surface, the lower valley fill facies association is composed of gray silty clay with cm- to dm-thick sand intercalations. This deposit records two distinct coarse-grained bodies, up to 2.5 m thick, consisting of medium-coarse sand with rare rounded pebbles. Fragments of mollusks and shells are found alongside vegetal remains. The mollusk collection is mostly made up of marine species, with *Corbula gibba* and *Bittium reticulatum* being the most prevalent. The sedimentological features and the fossil content of the clay fraction document the establishment of a shallow-marine environment subject to moderate fluvial influence.

There is currently no information about the timing of the initial incision of the Biferno Valley. According to Amorosi et al. (2016), the Biferno River excavated a deep incision in the bedrock after ca. 350 ky BP, based on the MIS 9 age assignment of the mature red argillic paleosol identified at the Apenninic margin, while the most plausible timeframe for the lower valley fill deposition appears to be the MIS 7.

Within the Biferno coastal plain, two distinct paleovalley systems are superimposed (Fig. 9). Stratigraphic interpretations of continuous cores indicate a compound architecture highlighted by the erosional boundary separating the coastal to shallow-marine lower valley fill from the overlying, essentially non-marine upper valley fill.

It has been documented that the study area and nearby coastal plains underwent significant tectonic uplift during the Middle Pleistocene. Following this uplift, the region remained stable until

the Holocene. In this context, it is likely that tectonic uplift, which resulted in the river downcutting, was the initial cause of the Biferno River paleovalley formation.

Most of these shallow-marine deposits were eroded during the subsequent sea-level lowering associated with MIS 6. Above the partly preserved MIS 7 coastal facies, the upper valley fill records the recent, prominent phase of fluvial incision and filling during the last glacial phase of sea-level fall and rising. According to Amorosi et al. (2016), the Late Pleniglacial period (MIS 3/2 transition), which occurred between 28 and 23 cal. ky BP, was likely the final stage of valley incision.

At the bottom of the upper paleovalley, about 30 m deep, an extensive and amalgamated, poorly sorted gravel body, up to 6 m thick, characterizes the valley floor. The gravel body exhibits a fining-upward trend and an erosional lower boundary. No fossils or plant debris were observed. This facies association represents a high-gradient and high-energy fluvial-channel deposit (LST).

Above fluvial gravels, the sharp transition to well-drained floodplain deposits, and overlying poorly-drained floodplain, swamp, and brackish-water clays indicate that the valley experienced increasing drowning between approximately 13 and 8 thousand years ago. As the sea level rose, the valley was flooded, and more extensive paludal and lagoonal areas could develop (TST).

During the middle-late Holocene, the Biferno coastal plain experienced progradation. A shallowing-upward facies trend characterizes the uppermost 15 m, with swamp clays overlain by discontinuous poorly-drained floodplain facies capped by the modern, well-drained alluvial plain (HST).

The facies and stratigraphic architecture of the Biferno paleovalley systems were reconstructed along a transversal cross-section using stratigraphic, sedimentological, geomorphological, and paleontological data. The Biferno River coastal plain exhibits considerable stratigraphic complexity and records multiple valley incision and infilling episodes.

Fluvial incision during the Middle Pleistocene was probably triggered by regional tectonic uplift. The nearshore to shallow-marine lower valley fill deposition is correlated to MIS 7, while the subsequent river erosion appears to have been controlled by climate and base-level drop during the last glacial sea-level fall, when a river valley deeply dissected the previous (MIS 7 and MIS 5e) highstand coastal wedges. The overprint of the Late Pleistocene–Holocene sea-level fluctuations onto the overall facies architecture, thus, was clearly identified.

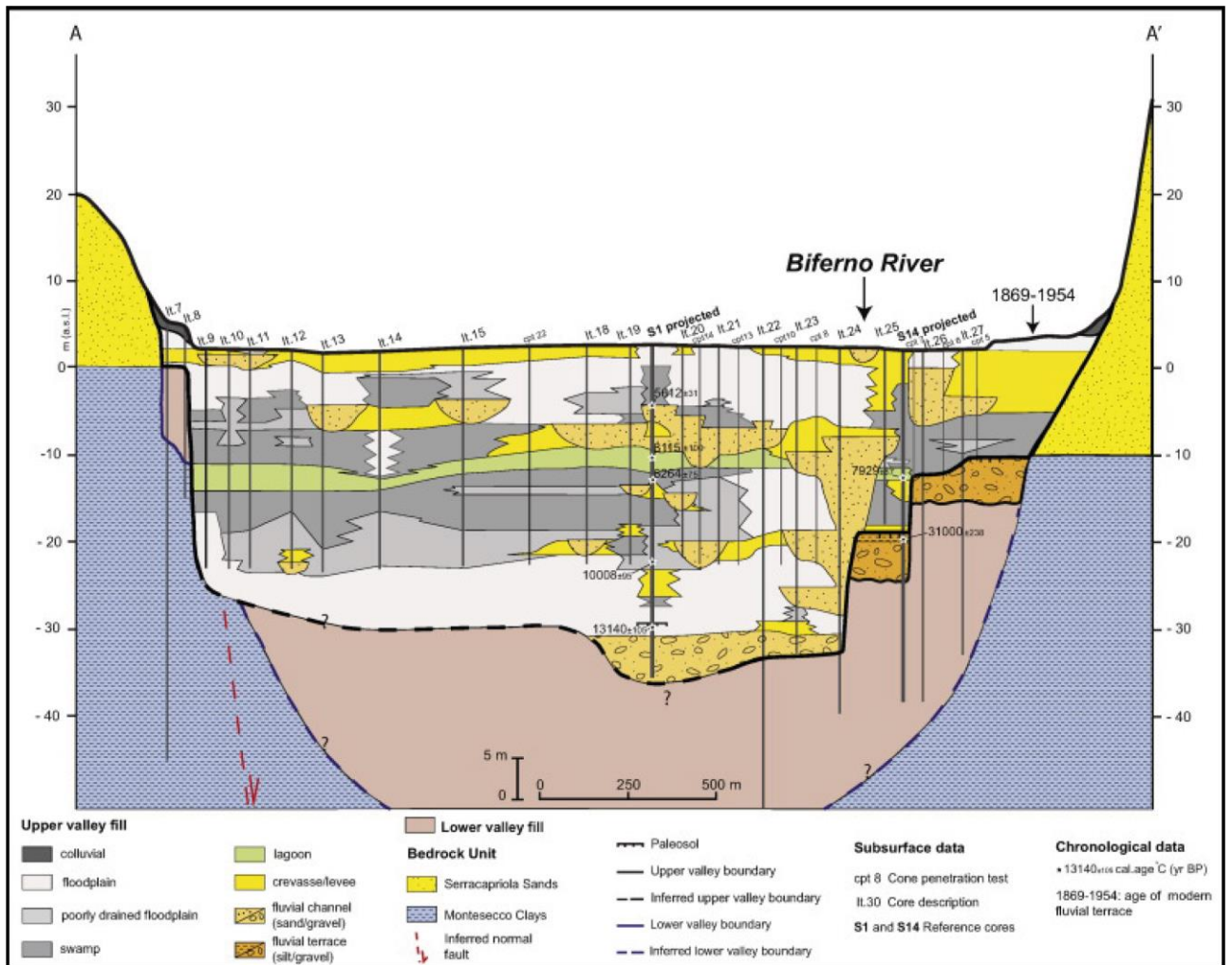


Fig. 9. Facies architecture of the Biferno Valley fill. The lower valley fill is undifferentiated (Amorosi et al., 2016).

### 2.1.7 The Manfredonia Paleovalley System offshore

The offshore segment of the Manfredonia Incised Valley (MIV) was identified in the southern Adriatic Sea by Maselli and Trincardi (2013), and Maselli et al. (2014 - Fig. 10). The MIV is located in the Gulf of Manfredonia, east of the Apulian Tavoliere, as a part of the Bradanic Trough region. The Apulian Tavoliere covers an area of 4300 km<sup>2</sup> and is bordered by three mountain ranges: the Daunia Mountains to the west, the Gargano Promontory to the north, and the Murge Plateau to the south. Currently, the Tavoliere Plain is drained by three main rivers: the Candelaro River has the widest drainage basin (2435 km<sup>2</sup>), the Carapelle River, with 1465 km<sup>2</sup>, and the Cervaro River, with 625 km<sup>2</sup>.

In this context, the offshore portion of the MIV was reconstructed using a dense network of geophysical data consisting of 3000 km of high-resolution chirp-sonar profiles, acquired with a Teledyne Benthos Chirtp-III SBP system, using a 2–7 kHz sweep-modulated bandwidth that allowed a vertical resolution in the order of 50 cm.

The landward segment of the MIV imaged by seismic data is located around 10-15 m water depth, close to the modern Candelaro and Cervaro River mouths. The valley is a wide incision with steep flanks and a maximum width of 7 km, exceeding 40 m in depth. Several units characterize the sedimentary infill of the valley, and high-resolution chirp profiles define the complex sedimentary deposits in its shallowest portion.

Above the basal erosional surface (ES1 in Fig 10), unit 5A is a 10 m-thick layer with sub-parallel seismic reflectors and low-angle internal downlapping surfaces; it mainly represents the fill of local erosional depressions. At the top of this unit, a sharp and laterally-continuous reflector is dissected by small-scale channel-like incisions (surface S1).

The valley section widens from approximately 700 m to over 2 km above surface S1. At this shallower level, a prograding body (Unit 5B), composed of high-angle downlapping reflectors, partially filled the incision. Surface S2 marks the top of Unit 5B, indicating it formed when the valley was still broadly incised, only partially filled with sedimentary units.

Unit 5C is about 10 meters thick and characterized by high amplitude sub-parallel reflectors that onlap northward onto surface S2. The shallowest part of Unit 5C consists of thin, well-defined reflectors draped over the valley flanks, just above surface S2.

Surface S3 separates Unit 5C from the overlying Unit 5D. Unit 5D is a prograding wedge up to 10 m thick with thin reflectors and multiple internal downlapping surfaces. It is characterized by foresets dipping about 5° southward and pinching out toward the valley flank.

The prograding wedge is capped by an erosional surface (surface S4) that plunges toward the valley axis and that suggests increasing energy conditions. Toward the valley center, the prograding wedge is replaced by a 10 m-thick, plane-parallel unit that reflects possibly a period of increased sediment flux or reduced energy conditions.

At the end of the deposition of Unit 5D, the paleovalley fill was asymmetrical, indicating a dominant sediment supply direction from the north. The last phases of the valley fill were then characterized by the deposition of homogeneous late-transgressive to highstand sediments (Units 5E and 5F).

These units are defined by strong reflectors whose amplitude increases towards shallower depths, onlapping towards the valley flanks. Nevertheless, minor internal erosional surfaces indicate repeated cut-and-fill events.

This large paleovalley system was filled with sediment during the post-glacial sea level rise, with about 2.95 km<sup>3</sup> of sediment, and then leveled off 5.5 kyr BP. Despite its small catchment area, the valley was rapidly filled in less than 15 kyr, which may have been due to high mountain relief, erodible catchment lithology, and short-term climate fluctuations.

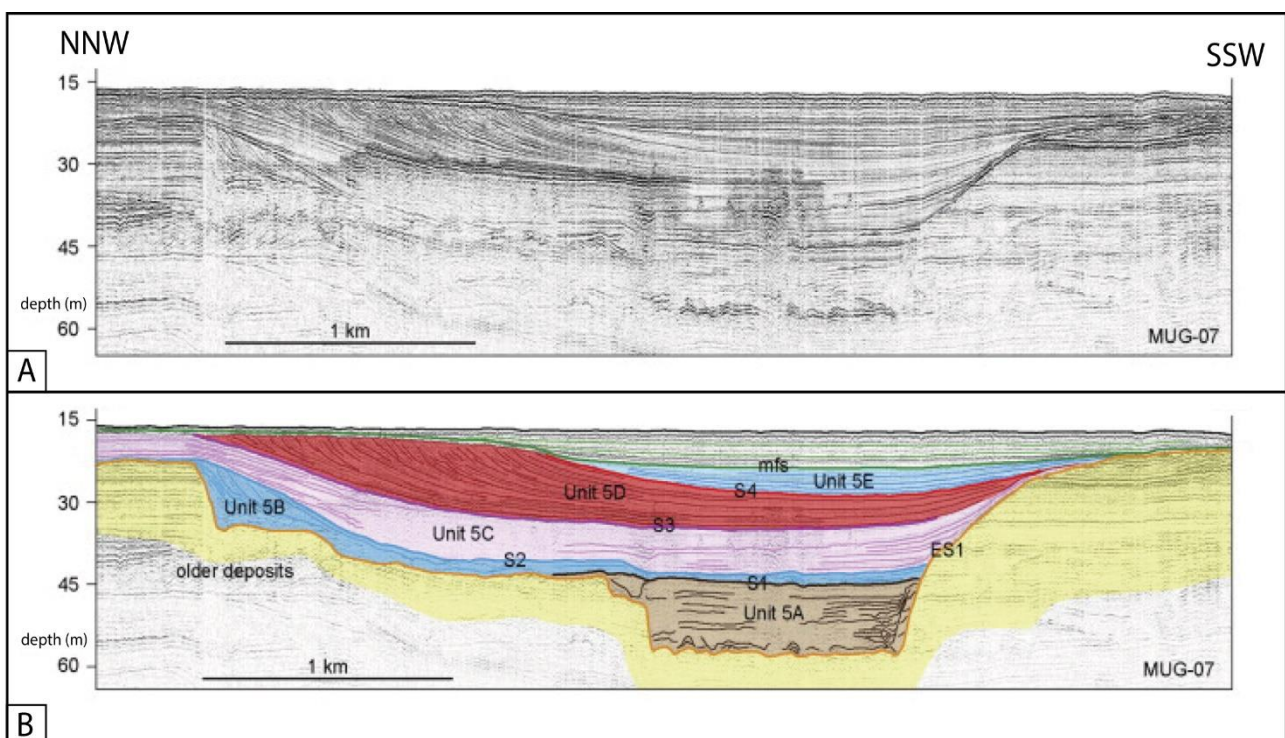


Fig. 10. A) Sparker profile MUG-07. B) representation of the lowstand to highstand infill of the MIV. (Maselli and Trincardi, 2013).

### 3. Methods

A multidisciplinary approach was applied to reconstruct the stratigraphy of paleovalley systems, characterize their seismic response, and analyze sedimentary facies on continuous cores.

In the Manfredonia area, the study was primarily based on the sedimentological analysis of undisturbed core material from three reference cores named MAN, ZS1, and ZS2. To achieve a more comprehensive reconstruction of the stratigraphic architecture of the study area, previous borehole descriptions and data from the early work of De Santis and Caldara (2016) and De Santis et al. (2020a, b, c) were also used (Fig. 11 A).

Combined sedimentologic and paleontologic investigations were carried out on reference cores. Sedimentary facies analysis (Fig 12 A) was conducted in the field by describing lithology, grain size, sedimentary structures, lamination styles, accessory components, and resistance to penetration measured through a pocket penetrometer. Mollusks, benthic foraminifera, and ostracods were then analyzed at Bologna University (Veronica Rossi, Daniele Scarponi, and Stefano Claudio Vaiani) to detect changes in environmental factors such as depth, salinity, confinement, substrate type, oxygen, and food availability. Spatial distribution patterns of modern meiofauna and mollusks were compared to interpret fossil assemblages. (Scarponi and Kowalewski, 2004; Rossi and Vaiani, 2008; Amorosi et al., 2014; Wittmer et al., 2014; Mazzini et al., 2017, 2022; Scarponi et al., 2014, 2022)

For macrobenthic analysis, core samples were collected from reference cores at intervals of ~1 m. The fossil assemblages were qualitatively analyzed under an optical microscope to identify key environmental taxa.

A total of 136 samples were collected to analyze foraminiferal and ostracod assemblages. To obtain paleoenvironmental interpretations, species were identified using original descriptions (e.g. Ellis and Messina, 1940; Debenay et al., 2000; Frezza and Carboni, 2009; Salel et al., 2016, Mazzini et al., 2022).

To perform a geochemical characterization of Southern Apennines sediment sources, 11 sediment samples from Southern Apennines rivers, including Candelaro, Cervaro, Carapelle, and Ofanto, were acquired. The samples were taken from exposed bars or subaqueous channel beds, and all particle sizes, from coarse sand to mud, were considered. Furthermore, geochemical analysis was conducted on 33 sediment samples from core MAN, taken between 8.70 and 43.10 meters

deep. The samples were tested for major element oxides, trace elements, and loss on ignition (LOI) at laboratories at Bologna University.

A total of 25 samples were collected from reference cores for radiocarbon dating, including a graded, light grey pumice layer (Mercato Pumice in De Santis et al., 2020b). The analysis was carried out at KIGAM laboratories in Daejeon City, Korea. The calibration of conventional radiocarbon ages was based on the IntCal20 dataset (Reimer et al., 2020), using OxCal 4.3. (Bronk Ramsey, 2009).

The three-dimensional stratigraphic architecture of the Pescara coastal plain succession (Late Pleistocene to Holocene) was reconstructed across two transects with NW-SE and SW-NE orientation, respectively, each about 2 km long. The stratigraphic correlation was carried out using geometric criteria and constrained by radiocarbon ages. The dataset includes a new reference core and 32 borehole descriptions (average depth ca. 45 m) available from the "Microzonazione Sismica Project" of the Pescara Municipality (Fig. 11 B).

The facies interpretation (Fig. 12 B) was based on an integrated sedimentological and paleontological (benthic foraminifera, ostracods, and mollusks) analysis conducted on the 52-meter-long reference core named Marconi.

The reference core was acquired in the Pescara coastal plain, about 1 km landward from the modern shoreline. The stratigraphic succession was analyzed, including texture, grain size, color, sedimentary structures, and accessory materials such as wood fragments, plant remains, fossil content, and carbonate concretions. Pocket penetration values were also considered for facies interpretations following the criteria outlined by (Amorosi et al., 2015).

A total of 79 and 50 samples were collected for analysis of meiofauna (ostracods and foraminifers) and malacofauna to obtain palaeoenvironmental information, such as organic matter concentration, paleosalinity, paleobathymetry, and substrate characteristics. For micropaleontological analyses, samples were analyzed using standard procedures previously adopted in other works on late Quaternary successions (e.g., Barbieri et al., 2021; Rossi and Vaiani, 2008).

Samples for mollusk-based inferences were collected at distinct stratigraphic positions. The material was analyzed under an optical microscope to describe fossil assemblages.

The identification of meiofaunal taxa was supported by original descriptions from Ellis and Messina (1940, 1952), integrated with selected papers from Athersuch et al. (1989), Barbieri and Vaiani (2018), and Henderson (1990).

The stratigraphic succession was chronologically constrained by a high-resolution framework consisting of seventeen AMS 14C dates performed on organic-rich samples at KIGAM Laboratory

(Daejeon, Korea). All samples were cleaned with deionized water, then dried at 40 °C to prevent mold growth. Conventional <sup>14</sup>C ages were calibrated using OxCal 4.4 with IntCal 20 and Marine 20 curves.

The reliability of the 17 new radiocarbon dates was tested using the Bayesian approach (Blockley et al., 2004), which incorporates prior information into the calibration process (Buck et al., 1991, 1992, 2003). The Markov Chain Monte Carlo (MCMC) analysis available in OxCal was utilized. An age-depth model (Lowe et al., 2007) was developed to reject dates of poor fit and objectively constrain the whole series.

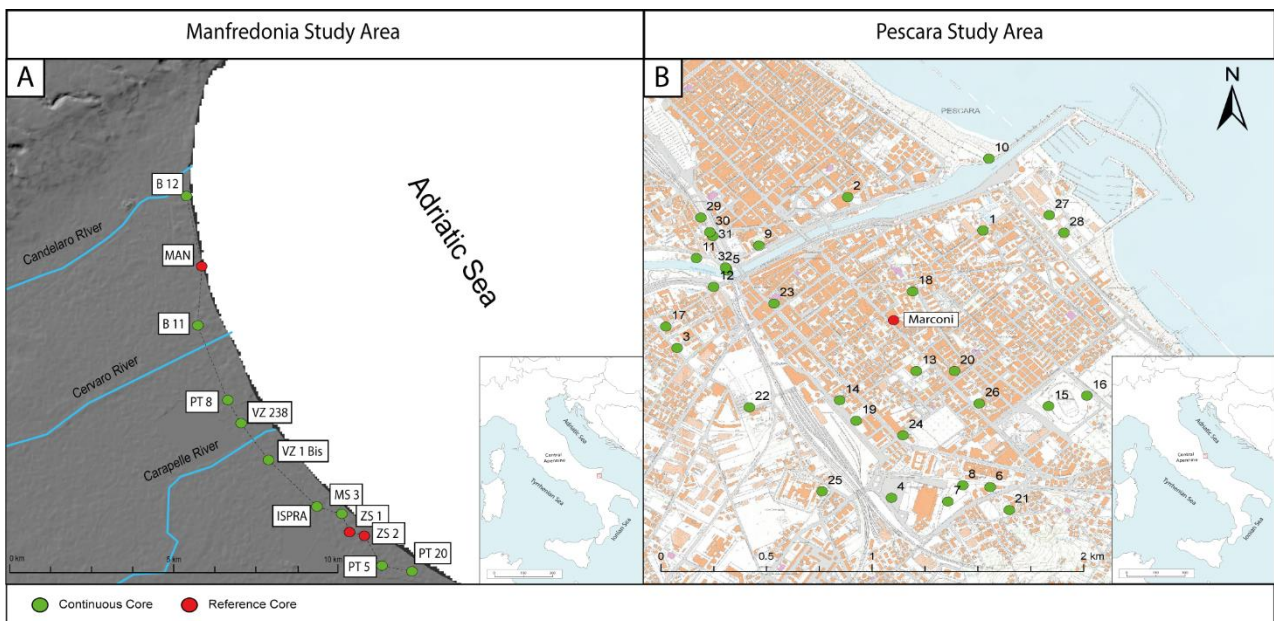


Fig. 11. Location of the two study areas. (A) Manfredonia area, and (B) Pescara area

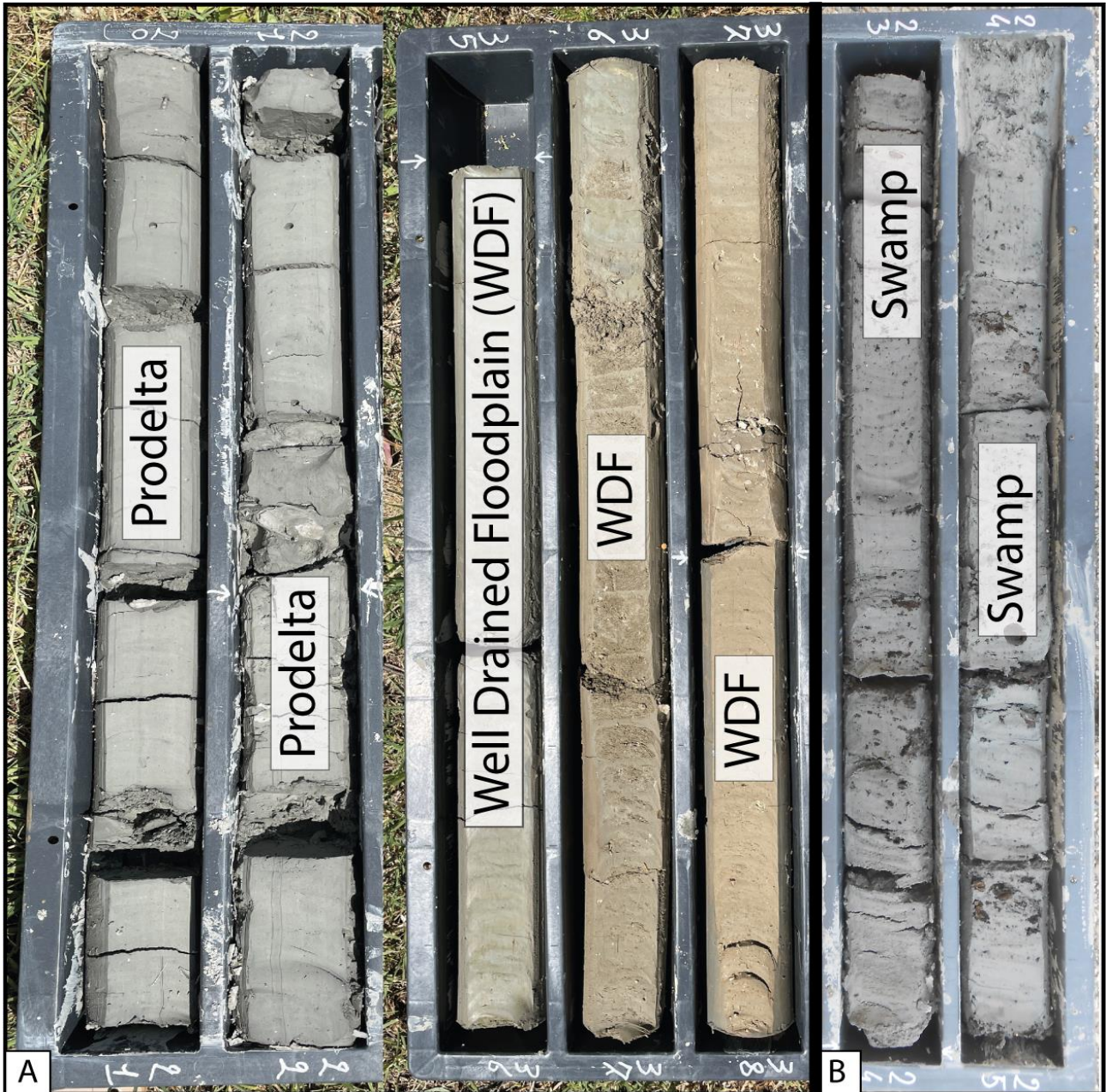


Fig. 12. Example of facies analysis performed on the MAN reference core, in the Manfredonia area (A), and on the Marconi borehole in the Pescara area (B)

The geophysical reconstructions and the study of seismic site effects mostly relied on the microtremor-based horizontal-to-vertical spectral ratio (m-HVSR).

Single-station microtremor recordings were acquired in both study areas, Pescara and Manfredonia. All microtremor measurements were performed using a Tromino<sup>®</sup> microtremor recorder by MoHo SRL (Italy). The Tromino is a small, lightweight, all-in-one seismograph designed for dynamic subsoil characterization with high accuracy and low effort (approximately 1 dm<sup>3</sup> volume and 1 kg weight, no external batteries/cables). Its versatility makes it useful for geology and engineering purposes. The instrument has three velocimetric and three accelerometric channels, with six amplification levels ( $\pm 0.5$  mm/s to  $\pm 40$  mm/s) and  $\pm 2g$  dynamic range.

The measurement sampling rate varies from 128 to 256 Hz, and the acquisition length was 16 to 60 minutes. The measurement length was determined by the estimated depth of the substrate and the amount of anthropic noise in the area. The instrument was securely placed in soft soil, devoid of vegetation, and protected from wind (Chatelain et al., 2008). Recordings were taken in free field conditions (Castellaro and Mulargia, 2009) at least 15 meters from buildings. Sensors were properly leveled and stabilized during recordings, and stiff material over soft soil was avoided. The instrument was aligned to the geographical North and leveled on the Earth's surface. Additionally, some measurements were repeated at the same locations using a longer acquisition time to confirm result stability.

All the measurements were processed with the Grilla software to perform the microtremor-based Horizontal to Vertical Spectral Ratio (mHVSR) (Fig. 13). The microtremor three-component time series was divided into 30-second non-overlapping windows. For each time window, Fourier spectra, computed using FFT, Fast Fourier Transform, were smoothed with triangular functions with a width equal to 10% of the central frequency. The resulting mHVSR curves were obtained by averaging the mHVSR ratios computed for each window, with component H being the geometric average of the instrumental N-S and E-W components.

To verify that the results were not affected by parameters basis, a few longer (30 min) measures were split into longer window lengths of 60 seconds and also smoothed with different smoothing functions like the Konno-Ohmachi smoothing algorithm. The results did not change.

To accurately correlate geological and geophysical data, we carried out microtremor measurements on the exact collocation of pre-existing borehole data; transforming the H/V form frequency to the spatial domain requires a precise constraint of the depth of the impedance contrast surface that can be obtained only with continuous cores.

In this regard, under the assumption of 1D site conditions and a  $V_s$  model for the sediment layer, the equation of 1D resonance links the thickness of the resonating layer with the fundamental ground resonance frequency and the shear wave velocity:

$$f_0 = \frac{V_s}{4h} \quad (1)$$

By means of equation 1, it is possible to obtain information about the depth of the impedance contrast surface. The geometry of the impedance contrast surface can be inferred by producing a geophysical cross-section composed of each mHVSr curve alongside contour plots of the curves interpolated as a function of the distance. These plots allow for visualization of the lateral correlation of the main resonance peaks and for identifying resonance frequencies associated with the primary impedance-contrast surfaces (Fig. 14).

Furthermore, relying on continuous core data, it is possible to produce a Frequency-Depth model and thus derive a  $V_s$  velocity profile valid in the area by correlating the observed depth of the impedance contrast surface and the measured resonance frequency at that point (e.g., Ibs-von-Set and Wohleberg, 1999).

In a paleovalley system, the impedance contrast surface can be identified as the surface that marks the abrupt lithologic contrast between the soft clay-dominated, transgressive paleovalley fill and the underlying lowstand fluvial gravel body at valley floor. However, it can locally reflect pedogenized horizons or the direct contact between the valley fill and the overconsolidated substrate at a slightly higher stratigraphic level.

A frequency-depth model can be derived using a power-law relation for increasing  $V_s$  with depth by fitting the resonance frequency with the identified depth of impedance contrast. This method was proposed by Ibs-von Seth and Wohleberg in 1999 and has been used in several geological contexts by numerous authors, such as Parolai et al. (2002), Paolucci et al. (2015), and Tün et al. (2016).

To test the accuracy of the obtained geophysical model, the Mean Square error (MSE) and mean Absolute Error (MAE) were computed, and a residual error plot was performed to validate further the model performance verifying the presence of bias that can lead the model to overestimate or underestimate the prediction consistently.

A Down Hole test was conducted at the reference core Marconi, to measure P and S wave velocities. The procedure involves lowering a geophone to a specified depth in the borehole and

clamping it to the casing. An energy source is placed at the surface and struck vertically or horizontally onto a steel plate to transmit P or S waves. Travel time from source initiation to reception at the geophone is recorded, and interval velocity is determined by comparing successive readings at specified depth intervals. The travel times of P and S waves are found by identifying their first arrivals on the seismic trace through manual or automatic picking. These travel times and known source-receiver distances are used to calculate seismic wave velocities for each depth measurement.

The resonance column test was performed on two undisturbed soil samples from core Marconi for the soil dynamic characterization. The Resonant Column Test is a laboratory method for determining soil's shear elastic modulus and damping properties. A cylindrical soil sample is confined between two ends, with the bottom end being fixed. The top of the sample is free and excites by torsional or longitudinal vibration. The vibration is applied using an electromagnetic drive system with variable frequency. The test starts by vibrating the cylindrical soil specimen at the top end, while the sample is restrained at the bottom. Vibration frequency is gradually increased until the first-mode fundamental frequency is reached. The resonance frequency and vibration amplitude are then measured. Knowing the geometry and the end constraints of the sample, the measured resonance frequency is then used to calculate the wave propagation velocity using the wave propagation equation and the theory of elasticity. The shear modulus is then obtained directly from the derived velocity and the density of the sample.

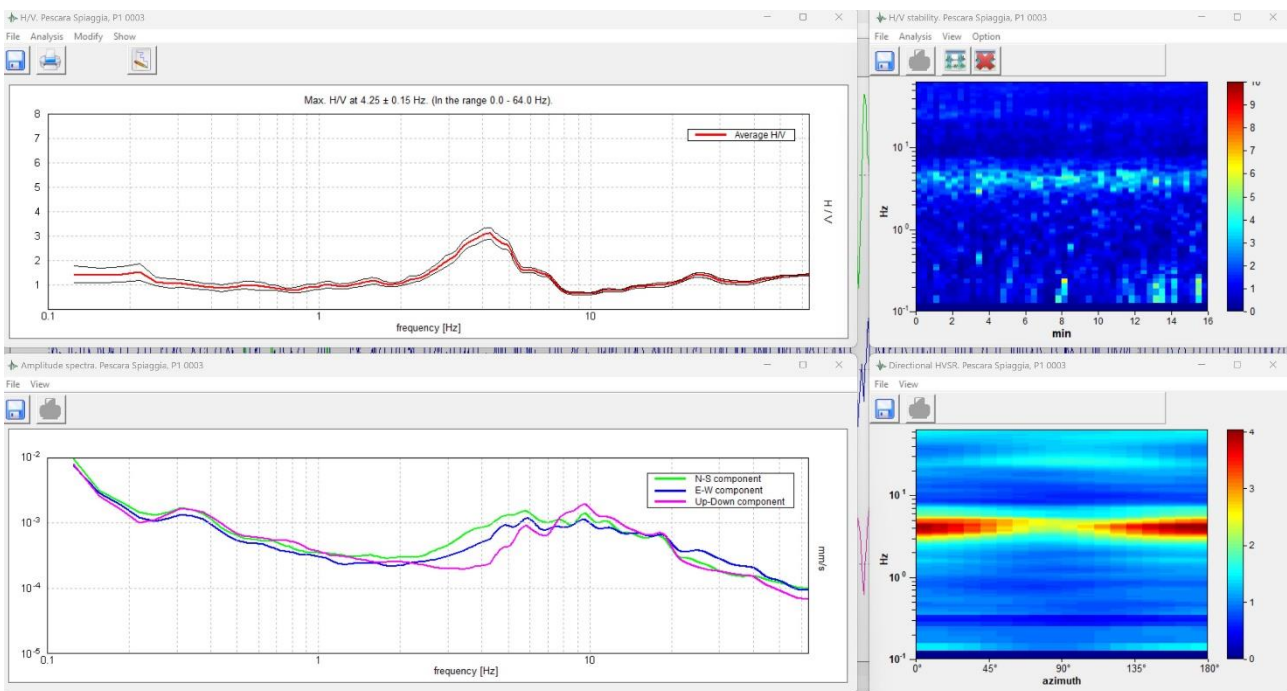


Fig. 13. Example of Grilla software interface for mHVSR analysis.

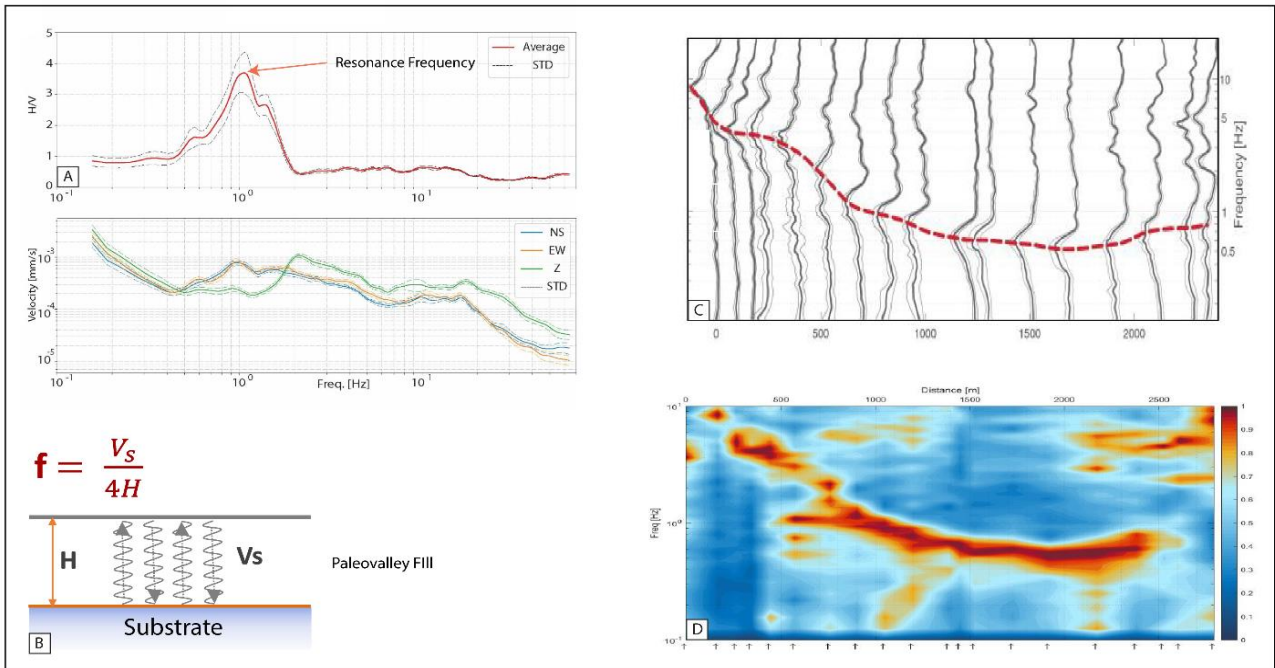


Fig. 14. (A) Example of an H/V curve with individual spectra of the motion. (B) Example of general conditions that generate stratigraphic resonance. (C) Lateral correlation of H/V curves. (D) Contour Plot of the H/V curve.

In order to conduct a seismic response analysis in the Pescara area, we integrated the reconstruction of resonance frequencies with 85 microtremor measurements. The new data were utilized to produce a resonance frequencies map, which, through a Frequency-Depth model, were subsequently transformed into a 3D geophysical model of the buried subsurface geometry of the Pescara paleovalley system. A local seismic response analysis requires accurate characterization of the velocity profile and clear identification of the main seismic layers. To this end, we directly measured the P and S wave velocities through a Down Hole test performed on the reference core Marconi.

*Down Hole Test* (Fig. 15 A) is a geotechnical method utilized to measure the properties of subsurface soil or rock layers. This test involves lowering a geophone into a borehole to record the arrival of seismic waves produced at the surface. The seismic wave velocities can be calculated by analyzing the required time for the seismic waves to travel from the surface to the geophone at varying depths. Thus, with this test, it is possible to identify the main seismic layers, especially when calibrating the geophysical results with the stratigraphy of the reference borehole.

An additional parameter to consider is the nonlinear behavior of the soil, described by the normalized shear modulus ( $G/G_0$ ) versus strain ( $\gamma$ ) and damping ratio ( $D$ ) versus ( $\gamma$ ) curves. We performed the resonant column test (Fig. 15 B) on two undisturbed samples acquired on the reference core Marconi to characterize this value. The Resonant Column Test is a laboratory test method utilized in geotechnical engineering to determine the dynamic properties of soil, e.g., the shear modulus ( $G$ ) and damping ratio ( $D$ ).

In a Resonant Column Test, a cylindrical soil sample is vertically confined and subjected to a torsional oscillation at its top, while its bottom is fixed. The oscillation induces shear waves that propagate through the soil sample. By varying the frequency of the applied torsional oscillation, a resonance frequency is found where the sample oscillates with the maximum amplitude. This resonance frequency, along with the dimensions of the sample and the applied confining pressure, is used to determine the shear modulus of the soil. Additionally, the damping ratio of the soil, which describes its energy dissipation characteristics, is determined by observing the decay of the oscillation amplitude after stopping the applied torsional load. The Resonant Column Test allows engineers and researchers to understand the dynamic behavior of soils, providing crucial data for seismic design and analysis.

The seismic response simulation was conducted on a simplified stratigraphic cross-section running through the depocenter of the paleovalley. The cross-section was reconstructed using the

3D geophysical model of the study area and subsequently refined through the geological data available in the Pescara seismic microzonation database. Based on sedimentological and stratigraphic criteria, the main seismo/stratigraphic layers were laterally correlated, reconstructing their buried geometries.

The seismic input (Fig. 16) was applied to the bedrock, and to maximize the reliability of the simulation, both synthetic input signals (Ricker Wavelet at 0.9 Hz and 3 Hz) and signals from real earthquakes were utilized.

The selection of real input signals was based on the criteria proposed by seismic disaggregation, which thus led to the use of only 'spectrum-compatible' signals in accordance with the Italian building code (Fig. 16). Seismic disaggregation is used to analyze the seismic hazard in a specific area. This process breaks down different earthquake scenarios and provides detailed insights into potential seismic events that pose a significant threat. It dissects the probabilistic seismic hazard into earthquake magnitudes, source-to-site distances, and possible faulting mechanisms, thereby revealing which scenarios are most likely to produce the most severe ground motions at the site. This technique is crucial for comprehending the potential sources and characteristics of future earthquakes that could impact a site.

In the Pescara area, the most probable seismic events are characterized by a magnitude ranging from 4.5 to 6.5 and by a distance between 0 and 30 km. The maximum predicted PGA from the Italian building code is 0.17g.

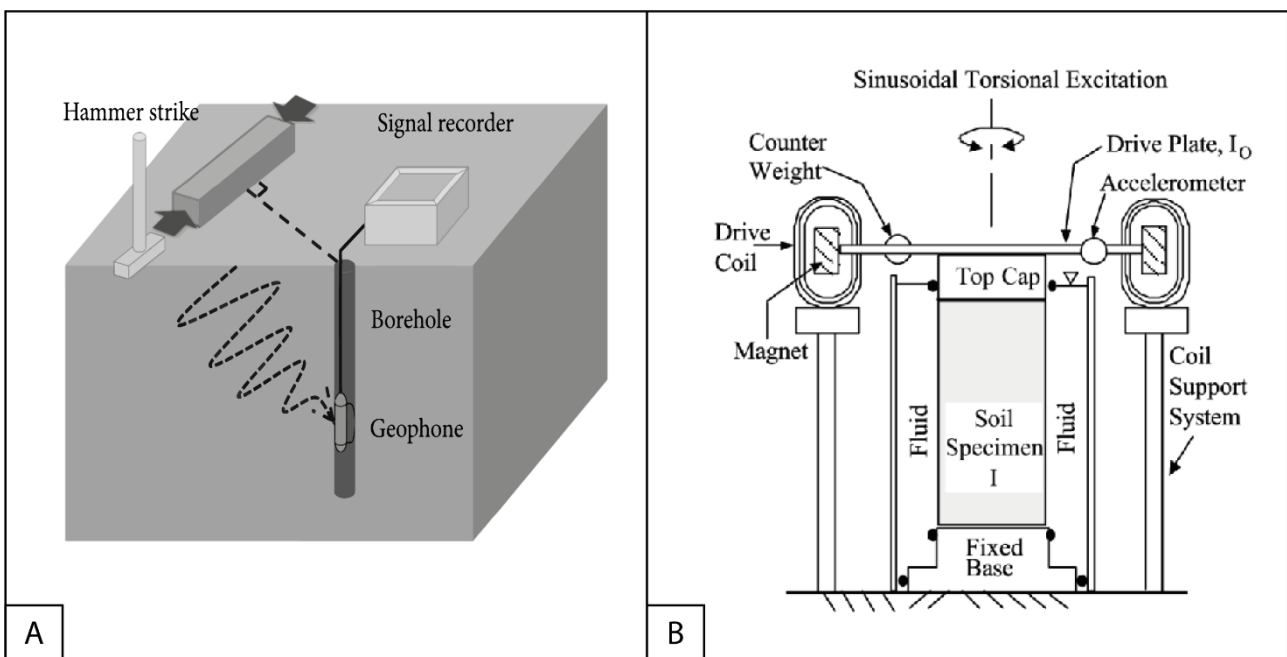


Fig. 15. Simplified diagrams of the Down Hole testing (DH) (A) and the Resonant Column apparatus (B)

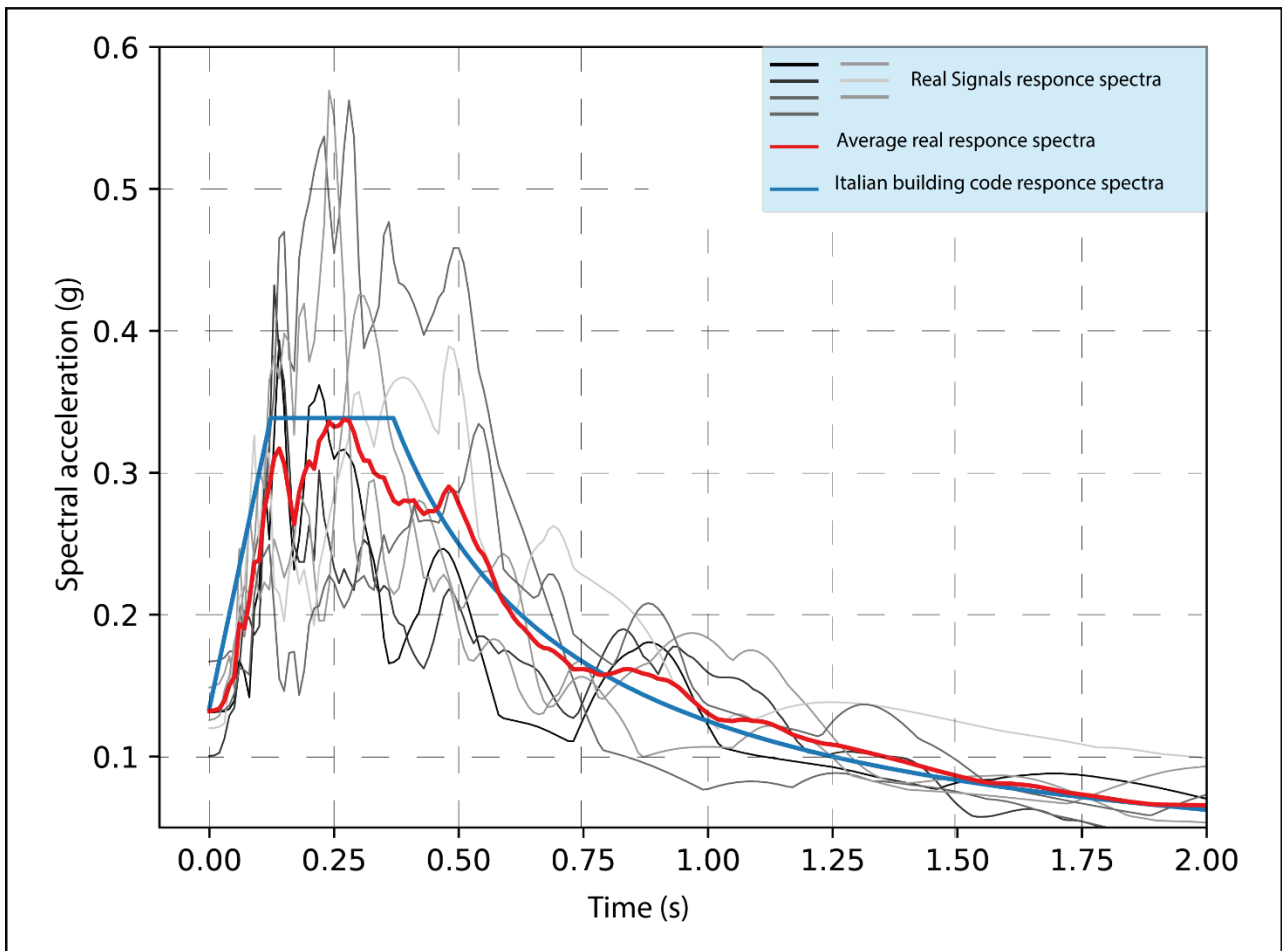


Fig. 16. Response spectra of the real signals at the bedrock used for the modeling of local seismic response. The spectra (in gray) are compared with the average response spectrum (in red) and the spectrum proposed by the Italian Building Code (in blue).

To perform facies analysis on sedimentary cores, we built an automatic method to perform semantic segmentation of sediment cores' digital images directly acquired in the field.

The dataset used in this study includes 82 digital images from 31 selected Holocene sedimentary cores in Italy acquired in the Po Plain and the Adriatic coastal plains of Marche, Abruzzo, and Apulia. Different devices, including compact cameras and smartphones, were used to take digital images in the field. The images had various resolutions, ranging from 1369×803 to 4605×2717 pixels, which were later resized to a homogeneous resolution of 3074 x 1538 pixels.

Using high-resolution stratigraphic reconstructions as a framework, we manually classified sediment cores into seven classes to produce ground truth segmentation masks for every image. The classes include six target classes corresponding to observed Holocene sedimentary facies and a seventh background class. The seven classes are as follows: Well-drained floodplain deposits (WDF), Poorly-drained floodplain deposits (PDF), Swamp deposits (Sw), Peat layers (PL), Prodelta deposits (P), Fluvial sand (FS), and Background (corresponding to the grey box containing the sediment core). The dataset was then divided into three, non-overlapping portions; 63 digital images were used for training, 9 for validations, and 10 for testing, corresponding to 76.83%, 10.97%, and 12.20% of the total, respectively. The data were stratified, so that each class was equally represented in every subset.

The image segmentation model used a U-Net (Ronneber et al., 2015) with an EfficientNetB3 backbone (Tan and Le, 2020) and pre-trained weights from ImageNet (Russakovsky et al., 2015). We used a network with relatively few parameters to prevent overfitting due to limited training samples. Additionally, a lightweight model can enable real-time predictions without powerful hardware requirements.

A U-Net (Fig. 15) is a convolutional neural network architecture designed for image segmentation tasks. Image segmentation involves classifying each digital image pixel, where each pixel corresponds to a specific object or class within the image. U-Nets are particularly useful for tasks requiring precise delineation of structures.

The U-Net architecture resembles the letter "U," with an encoder path on one side and a decoder path on the other. The encoder captures the context and extracts features from the input image, gradually reducing its spatial dimensions. The decoder then generates a segmented output with the same dimensions as the input image.

The encoder consists of multiple convolutional layers, often organized in a way that progressively reduces the spatial dimensions while increasing the number of features. This is usually done through convolutional layers, max-pooling layers, and activation functions like ReLU. The encoder's purpose is to learn hierarchical features from the input image. At the bottom of the "U," there is a point where the spatial dimensions are the smallest. This is often referred to as the "bridge" or "bottleneck" and contains the most abstract representations of the input image.

The decoder path starts from the bottleneck and aims to reconstruct the segmented output. It involves upsampling operations to gradually increase the spatial dimensions while decreasing the number of feature channels.

The critical innovation of U-Net is the incorporation of skip connections. These connections skip over layers in the encoder path and directly connect with corresponding layers in the decoder path. Skip connections help preserve spatial information lost during downsampling and aid the decoder in refining the segmentation map. When a skip connection is formed, the feature maps from the encoder are concatenated with those from the decoder. This helps the network learn to combine low-level and high-level features effectively, leading to accurate and detailed segmentations.

The final layer of the decoder typically consists of a 1x1 convolutional layer followed by an activation function. This layer generates the final segmentation map with pixel-wise class probabilities. The specific activation function depends on whether the task is binary (each pixel belongs to one of two classes) or multi-class (each pixel belongs to one of multiple classes).

Data augmentation (random rotation, brightness, and contrast transformations) was used to improve the model generalization capabilities. The categorical cross-entropy loss function was used for training.

We used the trained model to predict image patches in both the validation and test sets. Then, we computed the mean Intersection over Union (IoU), F1 score, balanced accuracy, and confusion matrix to evaluate prediction performance (Goutte and Gaussier, 2005; Hay, 1988).

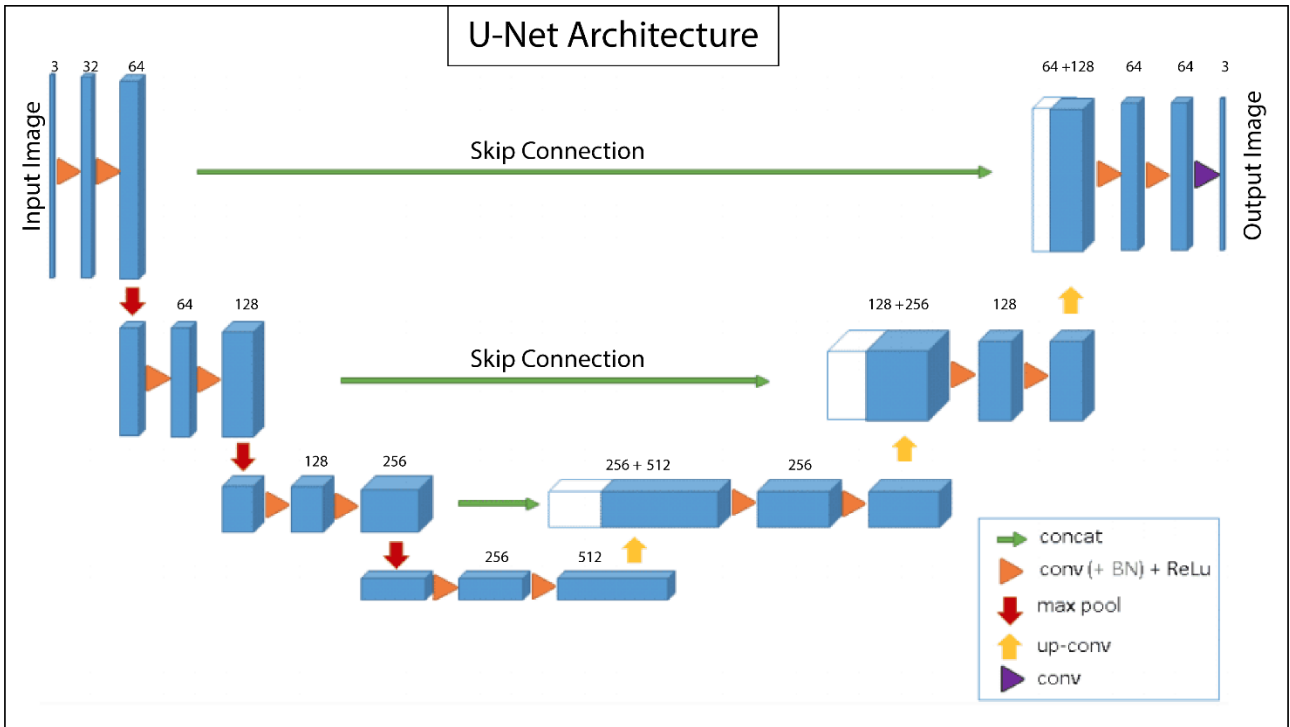


Figure 17. Simplified structure of the U-net convolutional neural network for semantic segmentation.

## 4. Late Quaternary sedimentary record of estuarine incised-valley filling and interfluvial flooding: the Manfredonia paleovalley system (southern Italy)

Alessandro Amorosi<sup>a</sup>, Luigi Bruno<sup>b</sup>, Massimo Caldara<sup>c</sup>, Bruno Campo<sup>a</sup>, Simone Cau<sup>a</sup>, Vincenzo De Santis<sup>c</sup>, Andrea Di Martino<sup>a</sup>, Wan Hong<sup>d</sup>, Giorgio Lucci<sup>a</sup>, Claudio Pellegrini<sup>e</sup>, Veronica Rossi<sup>a</sup>, Irene Sammartino<sup>e</sup> and Stefano Claudio Vaiani<sup>a</sup>

<sup>a</sup> Department of Biological, Geological and Environmental Sciences (BiGeA), University of Bologna. Piazza di Porta San Donato 1, 40126 Bologna, Italy, \*corresponding author, [alessandro.amorosi@unibo.it](mailto:alessandro.amorosi@unibo.it)

<sup>b</sup> Department of Chemical and Geological Sciences, University of Modena and Reggio Emilia, Via Campi 103, 41125 Modena, Italy

<sup>c</sup> Department of Earth and Geoenvironmental Sciences, University of Bari "Aldo Moro", Via Orabona 4, 70125 Bari, Italy

<sup>d</sup> KIGAM Korea Institute of Geoscience and Mineral Resources, 92 Gwahangro, Yuseong-gu, Daejeon Metropolitan City, Korea

<sup>e</sup> National Research Council (CNR), Institute of Marine Science (ISMAR), Via Gobetti 101, 40129 Italy

## Abstract

Multiple paleovalley systems of late Quaternary age have been widely explored in previous research from the Gulf of Manfredonia on the basis of seismic data, but only limited information is available on their proximal (onshore) segments. Through an integration of sedimentary, paleoecological (mollusks, benthic foraminifers, ostracods), and geochemical analyses from three 30-50 m-long onshore cores and a sequence-stratigraphic framework chronologically constrained by 25 radiocarbon data, we document the stratigraphic architecture of three contiguous paleovalley systems (Candelaro, Cervaro and Carapelle rivers) and their sedimentary response to Late Pleistocene valley excavation, Holocene filling and basinwide interfluvial flooding. Above a prominent sequence boundary formed during the Late Pleistocene relative sea-level fall, fluvial-channel gravels and sands (lowstand systems tract) are overlain by a deepening-upward, valley-fill succession of inner-estuarine (freshwater) to outer-estuarine (brackish) muds (lower transgressive systems tract – TST). The individual valley fills are overlain by laterally extensive bay deposits (upper TST) and by a progradational succession of prodelta/delta front and offshore/shoreface deposits that reflect normal regression under highstand conditions (HST). The transition from fluvial to inner-estuary (fluvial-dominated) and outer-estuary (wave-influenced) deposits records the progressive shift in sediment provenance from Southern Apennine source rocks to a mixed composition that reflects increasing alongshore sediment contribution from northern sources via the SE-directed Western Adriatic Current. The stratigraphic surface that demarcates the transition from estuarine to bay depositional systems (lower/upper TST boundary) represents the physical prolongation of interfluvial terrace surfaces, as valley margins were flooded during the Early Holocene transgression. This surface, typically recognizable on seismic profiles at the boundary between low-amplitude and overlying high-amplitude reflectors, has no obvious lithologic signature in core. However, it can be readily identified on the basis of paleoecologic features (sharp increase in species diversity and in the proportion of marine taxa) that reveal the abrupt transition from laterally confined to unconfined settings.

## Keywords

Sequence stratigraphy; Source-to-sink; Incised valley; Mollusk, Meiofauna; Geochemistry; Apulia; Adriatic Sea

## 4.1 Introduction

Incised valleys (Van Wagoner et al., 1990) or paleovalley systems (Blum and Törnqvist, 2000) are important features in the stratigraphic record: they represent fluvially-eroded, elongate topographic lows that are typically larger than single channel forms (Zaitlin et al., 1994; Boyd et al., 2006; Gibling et al., 2011). Beneath low-gradient Holocene coastal plains, paleovalleys typically display significant relief, with truncation of older strata and juxtaposition of fluvial/estuarine facies onto marine deposits (Van Wagoner et al., 1990; Blum et al., 2013).

Paleovalley systems develop during phases of base-level lowering, and their fill is associated with relative sea-level rise (Posamentier and Vail, 1988; Posamentier et al., 1988; Wright and Marriott, 1993). Examples from Quaternary across-shelf paleovalleys (Thomas and Anderson, 1994; Abdullah et al., 2004) have documented that the post-MIS 5e glacial-interglacial cycle, spanning approximately the last 125 kyr, includes multiple periods of incision punctuated by episodes of lateral migration, valley widening, and channel-belt deposition during relative sea-level fall, resulting in the formation of compound incised valleys (Blum and Törnqvist, 2000; Rittenour et al., 2005; Busschers et al., 2007; Labaune et al., 2010; Blum et al., 2013; Peeters et al., 2015; Mattheus et al., 2020).

Criteria for identifying paleovalley fills in the geological record have commonly been derived from coastal areas, where high-magnitude glacio-eustatic fluctuations generate predictable systems tracts (Boyd et al., 2006; Gibling et al., 2011). Paleovalleys buried at shallow depths beneath modern coastal plains are inferred to have formed during the most recent relative sea-level fall, at the MIS 3-2 transition (Blum and Price, 1998; Dabrio et al., 2000; Li et al., 2000; Autin and Aslan, 2001; Anderson et al., 2004; Busschers et al., 2007; Kasse et al., 2010; Amorosi et al., 2013; Fan et al., 2019). For such coastal-plain paleovalleys, the rate and magnitude of relative sea-level change is the primary control on stratigraphic organization (Wang et al., 2020) and paleovalley fills typically include estuarine successions formed during shoreline transgression (Dalrymple et al., 1994; Zaitlin et al., 1994; Boyd et al., 2006; Dalrymple, 2006; Blum et al., 2013).

Few paleovalley systems have been reported from offshore locations along the southern Adriatic coast of Italy. A deeply incised valley (the “Manfredonia incised valley” – MIV in Fig. 1) was first documented from the Gulf of Manfredonia, south of the Gargano Promontory, on the basis of seismic profiles interpretation (Maselli and Trincardi, 2013; Maselli et al., 2014). Three distinct paleovalley systems, deeply incised (40 m) in the substrate, were then identified off Apulia in a more southern position, about 80 km from the shelf edge (De Santis and Caldara, 2016; De Santis et al.,

2020a, b). While Quaternary incised valleys have been abundantly investigated along the Apulian shelf, little work has addressed the geometry and facies architecture of the onshore segments of the valleys (Amorosi et al., 2016).

This study relies on the integrated sedimentological, paleontological (mollusk, benthic foraminifer and ostracod) and geochemical analysis of a 50 m-long core (MAN) that was recovered in onshore position in May 2021, in front of the Manfredonia incised valley (Fig. 1). It is also based on insights from cores ZS1 and ZS2 recovered 15 km south of Core MAN, and from a 17 km-long transect with detailed geochronology of 25 radiocarbon ages (Fig. 1). For a preliminary description of core ZS2, the reader is referred to De Santis et al. (2020a).

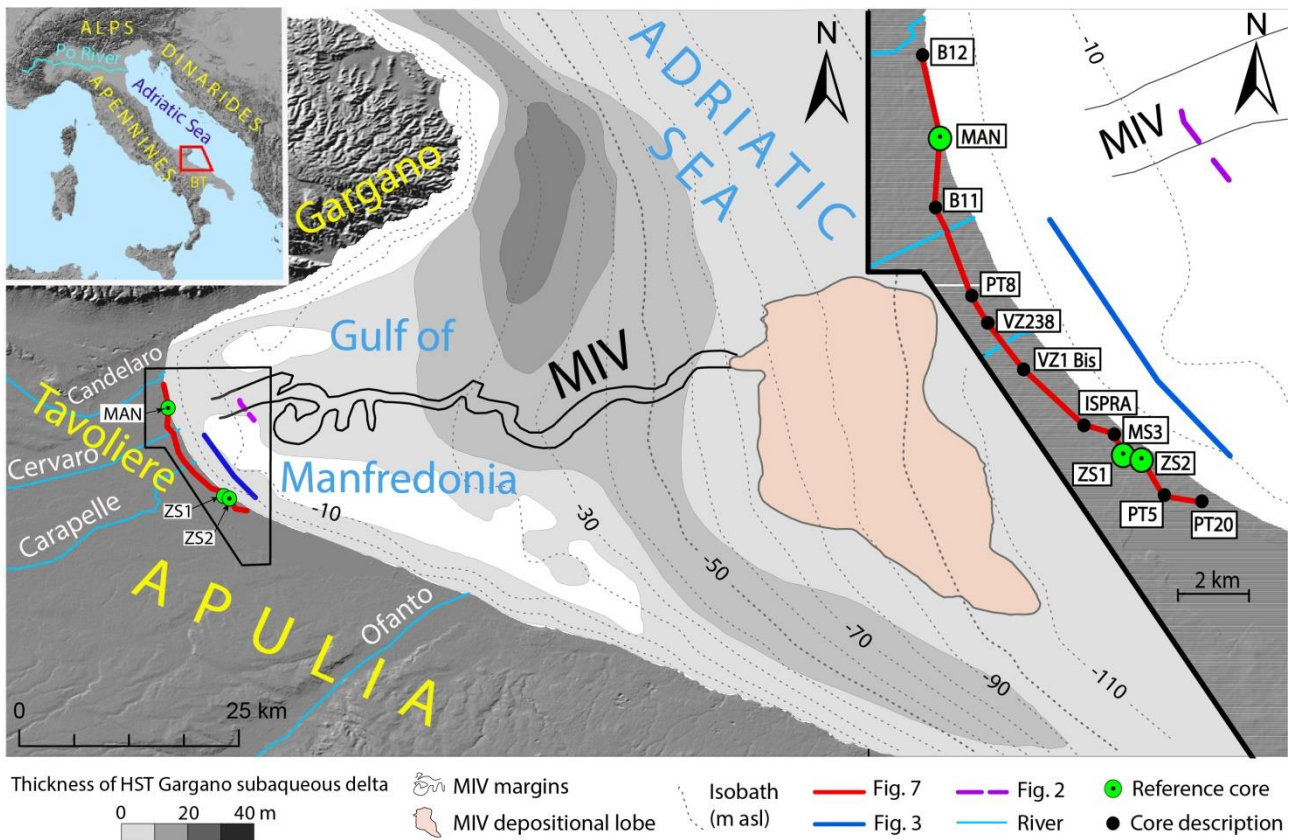


Fig. 1. Simplified bathymetric map of the Gulf of Manfredonia, with location of reference cores MAN, ZS1 and ZS2, offshore seismic profiles (Figs. 2 and 3) and the onshore stratigraphic panel (Fig. 7). The Manfredonia paleovalley (MIV), the contour of present-day bathymetry (after Maselli et al., 2014), and the Gargano subaqueous delta of Cattaneo et al. (2003) are also shown. BT: Bradanic trough.

## 4.2 Geological setting

The Tavoliere plain, in Apulia, is the second largest alluvial plain in Italy and represents the onshore prolongation of the Manfredonia Gulf (Fig. 1). It is drained by three short rivers, from north to south: Candelaro (70 km), Cervaro (30 km), and Carapelle (85 km). The longer Ofanto River (165 km) also flows into the southern part of the Manfredonia Gulf (Fig. 1). The Tavoliere plain belongs to the Bradanic Trough domain, which formed in the Early Pliocene, between the Southern Apennine chain and the Apulian–Dinaric foreland (Malinverno and Ryan, 1986; Royden et al., 1987; Patacca and Scandone, 1989, 2001; Doglioni, 1991). A generalised regional uplift took place in the area from the Middle Pleistocene (Ricchetti et al., 1992; Doglioni et al., 1994, 1996), as testified by a well exposed series of uplifted terrace deposits cropping out extensively along the Tavoliere (De Santis et al., 2010; 2013; 2014) and in other parts of Apulia (De Santis et al., 2020c).

Glacio-eustatic fluctuations superposed on this ongoing phase of regional uplift punctuated the overall regressive trend. As a consequence, terrace deposits of the Apulian Tavoliere record a complex pattern of alternating Pleistocene marine and continental deposits (Caldara and Pennetta, 1991; 1993; Boenzi et al., 1991; Apulian Tavoliere Supersynthem of Ciaranfi et al., 2011).

Apulian river catchments around the Gulf of Manfredonia comprise sedimentary rocks exposed in the Gargano Promontory and in the Southern Apennines. Mesozoic carbonates of the Apulia platform crop out in the Gargano massif, whereas silty clay hemipelagic deposits are the dominant lithology of the Bradanic Trough, which was supplied mostly from the southern Apennines (Ricchetti et al., 1992).

The Gulf of Manfredonia has a microtidal regime and a very gently sloping sea bottom toward the east. Distinct cross-shelf paleovalley systems related to the Last Glacial Maximum (LGM) have been described in detail from this region (Fig. 1). The Manfredonia incised valley, fed by Candelaro River, was described first by Maselli and Trincardi (2013), who identified a sinuous valley elongated for more than 60 km in W-E direction, from the inner to the outer shelf, with its prolongation into a depositional lobe, at 80-100 m depth (Fig. 1). Based on seismic surveys with sub-bottom profiler, the same valley was intercepted at relatively proximal locations by De Santis and Caldara (2016 - Fig. 2). More recently, two adjacent incised-valley systems, one linked to the Cervaro River, and the other one generated by incision of the Carapelle River (Fig. 1), have been illustrated by De Santis et al. (2020b).

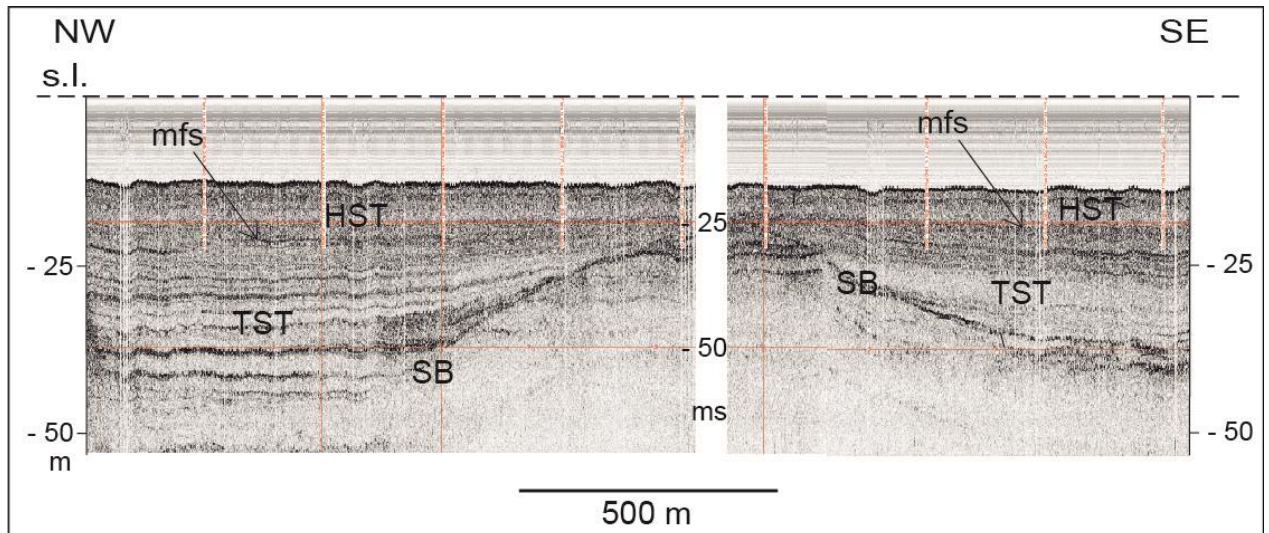


Figure 2

*Fig. 2. Seismic profile showing the Manfredonia paleovalley (left) and the adjacent Cervaro River paleovalley (right), both cut into the Quaternary substrate, and their sequence-stratigraphic interpretation (SB: sequence boundary, TST: transgressive systems tract, HST: highstand systems tract, mfs: maximum flooding surface). Slightly modified from De Santis and Caldara (2016). For section trace, see Fig 1.*

A regionally extensive stratigraphic surface represents the lowstand surface of subaerial exposure formed during the LGM (Maselli and Trincardi, 2013; Maselli et al., 2014). This surface separates a poorly reflective unit, of pre-LGM age, from overlying, reflective units of latest Pleistocene to Holocene age that represent the lowstand/transgressive systems tracts and exhibit distinctive onlapping geometries (De Santis and Caldara, 2016 – Fig. 2).

Above a regional downlap surface that marks the maximum flooding surface, highstand deposits in the study area include progradation of the mud-prone Gargano subaqueous delta (Cattaneo et al., 2003; Pellegrini et al., 2015), which represents the southernmost portion of the Western Adriatic mud wedge (Fig. 1).

## 4.3 Methods

This study is based primarily on the sedimentological analysis of undisturbed core material from three reference cores (Fig. 1): core MAN (41°32'55.528"N, 15°53'53.417"E), core ZS1 (41°27'22.008"N, 15°57'15.233"E), and core ZS2 (41°27'16.869"N, 15°57'35.449"E). For the stratigraphic analysis of the study succession, we also used archived borehole descriptions and data from earlier work (De Santis and Caldara, 2016; De Santis et al., 2020a, b). Reference cores were investigated through combined sedimentologic and paleontologic investigations. Sedimentary facies analysis of the study cores was carried out through description of lithology, grain size, primary sedimentary structures, lamination styles, accessory components and resistance to penetration measured through a pocket penetrometer. Mollusks, benthic foraminifers and ostracods were analyzed to detect changes in depth, salinity, degree of confinement, type of substrate, oxygen and food availability (Scarponi and Kowalewski, 2004; Rossi and Vaiani, 2008; Amorosi et al., 2014; Scarponi et al., 2014; Wittmer et al. 2014; Mazzini et al., 2017; 2022). Comparison with spatial distribution patterns of the modern meiofauna and mollusks allowed a robust environmental interpretation of fossil assemblages (Scarponi et al., 2022).

Core samples for macrobenthic analysis, ~250 cm<sup>3</sup> each, were collected at ~1 m intervals. Samples were dried (24 h at 40°C), soaked in 4% H<sub>2</sub>O<sub>2</sub> solution (~12 h), and wet sieved with 1 mm screen (Scarponi and Angeletti, 2008). The resulting material was qualitatively analyzed under an optical microscope to recognize environmental key taxa in each fossil assemblage. Macrobenthic remains of key taxa were counted as rare ( $n \leq 10$ ) or common ( $n > 10$  fossils) and identified, whenever possible, to species level.

A total of 136 samples, ~100 g of dry weight each, were collected for analysis of foraminiferal and ostracod assemblages (60 from core MAN; 41 from core ZS1; 35 from core ZS2). Samples treatment followed the standard method adopted in several studies from the Adriatic coastal plain (Rossi and Vaiani, 2008; Barbieri et al., 2017). Sediment samples were: (i) dried for 8 hours at 60°C, (ii) soaked in water, (iii) wet sieved through sieves of 63 µm (240 mesh), (iv) dried again for at least 8 hours and weighted, and (v) dry sieved at 125 µm. Size fractions >125 µm and 63-125 µm were analyzed separately.

Species identification was based upon: (i) original descriptions (Supplementary Table 1 – Ellis and Messina, 1940, 1952), (ii) reference papers that were also used for paleoenvironmental interpretations (Athersuch et al., 1989; Cimerman and Langer, 1991; Henderson 1990; Jorissen,

1988; Mazzini et al., 2022; Milker and Schmiedl, 2012; Sgarrella and Moncharmont Zei, 1993), and (iii) additional studies (Debenay et al., 2000; De Stigter et al., 1998; Frezza and Carboni, 2009; Jorissen et al., 2018; Murray, 2006; Salel et al., 2016). For the complete taxonomic reference list, see Supplementary Table 1.

The geochemical characterization of Southern Apennines sediment sources was carried out through analysis of 11 Apulian river samples collected from Candelaro (3 samples), Cervaro (3), Carapelle (2) and Ofanto (3). Samples were retrieved from exposed bars or subaqueous channel beds, and all particle sizes, from coarse sand to mud, were considered. Thirty-three samples from core MAN (between 43.10 and 8.70 m depth) were also analyzed for bulk-sediment geochemistry. Samples were analyzed at Bologna University laboratories for major element oxides, the loss on ignition (LOI) and trace elements. LOI, evaluated after overnight heating at 950°C (LOI<sub>950</sub>), represents a measure of volatile substances (weight %, wt%), including pore water, inorganic carbon and organic matter. The estimated precision and accuracy for trace-element determinations was 5%, except for elements with concentrations < 10 ppm, for which the accuracy was 10%.

A total of 25 radiocarbon dates (12 from core MAN, 1 from core VZ238, 4 from core ZS1 and 8 from core ZS2), including a graded, light grey pumice layer (Mercato Pumice in De Santis et al., 2020b) were carried out mostly at KIGAM laboratories, Daejeon City, Korea (Table 1). The calibration of conventional radiocarbon ages was based on the IntCal20 dataset (Reimer et al., 2020), using OxCal 4.3. (Bronk Ramsey, 2009). Before AMS counting, organic samples (for example, wood) were pre-treated with acid–alkali–acid method in order to remove CaCO<sub>3</sub> and humic-acids contamination. Shell samples were subjected to HCl etches to eliminate secondary carbonate component. Peat samples were treated with 0.5M NaOH at 80°C for 2 hours to extract humic acid without extraction of the humin fraction. Humic acids were then collected by adding concentrated hydrochloric acid to the solution. Results are summarized in Table 1.

Table 1. List of radiocarbon dates in Figs. 4 and 7.

Lab code	Sample name and depth (m)	Material	conventional <sup>14</sup> C age (year BP)	d13C (‰)	calibrated <sup>14</sup> C age (year BP)
KGM-OCa210086	MAN 4,1	shell	786 ± 31	-4,4 ± 1,7	240 ± 160
KGM-OCa210088	MAN 9,75	shell	1264 ± 30	6,69 ± 1,45	655 ± 120
KGM-OCa210089	MAN 13,7	shell	1488 ± 32	0,78 ± 1,43	865 ± 140
KGM-OCa210090	MAN 20,27	shell	6479 ± 42	-1,64 ± 2,3	6240 ± 210
KGM-OCa210091	MAN 21,8	shell	6522 ± 42	-0,95 ± 2,63	6285 ± 210
KGM-OCa210092	MAN 23,45	shell	6708 ± 44	-0,96 ± 2,42	6485 ± 220
KGM-OCa210093	MAN 24,8	shell	6986 ± 43	-1,25 ± 1,53	6800 ± 230
KGM-OCa210094	MAN 25,8	shell	8376 ± 45	0,59 ± 1,09	8200 ± 200
KGM-OCa210096	MAN 27,83	shell	8554 ± 46	-3,79 ± 1,41	8390 ± 220
KGM-OCa210097	MAN 28,45	shell	8841 ± 47	-4,69 ± 1,26	9380 ± 140
KGM-OWd210410	MAN 30,9	wood	8722 ± 44	-31,03 ± 0,92	9690 ± 200
KGM-OWd210411	MAN 31,2	wood	8819 ± 40	-25,92 ± 1,95	9890 ± 260
KGM-OCa210076	ZS1 3,4	shell	2488 ± 33	1,24 ± 1,73	1425 ± 90
KGM-OCa210077	ZS1 19,75	shell	4633 ± 36	0,96 ± 2	4055 ± 240
KGM-OCa210078	ZS1 24,38	shell	8357 ± 45	-3,34 ± 2,22	8735 ± 210
KGM-OCa210079	ZS1 25,55	shell	8021 ± 44	-2,65 ± 1,28	8345 ± 120
D-AMS 007669	ZS2 4,8	shell	2090 ± 23	5,8 ±	1020 ± 95
KGM-OCa210080	ZS2 12,3	shell	2801 ± 34	-2,2 ± 1,24	1780 ± 220
KGM-OCa210081	ZS2 14,1	shell	2874 ± 35	0,01 ± 1,24	1870 ± 210
KGM-OCa210082	ZS2 16,3	shell	4369 ± 37	7,12 ± 2,15	3705 ± 230
KGM-OCa210083	ZS2 19,1	shell	4309 ± 37	3,32 ± 0,99	3630 ± 230
KGM-OCa210084	ZS2 27,7	shell	8398 ± 51	1,31 ± 3,15	8800 ± 210
D-AMS 007669	ZS2 28,65	wood	8401 ± 37	-14,3 ±	9160 ± 163
KGM-OSa210085	ZS2 29,95	sediment	8418 ± 39	-20,87 ± 1,69	9450 ± 100
KGM-OCa210085	VZ238 4	shell	6576 ± 43	0,83 ± 0,71	6350 ± 210

With the aim of building a model for routing of sediment across all segments of the Apulian source-to-sink system, we also reinterpreted the seismic profile by De Santis et al. (2020b), located about 2.5 km seaward of the study cores (Fig. 1), which allowed us to carry out onshore-to-offshore stratigraphic correlation.

#### 4.4 Offshore seismic stratigraphy

The stratigraphic architecture of two adjacent incised-valley systems, generated by incision of the Cervaro and Carapelle rivers, respectively, has been illustrated in detail by De Santis et al. (2020a), who identified four seismic units with clear sequence-stratigraphic significance. In this study, we expand upon previous work by differentiating two additional seismic units that characterize the post-LGM succession in the study area (Fig. 3). Seismic units 1-3 are laterally confined by the pre-LGM substrate and represent the paleovalley fill, whereas units 4-6 are laterally extensive and overlie the adjacent interfluvial. The six seismic units that form the LGM/post-LGM sedimentary succession are illustrated in stratigraphic order (Fig. 3).

#### 4.4.1 Seismic Unit 1

This unit has onlapping geometry onto the sequence bounding unconformity, though the lack of coherent reflections obscures individual onlap reflection terminations onto the erosional depression. Unit 1 is characterised by low-amplitude, spaced, sub-horizontal to slightly wavy reflections, of low lateral continuity (Fig. 3). Overall, it is characterised by chaotic fill internal reflection configuration (Fig. 3).

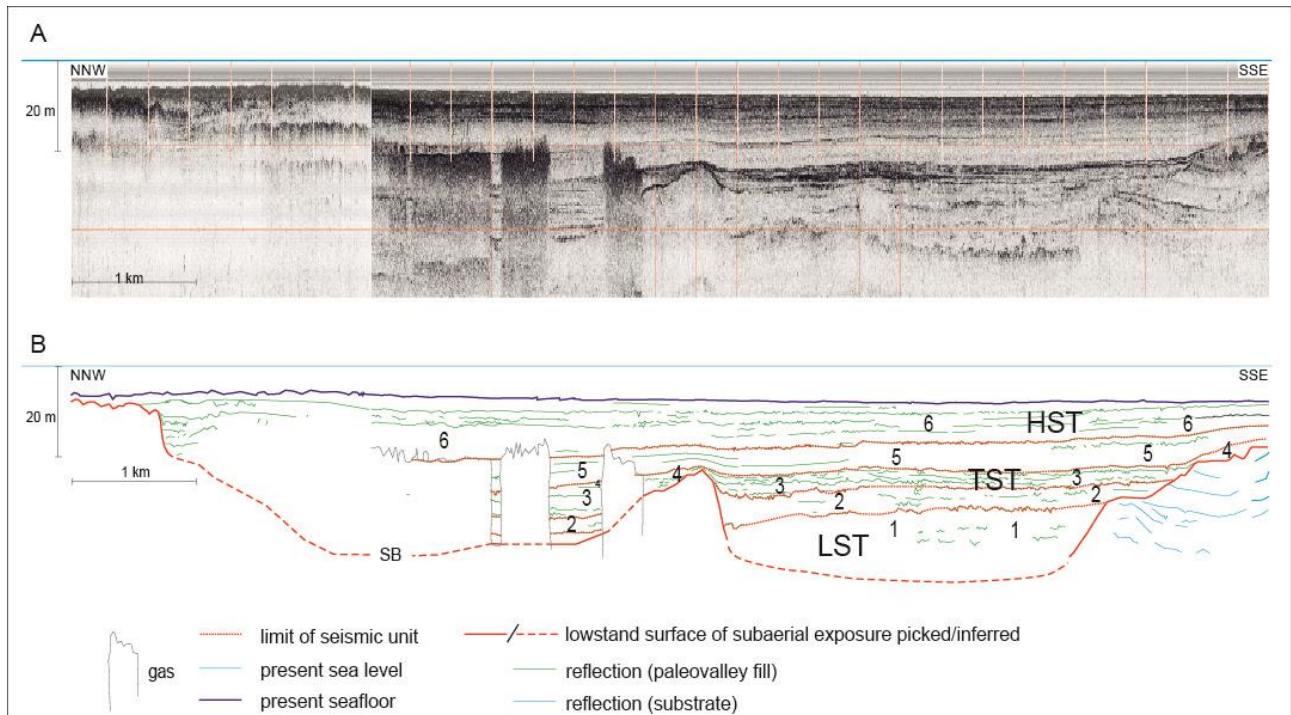


Fig. 3. Seismic profile (A) across the Cervaro (left) and Carapelle (right) paleovalleys, with subdivision of the LGM (Unit 1) and post-LGM (Units 2-6) sedimentary succession into six seismic units (B) and their sequence-stratigraphic interpretation (LST: lowstand systems tract, TST: transgressive systems tract, HST: highstand systems tract). Modified after De Santis et al. (2020a). Facies architecture is shown in Fig. 7. For section trace, see Fig. 1. SB: sequence boundary.

The chaotic fill reflection configuration of Unit 1 suggests the presence of poorly stratified sediment bodies filling the lower parts of paleovalleys, deposited in a relatively high-energy setting (Sangree and Widmier, 1977). Earlier documentations sustain interpretation of this unit as a fluvial deposit (Maselli and Trincardi, 2013).

#### 4.4.2 Seismic Unit 2

This unit is onlapping onto the sequence bounding unconformity. It consists predominantly of low-amplitude and low-continuity seismic reflections, with locally higher-amplitude reflections with sub-horizontal configuration (Fig. 3). Along the valley axis, Unit 2 shows meter-scale, channel-like incisions highlighted by high-amplitude reflections with scarce lateral continuity (Fig. 3).

Unit 2 is interpreted as a silt/mud facies affecting a broad section of the valley, which represents further valley filling in a locally high-energy depositional environment (Mitchum et al., 1977), as testified by the association with local cut-and-fill events.

#### 4.4.3 Seismic Unit 3

This unit, <5 m thick, is characterised by closely-spaced, discontinuous, parallel to sub-parallel reflections, with low- to high-amplitude. Locally, laterally continuous, very high-amplitude reflections lap onto the paleovalley flanks (Fig. 3). This unit shows internal onlap and downlap reflection terminations (Fig. 3).

Unit 3 represents the topmost part of the paleovalley fill. Its internal reflection configuration suggests multiple depositional events that resulted in compensational stacking patterns. These events led to deposition of stratified sedimentary bodies of variable grain size, as suggested by changes in seismic amplitude calibrated by sediment cores in the same area (Maselli and Trincardi, 2013).

#### 4.4.4 Seismic Unit 4

This unit consists of discontinuous, low-amplitude reflectors overlapping the interfluves and discontinuous, low- to high-amplitude reflectors above the valley fill (Fig. 3). On the paleovalley flanks, Unit 4 reaches a maximum thickness of 5 m. The topmost reflector of this unit dips toward the valley axis (Fig. 3).

The seismic reflection configuration of Unit 4 and its lateral changes in thickness and inclination suggest progradation of coarse-grained lithosomes above the southeastern paleovalley flank. The prograding sediment body suggests increasing accommodation compared to earlier phases of valley filling. In this context, the rollover point (i.e. the main breaking in slope) of the coarse-grained

lithosome approximates the coastline position and suggests a very shallow-water environment, with local (bay-head delta?) progradation (Pellegrini et al., 2020).

#### 4.4.5 Seismic Unit 5

This unit has low amplitude reflections, with only few, widely-spaced, parallel and slightly dipping high-amplitude reflections of high lateral continuity (Fig. 3). These reflections have slightly wavy geometry above the interfluves. Overall, Unit 5 shows prograding reflection patterns (Fig. 3).

The seismic pattern of Unit 5 suggests deposition of fine-grained clinoforms in a lower-energy (deeper) environment compared to underlying seismic units. Muddy clinoforms prograding from the north and along the Adriatic coast show a depocenter in the Gulf of Manfredonia and extend further south (e.g. Cattaneo et al., 2003; Pellegrini et al., 2015), being intersected along the seismic profile in Figure 3.

#### 4.4.6 Seismic Unit 6

This unit is characterised by closely-spaced, gently dipping reflections, with moderate to high amplitude and high lateral continuity. Locally, toplap and offlap terminations are present (Fig. 3). Unit 6 shows an overall prograding fill configuration (Fig. 3).

Unit 6 seismic configuration suggest the presence of stacked fine-grained prograding clinoforms with compensational stacking patterns (Mitchum et al., 1977). Similar prograding clinoforms have been documented from the central Adriatic Sea as the result of the interplay among sediment supply, accommodation, and oceanographic regime (Pellegrini et al., 2021).

## 4.5 Onshore sedimentary facies associations

Six facies associations were differentiated through the integration of sedimentological and paleoecological data from reference cores MAN, ZS1, and ZS2 (Fig. 4). These facies associations are illustrated below, in stratigraphic order. Unless specified otherwise, data refer to core MAN.

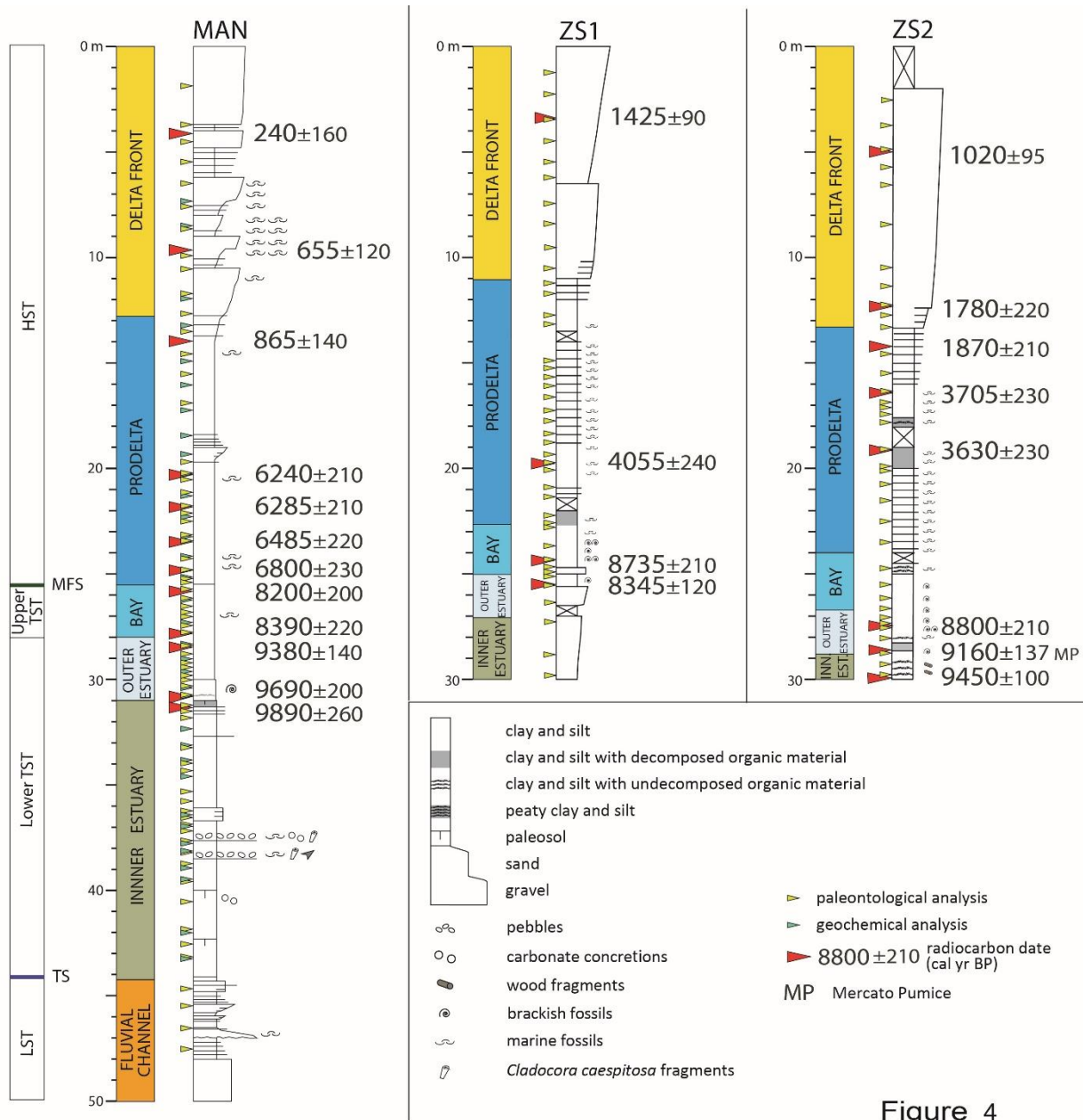


Figure 4

Fig. 4. Sedimentology and sequence-stratigraphic interpretation of reference cores MAN, ZS1, and ZS2 (see Fig. 1 for location), with stratigraphic position of samples for radiocarbon, paleontological and geochemical analyses.

#### 4.5.1. Fluvial-channel facies association

##### *Description*

This facies association, up to 10 m thick, but only partly recovered in core MAN (Fig. 4), was reconstructed using stratigraphic descriptions from adjacent continuously-cored boreholes (De Santis et al., 2010; 2013). It consists of laterally amalgamated, gravel and coarse to medium sand bodies that grade upwards into fine to silty sand and sand-silt alternations (Fig. 4). Gravel and sand bodies have concave-up, lens-shaped geometry, erosional lower boundaries and are locally separated by thin clay horizons. Gravels, of Apennine origin, are poorly sorted, with a locally abundant sandy matrix. Vegetal remains are rare, and no fossils were encountered (De Santis et al., 2013).

##### *Interpretation*

Thick packages of gravels and sands with concave-up geometry, erosional base, fining-upward trends and lack of fossils reflect a high-energy, continental depositional environment and are interpreted as fluvial-channel deposits (Miall, 1992). The high ratio of bedload versus suspended load and poor sorting suggest braided stream facies that accumulated in steep gradient environments under strong morphological confinement.

#### 4.5.2. Inner estuary

##### *Description*

This facies association, up to 13 m thick in core MAN (Fig. 4), is made up predominantly of bioturbated silt and clay. In its lower part (8 m in Fig. 4), it is varicolored, with abundant yellowish and reddish mottles due to Fe oxides (facies WdF in Fig. 5a), and locally hardened, with pocket penetration values invariably  $> 2.5 \text{ kg/cm}^2$ . Higher values, around  $4\text{-}6 \text{ kg/cm}^2$ , were observed in stiff clays with an abundance of mm- to cm-sized carbonate nodules. Upsection, this facies association exhibits a greenish grey color, root traces and occasional mottles due to Mn and Fe oxides (facies PdF in Fig. 5a). Silty sand and sand layers, generally less than 30 cm thick, are subordinate. Sharp-based sand bodies, up to 5 m thick, are locally embedded in the clay. Pocket-penetration tests record

values in the range of 1.7-2.5 kg/cm<sup>2</sup>. The uppermost part of this facies association, < 1 m thick in core MAN, consists of soft, organic-matter-rich clay, with a characteristic dark color, an abundance of plant debris, wood fragments and peat (facies Sw in Fig. 5a). Pocket penetration values in this stratigraphic interval drop to 0.4-0.9 kg/cm<sup>2</sup>.

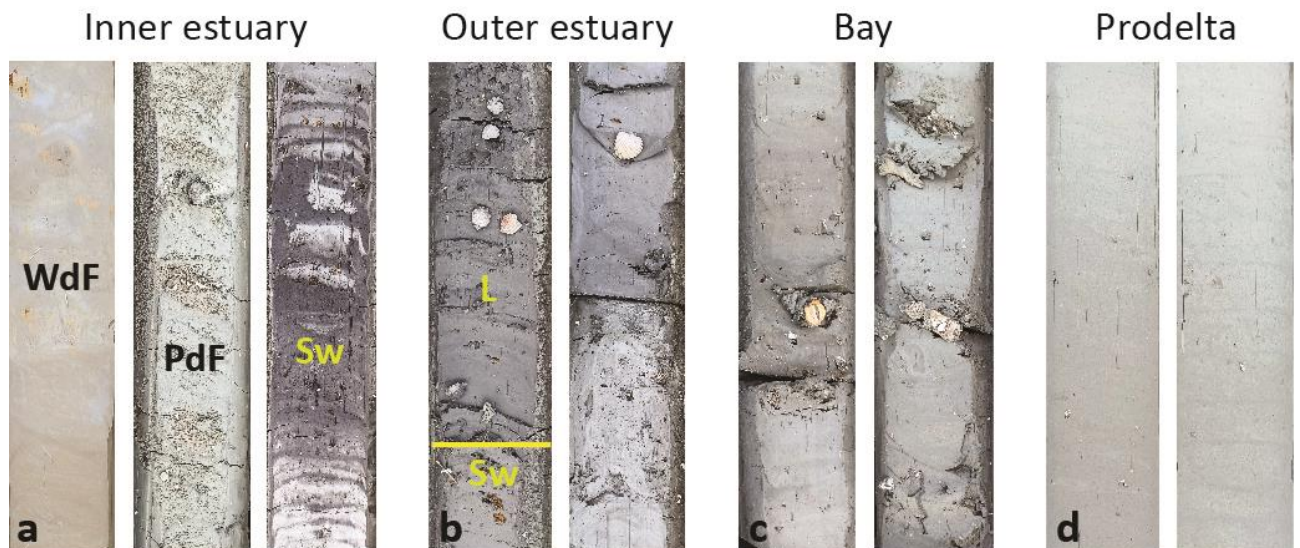


Fig. 5. Representative core photographs of the Manfredonia paleovalley fill (core bottom: lower left corner; core top: upper right corner). All photographs from core MAN (see Fig. 1 for location). a: 43-42 m core depth (WdF), 32-31 core depth (PdF and Sw); b: 31-30 m core depth; c: 28-27 m core depth; d: 18-17 m core depth. WdF: well-drained floodplain, PdF: poorly-drained floodplain, Sw: swamp, L: lagoon.

Macrofossils are rare. Coral fragments (*Cladocora caespitosa*), rare *Bittium* sp. and *Varicorbula gibba*, and rare specimens of the pulmonated gastropod *Cerastoderma glaucum* were encountered around 37-38 m core depth (Fig. 4). Only rare and poorly preserved foraminifera, such as *Ammonia*, *Bulimina*, *Globigerina*, *Globigerinoides*, and *Gyroidina* were observed within this facies association. The uppermost layers show abundant hydrobiids, thin-shelled *Cerastoderma glaucum* and rare *Abra segmentum* plus few fragments of pulmonated gastropods. Specimens of freshwater ostracods (*Pseudocandona*) were locally recognized in cores ZS1 and ZS2.

## Interpretation

The dominance of stiff, varicolored and oxidized fine-grained material grading upward to homogeneous silt and clay with lack of oxidation and generally low soil consistency suggest that deposition of this facies association took place in a fluvial-dominated, low-energy, well-drained (facies WdF) to poorly-drained (facies PdF) floodplain environment with low to high groundwater table, occasionally inundated by overflow waters. Isolated sand bodies likely reflect single-thread rivers (Potter et al., 1967; Hayes, 1975). The presence of indurated horizons and carbonate concretions is suggestive of local soil development. Based on its remarkable thickness and diagnostic fossil content (freshwater ostracods), this unit is argued to represent overbank sedimentation in a laterally confined environment, such as the inner part of an estuary, in which poorly preserved foraminifers and the rare mollusk fauna are interpreted to represent reworking of Pleistocene deposits (De Santis et al., 2010). Within facies Sw, dark gray to black colors reflect high proportion of organic matter. Abundant undecomposed vegetal remains, peat layers and very low (< 1 kg/cm<sup>2</sup>) pocket penetration values associated to common hydrobiids, rare brackish and thin-shelled bivalves reflect ephemeral bodies of stagnant waters under generally reducing conditions, such as hypohaline swamps adjacent to brackish marshes (Quarta et al., 2019).

### 4.5.3. Outer estuary facies association

This facies association, 2-3 m thick in reference cores (Fig. 4), is dominated by a homogeneous succession of soft clay and silty clay, with faint silt laminae, a few mm to cm thick. At the transition to underlying swamp clays, this unit exhibits dark grey color, plant debris and wood fragments (Fig. 5b). Upsection, the color is lighter grey. No pedogenic features were observed. Pocket penetration tests yielded values in the range of 0.7-1.0 kg/cm<sup>2</sup>.

Within facies L (Fig. 5b), samples show a very similar stock of mollusk species represented by abundant, cm-sized shells (hydrobiids, *Cerastoderma glaucum*, and *Abra segmentum*). In the uppermost part of the unit, *Bittium reticulatum*, ostreids and rissoids are also abundant.

The meiofauna assemblage is dominated by well-preserved euryaline foraminifers and ostracods, such as *Ammonia tepida*, *Haynesina germanica* and *Cyprideis torosa*, with subordinate other foraminifers commonly found in lagoon settings (*Ammonia parkinsoniana*, *Aubignyna perlucida*, *Criboelphidium gunteri*, *Elphidium fichtelianum*, *Elphidium oceanense*, *Porosonion granosum*,

*Miliolinella* spp., and *Quinqueloculina seminulum*). Poorly preserved specimens of *Adelosina* and *Triloculina* are locally present.

### *Interpretation*

This sedimentary unit is dominated by a low-diversity meiofauna able to tolerate changes in salinity and organic matter content. The macrobenthic associations recovered has been well documented in Quaternary paralic successions of Italy (e.g., Amorosi et al., 2014; Scarponi et al., 2017) and all over the Mediterranean (Pérès and Picard, 1964). As a whole, this facies association likely accumulated in a low-energy, mesohaline environment subject to short-lived salinity fluctuations, such as an outer estuary. The upward increase in mollusk taxa distributed also in shallow-marine settings (*Bittium*, ostreids, and rissoids) suggests development of less confined (more open) and higher-salinity conditions (Cau et al., 2019). Similarly, poorly preserved specimens of *Adelosina* and *Triloculina* are interpreted as transported from nearby marine environments.

#### 4.5.4. Bay facies association

This facies association, about 2.5 m thick in reference cores (Fig. 4), consists of homogeneous medium grey clays with an abundance of body fossils concentrated at discrete horizons (Fig. 5c). A condensed fossil horizon was observed at 25.7 m depth in core MAN. From a lithological perspective, this unit is hardly distinguishable from underlying outer estuarine deposits, which have similar geotechnical characteristics (pocket penetration values between 0.8 and 1.0 kg/cm<sup>2</sup>).

Within this facies association, the macrobenthic assemblage is characterized by a diversified stock of brackish species, with an upward increasing number of fully marine species, variable mollusk content and taphonomic damages. The lower part of this unit shows ecologically mixed assemblages of brackish to shallow-marine taxa (e.g., *Cerastoderma* and nuculids, respectively) with variable taphonomic damage (i.e., from pristine to highly damaged shells), mainly represented by bioerosion, chemical dissolution and encrustation. The topmost sample (at 25.7 m core depth) records an ecologically coherent stock of marine taxa represented by *Varicorbula gibba*, *Antalis* cf. *dentalis* (both common), and rare *Kurtiella bidentata*, *Sorgenfreispira brachystoma*, *Cerithidium submammilatum* and other mud-loving taxa. In core ZS2, the mollusk stock is mainly represented by

*Ostea edulis*, *Modiolus barbatus*, and *Kurtiella bidentata*. Upwards, it is enriched in several marine taxa (e.g., *K. bidentata*, *Nucula nitidosa*, *Abra nitida*, and *Antalis inaequicostatum*).

The meiofauna is dominated by benthic foraminifera, mainly *Ammonia tepida*, *Aubignyna perlucida*, *Haynesina depressula*, *Elphidium* spp., *Porosononion granosum*, *Porosononion lidoense*, *Quinqueloculina seminulum* and several *Triloculina* species (*T. affinis*, *T. inflata* and *T. trigonula*). Other Milioloidea, such as *Adelosina*, *Miliolinella* and other *Quinqueloculina* are subordinate. Low amounts of *Ammonia beccarii*, *Ammonia parkinsoniana*, *Criboelphidium* spp., and *Rosalina bradyi* are commonly observed.

### *Interpretation*

Within this stratigraphic interval, mollusk assemblages record the rapid transition from oligotypic assemblages, typical of an open lagoon setting to a more open, marine habitat, such as a relatively sheltered embayment (Maselli et al., 2014), as suggested by the more diversified marine fauna and the abundance of ostreids in the upper part of this unit. The 50 cm-thick fossil-rich interval between 27.2-26.7 m, characterized by variable taphonomic damages and variable mollusk content, is retained to represent a transgressive lag. Finally, the relatively rich mollusk association retrieved at 25.8 m records a typical assemblage characterizing the transition to shelf marine environments commonly between 20-40 m water depth in the Adriatic Sea (e.g., Kowalewski et al., 2015; Scarponi et al., 2017; Tomašových et al., 2019).

The microfossil assemblage exhibits the particular co-occurrence of species tolerant (*Ammonia tepida*, *Aubignyna perlucida*, *Quinqueloculina seminulum* and *Porosononion* spp.) or sensitive (*Adelosina* spp., *Ammonia parkinsoniana*, *Miliolinella* spp. and *Triloculina trigonula*) to organic matter enrichment (Jorissen et al., 2018). These species are considered to reflect a shallow-marine environment moderately influenced by river water. The presence of epiphytic taxa (*Triloculina trigonula* and *Rosalina bradyi*) indicates local vegetation cover at the sea bottom.

In general, the faunal assemblage displays the highest species diversity and relative abundance of open-marine species and thus reflects the deepest water depths attained during the Holocene.

#### 4.5.5. Prodelta facies association

This facies association, up to 12 m thick, is dominated by homogenous light grey clay (Fig. 5d), with common silt intercalations. Sand layers are abundant in the upper part of this unit and show a characteristic upward increase in thickness and frequency. Plant debris and other organic matter are locally observed. Pocket penetration values are very low (0.5-0.7 kg/cm<sup>2</sup>). The boundary with underlying bay deposits is transitional and has poor lithologic expression. It is, however, recognizable under visual inspection of the core by the sudden disappearance of large shells.

Within this ten-meter-thick stratigraphic interval, all samples hold an ecologically compatible set of mollusk taxa, with abundant *Turritellinella tricarinata*, nuculids, *Kurtiella bydentata* and *Antalis* sp., and rare *Abra prismatica*, *Bela brachystoma* (among others) and *Varicorbula gibba*. In core ZS2, the most common species are *Moerella distorta*, *Varicorbula gibba*, *Kurtiella bidentata*, *Pitar rudis*, *Gouldia minima*, *A. nitida*, *Lembulus pella*, *Nucula nitidosa*, and *Antalis inaequicostatum*. Many ossicles of Asteroidea and vertebrae of Ophiuroidea are present.

The benthic foraminifera assemblage includes the same species found in the underlying bay facies association, but with remarkable differences in the relative abundance of individual taxa. In particular, an overall increase in *Ammonia tepida*, *Aubignyna perlucida*, *Porosonion granosum* and *Porosonion lidoense* is paralleled by the decrease in Milioloidea and *Elphidium* species.

#### *Interpretation*

The assemblage retrieved in this facies association is well documented from Pleistocene and Holocene muddy units of the Mediterranean basin (Angeletti and Scarponi, 2008; Scarponi et al., 2014; 2017; Rossi et al., 2021). This assemblage points toward marine muddy substrates characterized by moderate to sustained sedimentation rates. The relatively high diversity and turnover of the dominant mollusk species suggest episodic sedimentation.

As a whole, the faunal stock is commonly retrieved in marine environments typified by high rates of deposition. High amounts of foraminiferal taxa tolerant to organic matter enrichment (Jorissen et al., 2018) are typical of the prodelta and reveal a progressive increase in river influence (e.g., Barbieri et al., 2017). Occasional, thin-bedded intercalations of very-fine to fine sand, with sharp

base and fining-upward trend, represent flood layers (Pellegrini et al., 2021), though the delta front (topset)–prodelta (foreset) transition is not resolved geometrically (Trincardi et al., 2020).

#### 4.5.6. Prograding delta front/beach barrier

This facies association, up to 14 m thick, displays a gradational lower boundary to the prodelta/offshore facies association. It is made up predominantly of upward-coarsening and shallowing packages of well sorted, fine to medium sand separated by finer-grained intervals, 1-3 m thick, including silt admixed with very fine sand and abundant sand intercalations. This unit has a morphological expression, cropping out in elongate beach ridges parallel to the modern shoreline. On vertical profiles, silt-interlamination frequency and thickness decrease upwards.

In the lower part of this facies association, the mollusk content is relatively well diversified: the most abundant species are *Dosinia lupinus* and *Moerella distorta*, rare *V. gibba* and *Tritia* spp., along with a long list of other shallow-marine mollusks. Upwards, samples are represented by a well-diversified stock of species, mostly (semi-)infaunal or associated to seagrass cover and living in coastal environments with muddy-sands and sands (e.g., *Acanthocardia tuberculata*, *Loripes orbiculatus*, and various nassarids, tellinids and rare donacids species), together with epiphytic taxa (e.g., *B. reticulatum*) and species of wave-protected environments (*Lucinella divaricata*). This latter is abundant in nearly all samples. *Glycymeris nummaria* and *Donax* increase upwards. The upper four meters show a relatively rich mollusk association, dominated by *Loripes orbiculatus*, *Donax semistriatus* and *D. trunculus*, along with a variety of rare epifaunal or byssally attached taxa that prefer hard or mixed substrates (e.g., *Arca noae*). The uppermost samples record rare pulmonated gastropods (*Cochlicella* spp.) or are barren, with only fragments of shallow-marine mollusks.

In the lower part of this facies association, the benthic foraminiferal assemblage includes high amounts of *Ammonia beccarii*, *A. tepida*, *Aubignyna perlucida*, *Porosonion granosum*, *P. lidoense* and Milioloidea (mainly *Adelosina* and *Triloculina*); *Rosalina bradyi* is locally common. Microfossils become progressively less abundant upwards, where *Ammonia beccarii* and Milioloidea are dominant, with common evidence of abrasion and size selection.

### *Interpretation*

The mollusk fauna of this facies association is typical of shoreface Mediterranean settings (SFBC unit in Pérès and Picard, 1964) and the general abundance of sand reflects deposition above the storm wave base. Paucity of sand in the lower part of this facies association indicates a lower-energy depositional regime.

Ecological requirements of the retrieved mollusk species point toward coarser-grained settings (transition to lower shoreface environments). The presence of species living in wave-protected environments (*L. divaricata*) and ehiphyte taxa (e.g., *B. reticulatum*), however, suggests a more heterogeneous substrate with quieter areas (see also Crippa et al., 2019).

Upwards, the increase of donacis, and especially *G. nummaria*, which can also thrive in low-salinity settings (e.g., Crnčević et al., 2013), suggests river-influenced, upper delta front settings. The paucity of fossil remains, the presence of sub-fossilized shoreface diagnostic taxa and land snails suggest a coarse-grained or mixed, upper shoreface to foreshore environments transitioning upwards to backshore deposits. Indeed, the pulmonated retrieved are present in sandy and dry habitats, like vegetated dunes (Grano and Di Giuseppe, 2021).

The foraminiferal assemblage is consistent with a coastal environment with moderate fluvial influence and with a shallowing-upward trend, as documented by the number and preservation state of specimens observed in the upper part of the unit.

## 4.6 Geochemical signature of valley-fill deposits

According to previous work from the Southern Adriatic area (Cattaneo et al., 2003; Weltje and Brommer, 2011; Goudeau et al., 2013), the Gulf of Manfredonia and the adjacent Apulian offshore receive sediment from two major sources (Fig. 1): (i) direct supply from the Southern Apennines, with Candelaro, Cervaro, Carapelle and Ofanto river catchments as major feeding sources; (ii) significant, though subordinate, mixed sediment contribution from the Po River (Fig. 1) and Central Apennine rivers, via the Western Adriatic Current.

Sediment dispersal from the Central Apennines and the Po River delta occurs preferentially through SSE-directed transport pathways. A powerful longshore drift under dominant southerly currents has been ascertained by a large number of studies in the Western Adriatic area (Cattaneo et al., 2003; Ravaioli et al., 2003; Weltje and Brommer, 2011; Goudeau et al., 2013; Spagnoli et al., 2008; 2014; 2021; Rovere et al., 2019). The Po River is the main source of trace metals into the Western Adriatic Sea and accounts for 45-50% of Cr and Ni delivered to the mud wedge along the Western Adriatic shelf (Lopes-Rocha et al., 2017).

It has been documented that chromium is a trace element able to fingerprint local source-rock composition from mafic/ultramafic successions. This key marker can carry clear provenance signals even in distal segments of the routing system (von Eynatten et al., 2003; Amorosi, 2012; Garzanti, 2016; Sarti et al., 2020). As sediment composition also reflect hydraulic sorting (Garzanti et al., 2009), normalization of geochemical data using one element as grain size proxy is necessary to compensate for mineralogical and granular variability of metal concentrations.

A characteristic element ratio that has been tested successfully as a geochemical marker of sediment provenance from the Po River catchment is Cr/V (Amorosi and Sammartino, 2007). This ratio, which proved very effective in reducing the grain size effect, exhibits distinctly higher values for sediment generated from mafic/ultramafic (ophiolite) sources, irrespective of sample lithology. In particular, prodelta deposits collected at the Po River mouth yielded a mean Cr/V value of 1.69 (Amorosi et al., 2008).

In order to capture the geochemical signature of local (ophiolite-free) source rocks versus possibly Po-derived (ophiolite-bearing) sediment contribution, we applied the Cr/V ratio to 16 inner-estuary (freshwater) and 17 outer-estuary (brackish) to marine deposits from core MAN, and matched these values against 11 samples from Apulian rivers (Candelaro, Cervaro, Carapelle and Ofanto), which we used as a Southern Apennine end-member (Fig. 6; Supplementary Table 2).

Vertical changes in trace metal contents within transgressive, valley-fill deposits are interpreted to reflect changes in the relative contribution of fluvial (ophiolite-free) versus marine (ophiolite-bearing) supply (Fig. 6): in particular, the mean Cr/V value of inner-estuarine samples (0.84) is slightly higher than the mean value of Apulian river deposits (0.82), whereas the maximum Cr/V value (0.88) is recorded up-section, within outer-estuarine to open-marine samples.

Although the prominence of the Gargano Promontory may represent an obstacle to SE-directed currents along the Western Adriatic mud belt, systematically increasing Cr/V values from hinterland (alluvial) to inner-estuarine and outer-estuarine/marine environments are interpreted to reflect mixed contribution from transversal (southern Apennines) and longitudinal (Po River+central Apennines) sediment sources, thus supporting the hypothesis of conspicuous alongshore sediment transport from the Po River to the Apulian offshore via the Western Adriatic Current.

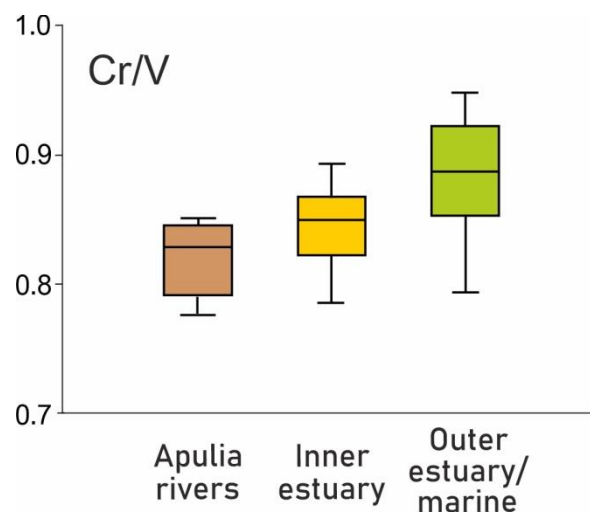


Fig. 6. Box plots of Cr/V ratios for fluvial, inner estuary, and outer estuary/marine muds from core MAN, showing increasing values with increasing marine influence. The lower boundary of each box is the 25th percentile, the upper boundary is the 75th percentile, the bold line within the box corresponds to the median, the “whiskers” define the minimum and maximum values.

## 4.7 Stratigraphic architecture of Apulian paleovalleys

The internal anatomy of three Apulian paleovalleys, linked to the Candelaro, Cervaro and Carapelle rivers, respectively, was reconstructed through a 17-km-long stratigraphic panel oriented roughly parallel to the modern shoreline and transversal to the paleovalley axes (Fig. 7). Along the transect, all paleovalley systems show prominent paleotopography (25-30 m relief), with width/thickness ratios around 150-200 (narrow sheets of Gibling, 2006). The Candelaro paleovalley represents the inland sector of the Manfredonia incised valley identified in shelf areas by Maselli and Trincardi (2013), Maselli et al. (2014) and De Santis and Caldara (2016). The Cervaro and Carapelle paleovalleys are the updip counterparts of the paleovalleys identified in offshore position by De Santis et al. (2020a, b – Fig. 3).

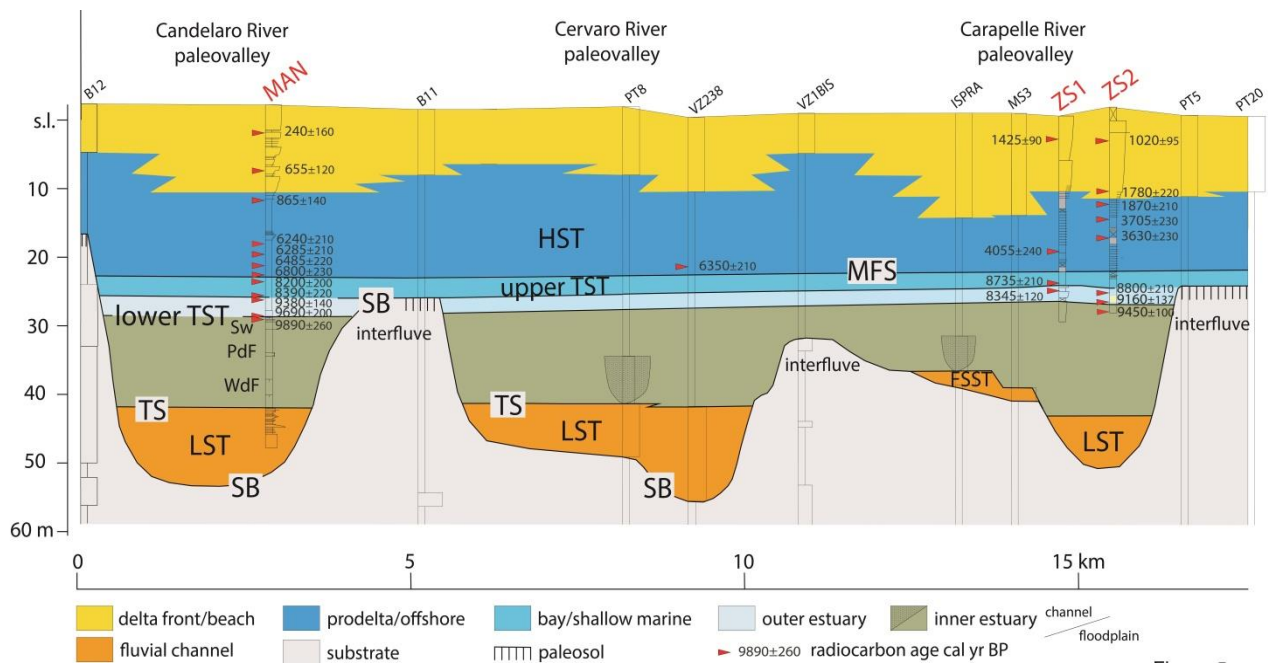


Fig. 7. Stratigraphic architecture of Candelaro, Cervaro and Carapelle paleovalleys. Compare with seismic line interpretations in Figs. 2 and 3. FSST: falling-stage systems tract, LST: lowstand systems tract, TST: transgressive systems tract, HST: highstand systems tract, SB: sequence boundary, TS: transgressive surface, MFS: maximum flooding surface. WdF: well-drained floodplain, PdF: poorly-drained floodplain, Sw: swamp.

In general, there is close correspondence between the vertical stacking of fluvial, inner-estuarine, outer-estuarine, bay, prodelta and delta front deposits reconstructed from core analysis (Fig. 7) and seismostratigraphic stacking patterns of paleovalley systems identified offshore (Fig. 3). Integrated sedimentological and paleontological analysis of sediment cores allows to define the key surfaces for sequence-stratigraphic interpretation (Zecchin et al., 2021).

The sequence boundary (SB) at the base of paleovalley systems is a prominent stratigraphic surface that is clearly recognizable from seismic profiles (Fig. 3). This erosional surface truncates much older marine strata attributable to the MIS5e coastal prism (De Santis et al., 2010; Maselli et al., 2014), indicating deep fluvial incision along major drainage axes. The basal valley-fill surface is marked (i) by the base of laterally amalgamated fluvial-channel gravel or sand bodies, up to 5 km wide, or (ii) by the sharp contrast between soft (valley-fill) deposits and stiff continental deposits into which valleys are incised (Fig. 7). Though poor quality stratigraphic descriptions provide no clear evidence of soil formation at the valley margin, we used overconsolidation as an indicator of the interfluvial sequence boundary (Amorosi et al., 2017b). Highly dissected, narrow interfluvial surfaces with thin, lenticular gravel bodies, interpreted as fluvial terraces, suggest periods of floodplain degradation that we interpreted as forced regressive deposits or Bond-scale falling-stage systems tract (Csato et al., 2014 - FSST in Fig. 7).

The complete sedimentary succession records three distinct stages in the evolution of the valley fill (Fig. 7), represented by seismic units 1-3 (Fig. 3). Sharp-based, amalgamated gravel or sand bodies in the lower parts of paleovalley fills (seismic unit 1) testify to a period of persistent channel activity likely attributable to lowstand conditions (lowstand systems tract or LST) and that may accord with a LGM attribution (Maselli and Trincardi, 2013), although these strata are not chronologically constrained by dates.

The abrupt boundary between sheet-like, amalgamated fluvial bodies and overlying lenticular bodies isolated within a mud-dominated, well-drained floodplain succession (facies WdF) marks the change from low-accommodation to relatively higher-accommodation conditions, which is traditionally interpreted as the landward expression of the initial transgressive surface (Shanley and McCabe, 1991; 1994; Labourdette and Jones, 2007; Catuneanu, 2017). Changes in the geometry of fluvial-channel bodies and their association with abundant floodplain deposits reflect development into the valley of a muddy floodplain with narrow and deep, single-thread alluvial streams (Aslan and Autin, 1999; Kasse et al., 2010; Li et al., 2010; Tanabe, 2020), which is interpreted to reflect the fluvial-estuarine transition.

The abundance of poorly-drained floodplain deposits (facies PdF) indicates that early stages of transgression in the study area were accompanied by fluvial aggradation in a strongly confined environment (Maselli and Trincardi, 2013 - seismic unit 2), landward of the transgressive estuarine-marine limit (lower transgressive systems tract or TST). Although this portion of the valley fill is not constrained chronologically, we tentatively assign this unit to the Lateglacial. The thin, dark interval rich in wood debris penetrated by the study cores atop the lower estuarine unit (facies Sw) yielded dates ranging between about 9.9 and 9.5 cal kyr B.P. (Fig. 7). This unit records transgressive inundation of a coastal setting, with rapid transition to generalized wetland sub-environments.

The vertical succession of inner estuary to outer estuary deposits observed in cores MAN, ZS1 and ZS2 is mostly associated with incised valley systems that were typically filled as sea-level rise promoted accommodation increase during transgression (Dalrymple et al., 1994; Zaitlin et al., 1994). Between about 9.5 and 9.2 cal kyr B.P., the three paleovalley fills record a deepening-upward trend that reflects transgressive influx of brackish waters. Outer-estuarine deposits are laterally confined (seismic unit 3 in Fig. 3) and there is no indication of early transgressive deposition above the valley margins, which were still undergoing degradation (and likely pedogenesis) during valley filling.

The stratigraphic surface that demarcates the estuarine-marine transition is dated to about 8.5 cal kyr B.P. and is interpreted to represent the boundary between the lower and upper TST (Figs. 4 and 7). Although this surface has poor lithologic expression, being represented by a clay-on-clay contact, the boundary between brackish (estuarine) clay and overlying bay/open marine clay has a diagnostic fossil signature, bearing invariably strong indication of increasing salinity and relative deepening. This surface can be correlated above three distinct paleovalley fills (Fig. 7) and has regional stratigraphic significance.

The development of an open-marine environment testifies to the filling of the valleys, with subsequent basinwide flooding of the interfluves. This prominent paleoenvironmental change is marked by the boundary between laterally confined estuarine deposits and poorly confined to unconfined bay deposits (Fig. 7). At the valley margins, where no lowstand or early transgressive deposition occurred, upper TST deposits directly overlie the interfluve sequence boundary (McCarthy and Plint, 1998) and SB merges with the transgressive surface. Higher up in the stratigraphic column, discrete shell layers within the bay/open-marine succession are interpreted to represent fossil lags due transgressive reworking, probably associated with renewed eustatic rise during the Early Holocene.

A surface of stratigraphic condensation is recorded atop the bay/open-marine facies association: this condensed interval, chronologically constrained between 8.0 and 7.0 cal kyr B.P. (Fig. 7), includes the maximum flooding surface (MFS). The MFS has a combined taphonomic evidence: (i) the mixing of autochthonous taxa, forming a concentration of relatively well-diversified skeletal parts, and (ii) the presence of highly damaged shells and encrusting biota (Scarponi et al., 2017). At this stratigraphic level, the mollusk content is dominated by *V. gibba*, *K. bidentata* along with scaphopods (i.e., *Antalis*). The abundance of *K. bidentata* also points out to the presence of ophiuroid-dominated communities (Ockelmann & Muss, 1978). Based on present-day environmental requirements (Oliver et al., 2016) and estimated preferential bathymetric distribution of the retrieved mollusk taxa (Wittmer et al., 2014), a depositional environment bracketed between 10 m and 30 m water depth can be hypothesized.

A normal regressive stacking pattern typifies the highstand systems tract (HST), where superposed prodelta and delta front facies associations indicate enhanced sediment flux under relatively stable sea-level conditions.

The response of transgressive units to stepped, post-LGM sea-level rise has been widely documented on Central Mediterranean shelves (Zecchin et al., 2015). In the southern Adriatic, it has been recently reconstructed offshore Apulia, within the Ofanto incised valley (Fig. 1), where short-lived progradation of coastal barrier complexes was interrupted by rapid relative sea-level rise linked to increased rate of ice melting and eustatic rise, namely meltwater pulses 1A and 1B (De Santis et al., 2020a).

In this study, through identification of two flooding surfaces, formed around 9.5 and 8.0 cal kyr B.P., respectively, and across which there is evidence of a relative increase in water depth (onset of brackish conditions and maximum marine ingressions, respectively), we reconstructed two additional phases of rapid relative sea-level rise that have clear expression on land. Coeval backstepping of estuarine environments locally associated with stratigraphic condensation has been recorded in other paleovalley systems of the Adriatic area (Amorosi et al., 2016; 2017a; Ronchi et al., 2021; Campo et al., 2022) and worldwide (Hori et al., 2004; Sloss et al., 2005; Hijma et al., 2009; Zong et al., 2009; Simms et al., 2010; Tanabe et al., 2015). Based on radiocarbon dating, the two flooding surfaces identified in the Manfredonia paleovalley system coincide with meltwater pulses 1C and 1D, at 9.5-9.0 and 8.0-7.0 cal kyr B.P., respectively (Blanchon et al., 2002; Liu et al., 2004), suggesting that abrupt deepening was driven primarily by sea level.

## 4.8 Conclusions

We reconstructed a Late Pleistocene to Holocene history of valley excavation and infill in the Southern Adriatic region through combined sedimentological, paleoecological and geochemical analysis of three sediment cores from onshore Apulia and their comparison with offshore seismic stratigraphy. Sequence stratigraphic interpretation, chronologically constrained by 25 radiocarbon dates, provides an integrated picture of multiple valley and interfluvial development in which stratigraphic architecture of paleovalley fills was largely driven by relative sea-level changes.

Above coarse-grained fluvial deposits that form the amalgamated lower paleovalley fill, the upper valley fill includes a vertical succession of mud-dominated, inner to outer estuary deposits. These, in turn, are overlain by bay/open-marine clays and by a shallowing-upward succession of prodelta and delta front facies associations. Stratigraphic discontinuities characterize the valley interfluvial, where Holocene transgressive deposits overlie indurated and pedogenized, pre-LGM deposits. Three stratigraphically significant surfaces were recognized: the sequence boundary and the transgressive surface have clear sedimentologic expression, whereas the maximum flooding surface demarcates subtle changes in paleoecological features and is marked by a condensed section.

Geochemical fingerprinting of inner-estuary deposits reveals enhanced sediment supply from Apulian river catchments in the early stages of paleovalley filling. Increasing contribution of material sourced from mafic/ultramafic rocks at the fluvial-marine transition is interpreted to reflect influence of the SE-directed (longshore) Western Adriatic current, which carries the unique (Cr-rich) compositional signature of Po River sediments.

This study shows that integrated paleoecological data, including mollusks, benthic foraminifers and ostracods are highly effective in assisting the paleoenvironmental interpretation of late Quaternary paleovalley successions. The dramatic paleoenvironmental change linked to Holocene valley filling and basinwide interfluvial flooding corresponds on seismic profiles to the obvious transition from laterally confined to unconfined settings. In the core record, though lacking a clear lithologic expression, this stratigraphic surface is readily identified by its diagnostic paleoecological signature.

## Acknowledgments

This work was supported by the Italian Ministry of University and Research under the PRIN 2017 program, project number 2017ASZAKJ “*The Po-Adriatic Source-to-Sink system (PASS): from modern sedimentary processes to millennial-scale stratigraphic architecture*”, grant to Alessandro Amorosi. The funding source had no involvement in study design; in the collection, analysis and interpretation of data; in the writing of the report; and in the decision to submit the article for publication. We thank Claudio Di Celma and an anonymous reviewer for their constructive criticism.

## 5. Late Pleistocene to Holocene glacio-eustatic history as recorded in the Pescara paleovalley system (Central Italy, Adriatic basin)

Campo B.<sup>a</sup>, Barbieri G.<sup>a</sup>, Di Martino A.<sup>a</sup>, Hong, W.<sup>b</sup>, Scarponi D.<sup>a</sup>, Vaiani S.C.<sup>a</sup>, and Amorosi A.<sup>a</sup>

<sup>a</sup> Dipartimento di Scienze Biologiche, Geologiche ed Ambientali (BiGeA), Università degli Studi di Bologna, Piazza di Porta San Donato 1, 40126, Bologna (Italy). \*Corresponding author. E-mail address: bruno.campo@unibo.it.

<sup>b</sup> KIGAM Korea Institute of Geoscience and Mineral Resources, 92 Gwahangro, Yuseong-gu, Daejeon Metropolitan City, South Korea

## Abstract

A buried paleovalley system, about 50 m deep and 2 km wide, is documented from the Pescara coastal plain. Based on stratigraphic, sedimentological, paleontological, chronological and geotechnical data, the paleovalley profile and 3D facies architecture of the paleovalley fill (PVF) were reconstructed.

The lowermost PVF is a laterally extensive fluvial gravel body, up to 13 m-thick, that represents the lowstand systems tract (LST; pre-11.3 ka cal BP). Above lowstand deposits, the transgressive systems tract (TST), 21 m-thick, shows a deepening-upward trend, from freshwater/inner-estuarine to brackish/outer-estuarine facies associations (11.3-8.0 ka cal BP). The upper part of the succession (highstand systems tract – HST) shows a shallowing-upward tendency from paludal to fluvio-deltaic deposits.

Seven millennial-scale parasequences (Ps) were identified within the Pescara Holocene (TST+HST) succession. Transgressive Ps1-3 exhibit a distinctive retrogradational stacking pattern. Highstand Ps4-7 are aggradationally-to-progradationally stacked. During the aggradational phase (P4), the estuary was gradually filled and swamp environments spread onto the valley interfluvium. Because of subsequent progradation (Ps5-7), delta plain conditions established. In the research core, TST parasequences show higher accumulation rates (up to 9.4 mm/y) than HST ones (1.3-1.8 mm/y). Thus, the study area evolved from a region of sediment storage (11.3-8.0 ka cal BP) into a sector of prevalent sediment bypass (last 8.0 ky).

Major early Holocene flooding events were possibly triggered by Melt-Water Pulses (MWP) 1B, 1C and 1D. The eustatic rise linked to MWP-1B reasonably caused the P1 flooding event (11.3 ka cal BP). Post-MWP 1C and 1D sea-level rises likely provoked the complete drowning of the paleovalley system and the subsequent maximum landward migration of the shoreline (about 8.0 ka cal BP).

This study provides new evidences, in terms of sedimentary response, of the poorly-documented MWPs 1C and 1D, and the first documentation of MWP-1B eustatic effects in an onshore sector of the Central Adriatic.

## Keywords

Paleovalley system; facies analysis; millennial-scale parasequences; glacio eustasy; melt water pulses; Adriatic basin

## 5.1 Introduction

The unquestionable importance of paleovalley systems (PVSs) is signaled by numerous studies that have documented these features in the stratigraphic record. During the last decades, the focus on PVSs was primarily due to their relevance as hydrocarbon reservoirs (Dalla et al., 1997; Dalrymple et al., 1994; Hampson et al., 1999; Harms, 1966; Jennette et al., 1991; Salem et al., 2005) and for the identification of sequence bounding unconformities (Posamentier et al., 1988; Shanley and McCabe, 1994; Van Wagoner et al., 1990, 1988). Following first sequence stratigraphic studies, several authors analyzed ancient (i.e., pre-Quaternary) paleovalley systems to refine concepts and models (Allen and Posamentier, 1993; Legarreta and Uliana, 1998; Shanley and McCabe, 1991; Shanley et al., 1993; Walker, 1995; Wright and Marriott, 1993), and reorganize them into a modern sequence-stratigraphic framework (Catuneanu, 2019, 2006; Catuneanu et al., 2009; Neal and Abreu, 2009; Neal et al., 2016). Paleovalley fills (PVFs) are stratigraphically expanded sedimentary successions that allow preservation of generally poorly-documented stratigraphic intervals (falling-stage and lowstand systems tracts - Blum et al., 1995; Blum and Aslan, 2006; Blum and Price, 1998; Payenberg et al., 2006; Rittenour et al., 2007; Thomas and Anderson, 1994) that can shed new lights on climatic variations in the past and, especially during glacial/tardiglacial periods (Busschers et al., 2007; Drago et al., 2006; Hanebuth and Stattegger, 2004; Ishiara and Sugai, 2017; Peeters et al., 2015; Simms et al., 2010). In this perspective, Late Quaternary PVSs have been considered as important geological archives and exceptional analogues for the comprehension of ancient systems (Blum and Törnqvist, 2000; Boyd et al., 1989; Kroonenberg et al., 2005; McGhee et al., 2022; Rodriguez et al., 1998; Wang et al., 2020, 2019) and environmental changes driven by allogenic/authogenic forcings (Amorosi et al., 2009; Chaumillon et al., 2010; Durand et al., 2018; Horozal et al., 2021).

More recently, PVSs have been considered as fundamental components of the source-to-sink (S2S) sediment-routing system (Blum et al., 2013). The study of Quaternary PVSs, in particular, may be useful to understand the dynamics of basin-scale sediment transportation pathways from source areas to the deep basin (Sømme et al., 2011; Sweet et al., 2020; Zhang et al., 2021) and to assess reliable sediment budget calculations (Forzoni et al., 2015; Mattheus and Rodriguez, 2014; Phillips et al., 2004). Late Quaternary PVs are also important geological objects in hydrogeological (Barnes et al., 2021; Goetz et al., 2021; Hickin and Best, 2013; Jessen et al., 2008; Seifert et al., 2008; Shaver and Pusc, 1992) and geotechnical (Bishop et al., 2010; Chua et al., 2020; ; Rossi et al., 2011; Truong

et al., 2011; Wu et al., 2015; Yanbin and Tongyu, 2016) perspectives. Finally, unconsolidated, post-LGM PVFs have great practical importance, as they can induce significant lateral variations in the effects of ground motions associated with earthquakes (Tanabe et al., 2021, 2015).

Considering the Po-Adriatic system as an ideal natural laboratory for S2S investigations (Amorosi et al., 2016a), this study aims at the identification of a PVS beneath the Pescara coastal plain (Fig. 1) as a fundamental onshore component of the complex sediment-routing system from the Apennine catchments to the Mid-Adriatic Deep (MAD) basin (Trincardi et al., 1996, 1994; Fig. 1a). In Italy, several PVSs have been documented beneath the Tyrrhenian and Ionian coastal plains (Aguzzi et al., 2007; Amorosi et al., 2013, 2012; Bellotti et al., 2004; Cilumbriello et al., 2010; Grippa et al., 2011; Milli et al., 2016, 2013; Tropeano et al., 2013). In the Adriatic basin, PVSs have been reported from offshore regions, such as the Tavoliere Plain, in Southern Italy (De Santis et al., 2020a, 2020b; De Santis and Caldara, 2016; Maselli et al., 2014; Maselli and Trincardi, 2013), and the Po Delta, in Northern Italy (Ronchi et al., 2018). On the other hand, onshore PSs have only been identified beneath the Venetian-Friulian Plain, in Northern Italy (Ronchi et al., 2021) and the Biferno coastal plain, in Southern Italy (Amorosi et al., 2016b).

Thus, a documentation gap exists for the Central Adriatic, characterized by a 50 km and 0.2° dip shelf descending directly into the small MAD basin (Maselli et al., 2011). Whereas the stratigraphic setting of this offshore basin is already well-known (Cattaneo et al., 2007; Correggiari et al., 1996; Gamberi et al., 2020; Pellegrini et al., 2021, 2018; Piva et al., 2008a, 2008b), the stratigraphy of coeval successions onshore is almost unexplored in this sector of the Central Adriatic. This work aims at filling this gap documenting the first Late Pleistocene-Holocene coastal plain paleovalley in front of the MAD, as the preliminary study for future and ongoing basin-scale S2S investigations with important implications for refining and improving hydrocarbon exploration models (Bhattacharya et al., 2016; Leithold et al., 2016; Liu et al., 2019; Zeng et al., 2019).

The occurrence of a late Quaternary PVS beneath the city of Pescara was suggested by Desiderio et al. (2007) in a preliminary hydrostratigraphic study on the basis of basic lithological descriptions. This study showed that the Plio-Pleistocene marine substrate (Fig. 1c) is unconformably overlain by Holocene alluvial deposits (up to 50 m thick), with a lower, < 10 m thick gravel body overlain by a thicker fine-grained interval with isolated sand bodies (Fig. 1c). More recently, Parlagreco et al. (2011) analyzed the uppermost 19 m of a distal sector of the Pescara coastal plain. They dated a brackish/lagoonal interval (ca. 13-9.4 m core depth) to about 7.7-6.8 ka cal BP, and uppermost coastal/continental sands to the last 4.0 ky. No other scientific studies are available from this area.

As a result, the stratigraphic architecture of the Pescara PVF and general paleoenvironmental evolution of the study during the last 30 ky are poorly known. Our investigation mostly focused on the paleovalley depocenter, south to the modern Pescara River axis (Fig. 1c, d), with the aim of exploring all stratigraphic components of the valley fill.

The main objectives of this work are: to achieve the high-resolution (millennial-scale) stratigraphic analysis of the Pescara valley fill; to reconstruct the three-dimensional (along-dip and along-shore) facies architecture; to accomplish the sequence stratigraphic interpretation of the investigated succession; to evaluate the glacio-eustatic control on facies architecture and sediment accumulation during the last 30 ky.

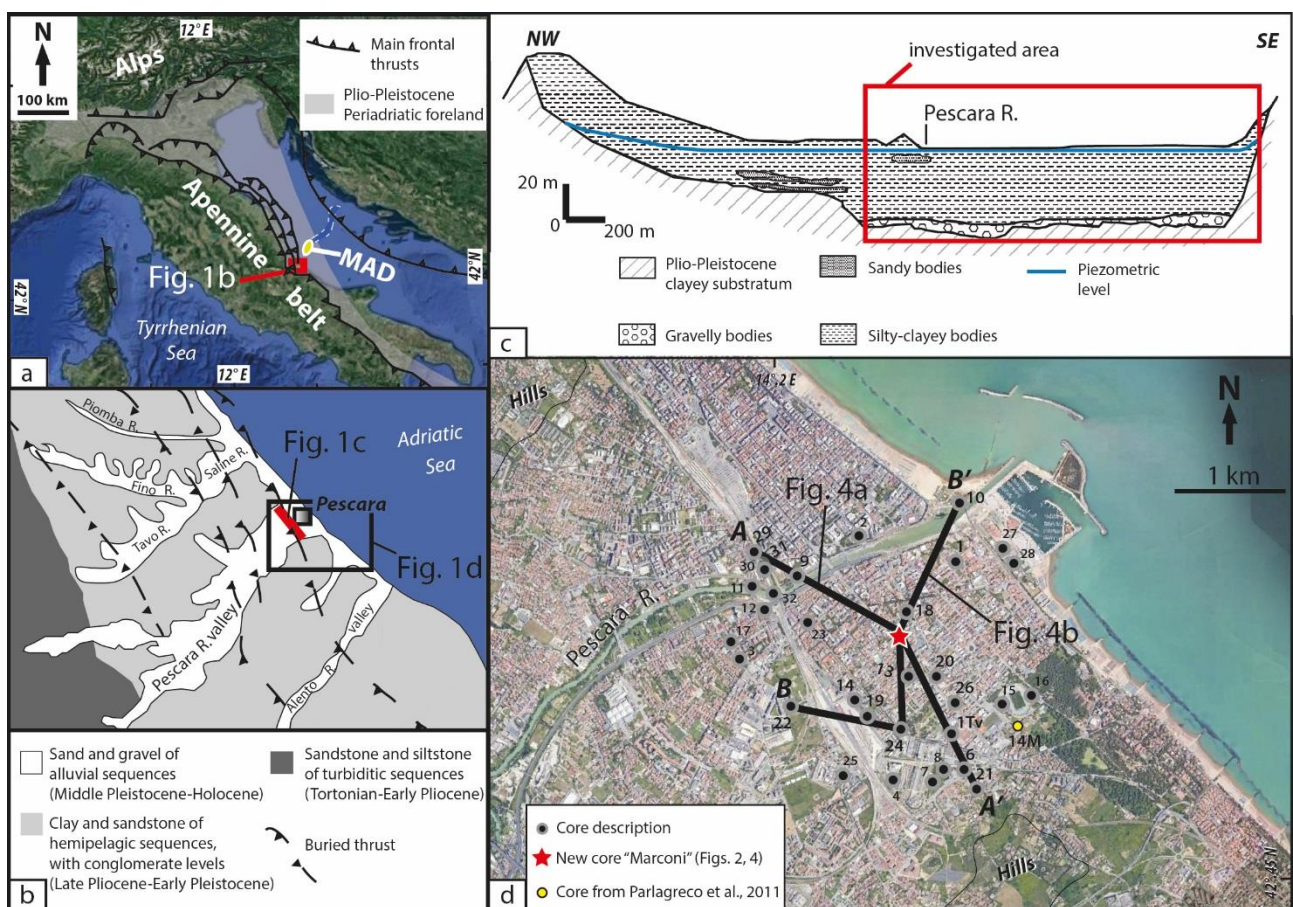


Fig. 1 – Location of the study area in the Italian peninsula (a), with indication of the main structural features of the northern and central Adriatic basin (modified from Carruba et al., 2006). The black rectangle highlights the schematic tectonic and geological map (b) of Abruzzo piedmont and coastal areas (modified from Parlagreco et al., 2011). The red line is the trace of the schematic lithological section (c) across the lower alluvial valley of the Pescara River (modified from Desiderio et al., 2007). The red rectangle represents the (d) investigated sector of the Pescara coastal plain, with indication of stratigraphic data used in this paper and stratigraphic panels of Fig. 4.

## 5.2 Geological and geomorphological setting

The Pescara coastal Plain represents the distal sector of the Pescara River valley (Fig. 1). The latter, several kilometers in width (D'Alessandro et al., 2001), is drained by the Pescara River (45 km long), which is fed by the Aterno and Sagittario tributaries. As a whole, the hydrographic basin is about 3170 km<sup>2</sup> (Urbano et al., 2017). The average sediment discharge of the Pescara River is about 1,500 kT/yr (Syvitski and Kettner, 2007).

The Pescara coastal plain is located along the Central Adriatic coast, between the Apennine thrust belt and the Periadriatic foreland (Fig. 1a). An eastward-dipping regional monocline characterizes the structural setting (Ascione et al., 2008; D'Alessandro et al., 2008). Fold and fault systems, buried underneath sedimentary strata, mainly show SW-NE direction (Fig. 1b) and alluvial valleys display similar orientation (Desiderio et al., 2007). Beneath the Pescara coastal plain, the main fault systems consist of buried thrusts (Della Seta et al., 2008).

The study area and the adjacent coastal plain experienced generalized tectonic uplift during the Middle Pleistocene (Bracone et al., 2012a), and then remained stable up to the Holocene (Antonioli et al., 2009; D'Amico et al., 2013). Based on sedimentological, paleontological and chronological data from a continuously-cored borehole retrieved in the study area (Fig. 1 for location) and the identification of five "sea-level markers", after paleo-sea level corrections and correlations with additional stratigraphic and morphotectonic data, Parlagreco et al. (2011) concluded that during the last 7,000 years, along the lower trunk of the Pescara valley, vertical tectonic displacements were negligible. Seawards, subsidence rate is about 0.3 mm/y in the Central Adriatic, the (Maselli et al., 2010).

The piedmont reliefs are characterized by the Plio-Pleistocene syn-orogenic marine succession (Ori et al., 1991; Bigi et al., 1995; D'Alessandro et al., 2003), which is made of siliciclastic clay, sands and conglomerates (Fig. 1b). These marine deposits mostly belong to the Mutignano Formation (Crescenti and D'amato, 1980). This unit crops out at the Apennine foothills between the valleys (Fig. 1b) as a wide homocline that gently dips north-east (Urbano et al., 2017), and that consists of offshore to shoreface facies associations (Ori et al., 1986; Geological Map of Italy at 1:50,000 scale, Sheet 351). The Plio-Pleistocene succession unconformably overlies the Messinian-Early Pleistocene turbidites of the Periadriatic foredeep (Della Seta et al., 2008) and typically includes the upper part of the Argille Azzurre Formation (Bracone et al., 2012b). Beneath the Pescara River, the thickness of the Plio-Pleistocene succession ranges between 2,000 m and 500 m in the main depocenters and

atop structural highs, respectively (Desiderio et al., 2007). This sequence is overlain with a Middle Pleistocene-Holocene continental succession composed of alluvial, transitional to coastal deposits (D'Alessandro et al., 2003). Four orders of alluvial terraces (Middle-Late Pleistocene), mostly made up of gravel and sand bodies, have been recognized on the W-NW flank of the Pescara valley (Parlagreco et al., 2011; Geological Map of Italy at 1:50,000 scale, Sheet 351). The origin of these terraces has been related to the interaction between Quaternary tectonics and high-frequency glacio-eustatic and climatic variations (Della Seta et al., 2008). In the proximity of the Pescara River mouth (Fig. 1b), the alluvial valley fill of Holocene age consists of a 10 m-thick gravel body capped by 50 m thick silty-clay sediments (Fig. 1c; Desiderio et al., 2007).

Offshore, the Adriatic continental shelf reaches the Mid-Adriatic Deep (MAD; Fig. 1a). While the shelf is characterized by sandy-silty depositional sequences (Ridente et al., 2008; Trincardi et al., 1994) the MAD is a small slope basin, up to 260 m deep, where fine-grained sediments accumulated almost continuously during the last 370 ky (Piva et al., 2008a, b). The MAD was progressively filled by Po River sediments during several Quaternary phases of sea-level fall and lowstand (Dalla Valle et al., 2013a, b). The stepwise sea-level lowering that followed the Last Interglacial (Marine Isotope Stage 5e or MIS 5e, ca., 130 ka cal BP) caused a marked basinward shift of the shoreline, the formation of an unconformity of regional extent, and alluvial plain sedimentation took place in the northern Adriatic shelf (Amorosi et al., 2016a). At the end of the Last Glacial Maximum (MIS 2), the MAD was partially filled with the Po River Lowstand Wedge (Pellegrini et al., 2018). This lowstand delta prograded 40 km throughout the shelf edge forming a 350 m-thick complex sedimentary body between 30-14 ka cal BP (Pellegrini et al., 2017).

## 5.3 Methods

### 5.3.1 Facies analysis

The three-dimensional stratigraphic architecture of the Pescara coastal plain succession (Late Pleistocene-Holocene) was reconstructed across two transects with NW-SE and SW-NE orientation, respectively, each about two kilometers long (Fig. 1d). Stratigraphic correlation was carried out based on geometric criteria constrained by radiocarbon ages. The dataset consists of 32 borehole descriptions (average depth ca. 45 m) available from the “Microzonazione Sismica Project” of the Pescara Municipality.

Facies interpretation was based on integrated sedimentological and paleontological (benthic foraminifer, ostracod and mollusk) analyses that were carried out on the 52 m-long reference core “Marconi” (Fig. 1d). This core was specifically acquired as part of the study from the Pescara coastal plain, about 1 km landward of the modern shoreline, at 1.35 m asl. Core Marconi was described in terms of texture, mean grain-size, color, sedimentary structures, and accessory materials, such as wood fragments, plant remains, fossil content and carbonate concretions (Fig. 2). Pocket penetration (compressive strength) values from fine-grained deposits (Fig. 2) were also considered for facies interpretation following the criteria outlined by (Amorosi et al., 2015). For stratigraphic correlation in a predominantly freshwater environment, we used the techniques adopted from recent work in the Po coastal plain. In particular, it expands the parasequence concept (Van Wagoner et al., 1990, 1988) to the paralic/estuarine realm, where paludification surfaces at the base of peats may delineate the updip (freshwater) equivalents of brackish/marine flooding surfaces more readily identified at seaward locations (Amorosi et al., 2021) due to sharp (marine to brackish) facies changes.

A total of 79 and 50 samples (Fig. 2) were collected for meiofauna (ostracods and foraminifers) and malacofauna analyses, respectively. These data allowed to retrieve palaeoenvironmental information about organic matter concentration, paleosalinity, paleobathymetry and substrate characteristics. For micropalaeontological analyses, samples (100-150 g) were treated according to standard procedures previously adopted in other works on late Quaternary successions (e.g., Barbieri et al., 2021; Rossi and Vaiani, 2008). Samples were dried at 60 °C, soaked in 10% H<sub>2</sub>O<sub>2</sub>, water-screened with a 63 µm sieve, dried again and dry-sieved at 125 µm.

Samples (400-700 g, depending on lithology) for mollusk-based inferences were collected at selected stratigraphic positions along the stratigraphic succession (Fig. 2). Based on (Azzarone et al.,

2020), samples were dried at 40°C, soaked in hydrogen peroxide solution 4% and wet sieved at 1 mm screens. The resulting material was qualitatively analyzed under an optical microscope to describe fossil assemblages. For each sample macrobenthic remains were speditively counted as rare ( $n \leq 10$ ) or common ( $n > 10$  fossils, respectively) and identified, whenever possible, to species level.

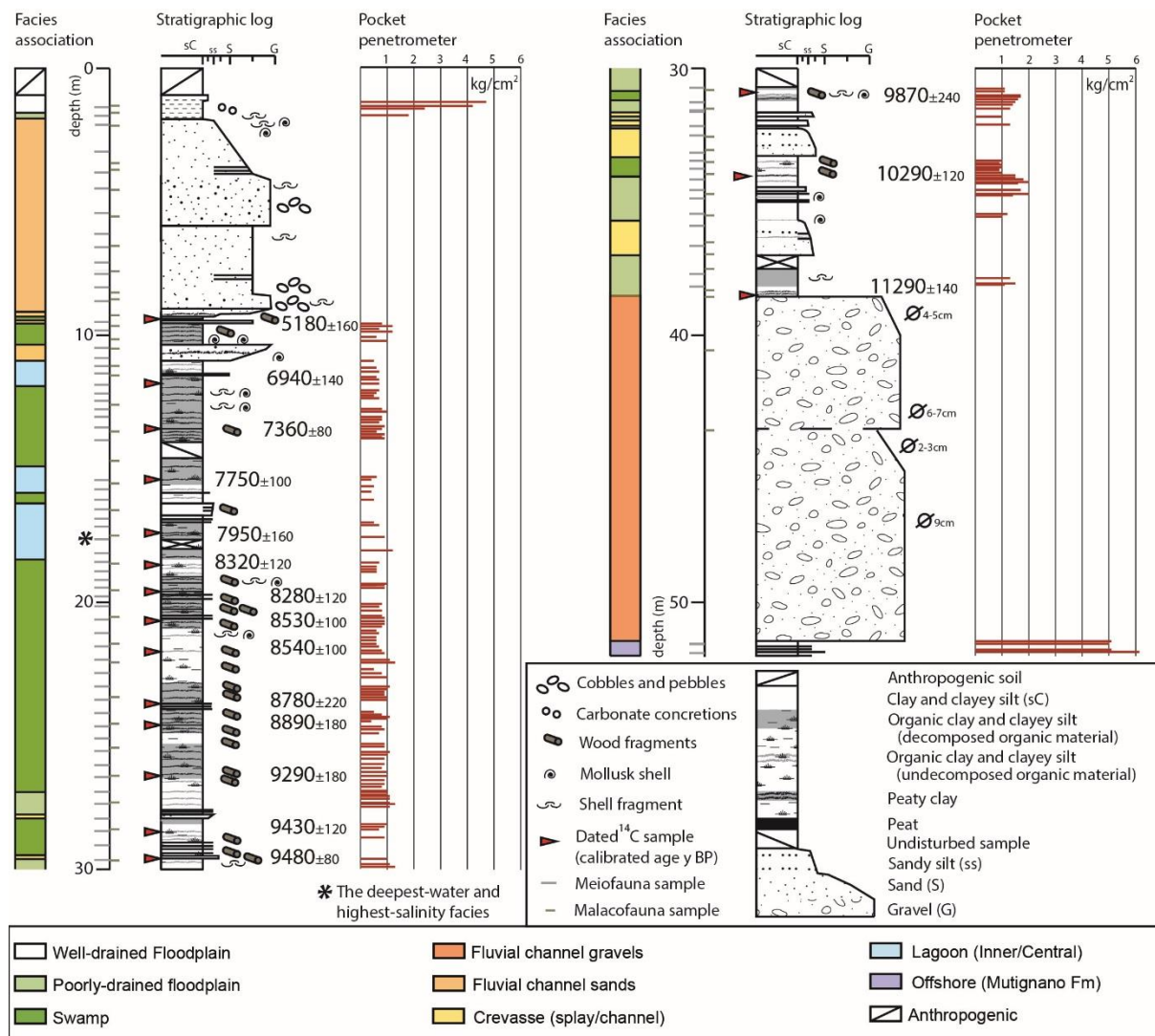


Fig. 2 – Facies interpretation and pocket penetration values of reference core Marconi (see Fig. 1d for location).

The identification of meiofaunal taxa was supported by original descriptions (Ellis and Messina, 1940, 1952), integrated with selected papers (Athensuch et al., 1989; Barbieri and Vaiani, 2018; Henderson, 1990). Autoecological characteristics and modern distribution of ostracods and foraminifers derive mainly from Coccioni (2000), Debenay et al. (2000), Meisch (2000), Milker and Schmiidl (2012), and Pint and Frenzel (2017). Mollusk identification relied on the late Quaternary

fossil collections of the Stratigraphic Paleoecology Laboratory of the Department of Biological, Geological and Environmental Sciences, University of Bologna.

### 5.3.2 Chronology

The high-resolution chronological framework rests on seventeen AMS  $^{14}\text{C}$  dates (Fig. 2 and Table 1) performed on organic-rich samples (wood fragments and charcoals) at KIGAM Laboratory (Daejeon, Republic of Korea), after acid-alkali-acid pretreatment. All samples were previously cleaned with deionized water and dried at  $40^\circ\text{C}$  to prevent mold formation. Conventional  $^{14}\text{C}$  ages were calibrated using OxCal 4.4 (Ramsey, 1995; Ramsey and Lee, 2013) with the IntCal 20 and Marine 20 curves (Reimer et al., 2020). Five dates on shells from Parlagreco et al. (2011) were recalibrated following facies attribution (brackish/lagoon vs marine) and the suggested correction of  $487 \pm 29$  y for the Central Adriatic Sea (Table 1).

The reliability of the 17 new radiocarbon dates (Fig. 2; Table 1) was tested by using the Bayesian approach (Blockley et al., 2004), which allows incorporating prior information into the calibration process (Buck et al., 2003, 1992, 1991). In particular, the form of Markov Chain Monte Carlo (MCMC) analysis available in OxCal has been utilized. An age-depth model (Lowe et al., 2007; see Supplementary materials) was developed to eventually reject dates of poor fit and constrain the whole series objectively. The General setting was adopted for the Outlier-Model analysis, and the prior probability fixed to 0.05. Similar Bayesian methodology was used by Tesi et al. (2017) for the investigation of coeval (Holocene) offshore-deep marine deposits in the Central and Southern Adriatic.

Lab Nr.	Material	Core Depth (m)	C14 age (BP)	Cal year BP (2 $\sigma$ range)	C14 age (2 $\sigma$ ) Cal BP (mean error)	Figure
KGM-OWd210391	wood fragments	9.4	4535 $\pm$ 33	5200-5050	5180 $\pm$ 160	2, 3, 4
KGM-OWd210392	wood fragments	11.8	6079 $\pm$ 37	7030-6790	6940 $\pm$ 160	2, 4
KGM-OWd210393	wood fragments	13.5	6444 $\pm$ 37	7430-7270	7360 $\pm$ 80	2
KGM-OWd210394	wood fragments	15.4	6919 $\pm$ 41	7850-7660	7750 $\pm$ 100	2, 4
KGM-OWd210396	wood fragments	17.4	7134 $\pm$ 39	8020-7920	7950 $\pm$ 160	2, 3, 4
KGM-OWd210397	wood fragments	18.6	7522 $\pm$ 40	8410-8280	8320 $\pm$ 120	2, 3, 4
KGM-OWd210398	wood fragments	19.6	7473 $\pm$ 44	8370-8190	8280 $\pm$ 120	2
KGM-OWd210399	wood fragments	20.7	7766 $\pm$ 42	8610-8420	8530 $\pm$ 100	2
KGM-OWd210400	wood fragments	21.85	7778 $\pm$ 43	8640-8430	8540 $\pm$ 100	2
KGM-OWd210401	wood fragments	23.8	7925 $\pm$ 40	8990-8600	8780 $\pm$ 220	2
KGM-OWd210402	wood fragments	24.6	8035 $\pm$ 43	9030-8720	8890 $\pm$ 180	2
KGM-OWd210403	wood	26.5	8288 $\pm$ 44	9440-9120	9290 $\pm$ 180	2, 4
KGM-OWd210404	wood	28.6	8405 $\pm$ 40	9530-9390	9430 $\pm$ 120	2, 4
KGM-OWd210405	wood fragments	29.6	8458 $\pm$ 47	9540-9410	9480 $\pm$ 80	2

KGM- OWd210406	wood fragments	30.9	8812 ± 39	9970- 9680	9870 ± 240	2, 4
KGM- OWd210407	wood fragments	34.05	9123 ± 43	10410- 10200	10290 ± 120	2, 4
KGM- OWd210408	charcoal	38.5	9874 ± 48	11410- 11190	11290 ± 140	2, 3, 4
6009*	Marine shell	3.0	2880 ± 30	2040- 1680	1850 ± 180	4
6010*	Marine shell	6.4	4125 ± 35	3550- 3200	3380 ± 180	4
6011*	Lagoon shell	8.4	6400 ± 40	6850- 6570	6710 ± 120	4
6012*	Lagoon shell	9.0	6870 ± 40	7410- 7160	7260 ± 120	4
6013*	Brackish shell	11.0	6860 ± 40	7410- 7150	7250 ± 120	4

*Table 1 – List of radiocarbon dated samples from reference core Marconi and 14C dates\* (AMS) from Parlagreco et al. (2011; recalibrated) shown in Figs. 2, 3 and 4*

## 5.4 Substrate and Facies associations

Based on the integrated sedimentological and paleontological analysis of core “Marconi”, seven facies associations were identified (Fig. 2) above the Mutignano Formation substrate. Substrate and facies associations are described in detail below in stratigraphic order. Their interpretation is based on sedimentological features, fossil (meiofauna and mollusk) content, stratigraphic relationships, and geotechnical properties (pocket penetration measurements).

### 5.4.1 Mutignano Formation (Mt Fm) substrate

**Description.** This sedimentary unit consists of gray to brownish clays and silty clays with cm-thick sand intercalations (Fig. 3). Horizontal lamination is common. Bioturbation is locally present. This sedimentary unit was encountered in the lowermost part of the reference core, up to about 51.5 m core depth (Figs. 2-3). It is characterized by very high pocket penetration (Pp) values, invariably > 5 kg/cm<sup>2</sup> (Fig. 2).

The foraminiferal assemblage consists almost entirely of benthic species, mainly *Bolivina* spp. (including common *Bolivina seminuda*), *Bulimina marginata*, *Globobulimina affinis*, *Globobulimina pyrula*, with the subordinate occurrence of *Bulimina etnea*, *Cassidulina carinata* and *Sigmoilopsis schlumbergeri*.

**Interpretation.** Sedimentological and paleontological data are considered to reflect a shelf depositional environment. Specifically, the assemblage is dominated by foraminifers indicative of high organic matter and low oxygen concentration at the sea floor (e.g. Jorissen et al., 1992; Rasmussen, 2005) the occurrence of *Bulimina etnea* is consistent with an age attribution to the Calabrian (Pasini and Colalongo, 1996; Pillans and Gibbard, 2012). This unit represents the distal (i.e., offshore) equivalent of the sandier to conglomeratic (i.e., shoreface) Mutignano Fm cropping out inland (Geological Map of Italy at 1:50,000 scale, Sheets: 351, 361).

Very high Pp values are consistent with consolidated substrate deposits that likely experienced relatively long (lithostatic) sediment compaction due to subsequent sediment loading.

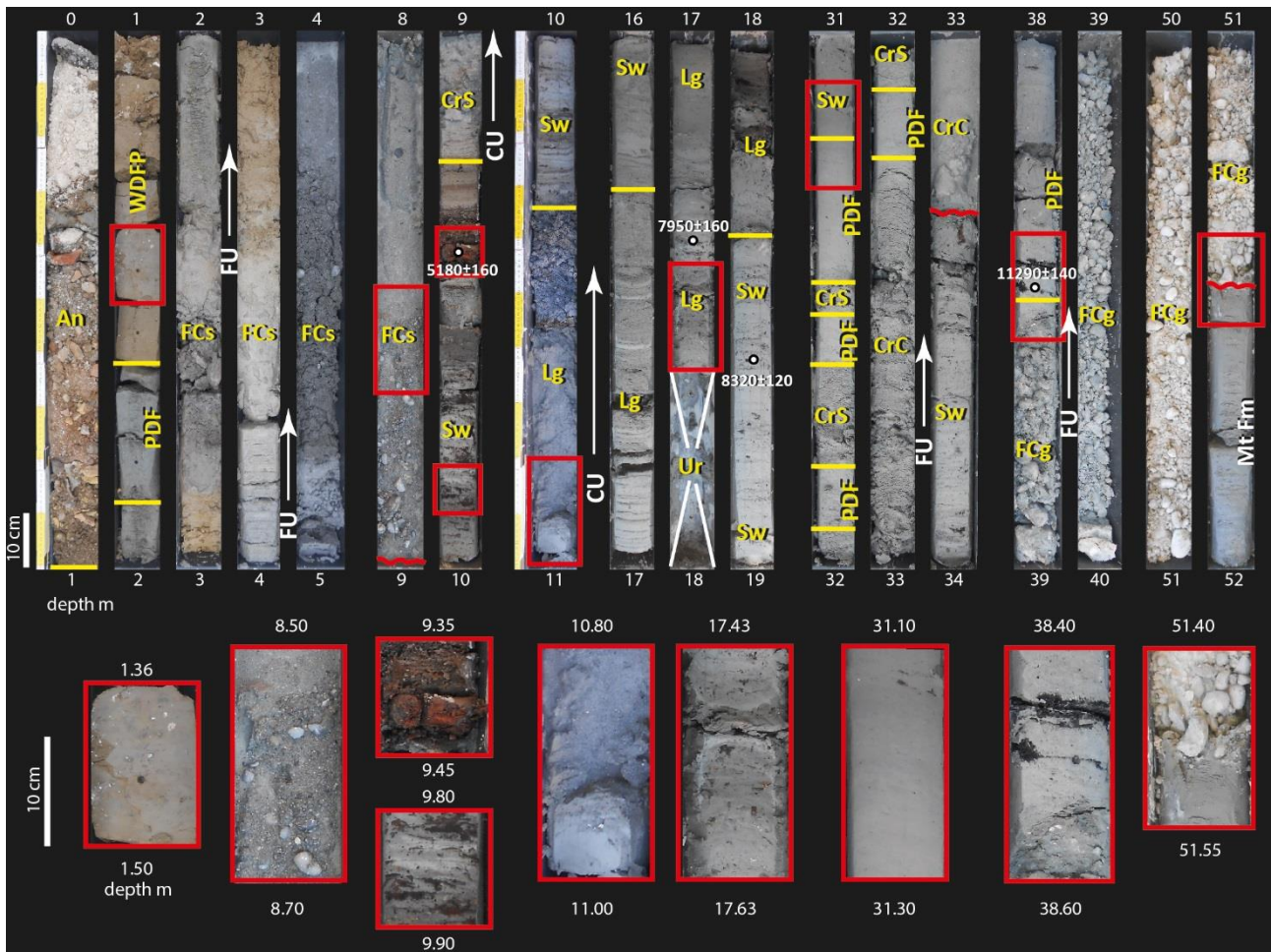


Fig. 3 – Representative photographs of the incised substrate and facies associations identified in core Marconi. Silty clays with cm-thick sand intercalations of the marine substrate (Mutignano Formation – Mt Fm). Fluvial-channel gravels (FCg) with calcareous rounded pebbles and cobbles, showing erosional lower base (red line) and fining-upward (FU) tendency. Massive, gray to darkish poorly-drained floodplain (PDF) silty clays. Swamp (Sw) dark gray to blackish clays with very high organic matter content, abundant vegetal/wood remains and peat layers. Silty sands with FU trend and erosional base of crevasse-channel (CrC) deposit. Coarsening-upward (CU) tendency within crevasse splay (CrS) sediments. Lagoonal (Lg) gray to darkish clays and silt clays with abundant wood fragments, bioclasts and decomposed organic content. Unrecovered (Ur) core interval. Fluvial-channel sands (FCs) with FU trend and erosional lower base. Mottled well-drained floodplain (WDFP) gray to brownish clays and silty clays. Anthropogenic (An) deposit. Calibrated ages (a BP; white color).

## 5.4.2 Facies associations

### *5.4.2.1. Fluvial-channel (gravel - FCg) facies association*

Description. This facies association, up to 13 m thick, includes amalgamated and poorly sorted gravel deposits with calcareous rounded pebbles and cobbles (ranging from 2 to 9 cm in diameter) locally embedded in a silty-sandy whitish matrix (Fig. 3). An erosional lower boundary cutting into the marine substrate characterizes this composite facies association, made of two vertically-amalgamated gravel bodies with peculiar fining-upward trends (Figs. 2 and 3). Microfossils are absent. Neither mollusk shells nor wood fragments were encountered. For this facies association, radiocarbon ages are not available.

Interpretation. The very coarse texture, internal FU trends and the erosional lower boundary are characteristic of high-energy and high-gradient fluvial-channel (FC) deposits (Miall, 1992). Poor sorting, presence of cobbles and pebbles along with amalgamation surfaces are consistent with a braided stream facies that accumulated in a confined and very high-energy flow setting, probably characterized by high topographic gradient and morphological confinement, within the narrow, piedmont Pescara valley (Fig. 1). The lack of fossils and of vegetal remains is consistent with this interpretation.

### *5.4.2.2 Channel-related (CrS-CrC) facies association*

Description. This facies association consists of two different lithofacies: silty sand deposits with maximum thickness of 1.3 meters with FU trend, erosional base and gradational top (Fig. 3); and sandy silt to coarse sand bodies, a few decimeters thick, displaying general coarsening-upward (CU) tendency with gradational lower boundary and sharp top (Fig. 3). Silty intercalations are locally encountered, along with scarce wood and shell fragments. Samples retrieved for palaeontological analyses are barren or include few freshwater mollusk remains (*Pisidium* sp. and *Bithynia* opercula).

Interpretation. Sedimentological and paleontological characteristics suggest a variety of sub-environments dominated by fluvial processes, close to the river axis. The presence of vegetal remains and fragments of freshwater bivalves (e.g., *Pisidium*) or gastropods opercula (e.g., *Bithynia*) is consistent with overbank sub-environments exposed to frequent river floods. Thin sand bodies with CU tendency and gradational base are interpreted to be crevasse splays (CrS). Fining-upward sandy deposits, less than 1.5 m thick, with erosional lower boundary are supposed to represent crevasse channels (CrC).

#### 5.4.2.3 Poorly-drained floodplain (PDF) facies association

Description. This facies association, generally less than 1.5 m thick (Fig. 2), is made up of massive gray to darkish gray clay and silty clay (Fig. 3). Pedogenic features are absent. Thin layers of decomposed organic material, a few cm-thick, are common, whereas wood and charcoal debris are scattered (Fig. 3). Silty sand intercalations, a few mm to cm-thick, are scattered within this facies association, which occurs at various stratigraphic levels in the reference core between 27 and 35 m core depth (Fig. 2). Radiocarbon dates available for this interval indicate an age ranging between 11.3 and 9.2 ka BP. Pocket penetration measurements fall in the interval of 1.0-1.7 kg/cm<sup>2</sup> (Fig. 2). Ostracod assemblages consist of low amounts of freshwater species, such as *Candona neglecta*, *Ilyocypris* spp. and *Pseudocandona albicans*. The macrobenthic content is represented by sparse fragments of freshwater and terrestrial gastropods, though mollusk shells are locally present (i.e., 38.4 m and 27.5 m core depth; Figs. 2 and 3). The lowermost fossil-rich horizon is dominated by the calciphile and pulmonate gastropod *Pomatias elegans* (common). Whereas the uppermost one is characterized by *Bithynia opercula* (common) and *Valvata* sp. specimens (common).

Interpretation. The fine-grained lithology, absence of pedogenic features and oxidation combined with the occurrence of a freshwater fauna (*Candona neglecta*, *Ilyocypris* spp. and *Pseudocandona albicans*) and shell fragments (from *Pomatias elegans* to *Bithynia* and *Valvata* remains) are consistent with deposition in a low-energy environment, most likely characterized by low topography, frequent river floods and generally high-water table or ephemeral standing bodies of freshwater typical of poorly-drained floodplain settings. The microbenthic content at 38.4 m and 27.5 m depth reflects locally increasing water table. Pocket penetrometer data support this interpretation, suggesting a depositional setting with high water content that produced relatively low soil consistency, transitional between well-drained floodplain and paludal deposits.

#### 5.4.2.4 Swamp (Sw) facies association

Description. This facies association, up to 9 m thick in the reference core (Fig. 2), is composed of very soft dark gray to blackish clays (Fig. 3). Organic matter content is very high, including abundant millimetric to centimetric-sized plant debris and wood fragments (Fig. 3). Peat layers (less than 15 cm-thick) occur at different stratigraphic intervals. Silt and silty sand intercalations, a few centimeters thick are also present. A rich ostracod fauna is commonly found within this facies association: it is dominated by the same species found in PDF sediments, with the local occurrence of other subordinate taxa, such as *Cypria ophtalmica*, *Fabaeformiscandona* sp. and *Cyclocypris* sp. In the upper part of the unit, rare specimens of euryhaline ostracods (*Cyprideis torosa*) and benthic foraminifers (*Ammonia tepida*) are observed in association with dominant freshwater to mesohaline ostracods. Mollusk shell fragments are abundant. A relatively rich macrobenthic assemblage was observed at 29.7 m and 12.6 m core depth, respectively (Fig. 2). This fossil assemblage includes a suite of freshwater-to-oligohaline taxa, such as *Planorbis* spp. (common), *Valvata* sp. (common), *Pisidium* spp. (rare), *Succinea* sp. (rare), *Theodoxus fluviatilis* (rare) and hydrobiids.

Pocket penetrometer measurements are generally lower than 1 kg/cm<sup>2</sup> with slightly higher values (up to 1.2 kg/cm<sup>2</sup>) recorded into peaty intervals (Fig. 2). This facies association commonly overlies poorly-drained floodplain deposits and is dominant between 18-30 m core depth (Fig. 2). Radiocarbon dates from this facies association suggest an age ranging between 9.4-8.3 ka BP (Fig. 2, Table 1). Between 16.3 and 9.4 m core depth, this facies association is sandwiched between lagoonal and fluvial deposits. Two ages of 7.3 and 5.2 ka cal BP are available for this interval (Figs. 2, 3 and Table 1).

Interpretation. Lithological characteristics, very-high amounts of organic matter, the presence of peat and very low Pp values are coherent with a low-energy environment, such as a wetland. Lack of traces of oxidation, rare coarser beds and abundant organic matter content are consistent with waterlogging and reducing conditions typical of a paludal environment, away from an active channel (Bruno et al., 2019). The rare occurrence of euryhaline taxa suggests the local onset of mesohaline conditions. Freshwater to low-brackish conditions are typical of swamps in the inner sector of an estuary.

#### 5.4.2.5 Well-drained floodplain (WDFP) facies association

Description. This facies association is encountered only in the topmost 2 m of the reference core (Figs. 2-3), but also at different stratigraphic levels in cores 9 and 6 (see Fig. 1 for location), between 34-37 m bsl. It is less than 1 m thick, and consists of rooted, pedogenized gray to brownish clay and silty clay with yellowish mottles due to manganese and iron oxides. Silty sand intercalations and carbonate nodules can be present. The meiofauna is absent. Shell-rich horizons dominated by the continental mollusk *Cernuella* and few reworked/transported shells of shoreface bivalves are locally observed (e.g., 1.7 m core depth Fig. 2). Based on the sedimentological data from available core descriptions and stratigraphic correlations, this facies association displays a remarkable lateral continuity extent in the uppermost interval of the succession. Pocket penetration values range between 2.4 and 4.7 kg/cm<sup>2</sup> (Fig. 2).

Interpretation. Lithology, pedogenic features and geotechnical characteristics allow interpreting this facies association as accumulated in a well-drained floodplain. Fine-grained lithologies, presence of roots and pedogenized horizons are consistent with a low-energy depositional environment typified by subaerial exposure under well-drained conditions, due to a very low water table position. The presence of land mollusks characteristic of dry coastal plain settings and open habitats, such as *Cernuella* (Grano and Di Giuseppe, 2021), along with the lack of meiofauna, also support this interpretation.

#### 5.4.2.6 Lagoon (Lg) facies association

Description. This facies association, up to 2 m thick in the reference core (Fig. 2), consists mostly of very soft gray to darkish clays. Silt clays with sandy silt and silty sand intercalations showing a CU trend are also encountered (10.35-10.90 m core depth, Fig. 3). Wood fragments and vegetal remains are abundant (Fig. 3). Decomposed organic matter is also diffused, and millimetric-sized shell fragments are locally widespread (Fig. 3). This facies association shows vertical transition to paludal clays, within 11-18 m core depth (Fig. 2). The lower and upper parts of this facies association were radiocarbon dated to about 8.0 and 7.0 ka cal BP, respectively (Fig. 2). The meiofauna consists of abundant euryhaline ostracods (*Cyprideis torosa*) and foraminifers (*Ammonia tepida* and rare *Ammonia parkinsoniana* and *Haynesina germanica*). A more diversified assemblage, including other brackish to euhaline ostracods and foraminifers, such as *Loxoconcha elliptica*, *Xestoleberis aurantia* and *Criboelphidium oceanensis*, was found between 17 and 18 m core depth. As for mollusk

remains, most samples yielded only few brackish specimens. Two mollusk-rich assemblages were retrieved at 17.5 m and 11.20 m core depth (Fig. 2). The lower assemblage is dominated by the brackish to marine gastropods *Bittium reticulatum* and *Rissoa* spp. (both common), the brackish minute gastropod *Ecrobia* cf. *ventrosa* (common) along with few freshwater specimens of *Valvata* sp.. Whereas the upper mollusk association is characterized by *Ecrobia* cf. *ventrosa* (common) along with *Abra segmentum* (rare) and thin-shelled *Cerastoderma* spp. (rare). Pocket penetration values are very low, ranging between 0.4-0.9 kg/cm<sup>2</sup> (Fig. 2).

Interpretation. Sedimentological characteristics and fossil assemblages suggest a low-energy, lagoonal (or outer-estuary) depositional environment, typified by generally abundant organic content, and brackish conditions. Fossils in the lower part of this unit (between 18 and 17 m core depth) reveal a relatively high marine influence, consistent with a central lagoon environment, as indicated by i) a diversified, brackish and euryhaline meiofauna, and ii) mollusk taxa adapted to live in mesohaline to fully marine salinity settings (e.g., *B. reticulatum*), along with rare freshwater species. In contrast, in the upper part of this facies association, the meiofauna and mollusks are considered to reflect inner lagoon conditions with a low marine influence, as suggested by i) few species of ostracods and foraminifers and ii) the common presence of hydrobids, thin-shelled *Cerastoderma* and *A. segmentum*, taxa preferentially distributed in mesohaline to oligohaline settings elsewhere along the Adriatic and beyond (e.g., Amorosi et al., 2014; Scarponi et al., 2017).

#### *5.4.2.7 Fluvial/distributary-channel (sand - FCs) facies association*

Description. This facies association was identified in the uppermost 10 m of the reference core, above paludal deposits. Poorly-drained floodplain clays cap this facies association, which generally consists of sand bodies (about 7 m thick) with erosional lower base and FU trend: from basal gravelly-coarse to medium gray sands with rounded pebbles to silty sands (Fig. 3). Internal erosional boundaries can also be observed (Fig. 2). Silty and silty clay cm-thick intervals are locally encountered, along with a few shell fragments of shoreface bivalves. This facies association is generally barren of microfossils. In cores 9, 6 and 22 (Fig. 1 for location), this unit is sandwiched between swamp clays and shows a slight upward decrease in grain-size, with the dominance of silty sands and sandy silts.

Interpretation. Lithology, grain-size tendency, and erosional lower base allow the interpretation of this facies association as a sandy fluvial-channel deposit (Bridge, 2006). The local abundance of

rounded pebbles supports this interpretation. As regards sand deposits in cores 9 and 6, the vertical transition to paludal clays coupled with finer grain size suggest their interpretation as a distributary-channel deposit (Bhattacharya, 2006). As for the mollusk content, the local presence of shoreface shell fragments is considered to reflect exceptional on land transport and might point to a portion of the fluvial network adjacent to (or interfingering with) backshore settings, in a wave-dominated deltaic environment.

#### *5.4.2.8 Beach-ridges/Delta-front/Transgressive barrier facies association*

**Description.** This facies association was not penetrated by core Marconi. It crops out in the easternmost sector of the studied succession, in proximity of the modern shoreline, as reported by the stratigraphic description of core 10 (Fig. 1 for location). This facies association, up to 22 m thick, is composed of medium to fine sands with frequent pebble (rounded) intercalations, gradational lower boundary with underlying organic-rich clays and an overall CU trend. Bioclasts accumulation is a common feature of this deposit.

**Interpretation.** Lithology, sedimentological features and the distal position are consistent with a high-energy marine (coastal) setting for this outcropping sand body. Presence of scattered bioclasts alternating with rounded pebbles may suggest a marine environment highly influenced by fluvial activity, such as a delta-front setting. Based on the chronology available from the reference core (Fig. 2; Table 1), stratigraphic correlations suggested that this facies association started to accumulate above estuarine deposits in response to the Middle Holocene transgression, around 8.3 ka cal BP. The maximum thickness is linked to Middle-Late Holocene delta progradation (last 7.8 ky).

#### *4.2.9 Anthropogenic facies association*

**Description.** This facies association, up to 2.5 m thick, was identified between 0-1 m depth in the reference core (Fig. 2). It is characterized by chaotic, unconsolidated and unsorted deposits of different provenance (Fig. 3). The coexistence of materials of both natural (sediment, wood) and human (bricks, plastic and iron fragments) origin is peculiar of this deposit which was identified in several core descriptions (22, 1, 29, 31, 9, 13, 20, 2, 1Tv, 6 and 21) at the core surface. Widespread blocks and cobbles generally have undifferentiated origin and show angular, sub-angular or rounded shapes (Fig. 3). No sedimentary structures were observed.

**Interpretation.** Stratigraphic positions, lack of sedimentary structures and the presence of clearly man-made materials such as plastic fragments, allow the attribution of this facies association to

human activity. In particular, the unsorted and unconsolidated deposits are associated to landfill activities, whereas levels of sub-angular clasts may reflect building foundations.

## 5.5 Paleovalley fill architecture and sequence-stratigraphic interpretation

### 5.5.1 Stratigraphic architecture

Two stratigraphic panels, one transverse (Fig. 4a) and the other one parallel (Fig. 4b) to the valley axis (Fig. 1d for location), depict the stratigraphic architecture of the paleovalley fill. Their orientation allowed a basic three-dimensional reconstruction of the paleovalley profile and of facies relationships.

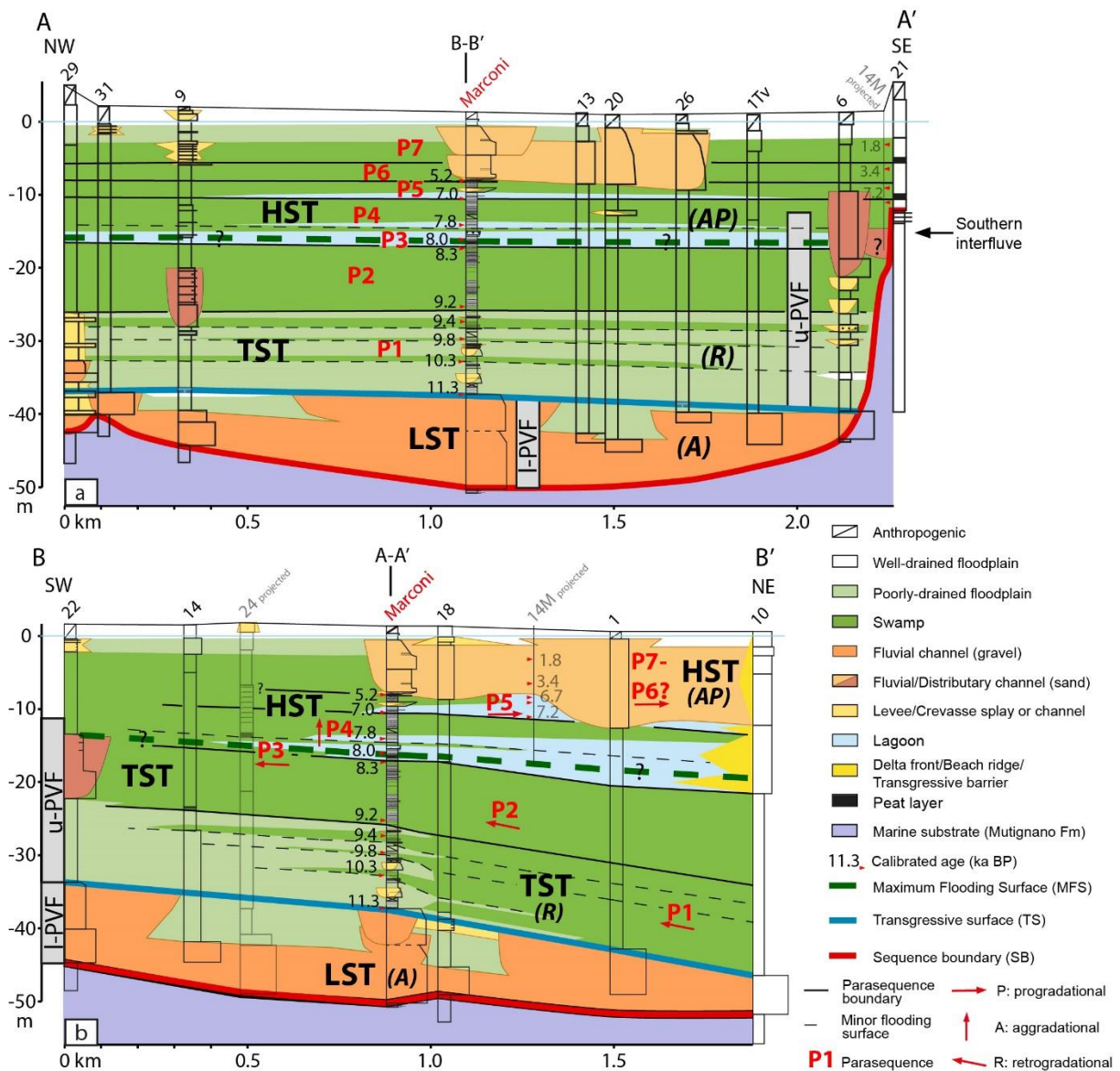


Fig. 4 – Stratigraphic panels illustrating the transversal (a) and longitudinal (b) facies architecture beneath the Pescara coastal plain (see Fig. 1 for section traces) with indication of lower (l-PVF) and upper (u-PVF) paleovalley fills; and sequence stratigraphic interpretation (LST: lowstand systems tract; TST: transgressive systems tract; HST: highstand systems tract). Seven parasequences are numbered in red. Reference core is also indicated in red.

Beneath the Pescara valley, the paleovalley profile and valley fill were identified and tracked from the depocenter (core “Marconi”) to the southern interfluvium (core 21; Fig. 4a) on the basis of the abrupt facies change between Early Pleistocene marine silty clays of the Mutignano Fm and continental deposits of Late Pleistocene-Holocene age (Fig. 4a, b). On the valley floor, between about 40-50 m depth (Fig. 4a, b), offshore deposits of the Mutignano Fm are overlain by laterally extensive, amalgamated fluvial gravel bodies (Fig. 4a, b). Southwards, at about 12 m depth (core 21, Fig. 4a), soft (mean  $P_p < 1.0 \text{ kg/cm}^2$ ) organic-rich Holocene deposits overlie the stiff (mean  $P_p > 5 \text{ kg/cm}^2$ ) substrate. Overall, the Pescara paleovalley is about 50 m deep and, at least, 2 km wide (Fig. 4a), possibly up to 3.5 km considering the unsurveyed northern sector shown in Fig. 1c.

The Pescara paleovalley fill is similar to many ancient and Late Quaternary PVFs (Allen and Posamentier, 1993; Aslan and Blum, 1999; Blum and Womack, 2009; Boyd et al., 2006; Busschers et al., 2007, 2005; Cross et al., 1993; Dalrymple et al., 2006; Gibling and Bird, 1994; Guijia and Congxian, 1996; Hori et al., 2002; Plint and Nummedal 2000; Shanley and McCabe, 1994, 1991; Tanabe et al., 2006; Van Wagoner, 1995; Zaitlin et al., 1994) in terms of facies architecture and fluvial stacking patterns: a laterally extensive fluvial body (i.e., the lower paleovalley fill or l-PVF; Fig. 4) with erosional base and upward transition to more isolated sand bodies within a mud-dominated succession (the upper paleovalley fill or u-PVF; Fig. 4). In the southernmost sector, a fluvial gravel body, > 3 m thick, was observed in proximal core 14M around 15-18 m depth (Parlagreco et al., 2011 - Fig. 4a). Since this core did not reach the Mutignano Fm substrate, the fluvial gravel body could represent a Holocene fluvial channel deposit of the u-PVF or, alternatively, a buried fluvial terrace generated by repeated fluvial deposition and incision following the MIS 5e/MIS 5d transition, as documented for the coeval Biferno “Upper PVF” (Amorosi et al., 2016b). The first interpretation is more likely, because of the presence of overlying “fine-grained sediments rich in wood fragments” (Parlagreco et al., 2011). These latter, in fact, are very similar to the swamp facies identified in core Marconi at the same stratigraphic level (Fig. 4a).

The l-PVF, between about 50-38 m depth (Fig. 4a), consists almost entirely of an up to 2 km wide (Fig. 4a, b) fluvial gravel deposit, in agreement with classic models (Gibling et al., 2011; Zaitlin et al., 1994). These basal gravels, assigned to the Late Pleistocene on the basis of a radiocarbon date of 11.3 ka cal BP at their top, have maximum thickness of 13 m in the valley depocenter (Figs. 2 and 4a, b). Amalgamation of fluvial bodies decreases upwards, between about 42-33 m depth, with the simultaneous appearance of poorly-drained muds and scattered well-drained and crevasse deposits (Fig. 4a, b).

The laterally extensive gravel deposit likely, despite repeated erosional episodes due to fluvial activity within a narrow valley, started to accumulate under lowstand conditions during the LGM (30-19 ka cal BP), when sea-level had dropped down to 120 m (Clark et al., 2009). In the lowermost interval, no preservation of overbank deposits may suggest that fine-grained sediment was completely eroded away by the lateral migration of a (braided?) river system within the narrow LGM valley and transferred to the deep basin. In the uppermost l-PVF (Fig. 4a, b), the occurrence of finer-grained facies and decrease in channel amalgamation are consistent with the gradual evolution of the fluvial system into a meandering alluvial plain during the early deglaciation. Similar changes in fluvial stacking pattern and the decrease in grain size have been linked to the glacial-interglacial transition, which caused significant reduction in stream competence of Holocene river systems compared to their high-energy, LGM counterparts (Amorosi et al., 2017a; Aslan and Autin, 1999; Campo et al., 2016; Kettner and Syvitski, 2008; Macklin et al., 2002; Milli et al., 2016).

The u-PVF is about 25 m-thick (38-11 m of reference core depth; Fig. 4a) and mostly composed of non-marine and organic-rich soft deposits (Fig. 4a, b) of Holocene age with Pp values ranging between 0.4-1.8 kg/cm<sup>2</sup>. As a whole, the u-PVF records an upward increasing marine influence in its lower interval (11.3-8 ka cal BP), but an opposite trend in the upper part (last 8 ky BP). The early Holocene succession is characterized by the vertical transition from poorly-drained floodplain facies to swamp clays to lagoonal deposits with scattered and narrow (< 100 m wide) distributary-channel sand bodies (Fig. 4a, b). Lagoonal clays identified in the reference core are in lateral transition to coastal sands and swamp deposits in distal and proximal sectors, respectively (Fig. 4b). The vertical facies change from freshwater/swamp to brackish/lagoonal deposits reflects progressive drowning of the valley, between 11.3 and 8 ka cal BP, under conditions of sea-level rise (Lambeck et al., 2011). During this transgressive phase, the Pescara valley drowned, transforming the studied reach into an estuary, as well as already documented for several coastal plains worldwide (Amorosi et al., 2008; Boyd et al., 2006; Dalrymple et al., 1992; Hijma et al., 2009; Hori et al., 2002; Milli et al., 2016, 2013; Ta et al., 2021; Tanabe et al., 2015, 2006; Zaitlin et al., 1994), and in other sectors of the Adriatic basin (Amorosi et al., 2016b; Bruno et al., 2017; De Santis et al., 2020a; Maselli et al., 2014; Ronchi et al., 2021; Rossi et al., 2021). Starting from about 7.8 ka cal BP, lagoonal clays were progressively overlain by swamp facies (Fig. 4a, b). Between 7.8 and 7.0 ka cal BP, sea level rose to the elevation of the southern interfluvium (Fig. 4a) and this sector was flooded, causing the progressively widening of paludal areas into the Pescara valley.

The uppermost interval (10-0 m depth; Fig. 4a, b) of the Pescara succession is dated to the last 5.2 ky, and reflects transition from lagoonal to poorly-drained depositional environments, up to the modern coastal plain with recent anthropogenic influence (Fig. 4a, b). A sandy fluvial channel-belt, about 500 m-wide (Fig. 4a), was identified within this interval. After 5.2 ka cal BP, under nearly stable sea-level conditions (Vacchi et al., 2016), fluvial activity increased (Benito et al., 2015) and the Pescara River likely started to deliver high amounts of sand to the coast, establishing, sustaining and growing a wave-dominated delta with beach ridges developing on either side of the river mouths (Fig. 4b). Subaerially exposed, barrier-beach and deltaic deposits form the uppermost interval (last 3.4 ky; Fig. 4b) of the Pescara coastal plain succession at distal locations of the study area (Urbano et al., 2017). Chronological, sedimentological and paleontological data from Parlagreco et al. (2011) are consistent with this interpretation.

The identification of an unconformable relationship between fluvial deposits and subjacent substrate of significantly older age, a methodology generally applied for the identification of ancient PVs (Blum et al., 2013), was also used for the recognition of the late Quaternary Pescara paleovalley fill.

### 5.5.2 Sequence stratigraphy

Stratigraphic and chronological data (Figs. 2, 4 and Table 1) allowed to interpret the Late Pleistocene amalgamated fluvial body with a general aggradational stacking pattern as the lowstand systems tract (LST; Fig. 4a, b). The erosional base of the LST gravel body, cutting into considerably (>1 My) older marine substrate corresponds to the classic sequence boundary (SB *sensu* Posamentier et al., 1988; Van Wagoner et al., 1990). At the location of the study area and further down shelf, the SB is genetically linked to the last stage of sea-level fall at the MIS 3-MIS 2 transition (about 30 ka cal BP; Pellegrini et al., 2018, 2017). Between 30-14 ka cal BP, mostly during lowstand conditions, laterally extensive fluvial-channel belts accumulated along the onshore sectors of the Adriatic basin (Amorosi et al., 2016a). The lowstand Pescara River system most likely delivered its fluvial sediments to the MAD basin, about 60 km to the northeast from the modern study area (Fig. 1).

Along the southern valley flank, the SB marks the stratigraphic unconformity between the Mutignano Fm and overlying Holocene swamp clays around 12 m depth (core 21; Fig. 4a). In this sector, SB formation could be related to the general phase of fluvial incision caused by the stepwise

post-MIS 5e (and pre-MIS 3) sea-level drop. Therefore, from the interfluvium to the depocenter, the SB shows a general diachronous nature (at least post-MIS 5e to MIS 2) that seems to be a characteristic feature of basal valley-fill surfaces, as discussed by Blum et al. (2013). The SB coincides with the paleovalley profile from the main depocenter up to the paleovalley interfluvium (Fig. 4a), where the low-quality data available did not allow the identification of a clear paleosol.

The abrupt facies change from the Late Pleistocene l-PVF to the Holocene u-PVF corresponds to the transgressive surface (TS; Fig. 4a, b), which is dated to about 11.3 ka cal BP. The maximum flooding surface (MFS), dated to about 8 ka cal BP (Fig. 4a, b), marks the most landward migration of the barrier-lagoon system, with lagoonal deposits reaching their innermost position about 1.5 km landward of the modern shoreline (Fig. 4b). Based on paleontological (micro- and macrofossils) indicators of marine influence in brackish settings, the MFS can be identified quite precisely on the reference core: it corresponds with the deepest-water or higher-salinity facies (i.e., central-lagoon, the sample at 17.6 m depth; Fig. 2), at the turnaround from deepening-upward to shallowing-upward trends (Fig. 4a, b). Hence, the Early Holocene (11.3-8.0 ka cal BP) interval with its characteristic deepening-upward trend, from poorly-drained to “the deepest and highest-salinity” lagoonal facies (Fig. 2), was interpreted as the transgressive systems tract (TST; Fig. 4a, b). On the other hand, the opposite, shallowing-upward trend, from lagoonal to modern coastal plain deposits, shown by the Middle to Late Holocene succession (last 8 ky), allowed its interpretation as the highstand systems tract (HST; Fig. 4a, b). The Middle to Late Holocene succession incidentally corresponds to HST.

Unlike the Biferno paleovalley system, located about 80 km south of the study area, where fluvial terraces at various depths were interpreted as the falling stage systems tract (FSST; Amorosi et al., 2016b), no equivalent deposits were identified in the Pescara system. However, the two PVSs share similar characteristics as comparable width (about 2 km) and downstream slope gradient (refer to the Geological Map of Italian Seas at 1:250,000 scale, available at [https://www.isprambiente.gov.it/Media/carg/marine/NK\\_33\\_5\\_PESCARA\\_SOTT/Foglio.html](https://www.isprambiente.gov.it/Media/carg/marine/NK_33_5_PESCARA_SOTT/Foglio.html)). In the Pescara PVS, gravel bodies that could be interpreted as fluvial terraces have been documented by Desiderio et al. (2007; Fig. 1c) only in the northern sector of the Pescara paleovalley, which was not investigated in this study.

## 5.6 Millennial-scale architecture and sediment accumulation rates

Seven parasequences (Ps 1-7 in Figs. 4 and 5) were identified and tracked within the whole Holocene succession (TST+HST; Fig. 4a, b). The lowest three parasequences (Ps 1-3; Fig 4a, b) are retrogradationally stacked and form the TST. The uppermost four parasequences (Ps 4-7; Fig. 4a, b), with an aggradational to progradational stacking pattern, make the HST.

Parasequence 1 (11.3-9.2 ka cal BP; P1 in Fig. 4), about 12 m thick, is mostly composed of poorly drained floodplain clays. Locally, towards the southern valley flank, scattered well-drained deposits can be found (Fig. 4a). Seawards, poorly drained floodplain sediments are progressively replaced by swamp clays (Fig. 4b). Three minor flooding surfaces were identified at the base of thin swamp intervals within P1 (Fig. 4). The basal flooding surface coincides with the TS (Fig. 4). Mean sediment accumulation rate is 5.7 mm/y (Fig. 5).

Parasequence 2 (9.2-8.3 ka cal BP; P2 in Fig. 4) is almost completely made up of organic-rich swamp clays, with isolated distributary-channel sand bodies (Fig. 4). No evident downdip facies change can be inferred from the stratigraphic panel of Fig. 4b. P2 has average thickness of 8.5 m (Fig. 4) and exhibits the highest sediment accumulation rate (9.4 mm/y in Fig. 5).

Parasequence 3 (8.3-8.0 ka cal BP; P3 in Fig. 4) is characterized by the appearance of lagoonal/outer-estuarine clays in the Pescara valley. Along-dip correlation (Fig. 4b) displays a genetically linked set of freshwater (swamp/inner-estuary), brackish (lagoon/outer-estuary) to nearshore (transgressive barrier?) facies, with an obvious retrogradational trend. P3 shows the minimum thickness (0.75 m) among TST Ps coupled with the lowest accumulation rate (2.5 mm/y; Fig. 5).

Parasequence 4 (8.0-7.0 ka cal BP; P4 in Fig. 4) displays a clear shallowing-upward trend (Fig. 4a), with basal ("the deepest"; Fig. 2) lagoonal deposits that are progressively replaced upwards by swamp clays. The internal stacking pattern is generally aggradational (Fig. 4b). The basal flooding surface is the MFS and highlights the transition from retrogradational (TST) to aggradational-to-progradational stacking patterns (HST; Figs. 4b and 5), consistent with the main sequence stratigraphic models described by Catuneanu et al. (2006) and Neal and Abreu (2009). Within P4, a minor flooding surface dated to about 7.8 ka cal BP marks another brackish interval. This deposit is less laterally extensive and includes faunal associations typical of a shallower (inner-lagoon) environment than underlying (outer-estuarine) clays (Fig. 5a, b). P4 is characterized by a mean

thickness of about 5.6 m (Fig. 4) and displays a relatively high sediment accumulation rate (5.6 mm/y in Fig. 5).

Parasequence 5 (7.0-5.2 ka cal BP; P5 in Fig. 4) shows similar facies architecture to P4, with basal lagoonal/outer-estuarine deposits overlain by swamp clays. In contrast, the overall stacking pattern is progradational (Fig. 4b). This parasequence is only 2.4 m-thick (Fig. 4) and marks the lowest sediment accumulation rate of the entire Holocene succession (1.3 mm/y; Fig. 5).

Parasequences 6 and 7 (post 5.2 ka cal BP; P6 and P7 in Fig. 4) are the youngest Ps within HST and are characterized by a marked progradational stacking pattern (Fig. 4b). P6 consists entirely of organic-rich swamp clays, whereas P7 includes basal swamp deposits overlain by poorly-drained floodplain and well-drained floodplain facies, in lateral transition to anthropogenic deposits. P7 displays a general increase in the sand/mud ratio, with a fluvial channel-belt sand body (up to 500 m wide) in the central sector of the study area (Fig. 4a) connected with coastal sands basinwards (Fig. 4b). The available data allowed to estimate only a cumulative sediment accumulation rate for P6 and P7, with values of about 1.8 mm/y (Fig. 5).

### 5.6.1 Sediment accumulation history of the Pescara PVs

Similar to what has been documented for the Northern Po-Adriatic sector (Amorosi et al., 2017b), landwards of the shoreline, TST Ps 1-3 generally display the highest accumulation rates (up to 9.4 mm/y; Fig. 5), whereas highstand Ps 4-7 are characterized by lower values (down to 1.3 mm/y; Fig. 5). As for their northern equivalent estuarine (TST) deposits, high accumulation rates could reflect generation of accommodation in the Pescara coastal plain due to the eustatic sea-level rise. During the Holocene transgression (11.3-8.0 ka cal BP), for 3.3 ky, the Pescara paleovalley acted as an area of sediment storage. Afterwards, under Late Holocene stable sea-level conditions (HST), sedimentation rates gradually started to decrease, suggesting rapid progradation of coastal systems. During this period, the study area turned into a region of prevailing lateral sediment distribution.

On the other hand, the very low sediment accumulation rate of 0.7 mm/y (estimated from the reference core) for the fully-alluvial I-PVF (LST) is not reliable. Accumulation of this unit took place in response to repeated phases of fluvial incision, valley widening, sedimentation and re-incision between 30-11.3 ka cal BP.

## 5.7 Holocene paleoenvironmental evolution and glacio-eustatic control at parasequence scale

### 5.7.1 Paleoenvironmental evolution

Comparing the age of retrogradational Ps 1-3 with sea-level curves from the last ca. 11.5 ky (Fig. 5) confirms that the estuary was formed during a phase of eustatic sea-level rise, similar to several coeval estuaries worldwide (Amorosi et al., 2013b; Boyd et al., 2006; Dalrymple et al., 1992; De Santis et al., 2020a; Hijma et al., 2009; Hori et al., 2002; Milli et al., 2016; Ronchi et al., 2021; Ta et al., 2021; Tanabe et al., 2006; Zaitlin et al., 1994). The available data clearly reveal that this phase was punctuated by high-frequency oscillations and short phases of deceleration in relative sea-level rise. Early stages of estuary development (after 11.3 ka cal BP, in proximity of the reference core) were characterized by a general rising of the groundwater table and by the accumulation of poorly-drained floodplain to swamp muds (Fig. 5), with progressively increasing organic matter contents above the TS, as also shown in Figs. 2, 3 and 4. After 9.2 ka cal BP, widespread accumulation of organic-rich facies took place (Fig. 4), and poorly-drained floodplains of P1 were waterlogged due to increasingly higher water table (P2; Fig. 5). Between 9.2 to 8.0 ka BP, the study area was progressively transformed into an estuary characterized in its proximal portion by predominantly freshwater/inner-estuarine conditions (Figs. 4b and 5). Further sea-level rise, between 8.3 and 8.0 ka cal BP, led to the maximum landward migration of a barrier-lagoon systems during deposition of P3 (Fig. 5). This is testified by paleontological data, which show that the “highest-salinity” (brackish) conditions occurred around 8.0 ka cal BP (at the reference core site), and by stratigraphic correlation with coeval coastal sands seawards (core 10, Fig. 4b). At the end of the transgression (onset of P4), with the shoreline in its innermost position, the estuary reached its maximum depth and inland extent (Fig. 4b). Coastal systems then started gradually to prograde basinwards, as suggested by characteristic shallowing-upward cycles of Ps 4-7. During the early aggradational phase recorded by P4, the estuary was progressively filled (Fig. 5). Laterally extensive brackish/outer-estuarine environments developed within the valley, in which sediment was accommodated at relatively high accretion rates (5.6 mm/y; Fig. 5), consistent with the aggradational stacking pattern of P4 (Figs. 4a, b and 5). Between 7.0-5.2 ka cal BP (P5), brackish environments were replaced by freshwater conditions in inland sectors of the study area (Figs. 4 and 5). At that time, as suggested by markedly lower sedimentation rates (1.3 mm/y in the reference core; Fig. 5), by the reduced parasequence

thickness (Fig. 4a) and by the clear progradational stacking pattern of P5 (Figs. 4b and 5), progradation of the coastal system quickened. In the last 5.2 ky (Ps 6-7), the study area experienced delta plain aggradation and further progradation of the coastal system (Fig. 5). Additional stratigraphic and chronological data from the relatively distal core 14M (Parlagreco et al., 2011; Fig. 1 for location) confirm that fluvio-deltaic sands accumulated during the last 4 ky as a result of the interaction between fluvial (Pescara River) and marine processes. The northeastern sector of the study area was probably characterized by a fluvio-deltaic system frequently exposed to high-energy coastal dynamics. Interestingly, based on the ages of the P6 basal flooding surface (about 5.2 ka cal BP) and of the MFS offshore (“a regional downlap surface” marking the base of the HST prograding wedge and dated  $6,160 \pm 60$  cal ky BP; Asioli et al., 1996; Trincardi et al., 1996), P6 and P7 are supposed to be coeval of the HST prograding wedge documented offshore the Apennine coast (Cattaneo et al., 2003).

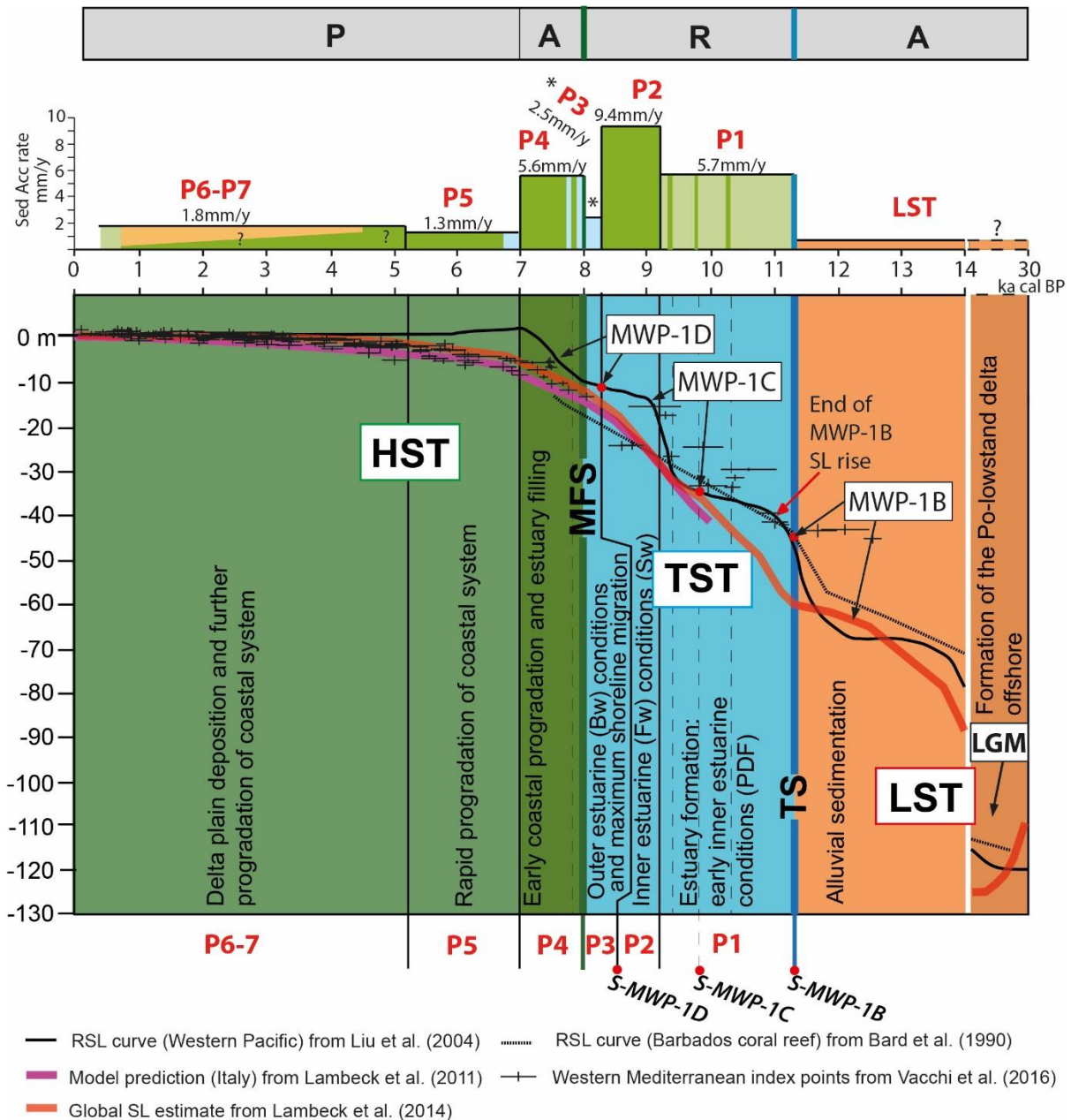


Fig. 5 – Comparison between millennial-to submillennial-scale sediment accumulation rates (Sed Acc rate) with indication of prevailing facies association (refer to Fig. 4 for legend), LGM to post-glacial sea-level curves from the Western Pacific (Liu et al., 2004), the Atlantic (Bard et al., 1990), the Mediterranean area (Lambeck et al., 2011) and the global one (Lambeck et al., 2014). Timing of parasequences (in red) evolution within the Pescara paleovalley system. Relative sea-level (RSL) index points from tectonically stable areas of the western Mediterranean are from Vacchi et al. (2016). LST: lowstand systems tract; TST: transgressive systems tract; HST: highstand systems tract; TS: Transgressive surface; MFS: Maximum flooding surface; LGM: Last Glacial Maximum; MWP: Melt water Pulse; S-MWP: Melt water pulse surface; A: aggradational stacking pattern; R: retrogradational stacking pattern; P: progradational stacking pattern; Bw: brackish water; Fw: freshwater; SL: sea-level. Modified after Amorosi et al. (2017b).

## 5.7.2 Influence of post-Younger Dryas episodes of glacio-eustatic sea-level rise

### 5.7.2.1. Melt Water Pulse 1B

Early Holocene poorly-drained conditions (P1) have also been documented for coeval (post-12 ka cal BP) successions within the Adriatic basin as the Biferno PVF (Amorosi et al., 2016b) and the Emilia-Romagna coastal sector (P1 of Amorosi et al., 2017b). Comparable and coeval transitional deposits between alluvial and fully-estuarine have also been recognized outside the Adriatic domain, beneath the Tyrrhenian coastal plains (Amorosi et al., 2008; Milli et al., 2016) but also worldwide from Northern Europe to the Asian coasts (Hijma et al., 2009; Tanabe et al., 2015; Hori et al., 2002). The basal surface of P1 is the TS: this surface, dated to about 11.3 ka cal BP, clearly marks the end of a remarkable phase of fluvial activity, as suggested by the upward change in fluvial stacking pattern atop LST deposits (Fig. 4), also illustrated by Campo et al. (2017) from the Po coastal succession. Chronological and stratigraphic data make the TS correlative offshore with the Melt Water Pulse (MWP) 1B (Fairbanks, 1989; Liu et al., 2004) surface (Zecchin et al., 2015; their Fig. 8). This latter, in turn, coincides with the “S2 surface” of Maselli et al. (2011) that separates middle from upper-TST units and that marks the end of a short-lived episode of subaqueous progradation assigned to the Younger Dryas reversal (i.e., 12.9-11.6 ka cal BP; Cheng et al., 2020). The P1 flooding event, thus, could have been triggered by the post-Younger Dryas sea-level rise linked to the MWP-1B dated to about 11.6-11.3 ka cal BP (Fairbanks, 1989; Fig. 5). MWP-1B is not well documented as MWP-1A, and defined as elusive in far-field sea-level records (Lambeck et al., 2014; Harrison et al., 2019; Tian et al., 2020). Abrupt change in fluvial stacking pattern and rapid establishment of inner-estuarine conditions documented for the Pescara coastal plain, along with data presented by Amorosi et al. (2017b) for the northern sector, strongly support evidences of the MWP-1B effects in the Mediterranean Sea. An estimated sea-level about 50 m below the present, around 11.3 ka cal BP (Lambeck et al., 2014, their Fig. 4), is only seemingly inconsistent contrast with the TS elevation (between 43-33 m bsl, Fig. 4b), for the following reasons: (i) possible unreliability of the sea-level curve (Lambeck et al., 2014) that does not take into account data from the Mediterranean Sea (their Fig. 1); (ii) the inland position of the study area (Fig. 1); (iii) the steepness of the Central Adriatic shelf (0.2°; Maselli et al., 2011). As for this latter aspect, the TS shows a remarkable change in elevation (10 m in less than 2 km; see Fig. 4b). As regard the position of the study area with respect to the coastline at about 11.3 ka cal BP, this is supported by the non-marine facies associations of P1 (poorly drained floodplain and swamp). Within P1, a minor flooding dated to 10.3 ka cal BP is coeval with a

barrier lagoon system identified in the northern Adriatic shelf by Storms et al. (2008) which was not correlated to the MWP-1B. On the contrary, MWP-1B sea-level rise effects have been documented in the Southern Adriatic, Manfredonia Gulf, by De Santis et al. (2020b). Here, MWP-1B has been thought to have caused the drowning and overstepping of previous coastal systems and the formation of a wave ravinement surface.

#### *5.5.7.2.2. Melt Water Pulse 1C*

Correlation of the overall stratigraphy with the sea-level curves (Fig. 5) documents the possible link between the minor flooding surface dated to about 9.8 ka cal BP and the beginning of MWP-1C, whereas the 9.4 cal ky BP flooding is simultaneous to the coeval glacio-eustatic event. Following Zecchin et al. (2015), the 9.8 ky BP flooding has been labelled as the MWP-1C surface (S-MWP1C of Fig. 5). Major effects of the post-MWP-1C sea-level rise are distinctly recorded by P2, which shows the most widespread landward incursion of inner-estuarine environments in the study area. Comparable remarkable effects of the post-MWP 1C sea-level rise are well documented in the Northern Adriatic sector. In the Po coastal Plain, Amorosi et al. (2017b) and Bruno et al. (2017) showed the widespread landward incursion of inner-estuarine environments. The age of their P2 is almost identical (9.2-7.7 ka cal BP) to the age of the Pescara parasequence P2 (9.2-8.3 ka cal BP; Fig. 5). Similarly, in the Tagliamento River Plain, Ronchi et al. (2021) dated to about the same age interval (9.4 to 8.4 ky BP) equivalent organic-rich deposits termed as “basal-peat”. To the south, the Biferno VF (Amorosi et al., 2016b), between 18 and 11 m depth, is also characterized by a coeval and predominantly swampy interval. As for the Pescara P2, the top of this interval is dated to about 8.3 ka cal BP (8,264±65 ka cal BP; their Fig. 5). Even more interesting, is the chronological equivalence with the “Eu-transgressive unit” of the Manfredonia Gulf, dated to 9.2-8.3 ka cal BP (De Santis et al., 2020a). Similar successions have been documented for the Tyrrhenian coast (Amorosi et al., 2013a), and worldwide in the Rhine Delta (Amorosi et al., 2013b), in the Song Hong River (Hori et al., 2004) and the Pearl River (Zong et al., 2009). As different sectors of the Adriatic Sea and coastal plain successions around the world recorded concomitant deposition of similar organic-rich facies associations, it seems that post MWP-1C sea-level rise played a key role as eustatic factor not only at the basin-scale (Adriatic) but also globally.

### 7.2.3. Melt Water Pulse 1D

The transition to P3 marks the establishment of brackish environments in the study area. The basal P3 flooding was identified as the MWP-1D surface (MWP1D-S of Fig. 5), because it post-dates an 8.3 ka cal BP swamp deposit (Fig. 4). The Biferno and the Po coastal Plain successions present similar ages (about 8.3 ka cal BP) for the transition from swamp (inner-estuarine) strata to overlying brackish (outer-estuarine) deposits, dated to 8.0-7.7 ka cal BP respectively (Amorosi et al., 2017b, 2016b). Most likely MWP-1D produced the maximum landward migration of the barrier-lagoon systems, around 8.0-7.7 ka cal BP, as recorded for the study area (Figs. 4 and 5), for different sectors of the Adriatic (Amorosi et al., 2017b, 2016b; Ronchi et al., 2021) and beyond (Amorosi et al., 2013a, b). The age of the MFS is consistent with the 8.0-7.0 ka cal BP age documented for the same surface in several coastal successions (Amorosi et al., 2008; Breda et al., 2016; Hori et al., 2004; Milli et al., 2013; Tanabe, 2020; Tanabe et al., 2022, 2015). In particular, it matches the age of the MFS in the Biferno PVs (Amorosi et al., 2016b) and in the northern Adriatic sector (Amorosi et al., 2017b). A possible alternative position for the MFS is within P4 (i.e., intra parasequence) atop lagoonal deposits dated to 7.8 ka cal BP (Figs. 4 and 5). An age of about 7.7 ka cal BP fits the MFS age reported from different coastal successions mentioned above, especially the MFS documented from Amorosi et al. (2017b). As reported by Tanabe (2020), analogous sea-level rise events have been inferred for MWP-1D between 7.8 and 6.8 ka cal BP for different locations worldwide (Blanchon et al., 2002; Bird et al., 2007; Song et al., 2018; Yu et al., 2007). Comparison of sea-level curve from Lambeck et al. (2011) and index points from Vacchi et al. (2016; Fig. 5) shows that in the Mediterranean Sea, the maximum sea-level jump linked to the MWP-1D ended about 7.5 ka cal BP (Fig. 5). The effects of the flooding driven by MWP-1D are not recorded after 7.0 ka cal BP, when sea-level stabilized (Fig. 5). According to our reconstruction, the 7.0 ka cal BP flooding and its correlative lagoonal deposits likely represent the very “last ditch effort” of MWP-1D in this sector of the Adriatic before coastal system progradation took place.

The Pescara Holocene succession (TST+HST) has many similarities in terms of facies architecture with coeval successions along the Adriatic basin and worldwide (Amorosi et al., 2017b; Milli et al., 2016; Ruberti et al., 2018; Hijma et al., 2009; Tanabe et al., 2006; Hori et al., 2002; Blum et al., 1995; Blum and Aslan, 2006; Blum and Price, 1998; Payenberg et al., 2006; Rittenour et al., 2007; Thomas and Anderson, 1994; Ronchi et al., 2021; Jessen et al., 2008; Shaver and Pusc, 1992; Seifert et al., 2008; Hickin and Best, 2013; Barnes et al., 2021; Goetz et al., 2021; Ta et al., 2021), confirming the

basin-scale importance of the eustatic component as the major controlling factor during Termination 1 (Denton et al., 2010).

As a whole, this investigation has documented a clear influence of the stepwise sea-level jumps caused by the MWPs 1B, 1C, and 1D on the stratigraphic architecture of the Pescara paleovalley fill. These events are still considered as local phenomena by some authors (see Tanabe, 2020), because their effects were not identified globally and there is not yet full consensus on their timing and magnitude. However, as also reported in this study, many works documented that eustatic rise episode was not smooth and gradual, but punctuated. Compared to MWPs 1A and 1B (Bard et al., 2010; Abdul et al., 2016; Tian et al., 2020), MWPs 1C and 1D are thought to have been less marked (Zecchin et al., 2015) and poorly documented, especially in the Mediterranean area, as previously documented by Amorosi et al (2017b) for the Northern Adriatic. Hence, this study provides data for future refinements of the post-LGM sea-level curve for this Mediterranean sector.

## 5.8 Conclusions

A buried paleovalley system (PVS), about 50 m deep and up to 2 km wide, was recognized beneath the Pescara coastal plain through stratigraphic correlation based on sedimentological, paleontological (meiofauna and mollusks), chronological and geotechnical (pocket penetrometer measurements) data. Detailed facies analysis was carried out on a 52 m-long core specifically recovered in the valley depocenter.

Two NE-SE and SW-NE oriented stratigraphic panels provided the 3D-facies architecture of the Late Pleistocene-Holocene paleovalley fill (PVF), and allowed the reconstruction of the paleovalley profile, incised into Calabrian age marine deposits. The general facies architecture and fluvial stacking patterns resemble the stratigraphic organization of several ancient and Quaternary paleovalley systems worldwide, with the lower paleovalley fill (l-PVF), composed of up to 13-m-thick, amalgamated fluvial gravel bodies of Late Pleistocene age (30-pre-11.3 ka cal BP), interpreted as the lowstand systems tract (LST), because of its overall aggradational stacking.

The mud-dominated, Holocene upper paleovalley fill (u-PVF) with isolated sand bodies is about 25 m-thick and consists mostly of non-marine, organic-rich deposits with low pocket penetrometer values (0.4-1.8 g/cm<sup>2</sup>). The vertical transition from poorly-drained floodplain facies to swamp clays to lagoonal deposits reflects progressive drowning of the valley and formation of an estuary, as a result of the Holocene transgression. During the last 8.0 ky, the estuary was progressively filled up to the establishment of the modern wave-dominated delta plain environment.

The abrupt facies change from the Late Pleistocene l-PVF to the Holocene u-PVF corresponds to the transgressive surface (TS), dated to about 11.3 ka cal BP. The early Holocene (11.3-8.0 ka cal BP) interval with a deepening-upward trend represents the transgressive systems tract (TST). The maximum flooding surface (MFS), dated to about 8.0 ka cal BP was tracked at the turnaround from deepening-upward to shallowing-upward trend and marks the maximum landward migration of barrier-lagoon systems, with outer-estuarine deposits reaching their innermost position up to 1.5 km landward of the modern shoreline. The last 8.0 ky succession, with a characteristic shallowing-upward trend from estuarine to modern delta plain deposits, is interpreted as the highstand systems tract (HST). The age of the MFS is consistent with the 8.0-7.0 ka cal BP age documented for the same surface in several coastal successions worldwide.

Seven parasequences (Ps 1-7) were identified and tracked within the Holocene interval (TST+HST). The lower three (Ps 1-3) are retrogradationally stacked and form the TST, whereas the

uppermost four (Ps 4-7) with peculiar aggradational to progradational stacking pattern make the HST. Based upon paleontological data and consistent with the stacking pattern of parasequences (retrogradational-aggradational to progradational), the MFS is placed between 8.0 ka cal and 7.7 ka cal BP. However, its positioning can be debated and, an alternative position beyond parasequences and flooding boundaries could be within P4, at the transition from lagoonal and swamp deposits, dated to about 7.7 ka cal BP.

Transgressive Ps 1-3 record the overall drowning of the valley and the onset of estuarine conditions. Due to the general sea-level rise, progressively deeper conditions, from inner- (Ps 1-2) to outer-estuarine (P3), were established in the study area. Between 8.0-7.0 ka cal BP sea-level stabilized and once the estuary was filled with freshwater organic-rich deposits (aggradational P4), coastal progradation definitively started (P5). In the last 5.2 ka cal BP (Ps 6-7) further coastal progradation took place. Coastal plain facies accumulated landward, whereas a wave-dominated fluvio-deltaic system developed at distal locations.

In general, TST parasequences display higher accumulation rates (up to 9.4 mm/y) than HST ones. These latter are characterized by a mean value of about 2.9 mm/y. High-sediment accumulation rates may reflect generation of accommodation caused by the rapid eustatic sea-level rise. On the other hand, under highstand conditions, sedimentation rates progressively decreased suggesting rapid progradation of the coastal system basinwards.

The Pescara PVS is the first example of late Quaternary PVs identified in front of the Mid-Adriatic Depression (MAD) basin, and represents the essential “onshore component” of the Adriatic system in a source-to-sink (S2S) perspective. The paleovalley, from a region of sediment storage during the transgression (11.3-8.0 ka cal BP) turned into a sector of prevailing lateral sediment distribution under highstand conditions (last 8.0 ky).

A first correlation with offshore data and comparison with coeval successions along the Adriatic basin (and worldwide) show many similarities in terms of facies/stratigraphic architecture and confirm the key role of eustatic sea-level rise as the major controlling factor during the post-LGM transgression, providing new evidence for Melt Water Pulses (MWP) 1B, 1C and 1D. The eustatic rise linked to MWP-1B reasonably triggered the P1 flooding event and the first establishment of inner-estuarine conditions tens of kilometers landwards of the coastline.

The Pescara valley fill also records the influence of minor and still poorly documented around the world MWP 1C and 1D. Whilst the minor 9.8 ka cal BP flooding surface was linked to the beginning of MWP-1C, major effects of the post-MWP-1C sea-level rise in the study area are clearly recorded

by P2. Similar to what was documented for several coeval successions of the Adriatic, P2 is characterized by the most widespread landward incursion of inner-estuarine deposits in the study area. The onset of MWP-1D is marked by the basal P3 flooding that highlights the onset of the very last backstepping episode of a barrier-lagoon system in this Central Adriatic sector, consistent with data from Amorosi et al. (2017b) for the Northern Adriatic. Hence, MWP-1D can be considered as the most important trigger for the maximum landward migration of the shoreline at the basin-scale.

## Authors contribution

Bruno Campo: conceptualization, methodology, formal analysis, investigation, data curation, writing - original draft, visualization, project administration. Barbieri Giulia: formal analysis, investigation. Di Martino Andrea: investigation. Hong Wan: formal analysis. Scarponi Daniele: formal analysis, writing review & editing. Vaiani Stefano Claudio: formal analysis, writing review & editing. Amorosi Alessandro: supervision, writing review & editing, project administration, funding acquisition.

## Acknowledgments

This work was supported by the Italian Ministry of University and Research under the PRIN 2017 program, project number 2017ASZAKJ “*The Po-Adriatic Source-to-Sink system (PASS): from modern sedimentary processes to millennial-scale stratigraphic architecture*”, grant to Prof. Alessandro Amorosi. We are grateful to the two anonymous reviewers for their very useful and constructive comments.

## 6. Reconstructing late Quaternary paleovalley systems of Italy through mHVSR: A tool for seismic hazard assessment in modern coastal lowlands

Andrea Di Martino<sup>1</sup>, Giulia Sgattoni<sup>2</sup>, Gianluigi Di Paola<sup>3</sup>, Matteo Berti<sup>1</sup>, Alessandro Amorosi<sup>1</sup>

<sup>1</sup> Department of Biological, Geological and Environmental Sciences (BiGeA), University of Bologna.  
Piazza di Porta San Donato 1, 40126, Bologna, Italy

<sup>2</sup> Istituto Nazionale di Geofisica e Vulcanologia, Sezione di Bologna, viale Berti Pichat 6/2, 40127  
Bologna, Italy

<sup>3</sup>Department of Biosciences and Territory (DiBT), University of Molise, Pesche (Isernia), Italy

## Abstract

Effective site characterization in highly urbanized coastal lowlands requires accurate stratigraphic and geophysical investigations. In these regions, which typically host shallowly buried paleovalley systems formed in response to Quaternary glacio-eustatic fluctuations, the marked lithologic contrast between soft sediment paleovalley fills and the adjacent, stiff substrate has the potential to modify earthquake motions, and assessment of critical parameters, such as shear wave velocities ( $V_s$ ) and resonance frequencies ( $f$ ), should be coupled with detailed stratigraphic architecture. To evaluate the potential of the microtremor horizontal-to-vertical spectral ratio (mHVSr) for paleovalley recognition and mapping, we performed mHVSr measurements along the Adriatic coastal plain of Italy, where two paleovalley systems (Pescara and Manfredonia) have been recently identified. In both areas, we detected rapid lateral variations in resonance frequencies and highlighted laterally-continuous impedance contrasts. Relying on a robust stratigraphic framework, we carefully evaluated the relation between geological and geophysical data and identified the stratigraphic surfaces responsible for the observed resonances. We derived  $V_s$  models for the sediment fill, reconstructing the geometry of the two buried paleovalleys. We address the importance of evaluating the geological context when designing microzonation studies, for a reliable interpretation of changes in resonance frequencies.

## Plain Language Summary

When earthquakes occur, buildings shake differently based on several factors, including seismic wave velocity, natural resonance frequencies, and local geological characteristics. Beneath modern coastal lowlands, the presence of paleovalley systems can significantly modify the ground motion. Identification of these buried bodies is therefore essential to assess and reduce seismic hazard. Paleovalleys are shallow incisions formed under periods of fluvial erosion in response to Quaternary climate fluctuations, and subsequently filled with very soft clay. These bodies are found worldwide, and do not have any geomorphological evidence, making their recognition challenging. Geologists typically use expensive sediment core analysis to identify paleovalleys, but this method can only provide spotty information. Geophysical exploration techniques that rely on microtremors (small vibrations on the Earth) can complement mapping of these buried bodies. In this work, we tested this technique in Pescara and Manfredonia (Adriatic coastal plain, Italy), providing dense information about paleovalley geometries and geophysical parameters crucial for predicting how the ground will

shake during an earthquake. This study also highlights the importance of integrating disciplines to improve our understanding of subsoil and to design future studies to mitigate seismic hazards.

### Key Points

- Paleovalley fills are key sediment bodies made up of soft clay, tens of m thick and few km wide, buried beneath coastal lowlands worldwide
- Microtremor-based paleovalley profiles and stratigraphic cross-sections exhibit strong similarity
- Microtremors can provide shear-wave velocities and resonance frequencies of paleovalleys, key parameters for seismic hazard mitigation

### Index Term

Microzonation and macrozonation, Risk, Exposure, Earthquake ground motions and engineering seismology, Europe

### Keywords

Site characterization, Resonance frequency, Paleovalley, Ambient seismic noise, Single-station technique, Seismic hazard

## 6.1 Introduction

The prevention of earthquake disasters is an ever-evolving scientific field that relies on contributions from a wide range of disciplines, including civil engineering, geology, and geophysics. Comprehensive site characterization is essential for predicting seismic site effects; it requires accurate reconstruction of subsurface features, including the physical properties of rocks and sediments. In particular, for precise ground motion simulations, shear wave velocities ( $V_s$ ) and resonance frequencies are critical parameters [Chandler et al., 2006; Del Monaco et al., 2013] that should be coupled with detailed three-dimensional modeling of buried stratigraphic architecture.

Delineating lithology and sediment thickness, alongside geophysical and geotechnical properties, is essential in engineering geology, as it plays a critical role in ensuring stable building foundations and understanding local seismic effects (Suopios et al., 2007; Verma et al., 2014). Many site effects studies focus on the vertical 1D characterization of sediment thickness, usually by oversimplifying the lateral variability, while site-specific stratigraphic architecture may significantly influence the frequency content and amplitude of ground motion (Thompson et al. 2009; Boore, 2004; Hallal et al., 2023).

The thickness of soft, unconsolidated Quaternary deposits, in particular, may vary significantly in the subsurface of big cities where millions of people live and can dramatically be increased by the presence of buried paleovalley systems.

Late Quaternary paleovalley systems (Blum and Törnqvist, 2000), also known as incised valleys (Van Wagoner et al., 1990), are shallow subsurface incisions formed under prolonged periods of fluvial erosion due to base-level fall, followed by valley filling in response to the rapid sea-level rise (Blum et al., 2013). The paleovalley size is a function of relative sea-level change, water supply, sediment discharge, and local geology and may differ significantly from valley to valley. Paleovalley thickness, typically tens of meters, may exceed 50 m, while width can vary from 2 km to over 15 km (Maselli et al., 2014; Amorosi et al., 2016, 2023; Campo et al., 2022). Paleovalley fills typically have economic value, as they might contain abundant hydrocarbon and water reserves (Dalrymple et al., 1994; Posamentier and Vail, 1988). In addition, these sediment bodies have the potential to modify earthquake ground motion due to their complex lenticular geometry and sharp contrast in geotechnical properties between the very soft clayey fill and generally overconsolidated substrate (Ishihara et al., 2013; Tanabe et al., 2015; 2021).

Late Quaternary paleovalley systems are found worldwide (Li et al., 2000; Anderson et al., 2016; Ishihara and Suggai, 2017; Hori et al., 2023), buried beneath modern coastal lowlands and delta plains, and do not have any geomorphological expression; the progressive drowning of the valley, followed by sedimentation above the interfluves, leads to complete obliteration of the primary erosional feature, making paleovalley identification and reconstruction challenging. In Italy, the stratigraphic architecture of late Quaternary paleovalley systems has been documented from the Tyrrhenian Sea coast (Amorosi et al., 2009, 2012, 2013; Milli et al., 2013, 2016), the Ionian Sea coast (Tropeano et al., 2013) and the Adriatic Sea coast (Fontana et al., 2008; Maselli and Trincardi, 2013; Mozzi et al., 2013; Maselli et al., 2014; De Santis and Caldara, 2014; Amorosi et al., 2016, 2017, 2023; Morelli et al., 2017; Ronchi et al., 2018, 2021; Campo et al., 2022). However, detailed geophysical studies and accurate seismic site characterization including resonance frequencies and shear wave velocity of Quaternary paleovalley systems have never been undertaken, so far.

Recently, the Geological Survey of Japan has investigated the physical properties, geometry, and stratigraphic architecture of a Quaternary paleovalley fill beneath the Tokyo and Nakagawa lowlands of the Kanto Plain to mitigate earthquake damage (Ishihara et al., 2013; Tanabe et al., 2015). In this area, paleovalley fills mainly consist of unconsolidated clays, which can amplify seismic waves leading to higher ground shaking (Tanabe et al., 2021). Furthermore, based on data from the 1923 earthquake disaster, Tanabe et al. (2021) established a link between the spatial distribution of the buried paleovalley fill, resonance frequencies, and structural damage to buildings. Reconstructing paleovalley geometries, therefore, is fundamental for a better understanding of seismic site effects.

Buried paleovalley geometries may vary significantly on very short distances (hundreds of m), from the valley flanks (interfluves) to their deepest parts (depocenters) (Campo et al., 2022; Amorosi et al., 2023). Traditional sediment core analysis is a quite expensive exploration tool that can provide detailed lithologic characterization of the valley fill, but no information about its geometry. On the other hand, geophysical investigations, such as shallow seismic imaging and electromagnetic surveys, may be negatively affected by anthropic activities and the presence of large buildings, pipes, and power lines. In this scenario, seismic microtremor surveys, introduced by Aki (1957) and then developed by Okada and Ling (1994) and Okada and Suto (2003), can provide an effective exploration tool. Through microtremor recordings, it is possible to obtain shear wave velocity profiles (Horike, 1985; Ohori et al., 2002; Okada, 2003; Parolai et al., 2005; Köhler et al., 2007) and also perform the microtremor-based horizontal-to-vertical spectral ratio (mHVSR). The mHVSR

method, or simply H/V, was introduced in Japan by Nogoshi and Igarashi (1971) and then popularized by Nakamura (1989, 2000). This geophysical technique is widely used owing to its simplicity and the large amount of information it can provide. In addition, it is widely recognized that the H/V technique offers reliable estimations of the resonance frequency of the surface resonating layer, which is related to sediment thickness, making this technique a fast and powerful stratigraphic tool (e.g. Ibs-Von Seht and Wohlenberg, 1999; Parolai et al., 2001, 2002; Castellaro and Mulargia, 2009; Grippa et al., 2011; Tropeano et al., 2011; Sgattoni and Castellaro, 2020; 2021).

To evaluate the potential of mHVSr as an exploration tool for mapping *late* Quaternary paleovalleys, we performed a series of measurements in two areas (Pescara and Manfredonia) along the Adriatic coastal plain of Italy (Fig. 1). Here two paleovalley systems have been recently identified and thoroughly described in terms of high-resolution sequence stratigraphy (Campo et al., 2022; Amorosi et al., 2023). Using the robust stratigraphic framework around these sites as a reference and through the acquisition of microtremor measurements along two transects perpendicular to each paleovalley longitudinal axis, the aims of this paper are: (i) to identify variations in resonance frequencies along the transects highlighting laterally-continuous impedance contrasts, (ii) to carefully evaluate the relation between geological and geophysical data and possibly identify the stratigraphic surfaces responsible for the observed resonances, (iii) to derive  $V_s$  models for the sediment fill in the two paleovalleys, and (iv) to estimate the thickness of the soft Holocene valley fills, thus reconstructing the buried paleovalley geometries.

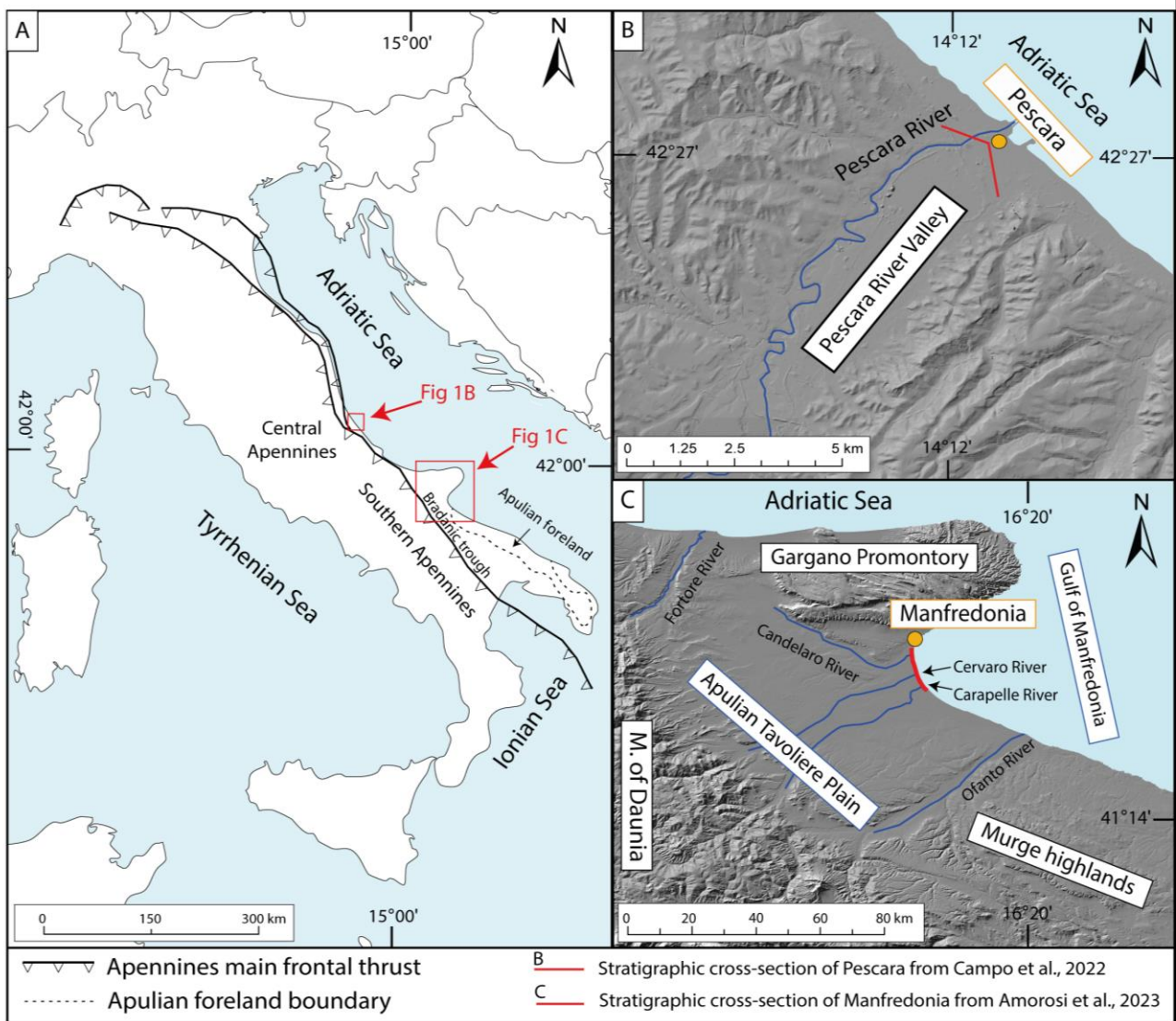


Fig. 1. Location of the two study areas (A): the Pescara (B) and Manfredonia (C) coastal lowlands

## 6.2 Geological background

### 6.2.1 Paleovalley systems: Formation, evolution, and facies architecture

Global climate changes, including cyclic variations in ice volume and sea level, controlled the origin and affected the evolution of paleovalley systems during the Quaternary (Blum et al., 2013). Middle to Late Pleistocene paleovalley systems, in particular, display characteristic cycles of erosion and sedimentation (Anderson et al., 2004; Busschers et al., 2007) that reflect glacial-interglacial cycles with a periodicity of ~100 kyr, following the eccentricity of the Earth's orbit. Higher-frequency rhythms predicted by the Milankovitch theory of orbital forcing, including ~43 kyr cyclic changes in axial tilt (Shackleton and Opdyke, 1973; Imbrie and Imbrie, 1986; Martinsen et al., 1987; Lisiecki and Raymo, 2007) and ~20 kyr precessional cycles (Prell and Kutzbach, 1992), played a major role in modulating facies architecture of glacial-interglacial depositional cycles. In particular, the late Quaternary paleovalley systems recognized worldwide in the subsurface of modern coastal plains reflect fluvial incision that took place at the transition from Marine Isotope Stages (MIS) 3 to MIS 2 (Amorosi et al., 2017), which was associated with a significant sea-level drop (Lambeck et al., 2014).

The evolution of late Quaternary paleovalleys in the coastal plain exhibits four distinct phases corresponding to a complete cycle of base-level fall and rise ([Fig. 2](#)):

(i) During period of relative sea-level fall, rivers cut into the substrate, and the valley system shows a degradational pattern with characteristic step-wise incision (Blum, 2007; Rittenour et al., 2007; Blum et al., 2008). Significant sediment by-pass characterizes the valley in this stage, though fluvial deposits may be preserved locally as alluvial terraces against the valley flanks. The erosional basal valley unconformity is the sequence boundary (SB, Fig. 2). In the adjacent interfluves, SB is generally expressed as a paleosol, i.e. a soil formed on a past landscape in response to subaerial exposure that was buried subsequently with valley evolution (interfluvial sequence boundary of Van Wagoner et al., 1990; Aitken and Flint, 1996).

(ii) Under lowstand sea-level conditions, fluvial sedimentation occurs within the valley, forming a characteristic amalgamated gravel or sand body at the valley bottom. This lower valley fill (Blum et al., 2013) is composed of fluvial channels and levee facies representing deposits of migrating and confined channels that cannot avulse outside the paleovalley boundaries (Gibling et al., 2011).

(iii) With relative sea-level rise, valleys are progressively drowned, and fine-grained estuarine facies are deposited above the fluvial deposits, forming the upper valley fill. The transgressive surface (TS, Fig. 2), which marks the first significant flooding event (Posamentier and Vail, 1988; Posamentier et al., 1988; Van Wagoner et al., 1990; Zaitlin et al., 1994) separates the gravel or sand fluvial channel-belt from the overlying mud-dominated upper valley fill. Generally, transgressive deposits include a vertical succession of freshwater to brackish estuarine facies formed within the zone of backwater effect during sea-level rise as a landward-tapering wedge (Blum et al., 2013).

(iv) With continuing relative sea-level rise, the valley is filled, the interfluves are drowned, and coastal to shallow-marine environments develop above the paleovalley fill. Above the maximum flooding surface (MFS, Fig. 2), which records the maximum marine ingressions, prograding coastal and deltaic facies typically cap the succession.

This work expands upon the recent, detailed sedimentological characterization of two paleovalley fills in the Adriatic coastal plain: the Pescara paleovalley (Campo et al., 2022) and the Manfredonia paleovalley (Amorosi et al., 2023). The simplified stratigraphic architecture of these two paleovalley systems is summarized in the following sections.

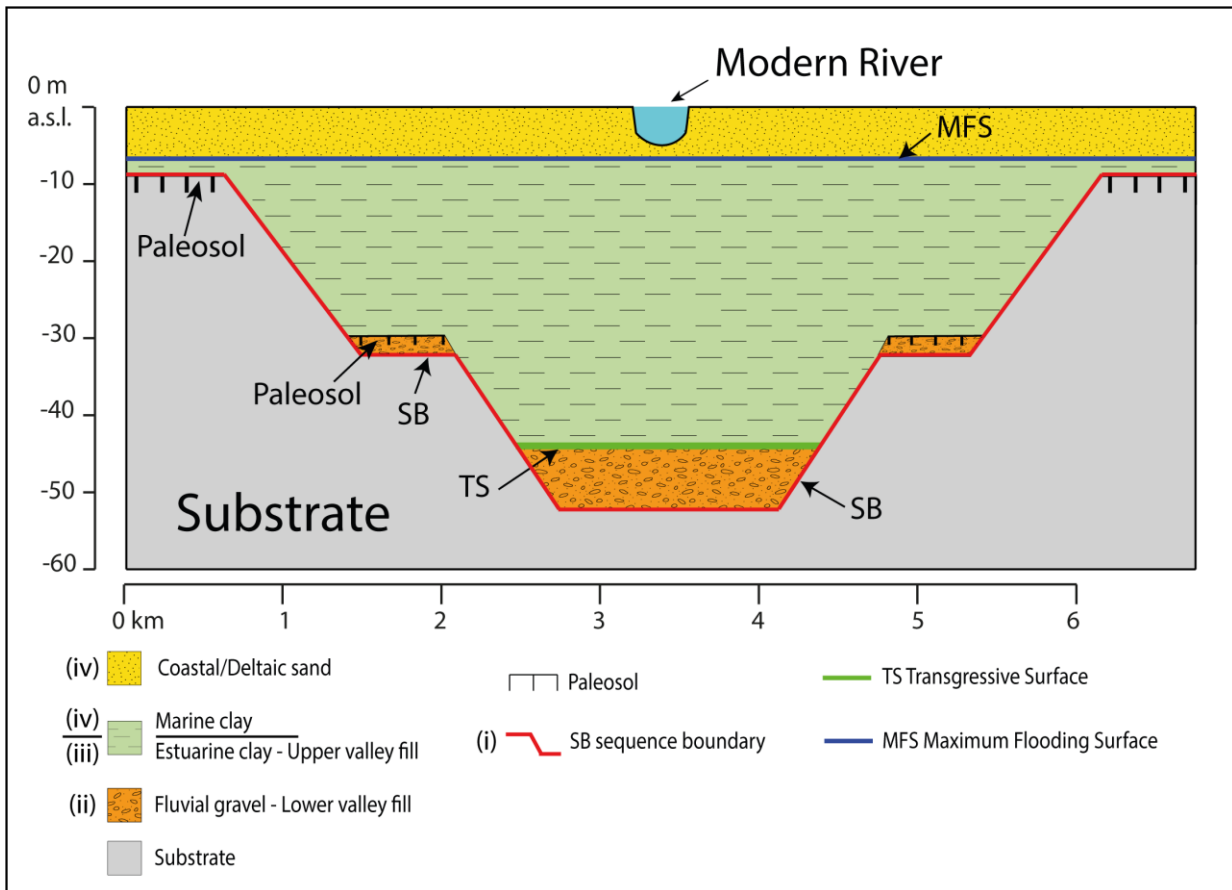


Fig. 2. Simplified conceptual paleovalley model, with typical sedimentary fill and key sequence stratigraphic surfaces: Sequence Boundary (SB), Transgressive Surface (TS), Maximum Flooding Surface (MFS). (i), (ii), (iii), and (iv) refer to the distinct phases of formation and evolution in chapter 2.1

### 6.2.2 The Pescara paleovalley

The Pescara coastal plain (Fig. 1B) in Central Italy is a 3.3 km<sup>2</sup> wide region, narrowly constrained between the Central Apennines and the Adriatic Sea, that hosts the Pescara River mouth. The Pescara River, fed by two main tributaries, Aterno and Sagittario, is the longest river in the Abruzzo region, at over 150 km, and drains a hydrographic basin of about 3170 km<sup>2</sup> (Urbano et al., 2017).

In the Pescara River valley, a Pliocene-Lower Pleistocene succession of marine deposits, up to 2000 meters thick, is overlain by a Middle Pleistocene-Holocene succession of alluvial deposits in transition to younger coastal facies.

The stratigraphic architecture of the Pescara paleovalley has been recently illustrated by Campo et al. (2022) (Fig. 3). The dataset (Campo et al., 2022) consists of borehole descriptions down to 45 m depth available from the seismic microzonation project of Pescara Municipality, supplemented by the 52 m-long reference core “Marconi”, for which seventeen closely-spaced radiocarbon dates are available (Campo et al., 2022). The paleovalley profile and facies architecture were reconstructed based on sedimentological, stratigraphic, geotechnical, and paleontological data. The sequence boundary (SB) is an erosional surface that marks the abrupt facies change between Lower Pleistocene marine silty clays (Mutignano Fm, and pocket penetrometer value > 5 kg/cm<sup>2</sup>) and the overlying paleovalley fill. The lower paleovalley fill consists of a laterally extensive, up to 14 m-thick fluvial gravel body accumulated during the Last Glacial Maximum (Fig. 3). The basal gravel body is overlain by the upper paleovalley fill of Holocene age, up to 25 m thick, composed of soft (pocket penetrometer values < 1 kg/cm<sup>2</sup>), organic-rich silty clay accumulated in poorly-drained (inner-estuarine) to brackish (outer-estuarine) depositional environments, in response to the post-glacial sea-level rise. The abrupt facies change from fluvial gravels to mud-dominated strata corresponds to the transgressive surface (TS, Fig. 3). The upper part of the Holocene succession consists of clay-sand fluvial-deltaic deposits, up to 10 m thick, in lateral transition with coastal sands (Campo et al., 2022).

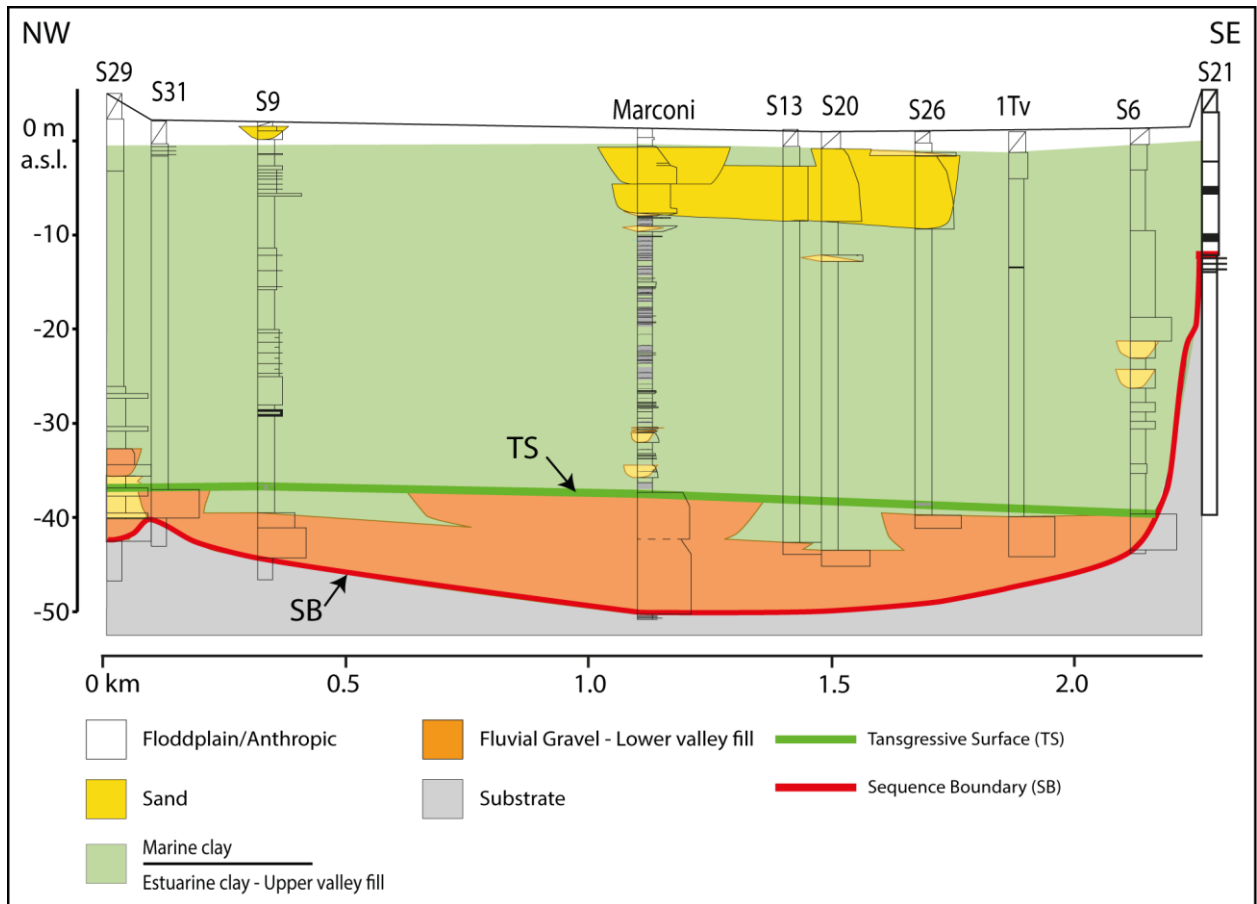


Fig. 3. Simplified stratigraphic cross-section of the Pescara paleovalley with vertical exaggeration (Campo et al., 2022). The stratigraphic cross-section is oriented perpendicular to the main paleovalley axis, the trace of the section is shown in Figure 1

### 6.2.3 The Manfredonia paleovalley system

In southern Italy, the Apulian Tavoliere coastal plain, about 4300 km<sup>2</sup> wide, is bounded by two mountain chains and a promontory (Fig. 1C): the Daunia Mountains to the west, the Gargano Promontory to the north, and the Murge highlands to the south. It extends north to south for about 90 km, from the Fortore River to the Ofanto River. The Tavoliere is the second-largest alluvial plain in Italy and consists of several Quaternary marine and alluvial terraces (De Santis et al., 2014). Four main rivers drain the modern Tavoliere Plain, from north to south: the Candelaro River, 70 km long with a drainage basin (db) of 2435 km<sup>2</sup>, Carapelle River (85 km long, db: 1465 km<sup>2</sup>), Cervaro River (30 km long, db: 625 km<sup>2</sup>), and Ofanto River (170 km long, db: 2780 km<sup>2</sup>).

The Gulf of Manfredonia (Fig. 1) represents the offshore prolongation of the Tavoliere: it is characterized by a microtidal regime and a sea bottom gently sloping to the east. A laterally extensive unconformity, marking the lower boundary of the Manfredonia paleovalley system related to the Last Glacial Maximum, has been recognized in the subsurface of the Gulf of Manfredonia and in the adjacent offshore areas (Trincardi et al., 2011; Maselli and Trincardi, 2013; Maselli et al., 2014; De Santis and Caldara, 2016). This paleovalley is sinuous and elongated for more than 60 km in a W-E direction, running to the mid-outer shelf. Its onshore prolongation has been recently documented through integrated sedimentological and paleontological analysis of three sediment cores, which enabled the detailed characterization of the stratigraphic architecture of the valley fill (Amorosi et al., 2023 and Fig. 4).

The recent stratigraphic analysis of a 50 m-long core from the Manfredonia area, corroborated by 25 radiocarbon data (Amorosi et al., 2023), enabled the reconstruction of the Candelaro paleovalley e.g. the onshore part of the “Manfredonia” incised valley identified by Maselli and Trincardi (2013) (Fig. 4). The internal anatomy of two adjacent Apulian paleovalleys, generated by the Cervaro and Carapelle rivers (Fig. 1C), respectively, was reconstructed based on sedimentological, stratigraphic, geotechnical, paleontological, and geochemical data through a 17-km-long stratigraphic panel (Amorosi et al., 2023 and Fig. 4) oriented roughly parallel to the modern shoreline and transversal to the paleovalley axes. Similar to the Pescara paleovalley system, the sequence boundary coincides with a prominent erosional stratigraphic surface that truncates older marine strata, indicating a deep fluvial incision along the major drainage axis. The lower valley fill (Last Glacial Maximum deposits) consists of laterally amalgamated, up to 10 m thick, fluvial-channel gravel and coarse-medium sand that grade upwards into fine to silty sand (Fig. 4). Above the fluvial

channel sand and gravel, a prominent pedogenized horizon is present, with pocket penetrometer value  $> 6 \text{ kg/cm}^2$ . The upper paleovalley fill succession, accumulated in response to the post-glacial sea-level rise, and includes a vertical succession of estuarine and bay deposits, up to 14 m thick, predominantly made of homogeneous silt and clay (pocket penetrometer value  $< 1 \text{ kg/cm}^2$ ) (Fig. 4). The boundary between the sheet-like amalgamated fluvial body and the overlying mud-dominated succession is interpreted as the transgressive surface (TS, Fig. 4). Above the paleovalley fill, 12 m thick, unconsolidated marine clay is overlain by 14 m-thick shoreface deposits made predominantly of upward-coarsening sand.

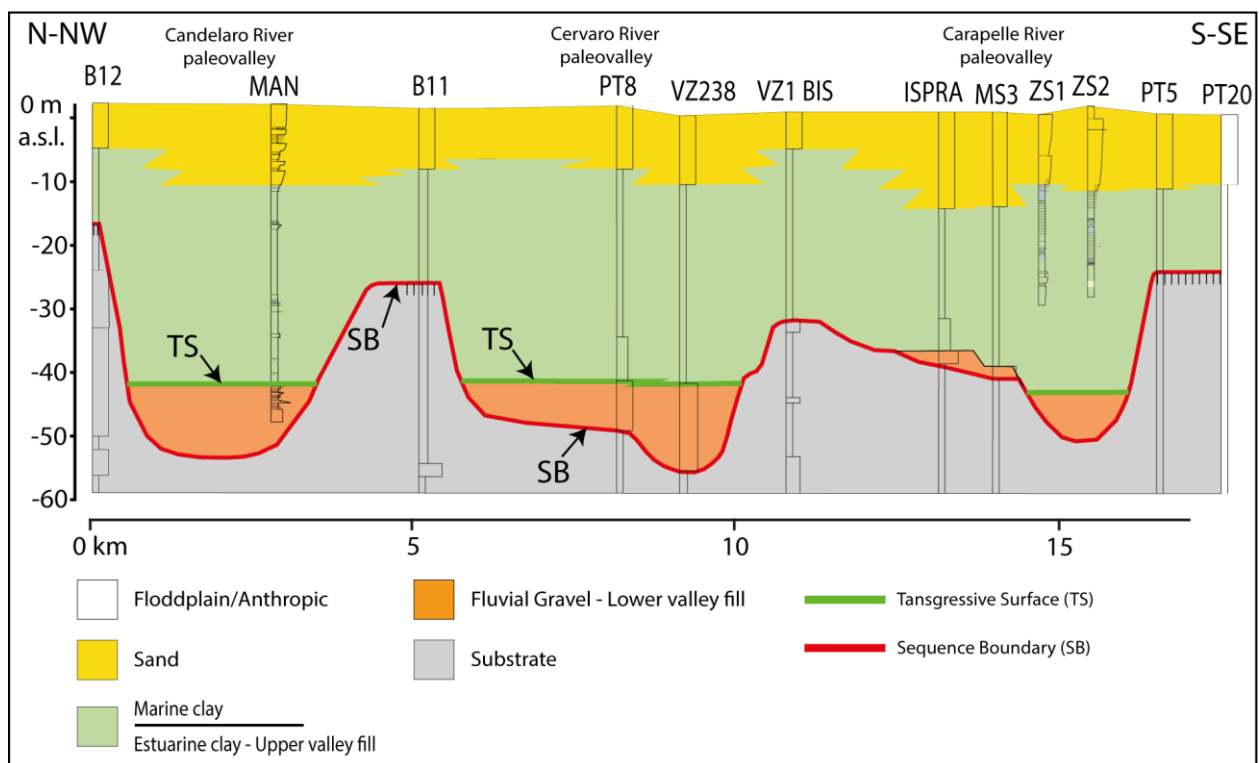


Fig. 4. Simplified stratigraphic cross-section of the Candelaro, Cervaro, and Carapelle paleovalley systems in the Manfredonia study area (Amorosi et al., 2023). The stratigraphic section is perpendicular to the paleovalleys axes; the trace of the cross-section is shown in Figure 1.

## 6.3 Materials and Methods

### 6.3.1 HVSR microtremor measurements

We collected single-station microtremor recordings (Table 1 and Fig. 5) in the Pescara and Manfredonia areas during three field campaigns: in April 2021 and May 2022 for Pescara, and in February 2021 for Manfredonia. All microtremor measurements were carried out using a Tromino® microtremor recorder by MoHo SRL (Italy). This is an all-in-one, 3-component velocity/acceleration portable instrument expressly designed to digitally record seismic noise. The sampling rate was 128 Hz, and the acquisition length was 16 to 30 minutes, chosen based on the supposed substrate depth inferred by previous stratigraphic studies (Campo et al., 2022; Amorosi et al., 2023) and the local level of anthropic noise. A few measurements were repeated at the same sites with a longer acquisition length to ensure stability of the results.

The instrument was oriented parallel to the geographical North-South direction and leveled on the Earth's surface; sensor leveling and ground stability were maintained throughout the record durations. Coupling the instrument to the Earth's surface is crucial; the sensor feet were firmly inserted into soft soil, vegetation was removed, and the sensor was protected from the direct wind (Chatelain et al., 2008). Although the urban environment presents a challenge to the natural free-field conditions (Castellaro and Mulargia, 2009), we collected all data, avoiding recordings on stiff material over soft soil and at least 15 meters away from buildings to minimize their effects (Castellaro and Mulargia, 2010).

The survey was designed to acquire microtremor measurements as close as possible to pre-existing geological data and, where possible, in coincidence with or parallel to the stratigraphic cross-sections of Figures 3 and 4 (see Figure 5 for an overview of all study areas). In Pescara, we acquired 29 mHVSR measurements (Table 1) with about 250 m spacing along an NW-SE oriented, 5 km-long shore-parallel transect crossing the Pescara River (Fig. 5A). In Manfredonia, we acquired 54 mHVSR measurements (Table 1), with spacing ranging from 500 to 1000 m. The recordings were acquired along an NW-SE oriented, 32 km-long shore-parallel transect crossing the Candelaro, Cercaro, and Carapelle rivers (Fig. 5B).

### 6.3.2 Data processing

To perform the microtremor-based Horizontal to Vertical Spectral Ratio (mHVSR), we processed the data with the Grilla software. Each three-component time series was split into non-overlapping windows of equal length (30 s). Fourier spectra were computed for each time window and smoothed with triangular functions having a width equal to 10% of the central frequency. We obtained the mHVSR curves by averaging the mHVSR ratios computed for each window, with H being the geometric average of the instrumental N-S and E-W components. The individual spectral components and mHVSR were calculated in terms of average  $\pm$  standard deviation; transient perturbations were carefully removed by manual selection. To rule out that the results were affected by the chosen processing parameters, a few longer (30 min) recordings were split into longer windows of 60 seconds, and the results did not change.

Pescara			Manfredonia					
Site Name	Resonance Frequency [Hz]	H/V Amplitude [-]	Site Name	Resonance Frequency [Hz]	H/V Amplitude [-]	Site Name	Resonance Frequency [Hz]	H/V Amplitude [-]
P1	3.05 Hz	2	M1	4.50 Hz	3.8	M28	0.95 Hz	3.2
P2	4.03 Hz	2.3	M2	2.97 Hz	3.8	M29	1.05 Hz	2.1
P3	4.20 Hz	3.1	M3	2.46 Hz	4.3	M30	1.1 Hz	2.5
P4	4.30 Hz	3.2	M4	1.62 Hz	2.7	M31	0.94 Hz	2.3
P5	3.8 Hz	4.6	M5	1.62 Hz	2.1	M32	1 Hz	2.8
P6	3.65 Hz	2.3	M6	1.15 Hz	2.1	M33	0.9 Hz	2.6
P7	1.86 Hz	2	M7	0.98 Hz	2.3	M34	0.83 Hz	3
P8	1.58 Hz	2.1	M8	0.92 Hz	2.7	M35	0.86 Hz	2.1
P9	1.24 Hz	1.6	M9	0.91 Hz	3.8	M36	1 Hz	2.3
P10	0.94 Hz	1.6	M10	0.96 Hz	3.9	M37	0.85 Hz	2.3
P11	1.09 Hz	1.7	M11	1.07 Hz	3	M38	1 Hz	2.5
P12	0.97 Hz	1.7	M12	1.14 Hz	2	M39	0.95 Hz	2.4
P13	0.97 Hz	1.8	M13	1.1 Hz	3.2	M40	0.93 Hz	2.3
P14	0.95 Hz	1.9	M14	1.21 Hz	1.5	M41	0.82 Hz	2
P15	1.08 Hz	1.9	M15	1.03 Hz	3.5	M42	0.8 Hz	2
P16	1.23 Hz	1.7	M16	1.06 Hz	2.2	M43	0.82 Hz	1.7
P17	1.14 Hz	1.5	M17	1 Hz	2.3	M44	0.8 Hz	2.1
P18	1.33 Hz	1.5	M18	1.26 Hz	2.3	M45	0.82 Hz	1.7
P19	3.54 Hz	1.6	M19	1.21 Hz	2.1	M46	0.86 Hz	1.6
P20	3.40 Hz	1.9	M20	0.98 Hz	1.9	M47	0.86 Hz	2.3
P21	3.34 Hz	1.8	M21	0.9 Hz	2	M48	0.85 Hz	2.4
P22	3.05 Hz	1.7	M22	0.93 Hz	2.1	M49	1.14 Hz	2
P23	3.56 Hz	1.5	M23	0.88 Hz	3	M50	1.6 Hz	2.5
S18	0.98 Hz	2.3	M24	0.85 Hz	2.9	M51	1.9 Hz	2.4
S19	1.06 Hz	2.6	M25	0.92 Hz	2.7	M52	2.3 Hz	1.3
S24	1.08 Hz	3.8	M26	1 Hz	3.4	M53	2.5 Hz	2.6
S2	1.10 Hz	2.5	M27	1.03 Hz	2.6	M54	2.5 Hz	2.4
S7	1.54 Hz	2.8						
Marconi	1.12 Hz	3.7						

Table. 1. Resonance Frequency and H/V Amplitude of the microtremor measurements acquired for this study.

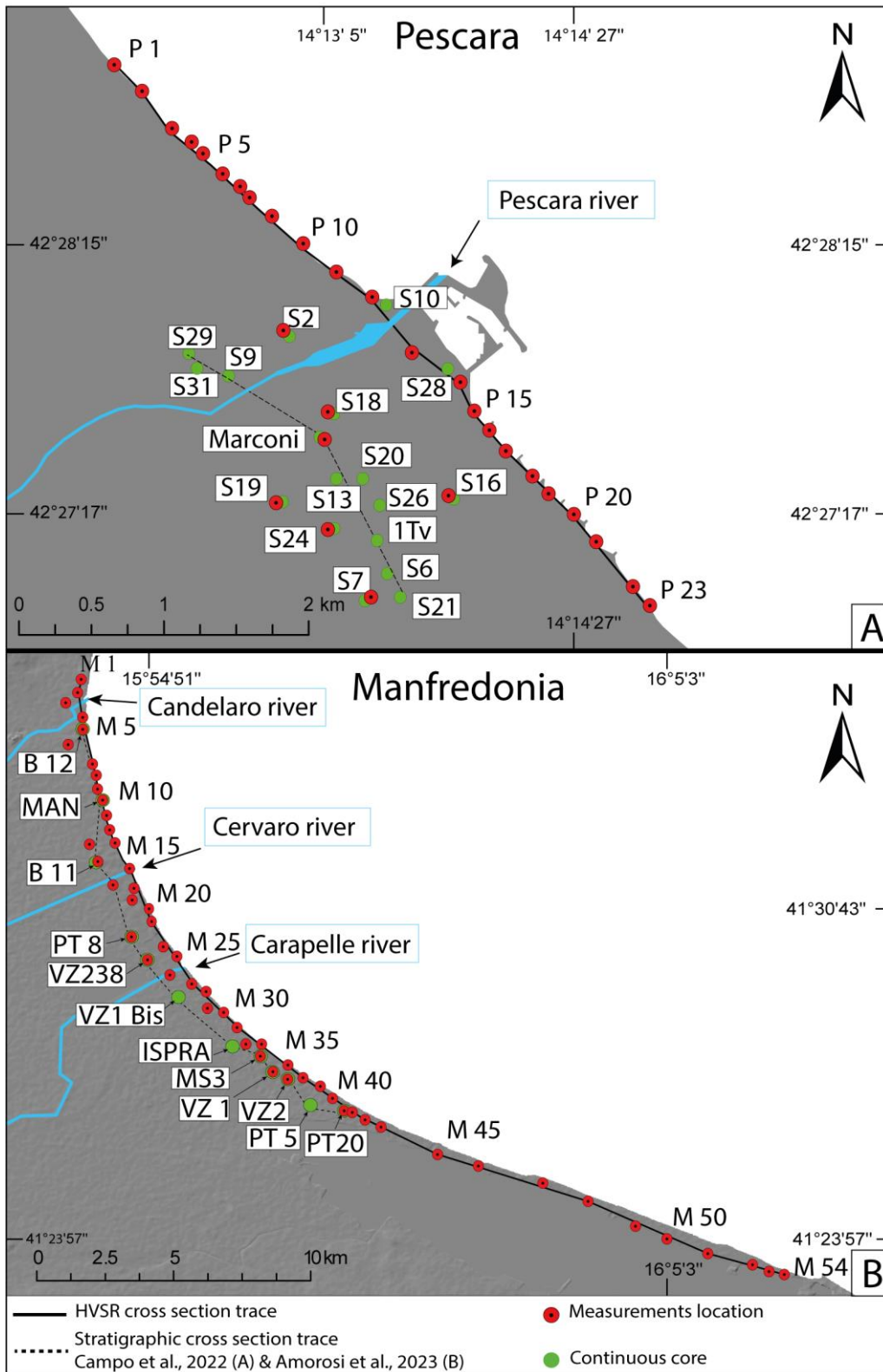


Fig. 5. Microtremor measurement locations in Pescara (A) and Manfredonia (B). The black dashed lines represent the two stratigraphic cross-sections of Figures 3 and 4.

### 6.3.3 Identification and lateral correlation of mHVSR peaks

The main resonance frequencies of the ground can be identified as distinct peaks on the mHVSR curves, as a function of the depths to the impedance contrasts below the measurement sites. For a correct stratigraphic interpretation, accurate correlation between geological and geophysical data is required. To this aim, we collected all available stratigraphic logs and analyzed our mHVSR curves to check for lateral peak correlation. We analyzed the data in three forms:

(i) Analysis of individual mHVSR curves in conjunction with the spectral components of motion. This type of analysis allows distinguishing the stratigraphic vs. anthropic nature of mHVSR peaks (Castellaro, 2016) and discerning the 1D/2D nature of a site (Sgattoni and Castellaro, 2020).

(ii) Lateral plots of mHVSR curves along the investigated lines. These plots allow identifying all mHVSR peaks at all sites, variations between sites, and possibly laterally-continuous impedance contrast surfaces.

(iii) Contour plots of mHVSR curves interpolated as a function of distance and color-coded for mHVSR amplitude, with each mHVSR curve individually normalized by its maximum computed within the frequency interval of interest. These plots allow enhancing lateral correlation of the main mHVSR peaks and identification of resonance frequencies associated with common impedance-contrast surfaces.

In Pescara, we identified low-amplitude resonance peaks (mHVSR amplitude mostly around 2) in a frequency range between 1 and 4 Hz. These peaks can be correlated laterally (Fig. 6A) to reproduce a U-shaped feature, marked with lower frequencies corresponding to deeper impedance contrasts in the central part of the profile and increasing frequency values towards the edges. A detailed picture of the impedance-contrast surface can be inferred from the contour plot of Fig. 6B, where dark-red colors denote the main resonance peaks. In this plot, each mHVSR curve is normalized by its maximum in the frequency range 0.9 – 4 Hz; by doing this, the detailed frequency features of the maxima associated with the U-shaped surface emerge clearly as a laterally nearly-continuous, dark red area and even the smallest lateral frequency variations are visible.

In the Manfredonia area, the mHVSR peaks are more prominent (with amplitudes up to 7) and two distinct resonance peaks characterize several sites. The lateral correlation of these peaks allowed us to identify two different U-shaped features: a relatively shallow impedance contrast at

frequencies between 0.9 and 4.5 Hz, and a deeper one at frequencies between about 0.4 – 1 Hz (Fig. 6C). This latter is tentatively associated with the carbonate substrate of Upper Jurassic age expected at 350 – 400 m depth (Geological Map of Italy, Sheet 409 - Zapponeta). Due to our particular interest in the shallow paleovalley system, which is approximately 50 m deep in its depocenter, we focused further analysis on the shallower layer. The contour plot in Fig. 6D shows the resonance frequencies identified along the profile within the frequency range of interest. Here, each mHVSR is individually normalized by its maximum in the frequency range of 0.75 – 2 Hz.

After inspection of each spectral component of motion, we verified the stratigraphic origin of mHVSR peaks following the criteria described by Castellaro (2016). Most of the resonance peaks are caused by local minima in the vertical spectral components of motion (Fig. 7 and Fig. 8), a feature related to the lateral propagation of surface waves observed under 1D conditions. The lateral variation of the observed resonance frequencies along the cross-section of both paleovalleys also supports the 1D nature of measurement sites. This suggests that the observed resonance frequency at each site depends on the local stratigraphy and does not represent a 2D vibration mode of the valley fill, which would be reflected in constant resonant frequencies across the valley (Sgattori and Castellaro, 2020).

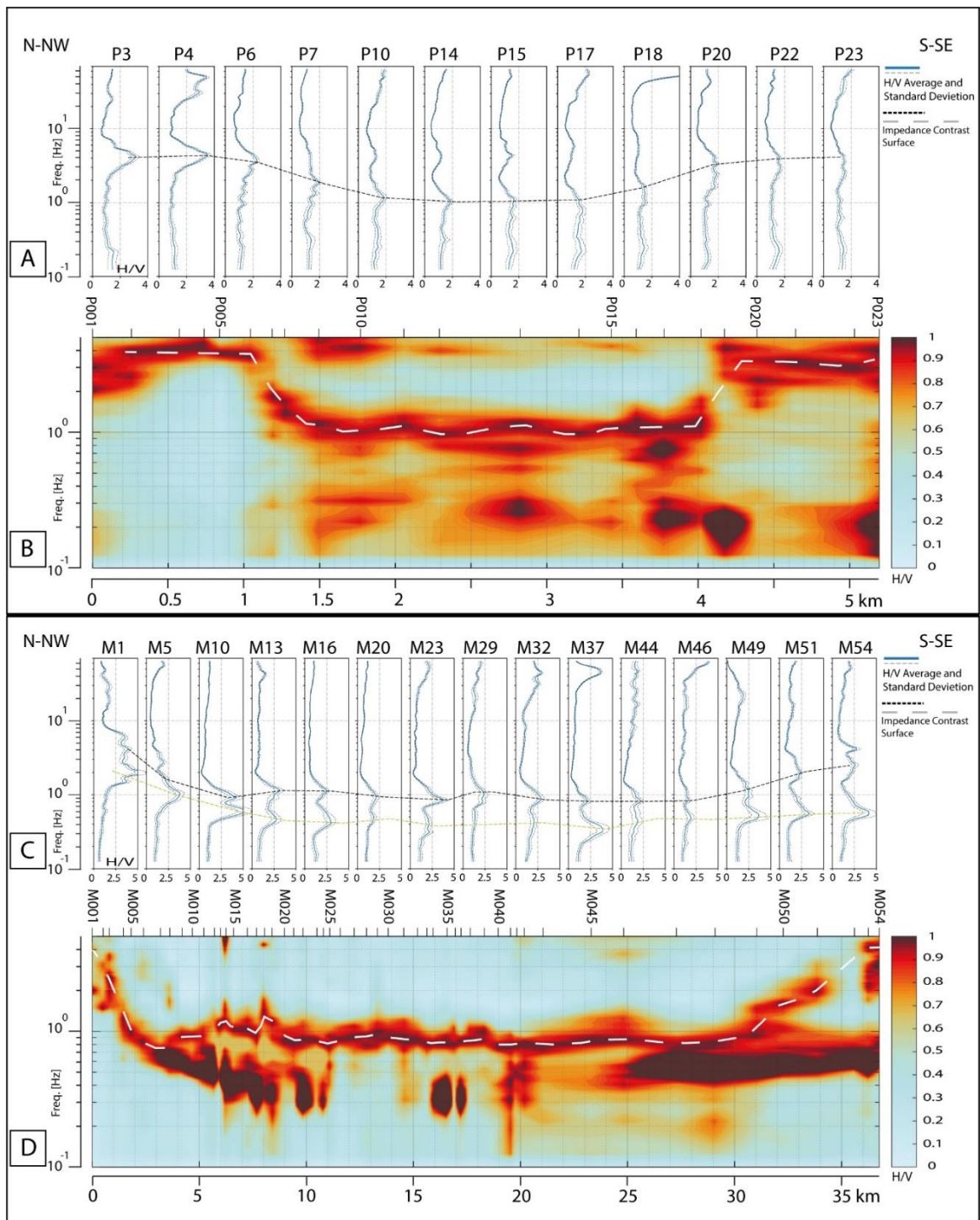


Fig. 6. Representative mHVSr curves of the Pescara (A) and Manfredonia (C) paleovalley systems and complete mHVSr frequency contour plots (B) and (D). The black dashed lines in A and D, and the white dashed lines in B and D, represent the lateral correlation of impedance contrast surface.

### 6.3.4 Frequency-to-depth conversion

This section describes the procedure to transform the mHVSr profiles from the frequency to the spatial domain. To do this, the 1D resonance equation can be used, which relates the fundamental ground resonance frequency ( $f_0$ ) with the S-wave velocity ( $V_s$ ) and thickness ( $h$ ) of the resonating layer:

$$f_0 = \frac{V_s}{4h} \quad (1)$$

The application of this equation requires i) the assumption of 1D site conditions at each measurement site, and ii) a  $V_s$  model for the sediment layer. The 1D assumption is verified in both study areas for the resonance frequencies of interest (highlighted with white dashed lines in [Fig. 6](#)). The  $V_s$  model can be derived by correlating the observed resonance frequencies with the known depths of impedance contrasts deduced from borehole data (e.g., Ibs-von-Set and Wohleberg, 1999). To this purpose, we carefully analyzed all microtremor data acquired at nearby sites, where continuous stratigraphic cores are available, and tentatively identified the stratigraphic surfaces that correlate with their corresponding resonance peaks. Four examples of stratigraphic-mHVSr curve correlation are shown in [Fig. 7](#) and [Fig. 8](#).

In the two paleovalley systems, the depth of the impedance contrast typically coincides with the marked lithologic contrast between the soft, clay-dominated upper paleovalley fill (pocket penetrometer values commonly  $< 1 \text{ kg/cm}^2$ ) ( [Fig. 7](#) and [Fig. 8](#)) and the underlying sand or gravel that typifies the lower valley fill. This major impedance contrast corresponds to the boundary between lowstand fluvial deposits and transgressive estuarine facies ([Fig. 2](#)). Although it can locally reflect pedogenized horizons (pocket penetrometer value commonly  $> 3 \text{ kg/cm}^2$ ) at a slightly higher stratigraphic level (core "MAN" - [Fig. 8](#)), or the direct contact with the substrate (pocket penetrometer value commonly  $> 5 \text{ kg/cm}^2$ ).

Several HVSr curves from both the Pescara and Manfredonia areas are characterized by mHVSr amplitudes lower than 1 at frequencies higher than about 2 Hz. This feature is typically related to velocity inversions, as described by Castellaro and Mulargia (2009), and is likely due to the shallow stiff sand layer that overlies the soft clay paleovalley fill ([Fig. 7](#) and [Fig. 8](#)).

The resulting frequency-depth constraint points are reported in [Fig. 9](#). Here, the column "Substrate depth" generally refers to the depth of the boundary observed locally between the soft,

unconsolidated estuarine clay (upper paleovalley fill) and the top of the underlying fluvial gravel (lower paleovalley fill).

A  $V_s$  model can be thus derived by fitting resonance frequencies with the identified substrate depths, following the method proposed by Ibs-von Seth and Wohleberg (1999) that assumes a power-law relation for increasing  $V_s$  with depth. This method has been used by numerous authors in several valley contexts (e.g., Parolai et al., 2002; Özalaybey et al., 2011; Paolucci et al., 2015; Tün et al., 2016; Sgattoni and Castellaro, 2021).

The regression analysis was conducted separately for the Pescara paleovalley and the Manfredonia study area, as shown in Fig. 9. The frequency-depth relation obtained for the Pescara sediment fill is the following:

$$H = 45.7f^{-1.26} \quad (2)$$

while for Manfredonia, we obtained:

$$H = 30.8f^{-1.39} \quad (3)$$

These relations are valid for the shallow subsurface within the depth range used for the regression analysis, which allows the conversion from the frequency to the depth domain of the mHVSR curves.

The data are fitted very well; in both cases, the coefficient of determination  $R^2$  is 0.99, and the mean square error is 0.27 m for the Pescara dataset and 0.30 m for Manfredonia. The resulting  $V_s$  models are also shown in Fig. 9. They denote very low  $V_s$  velocities, with equivalent  $V_s$  values in the fine-grained paleovalley depocenters, equal to about 180 m/s in Pescara and 140 m/s in Manfredonia.

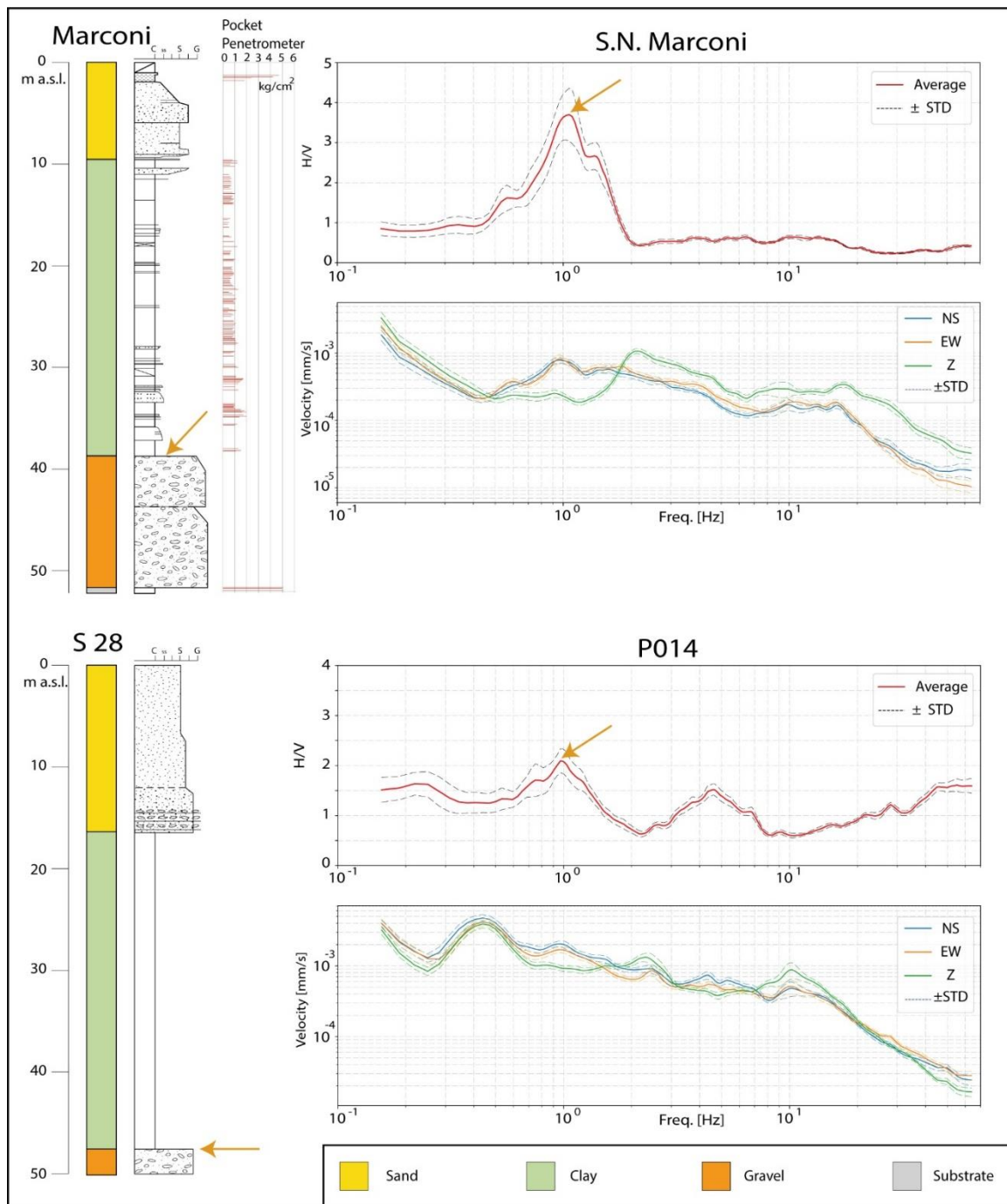


Fig. 7. Two cores from the Pescara area, with stratigraphy on the left and related mHVSr measurements with spectra on the right. Pocket penetrometer data from reference core Marconi are shown. Note paleovalley fill values  $< 1 \text{ kg/cm}^2$  and substrate values exceeding  $5 \text{ kg/cm}^2$ . The orange arrows indicate peaks in the resonance H/V curves and associated impedance contrast surfaces.

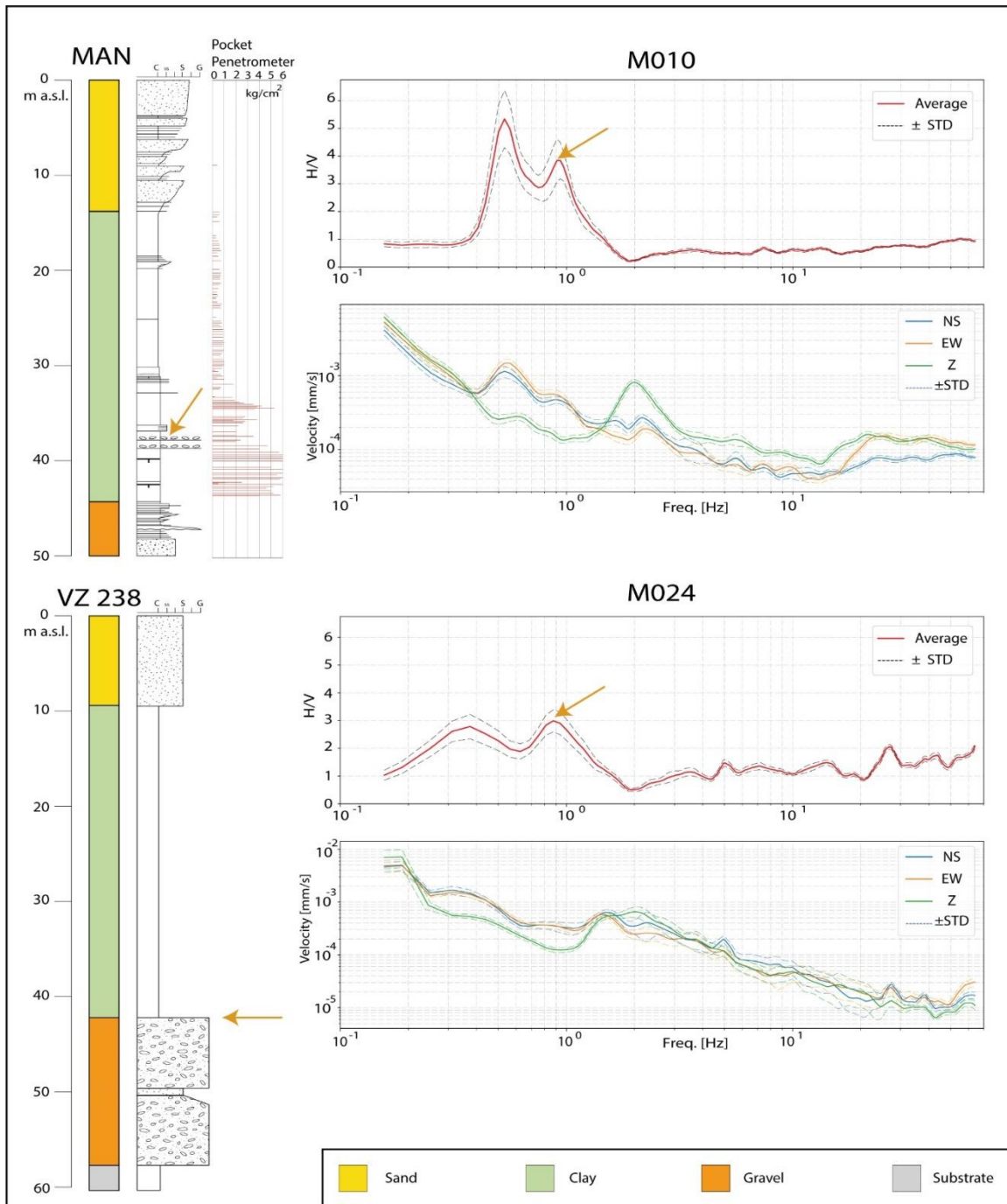


Fig. 8. Two cores from the Manfredonia area, with stratigraphy on the left and related mHVSr measurements with spectra on the right. Pocket penetrometer data from reference core MAN are shown. Note paleovalley fill values  $< 1 \text{ kg/cm}^2$  and the pedogenized horizon values  $> 5 \text{ kg/cm}^2$ . The orange arrows indicate peaks in the resonance H/V curves and associated impedance contrast surfaces.

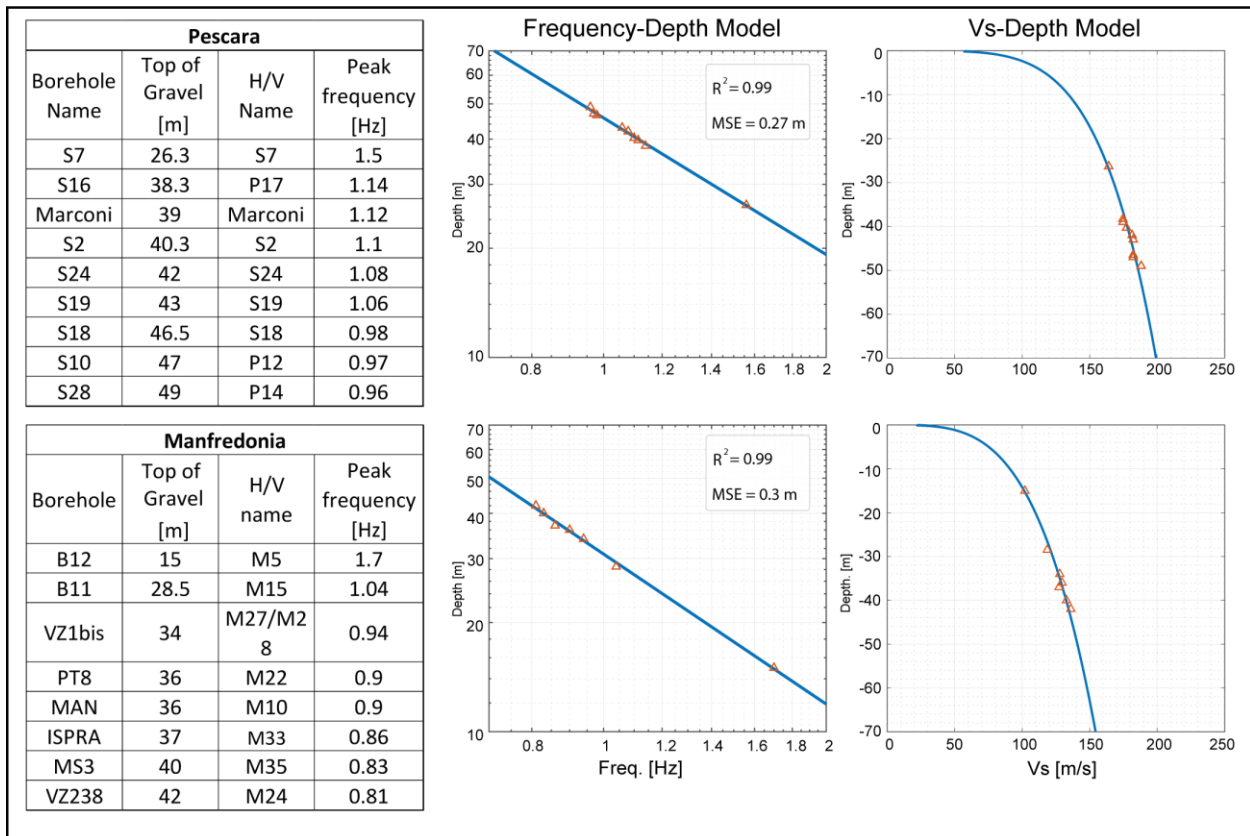


Fig. 9. Frequency-depth constraint points for the Pescara and Manfredonia paleovalleys. The two regression models from equations 2 and 3 and the resulting Vs-Depth model are shown.

## 6.4 Results

By means of equations 2 and 3, we transformed the mHVSr curves from the frequency to the spatial domain, down to the base of both paleovalleys. Given the purpose of mapping the shallowly buried paleovalley body, we pushed the reconstructions down to frequencies of approximately 0.9 Hz (corresponding to 50 m) in Pescara and 0.8 Hz (corresponding to 45 m) in Manfredonia. As a result, we obtained two new contour plots, with mHVSr amplitudes as a function of depth and distance along the profiles. Then, we compared the new mHVSr profiles with the corresponding geological cross-sections in [Fig. 10](#) and [Fig. 11](#).

### 6.4.1 The Pescara paleovalley

In the Pescara area ([Fig. 10](#)), the stratigraphic cross-section of [Figure 3](#) is parallel to the mHVSr profile, from which it is about 900 meters distant. The geological cross-section runs through the Pescara city center, while the mHVSr profile runs along the modern Adriatic Sea beach, as shown in [Fig. 5](#). The Pescara mHVSr profile is 5.2 km long and extends over a longer distance than the stratigraphic cross-section of the Pescara paleovalley. The stratigraphic transect covers the central portion of the mHVSr profile, approximately from measures P010 to P018 ([Fig.10](#)).

From measurements P001 to P006, at approximately 10-m depth, the mHVSr profile shows a clear impedance contrast ([Fig. 10](#)), interpreted to represent the northern interfluvium of the Pescara paleovalley. In this portion of the profile, unconsolidated sand from the modern beach ridge (see section trace in [Fig. 5](#)) likely overlies the substrate (e.g. Mutignano Fm), producing a high impedance contrast. The fundamental resonance frequency ( $f_0$ ) of this segment is around 4 Hz and rapidly decreases to 3 Hz at measurement P006 ([Fig. 6A-B](#)).

From measurements P006 to P010, the depth of the impedance contrast surface increases, from 10 m to 40 m below sea level (b.s.l.)([Fig. 10](#)). In this zone, the fundamental resonance frequency rapidly changes from 3 Hz at P006 to 0.95 Hz at measure P010, within only 700 meters distance ([Fig. 6A-B](#)). This area represents the northern flank of the paleovalley. From measurement P010 to P017, the impedance contrast surface stabilizes around 40 meters b.s.l. ([Fig. 10](#)), which is inferred to represent the paleovalley depocenter. In this portion of the profile, minor changes in impedance contrast depth are likely due to the marked thickness variability of the basal gravel body, as shown in the stratigraphic cross-section ([Fig. 3](#)). In the depocenter, the fundamental resonance frequency is systematically around 1 Hz ([Fig. 6A-B](#)), with some minor changes. For instance, at measure P013,

which is almost aligned with core Marconi in the center of the paleovalley,  $f_0$  is 1.17 Hz, consistent with the greater thickness of the fluvial gravel body.

The southern portion of the profile shows an abrupt change in impedance contrast depth from measurement P017 (38 m b.s.l.) to measurement P020 (10 m b.s.l.; Fig. 10). A much steeper slope, thus, characterizes the southern flank. From measurement P020 to P023, the depth of the impedance contrast remains stable at approximately 10 m b.s.l.. The sedimentary cover has comparable thickness as in the northern interfluve, as supported by stratigraphic information from core S21. As for the northern interfluve, the dominant resonance frequency varies from 3.5 to 4 Hz (Fig. 6A-B).

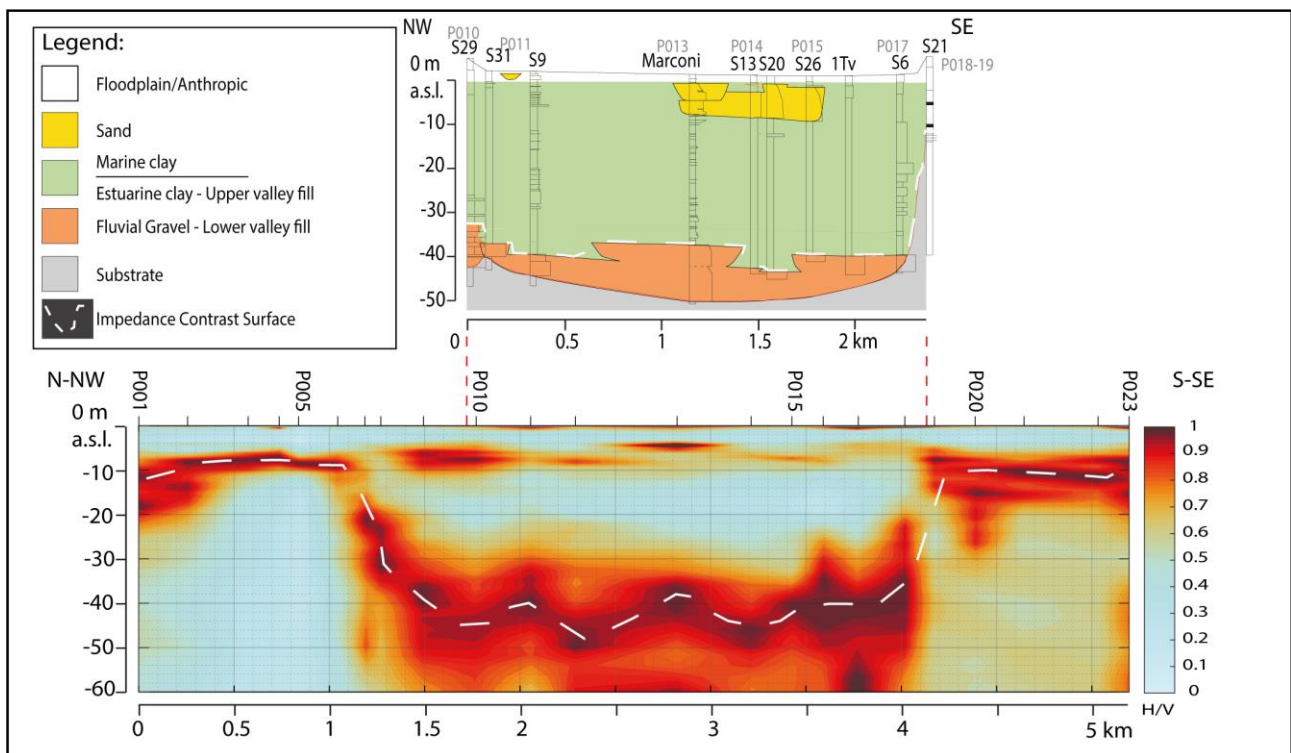


Fig. 10. Contour plots of the mHVSr amplitudes function of depth matched against the Pescara geological cross-section. The white dashed lines represent the inferred impedance contrast surfaces

## 6.4.2 The Manfredonia paleovalley

In the Manfredonia area (Fig. 11), the internal architecture of three Apulian paleovalleys, generated by the Candelaro, Cervaro, and Carapelle rivers, respectively, is summarized by the 17 km-long stratigraphic cross-section of Fig. 4.

Along the Manfredonia mHVSr profile, from measurement M001 to M008, the depth of the impedance contrast surface rapidly increases from 10 m b.s.l. at M001 to 45 m b.s.l. at M008, this latter representing the Candelaro paleovalley depocenter. In this segment, the resonance frequency varies from 4.5 Hz to 0.9 Hz in 3.5 km (Fig. 6C-D). Between measurements M009-10-11, the impedance contrast surface rises up to 36 m b.s.l. approximately. This change is due to a prominent paleosol observed in the reference core MAN (Fig. 8), which coincides with the site where measurement M010 was acquired. From measurement M011 to M019, the impedance surface varies only slightly, from 25 m to 30 m b.s.l., with a resonance frequency of around 1.2 Hz (Fig. 6C-D). Therefore, with core B11 as a support, this zone is interpreted as the interfluvium between the Candelaro and Cervaro paleovalleys.

The Cervaro paleovalley was encountered from measurement M020 to M030 (Fig. 11), with its depocenter between M022 and M025, consistent with stratigraphic data from cores PT8 and VZ238. In this segment, the depth of the impedance contrast decreases from 41 m b.s.l. (M024), with a resonance frequency of 0.85 Hz to 30 m b.s.l. (M030), with a resonance frequency of 1.1 Hz (Fig. 6C-D), marking a minor interfluvium that separates the Cervaro from the Carapelle paleovalleys.

While in the stratigraphic cross-section the Carapelle paleovalley wedges out with its southern interfluvium at core PT5 and PT20 (Fig. 4), the mHVSr profile does not show the same geometry (Fig. 11). Based on the mHVSr profile, the Carapelle paleovalley depocenter would be located, instead, between measurements M040 and M044, with an impedance contrast depth of about 42 meters b.s.l. and a resonance frequency of 0.8 Hz (Fig. 6C-D). Such contrasting interpretations likely reflect the low-quality stratigraphic descriptions of cores PT5 and PT20 on which the geological cross-section is based. The southernmost part of the mHVSr profile has a lower density of measurements and is not supported by stratigraphic information from drillings. Along this transect, the depth of the impedance contrast is systematically low, around 40 m below sea level. Between measurements M048 and M049, the impedance contrast rises up, reaching 10 m b.s.l. at the end of the profile (M054), with a resonance frequency that changes from about 0.8 Hz to 2.5 Hz in 8 km (Fig. 6C-D), marking the southern interfluvium of the paleovalleys system.

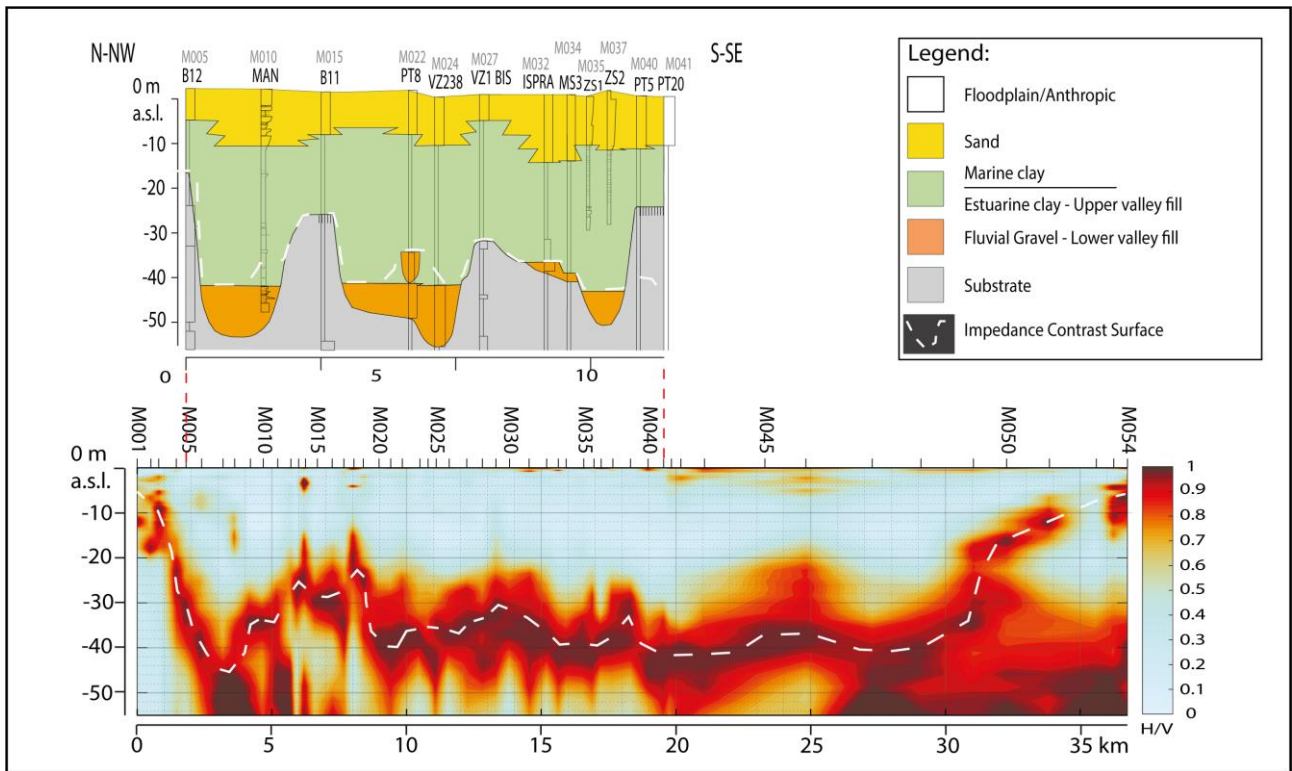


Fig. 11. Contour plots of the mHVSr amplitudes function of depth matched against the Manfredonia geological cross-section. The white dashed lines represent the inferred impedance contrast surfaces.

## 6.5 Discussion and Conclusion

Reconstructing a realistic subsurface stratigraphic model that considers the physical properties of rocks and sediments is fundamental for correct seismic site characterization. In this respect, the mHVSr technique represents a well-known and widely used tool to delineate the subsurface geometry and geophysical properties of the terrain. This method has been successfully applied in diverse geological contexts, including deep valley basins (Ibs-Von Seht and Wohlenberg, 1999; Sheib et al., 2016), shallow valley basins, and Alpine valleys (Gosar and Lenart, 2010; Le Roux et al., 2012; Mantovani et al., 2018; Mele et al., 2021; Sgattoni and Castellaro, 2021) and it is also used to investigate weathered rock profiles (Moon et al., 2019), unstable slopes and landslides slip surfaces (Del Gaudio et al., 2014).

Late Quaternary paleovalley systems buried beneath modern coastal lowlands are key geological features for which the efficacy of this geophysical approach is promising due to pronounced lithological contrasts. Paleovalley fills are made up predominantly of very soft, unconsolidated clay with poor geotechnical properties and low shear wave velocities: the combination of these factors may lead to increased structural damage in the event of an earthquake. Nonetheless, reconstructing in detail paleovalley geometries can be expensive, as these buried sediment bodies have no geomorphological expression, and precise identification of depocenters and interfluves in the subsurface requires collection of a large number of sediment cores.

The mHVSr technique proved to be a powerful tool for the subsurface identification of late Quaternary paleovalley systems along the Adriatic Sea coastal plain and an ideal complement to classic stratigraphic reconstructions based on different data sources. The mHVSr profiles from Pescara (Fig. 10) and Manfredonia area (Fig. 11) show that sharp impedance contrasts can be used effectively to delineate the interfluves of the paleovalley systems and the bases of soft sedimentary valley fills, especially where poor-quality stratigraphic descriptions or absence and scarcity of subsurface data may prevent from reliable stratigraphic reconstructions. This is the case of the southern flank of the Carapelle paleovalley systems in Manfredonia area (Fig. 11), where mHVSr data suggest a possibly different interpretation than the one derived from low-quality stratigraphic descriptions, thus contributing significantly to the paleovalley reconstruction.

In general, the mHVSr technique provides a picture of the paleovalley geometry, which is consistent with the one derived from the stratigraphic reconstruction, allowing recognition of important features within the major valley system, such as in the case of the Manfredonia area. The

H/V technique not only emphasizes the sharp contrast between the soft clayey valley fill and the underlying gravel but also detects impedance contrasts with prominent paleosols or older (and much more consolidated) substrates. The accurate reconstruction of buried valley geometries can be carried out only through acquisition of a dense network of microtremor measurements: cost-effectiveness and ease of deployment of the mHVSR technique make this approach appropriate for this purpose. Furthermore, the geometries derived from mHVSR reconstructions can be used to plan core drilling campaigns and characterize the paleovalley stratigraphic architecture.

As late Quaternary paleovalley systems have been generated under the global control of glacio-eustatic fluctuations and reflect generalized fluvial incision due to sea-level fall, their worldwide occurrence beneath modern coastal plains and deltas can be predicted in terms of location, size, and geometry. In this regard, the mHVSR technique could be used as a subsurface exploration tool of modern lowlands even where stratigraphic data from drillings are scarce, assuming that basic information on the impedance contrast depth or shear wave velocity is known.

Essential parameters of paleovalley systems other than valley profiles can be obtained through mHVSR investigations. Changes in resonance frequency can be detected by microtremor measurements. In paleovalleys with steep buried flanks, they can vary abruptly without any superficial morphologic evidence in a frequency range that can interact with common building types. In the northern flank of the Pescara paleovalley, the fundamental resonance frequency varies laterally from 3 Hz to 0.9 Hz in only 750 meters, remaining stable at 1 Hz in the depocenter (Fig. 6A-B). Another abrupt variation can be observed along the southern interfluve, where  $f_0$  varies laterally from 0.9 Hz to 3.3 Hz in 600 m only.

The northern portion of the Candelaro paleovalley in the Manfredonia area shows rapid changes in resonance frequencies that vary laterally from 4.5 Hz to 0.9 Hz in 3.5 km (Fig. 6C-D); other resonance frequency variations can be detected within the main paleovalley body, as part of the minor interfluves separating distinct river domains. For instance, the Candelaro-Cervaro and the Cervaro-Carapelle interfluves are marked by resonance frequency changes from 0.9 Hz to 1.2 and from 0.85 Hz to 1.1, respectively (Fig. 4).

In the southern portion of the Manfredonia area, the spacing between mHVSR measurements increases, enabling identification of major resonance frequency changes only and delineating the buried valley morphology, but possibly neglecting local changes that might affect the main paleovalley body, as shown in its northern portion. In this respect, a careful evaluation of the geological context is essential to design an effective microzonation measurements campaign and

detect rapid variations in resonance frequencies over short distances, fundamental to preventing building structural damage and can easily be missed in a paleovalley context.

Furthermore, the  $V_s$  model obtained for the two paleovalleys systems (Fig. 9) denotes generally low shear wave velocities, with comparable  $V_s$  values in the paleovalley depocenters (about 180 m/s in Pescara and 140 m/s in Manfredonia, respectively), placing both paleovalley fills into the ground type D of Standard Eurocode 8, which is a  $V_{s30}$ -based soil classification. Paleovalley geometries and this derived parameter, thus, can be used to improve the quality of local seismic microzonation, and for more accurate site characterization and seismic modeling. In this regard, the shallow velocity inversion due to the uppermost sand layer could also play a role in the seismic response of the paleovalleys, as noted in different contexts, e.g., Di Giulio et al. (2016). Further characterization of the velocity model with direct  $V_s$  measurements would help for exhaustive modeling of the seismic response.

In this study, we utilized the mHVSr technique to reconstruct the geometries of two buried late Quaternary paleovalley systems (Pescara and Manfredonia area) beneath the Adriatic coastal plain of Italy. The microtremor measurements were processed to perform the microtremor-based Horizontal to Vertical Spectral Ratio (mHVSr) and analyzed in conjunction with the spectral components of motion. We recognized clear resonance frequencies in both study areas that outlined the buried valley geometries. Then, assuming a power-law relation for increasing  $V_s$  with depth and the link between geological and geophysical data, we transformed each mHVSr curve from the frequency to the spatial domain.

We address the importance of integrating geophysical data with accurate stratigraphic reconstructions when performing microzonation studies to ensure reliable geophysical modeling of the critical parameters that control seismic amplification. In paleovalley systems, the resonance frequencies exhibit rapid lateral variation in a range of interactions with standard buildings. The buried paleovalley geometry is typically characterized by steep flanks that can result in 2D seismic effect. Moreover, low S-wave velocities of paleovalley fills can cause longer shaking and seismic amplifications, making this geological context a potential seismic hazard beneath modern coastal lowlands.

## Acknowledgments

This research was supported by the Italian Ministry of University and Research under the PRIN 2017 program to Alessandro Amorosi, project number 2017ASZAKJ “*The Po-Adriatic Source-to-Sink system (PASS): from modern sedimentary processes to millennial-scale stratigraphic architecture*”.

## Open Research

The data used for this work are preserved in the repository (AMSacta) hosted by the University of Bologna, Italy, and can be found at the link <https://amsacta.unibo.it/id/eprint/7295>. Refer to Table 1 for the name and geographic coordinates of each measure.

# 7. Seismic Amplification of Late Quaternary Paleovalley Systems: 2D-1D Seismic Response Analysis of the Pescara Paleovalley (Central Italy)

Andrea Di Martino<sup>1</sup>, Giulia Sgattoni<sup>2</sup>, Federico Purri<sup>1</sup>, Alessandro Amorosi<sup>1</sup>

<sup>1</sup> Department of Biological, Geological and Environmental Sciences (BiGeA), University of Bologna. Piazza di Porta San Donato 1, 40126, Bologna, Italy

<sup>2</sup> Istituto Nazionale di Geofisica e Vulcanologia, Sezione di Bologna, viale Berti Pichat 6/2, 40127 Bologna, Italy

Corresponding author: Andrea Di Martino (Andrea.dimartino4@unibo.it)

## Abstract

Effective site characterization and seismic response analysis require a thorough understanding of subsurface features, including geophysical properties and geometries of sediment bodies. Late Quaternary paleovalley systems, often overlooked in seismic hazard assessment, represent a potential threat due to their unconsolidated infill (with shear wave velocities  $< 200$  m/s) and sharp contrast with the adjacent substrate. Through an integrated approach that combined geological and geophysical data, we characterized the subsurface of the Pescara paleovalley system. Geostatistical interpolation of microtremor measurements enabled mapping resonance frequencies, highlighting abrupt changes and delineating the paleovalley boundaries. High-resolution core descriptions were then correlated with resonance frequencies, enabling the reconstruction of a 3D geophysical depth model of the buried paleovalley morphology. Furthermore, analyzing velocity profiles from down-hole tests led to the identification of five main seismic/stratigraphic layers within the valley fill. The geometry and facies architecture were reconstructed through a cross-section transversal to the paleovalley axis and then implemented into a 2D finite element model. Seismic response was computed, revealing significant amplification factors at frequencies closely matching the direct observation. Amplification factors peaked at frequencies between 0.9 and 1.3 Hz in the paleovalley axis and up to 5 Hz towards the flanks, reaching a factor of 4. These findings suggest a notable increase in amplification amplitude compared to simpler geological contexts and emphasize the potential impact on common building types. Response spectra show strong amplifications in the paleovalley system, potentially leading to a significant underestimation of spectral accelerations compared to Eurocode 8 guidelines. The comparisons of 1D and 2D modeling approaches revealed minimal differences, indicating that the generally flat geometry of the valley may not exhibit clear 2D effects. However, local subsurface stratigraphy strongly influences lateral changes in seismic response, emphasizing the importance of detailed subsurface knowledge for realistic seismic response estimates.

## Keywords

1D-2D Seismic Response Analysis, Seismic Amplification, Seismic Hazard Analysis, Non-linear Dynamic Analysis, Response Spectra, Paleovalley

## 7.1 Introduction

An adequate site characterization requires accurate reconstructions of subsurface features, including sedimentary facies, geometry, and variations in the engineering and geophysical properties of rocks and sediments. All these characteristics strongly influence site effects in terms of frequency content, intensity, and duration of an earthquake (Boore, 2004; Thompson et al., 2009). Furthermore, basin effects are known to have the potential to modify ground motions, leading to the generation of local surface waves or possible 2-D resonance (e.g., Bindi et al., 2009; Macerola et al., 2019; Poggi et al., 2014).

Several studies have attempted to model seismic site effects by focusing on simple one-dimensional (1D) simulations, with the assumption of lateral homogeneity (Fabozzi et al., 2022; Fehr et al., 2019; Hallal and Cox, 2023); Two-dimensional (and 3D) ground motion simulations are expected to provide more realistic results, as subsurface stratigraphy can rarely be assumed as 1D (Hallal and Cox, 2023). As further evidence, purely 1D simulations cannot explain the damage caused by many earthquakes, as demonstrated by the Loma Prieta earthquake in 1989 (Kiureghian and Neuenhofer, 1992) and the Kobe earthquake in 1995 (Kawase, 1996).

On the other hand, 1D simulations remain a reasonable approximation wherever the stratigraphic framework is simple and relatively homogeneous. A recent study (Hallal et al., 2022) used literature data from Afshari & Stewart, 2019; Laurendeau et al., 2018; Pilz & Cotton, 2019; Tao & Rathje, 2020 and Thompson et al., 2012, to examine the seismic response of 600 downhole arrays, and found that approximately 50% of them could be modeled with 1D assumptions. A seismic response study conducted in L'Aquila (Central Italy) also highlighted that within complex sedimentary basins, the reliability of 1D and 2D modeling varies spatially (Macerola et al., 2019).

In this context, late Quaternary paleovalley systems (Blum et al., 2013) represent an underestimated seismic hazard (Di Martino et al., 2023b). These systems include shallow subsurface incisions (tens of meters deep and a few km wide) formed in response to the latest episode of global sea-level fall (Amorosi et al., 2017) and filled with very soft/unconsolidated clay during the post-glacial sea-level rise. Paleovalleys are widespread beneath modern coastal lowlands worldwide, in the shallow (10-20 m) subsurface of large cities and of rapidly expanding urban areas. Their detection, however, may be challenging, as they lack any geomorphological expression (Strong and Paola, 2008). Where present, these sediment bodies significantly increase the thickness of soft late Quaternary deposits and modify their geometry, crucial parameters in engineering geology that play a significant role in foundation stability.

Besides the well-established economic importance of paleovalleys in the geological record (Blum and Törnqvist, 2000; G. P. Allen, H. W. Posamentier, 1993; Legarreta and Uliana, 1998; Salem et al., 2005), these buried features are increasingly studied worldwide, as they have the potential to modify earthquake motions due to their complex geometry and the sharp contrast between the unconsolidated clayey fill and the adjacent substrate, which may result in potential seismic amplification and rapid variations in resonance frequencies within the range of interaction with common buildings (Di Martino et al., 2023b).

Recently, the Geological Survey of Japan conducted investigations into the physical properties, geometry, and stratigraphic architecture of a paleovalley fill beneath the Tokyo lowland to mitigate earthquake risk (Ishihara et al., 2013; Tanabe et al., 2015). Additionally, based on data from the 1923 Kanto earthquake catastrophe, Tanabe et al., (2021) established a correlation between the structural damage to wooden houses and the spatial distribution and thickness of the soft paleovalley fill.

In complex geological contexts, such as paleovalley systems, numerous non-1D factors must be considered. These include significant heterogeneity in the stratigraphic layering and variable geometry of the substrate (Bard and Gariel, 1986; Semblat et al., 2005), resulting in the remarkable deviation from the assumption of shear waves propagating vertically in a homogeneous medium. A common limitation of 2D simulations lies in the difficulty of obtaining accurate site characterization, including velocity profiles, stratigraphic layering, and soil properties, through reliable subsurface models over large areas. However, detailed seismic site response analysis of late Quaternary paleovalley systems has never been undertaken, so far.

In this study, we aim to perform a comprehensive site response analysis of a buried paleovalley system beneath the city of Pescara (Central Italy; Fig. 1), leveraging a large amount of geological, geophysical, and geotechnical data, by integrating sediment body geometries, velocity profiles, and soil properties.

The central part of the Italian peninsula is well-known for being a high-risk seismic area. In recent years, numerous earthquakes have struck the regions of Marche and Abruzzo. In 2009, an earthquake of  $M_w = 6.3$  struck L'Aquila, resulting in a high number of losses and structural damage to buildings and infrastructures (Di Ludovico et al., 2017a, 2017b; Lagomarsino, 2012). In August 2016, a  $M_w=6$  earthquake hit Amatrice, causing significant loss of lives and damage to historical and cultural heritage (Fiorentino et al., 2018; Karimzadeh and Mastuoka, 2017; Luzi et al., 2017; Saganeiti et al., 2020).

Given the high seismic risk in central Italy, seismic microzonation of urban areas is needed, and high-resolution seismic site response studies should be performed to mitigate earthquake-induced damages (Cox et al., 2011; Iyengar and Ghosh, 2004; Moscatelli et al., 2020; Pergalani et al., 2020).

With this aim, we: i) mapped the main resonance frequencies in the study area, based on 85 microtremor measurements; ii) estimated an average  $V_s$  model for the paleovalley system, correlating the measured resonance frequencies with borehole stratigraphy, and thus enabling the 3D reconstruction of the paleovalley geometry; iii) compared the microtremor-based  $V_s$  model of the valley fill with  $V_s$  data from 6 Down Hole measurements, building a layering that integrates  $V_s$  and subsurface stratigraphy; iv) conducted 2D seismic response simulations along a cross-section in the paleovalley depocenter, comparing the results with 1D simulations; and v) compared the response spectra based on the EUROPEAN COMMITTEE FOR STANDARDIZATION, (2004) Eurocode 8 EC8) soil classification guidelines with the model-based response spectra, to achieve robust soil classification.

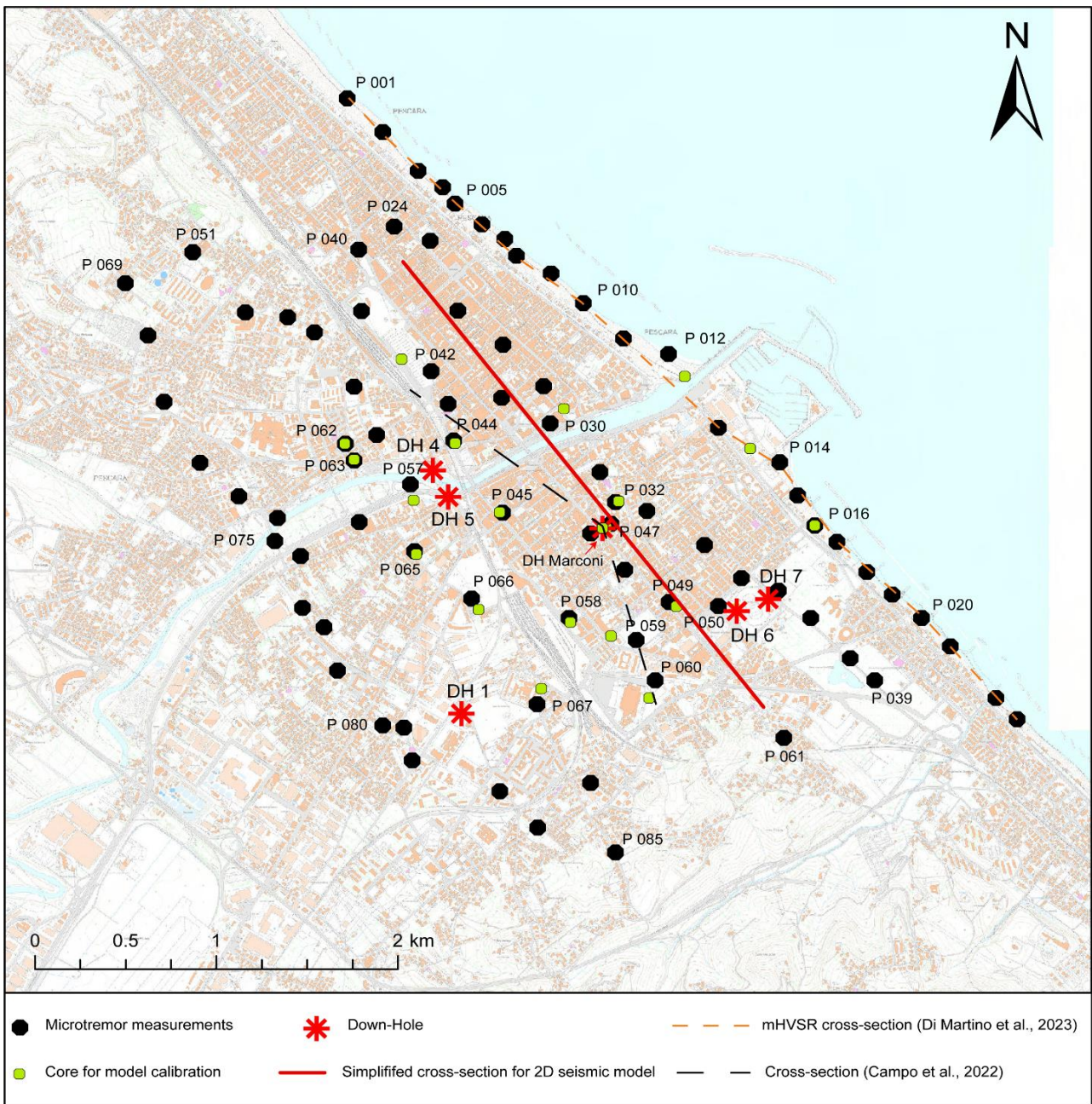


Fig. 5. Microtremor measurement points, boreholes used for model calibration ( $f_0$ -depth), and Down-Hole tests location in the urban Area of Pescara, Central Italy. The traces of the simplified geological cross-section used for the seismic model, the geophysical section from Di Martino et al. (2023), and the stratigraphic panel from Campo et al. (2022) are also shown.

## 7.2 Geological setting: The Pescara paleovalley system

Located in central Italy and bordered by the Central Apennines and the Adriatic Sea, the Pescara coastal plain is about 3.3 km<sup>2</sup> wide and represents the distal portion of the Pescara River valley. The Aterno-Pescara River is the longest in the Abruzzo region, with over 150 km and a hydrographic basin of 3170 km<sup>2</sup> (Urbano et al., 2017).

The Upper Pleistocene-Holocene paleovalley system buried beneath the Pescara River has been comprehensively described in the recent work, based on the sedimentological analysis of reference core “Marconi” (Campo et al., 2022a). A simplified cross-section that runs perpendicular to the paleovalley axis (Fig. 1) is shown in Figure 2.

The lower boundary of the paleovalley system is a prominent erosional surface (SB in Figure 2) that marks the abrupt facies change from the stiff (pocket penetrometer values > 5 kg/cm<sup>2</sup>) Pliocene-Pleistocene substrate (Mutignano Fm) to the overlying, Upper Pleistocene to Holocene valley fill (Fig. 2). The lower valley fill consists of a laterally extensive, fluvial gravel body, up to 14 m thick, that accumulated during the Last Glacial Maximum, between approximately 30 and 20 cal kyr BP.

The fluvial gravel is overlain by > 20 m of very soft, organic-rich clay (pocket penetrometer values < 1 kg/cm<sup>2</sup>, Campo et al., 2022) that accumulated in an estuarine depositional environment in response to the post-glacial sea-level rise (upper paleovalley fill). The soft clayey deposit is bounded laterally by steep flanks that separate the valley fill from the substrate, which confines the paleovalley in the north and south. Above the valley fill, the upper part of the succession consists of fluvial-deltaic deposits, up to 10 m thick, in lateral transition with coastal sands.

For a detailed description of the Pescara paleovalley system, including its sequence stratigraphic interpretation and comprehensive sedimentary facies analysis, the reader is referred to Campo et al. (2022).

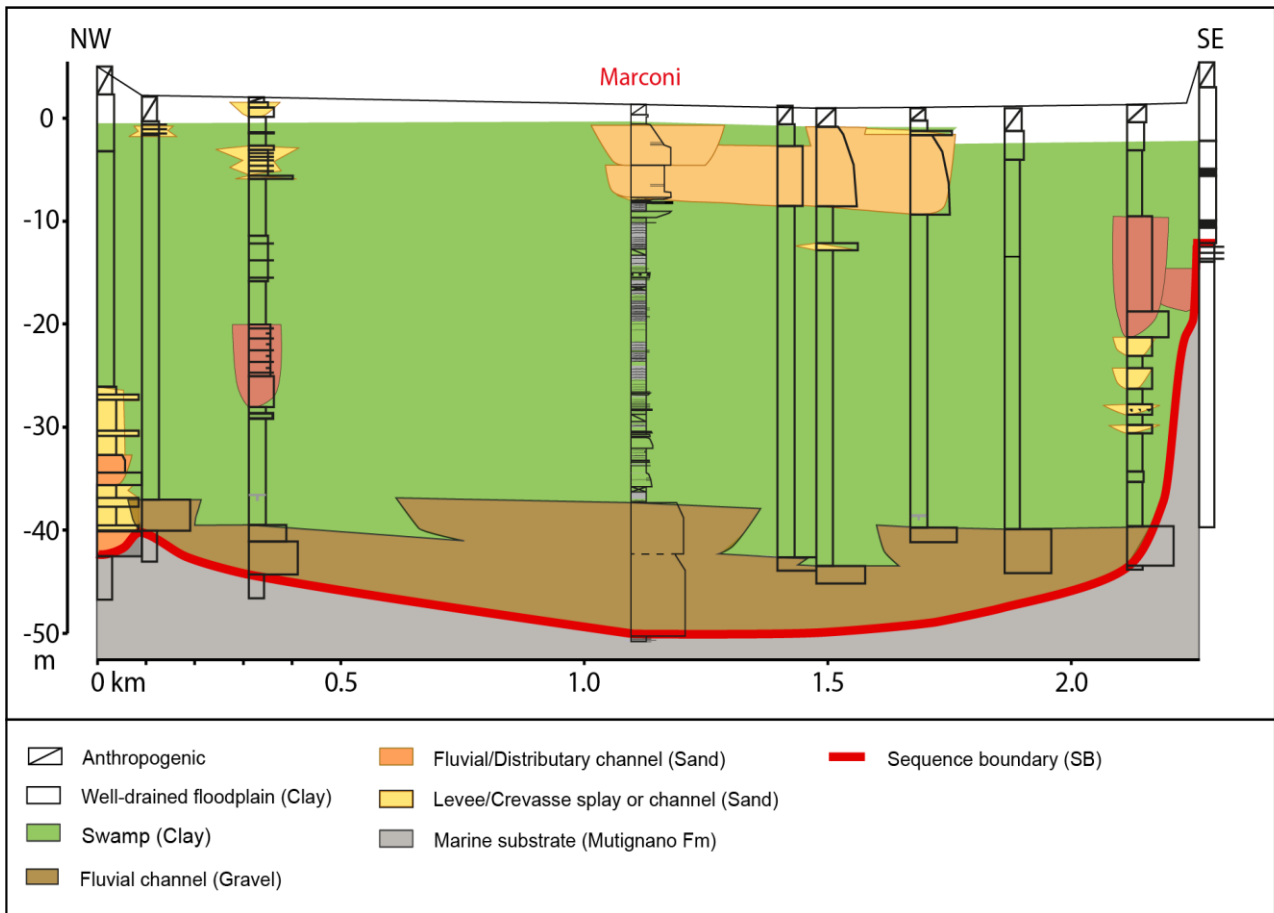


Fig. 2. Simplified stratigraphic cross-section of the Pescara paleovalley system (from Campo et al., 2022), transversal to the paleovalley axis (Fig. 1).

## 7.3 Resonance frequencies of the Pescara paleovalley

### 7.3.1 Microtremor measurements: Acquisition and processing

A total of 85 microtremor measurements were carried out in the study area, which is approximately 10 km<sup>2</sup> wide and centered in the city of Pescara. The microtremor measurements were acquired using a Tromino three-component seismometer designed by Moho SRL for digitally recording seismic noise. The duration of measurements was set at either 16 or 30 minutes, depending on local anthropic noise levels and on the inferred depth of the target substrate. The measurements were acquired with a sampling rate of 128 Hz. The seismometer was inserted firmly into soft soil and oriented toward the geographic north. The measurements were taken in free field conditions (Castellaro and Mulargia, 2010), > 15 meters away from buildings to minimize the influence of local structures on the recorded data. Sensors were properly leveled and stabilized during recordings.

The microtremor measurements were processed with Grilla software using the Horizontal to Vertical Spectral Ratio (H/V or HVSR) technique, which involves computing the Fourier amplitude spectra (FAS) ratio of the horizontal and vertical components of the ground motion. Each three-component time series was divided into 30-second non-overlapping windows. Within each window, the H/V ratio was computed. Ratios were then smoothed using triangular functions with a width equal to 10% of the central frequency. The resulting H/V curves were averaged to obtain microtremor-based H/V Spectral Ratio (mHVSR) curves; each curve was inspected to eliminate transient noise perturbations.

A few longer measurements (30 minutes) were split into longer window lengths of 60 seconds to ensure the robustness of the results and perform a parameter sensitivity check. Furthermore, different smoothing functions, like the Konno-Ohmachi algorithm, were applied, obtaining consistent results.

### 7.3.2 Resonance frequency map

Each mHVSR curve was analyzed to detect the dominant resonance frequency. The main resonance frequencies of the ground can be identified as distinct peaks on the mHVSR curves as a function of the impedance contrasts below the measurement site. We analyzed each mHVSR curve along with the single spectral components of motion to distinguish the stratigraphic *versus* anthropic

nature of mHVSr peaks and to discern the 1D/2D nature of the site (Castellaro, 2016; Sgattoni and Castellaro, 2020).

Most curves show one clear resonance peak, with observed resonance frequencies ranging from a minimum of 0.9 Hz to a maximum of 12 Hz and peak amplitudes between 2 and 4. In the study area, resonance peaks primarily result from local minima within the vertical spectral components of motion; this characteristic is associated with the lateral propagation of surface waves, as observed under one-dimensional conditions.

A microtremor measurement transect parallel to the shoreline (Fig. 1) revealed that resonance peaks can be correlated to reproduce a U-shaped feature (Fig. 3A), with lower frequencies in the center and higher frequencies towards the edges of the profile (Di Martino et al., 2023b). A clear picture of the impedance-contrast surface can be inferred from the contour plot of Fig. 3B. In this plot, the H/V curves are interpolated as a function of distance, each mHVSr curve being normalized by its maximum in the frequency range (0.9-4 Hz); the dark red colors indicate the main resonance peaks.

We reconstructed a frequency map covering the whole study area, using a total of 85 measurement points (Fig 4). The map was drawn with the ArcGIS software, relying on a Kriging geospatial interpolation, with each measured resonance frequency as input. The resonance frequency map was subdivided into six classes using the Jenks natural breaks classification, a data clustering method designed to determine the best arrangement of values into different classes. This map shows the resonance frequencies of the individual measurement points using the same spectrum of colors, with red indicating the highest resonance frequencies and green the lowest.

The northern sector of the study area is characterized by the highest resonance frequencies, with a gradual reduction towards the south-east. The maximum resonance (12 Hz) is specifically situated in the northeastern portion of the area (Fig. 4). In this section, an obvious transition is noticeable in the east, with resonance frequencies decreasing within 1 km, from 12 Hz to 4 Hz. Another pronounced decrease in resonance frequencies is observed from north to south. Within a distance of 2.5 km, resonance frequencies decline from 12 Hz to a minimum of 0.9 Hz in the center of the area. A transition zone, marked by the rapid drop in resonance frequencies from around 5 Hz to 1 Hz in only 700 m, is visually represented in Fig. 4 by shades of yellow and light green.

The central region, corresponding to the Pescara city center, exhibits relatively consistent frequencies that vary in the range of 0.9-1.5 Hz. The central portion of this sector hosts the lowest frequencies within this range (Fig. 4).

In the southern portion of the study area, limited measurement points may impact the precision of the statistical model. Nevertheless, a trend remarkably similar to the one recorded in the north can be observed from the center toward the south of the study area, with resonance frequencies varying from approximately 0.9 Hz to 7 Hz across 2 km. A comparable transition zone, about 600 meters long, is characterized by a rapid increase in resonance frequencies.

The concentration of the lowest resonance frequencies in the center of the study area, with increasing values towards north and south, alongside the lateral variation of resonance frequencies shown in the cross-section of Fig. 3, supports the 1D nature of the measurement sites and suggests a strong dependence on local paleovalley geometry.

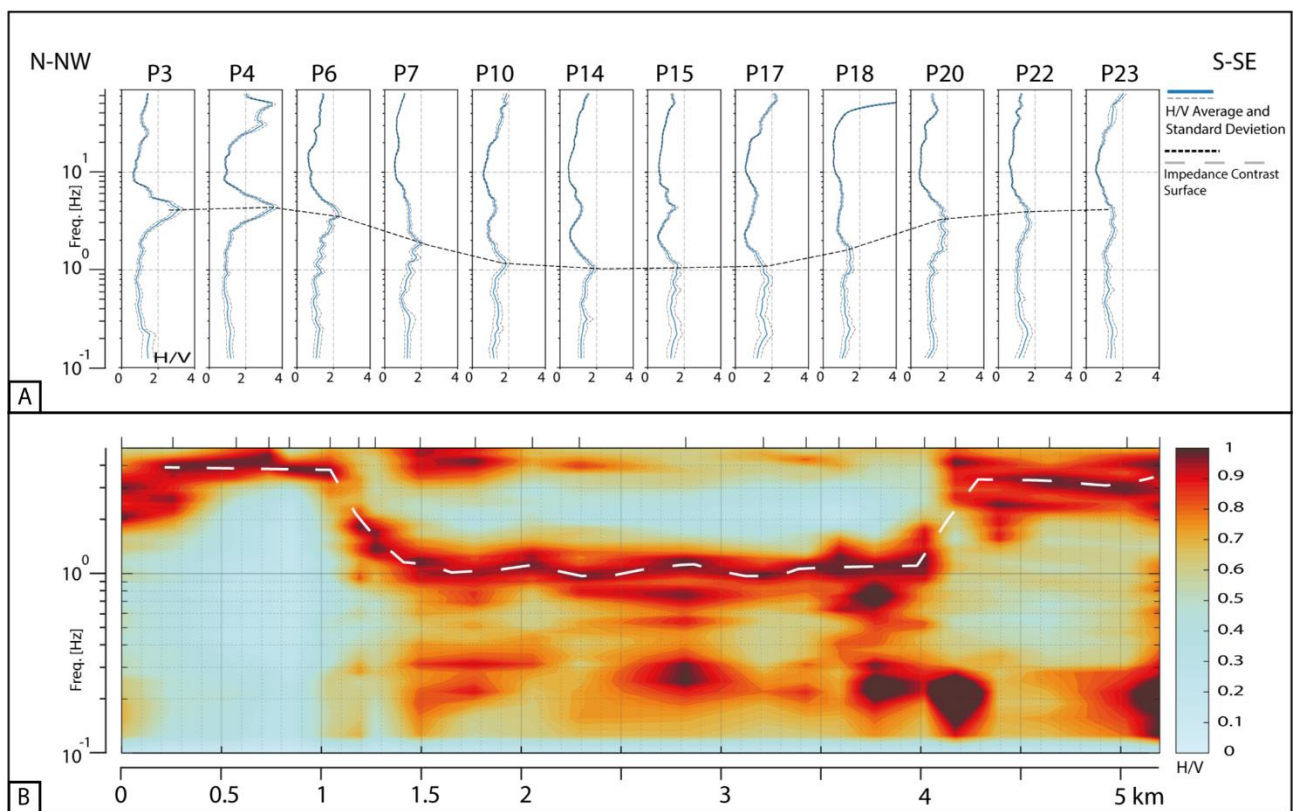


Fig. 3. Representative mHVSr curves of the Pescara paleovalley systems (A) and complete mHVSr frequency contour plots (B) from Di Martino et al. (2023). The black (A) and white (B) dashed lines represent the lateral correlation of the resonance frequency peak. Section trace in Fig. 1.

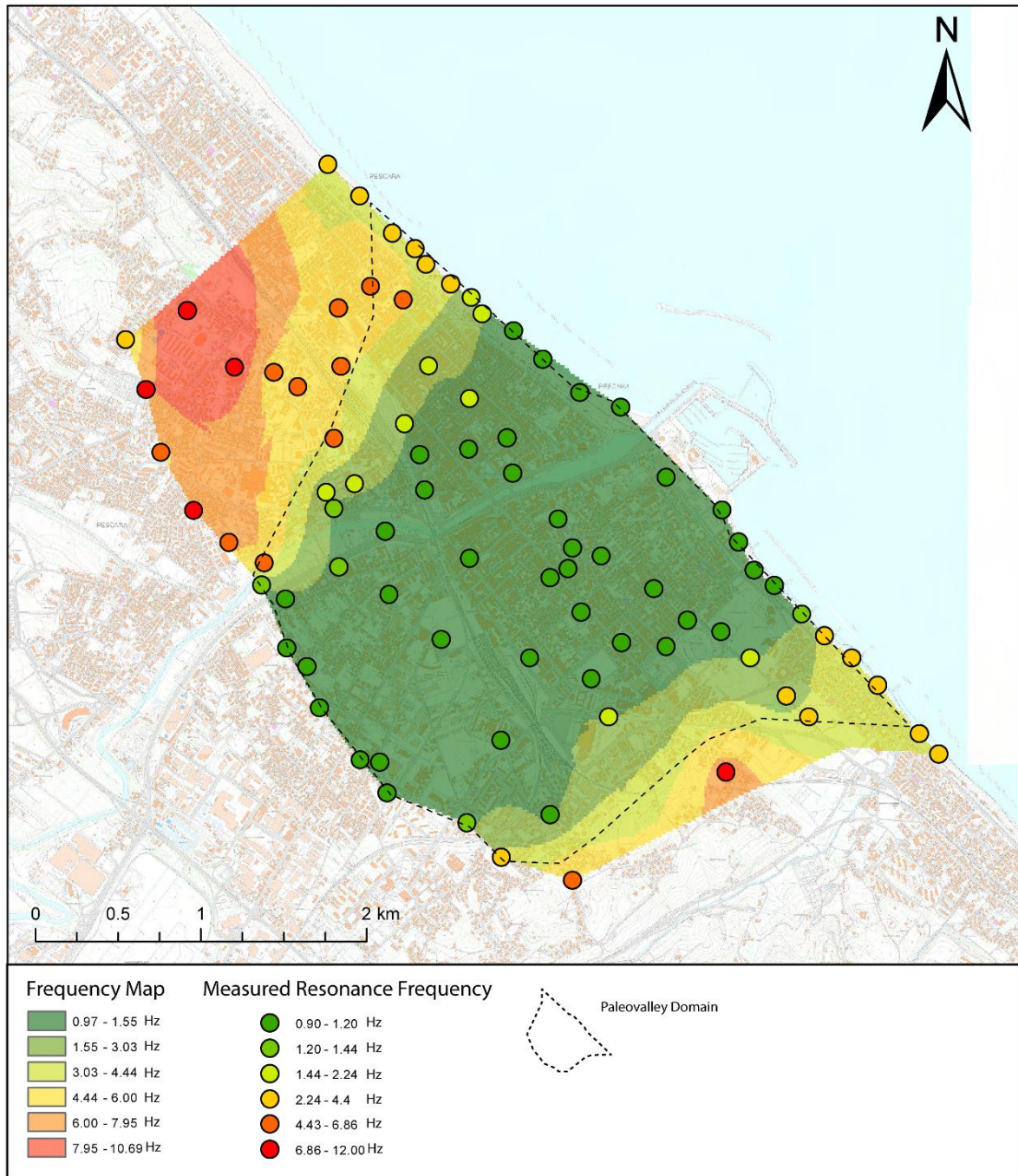


Fig. 4. Resonance frequency map: values are classified using the Jenks natural breaks classification method. Resonance frequencies measured at 85 data points are also represented.

## 7.4 Geophysical 3D modeling of the paleovalley system

### 7.4.1 Frequency-Depth conversion

Accurate correlation of geological and geophysical data is required to transform the H/V profiles from the frequency to the spatial domain and for a reliable interpretation of microtremor measurements. In this regard, the 1D resonance equation links the thickness of the resonating layer ( $h$ ) with the fundamental ground resonance frequency ( $f_0$ ) and the shear wave velocity ( $V_s$ ):

$$f_0 = \frac{V_s}{4h} \quad (1)$$

Equation 1 requires the assumption of (i) 1D site conditions at each measurement site, and (ii) a  $V_s$  model for the sediment layer.

Relying on continuous core data, it is possible to produce a frequency-depth model; thus a  $V_s$  velocity profile can be derived in the area by correlating the observed depth of the impedance contrast surface and the measured resonance frequency at that point (e.g., Ibs-von Seht & Wohlenberg, 1999).

For this purpose, we carried out microtremor measurements on the exact location of 20 boreholes used for the model calibration; we carefully analyzed all microtremor data acquired in nearby sites to identify the depths of the impedance contrast surfaces (Fig 5A). In the study area, a major impedance contrast surface was identified at the marked lithologic contrast between the soft, clay-dominated upper paleovalley fill and the underlying gravel that typifies the paleovalley floor; whereas, at the paleovalley flanks the impedance contrast is inferred to be the sharp boundary between the soft clayey fill and the overconsolidated substrate. For the detailed calibration of sediment cores with the corresponding mHVSr curves, the reader is referred to Di Martino et al. (2023b).

Assuming a power-law relation for increasing  $V_s$  with depth, a frequency-depth model can be derived by fitting the resonance frequency with the identified depth of the impedance contrast, following the method of Ibs-von Seth and Wohlenberg (1999), subsequently used by several authors (e.g., Paolucci et al., 2015; Parolai et al., 2002; Tün et al., 2016).

The derived frequency ( $f$ ) – depth ( $H$ ) fitting function is expressed as  $H = 45.071f^{-1.242}$  (2) (Fig. 5B). This function applies within the depth range used for the regression analysis.

The resulting model (Fig. 5B) is constrained with geological data between about 50 and 18 meters below sea level. However, within the range of 30 to 18 meters the model is less constrained, with only 4 out of 20 total constraint points falling in this interval. In spite of this, the model exhibits good performance with no significant outliers and a mean absolute error (MAE) of 0.66, which measures the average magnitude of errors between the predicted and observed values. A residual error graph (Fig. 5C) was produced to further validate the model performance. This graph compares the model-predicted depth values against the depths observed along the cores.

Figure 5C shows a maximum error of 1.8 meters between the predicted and observed values. Remarkably, most measurement points fall within the range delineated by the dotted green lines, corresponding to the MAE value of 0.66. Furthermore, the distribution of residual errors follows a Gaussian trend, with the model's errors distributed symmetrically around zero, implying that it does not consistently overestimate or underestimate the prediction. A Gaussian distribution indicates a random and unbiased distribution of errors to further support the robustness of the model.

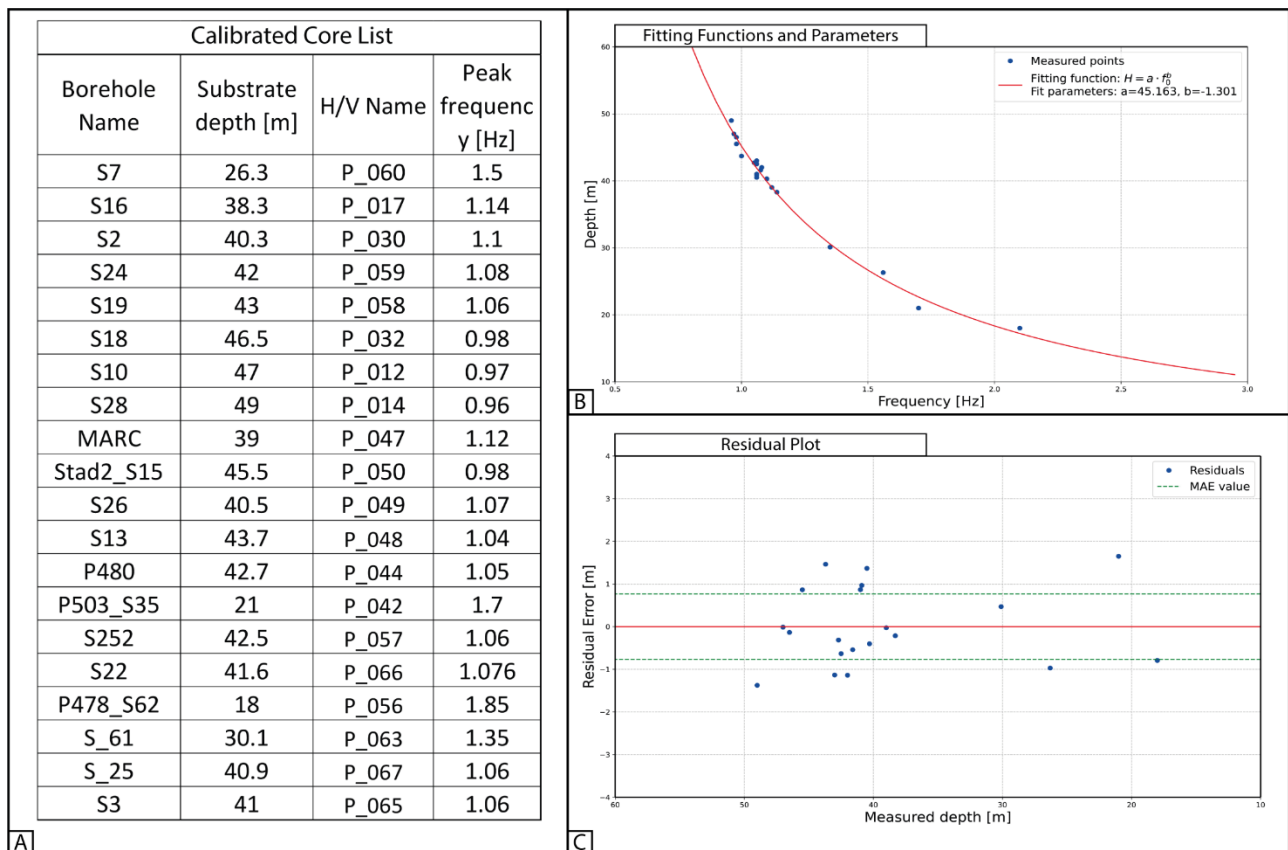


Fig. 5. A) Depths and resonance frequencies used to constrain the model. B) Correlation function, along with parameters 'a' and 'b. C) Plot of residual errors, with the green dashed line indicating a mean absolute error (MAE) value of 0.66 meters.

### 7.4.2 3D depth model

By means of equation 2, we transformed each H/V curve from the frequency to the spatial domain. We estimated 85 depth values corresponding to the resonance peaks correlated with the top of the gravel body along the paleovalley floor. To obtain a 3D model of paleovalley geometry, we performed the Kriging geostatistical interpolation on the resulting depth points. While the microtremor measurements cover a wider area, the 3D model is limited to the paleovalley. In the northern and southern portions of the study area, the paleovalley wedges out, and only a few meters of Quaternary deposits overlie the Pleistocene marine substrate, at these locations. Microtremor measurements, showing the rapid increase in resonance frequencies towards the north and south, significantly assist in constraining the paleovalley domain.

The 3D subsurface model (Fig. 6) outlines the buried paleovalley geometry, with relative depths ranging from 8 m to -51 m above sea level. The rapid change in resonance frequencies, converted from the frequency to the spatial domain, marks the presence of steep buried flanks that bound the paleovalley to the north and south. In the northern portion, the inferred paleovalley depth varies from -3 m. a.s.l. (interfluvial), to -40 m. a.s.l. (depocenter), in 650 meters. The southern flank is steeper; here, we observe changes in depth from -45 m a.s.l. to 8 m a.s.l. in 600 meters only. The maximum depth (about -51 m a.s.l.) is observed in the middle of the study area, beneath the city of Pescara, delineating the paleovalley depocenter.

Changes in depth are illustrated using a color spectrum ranging from dark blue to dark red; these hues represent deeper (depocenter) and shallower (valley margin) paleovalley portions, respectively, thus outlining the paleovalley morphology.

The geometry and thickness of the buried valley system inferred from the geophysical modeling are consistent with those reconstructed through stratigraphic investigations (Campo et al., 2022; Di Martino et al., 2023b).

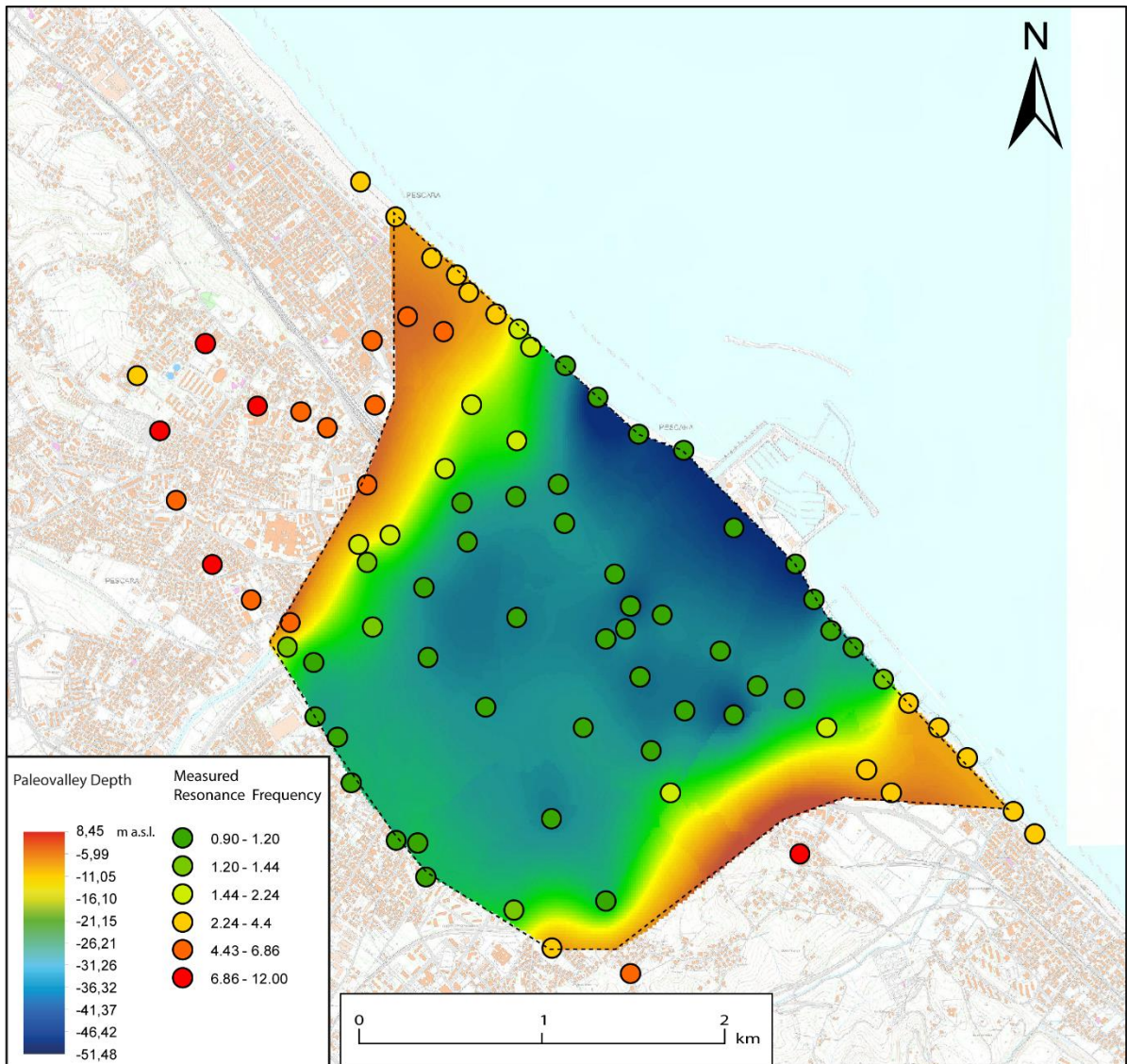


Fig. 6. 3D map of the Pescara paleovalley obtained using geostatistical Kriging interpolation.

## 7.5 Shear wave velocity of the paleovalley fill

Realistic velocity profiles are crucial to perform ground motion simulations. By means of equation 2, it was possible to obtain a  $V_s$  profile, which represents an average of the whole modeled body within the depth range used to constrain the regression model. Although this approach is not a direct  $V_s$  measure, several authors have applied this technique to characterize seismic velocity in many valleys and sedimentary basins (e.g. Castellaro & Mulargia, 2009; Ibs-von Seht & Wohlenberg, 1999; Parolai et al., 2001, 2002; Sgattoni & Castellaro, 2020, 2021).

Our model denotes very low  $V_s$ , with homogeneous values in the fine-grained paleovalley depocenters (about 180 m/s) and a  $V_{s30}$  of 165 m/s, which place the paleovalley fills at the boundary between ground types D and C of the EUROPEAN COMMITTEE FOR STANDARDIZATION, 2004 (EC8).

Given the low velocities that typify the paleovalley fill, we compared the paleovalley velocity profile with a selection of calibrated velocity profiles derived from frequency vs. depth relations, which represent  $V_s$  profiles from different sedimentary basins and river valleys (Chandler and Lively, 2016; D'Amico et al., 2008; Delgado et al., 2000; Di Martino et al., 2023; Garcia-Jerez, 2006; Gosar and Lenart, 2010; Hinzen et al., 2004; Ibs-von Seht and Wohlenberg, 1999; Le Roux et al., 2012; Moon et al., 2019; Motazedian et al., 2011; Özalaybey et al., 2011; Parolai et al., 2002; Tün et al., 2016).

To perform a reliable comparison, we selected 15 Holocene velocity profiles covering a broad range of geological features (Fig. 7). To avoid any possible bias due to significant differences in basin size, we only selected models with shallow constraint points in a depth range compatible with the Pescara paleovalley system (0-80 m).

Figure 7 highlights the remarkably lower velocity profile of the Pescara paleovalley system, alongside those from Manfredonia (Italy), the Segura River valley (Spain), and Ottawa. It is remarkable that subsurface stratigraphy in the Segura River Valley, Ottawa and Manfredonia delineates typical (paleo)valley geometries, making those sites very similar to the Pescara area. In these cases, the increase in shear wave velocity with depth as shown by the slope of the derived  $V_s$  model is not prominent and  $V_s$  values exhibit only minor variations with depth. On the other hand, in markedly different geological contexts, the increase in shear wave velocity with depth is appreciable even in the shallow subsurface.

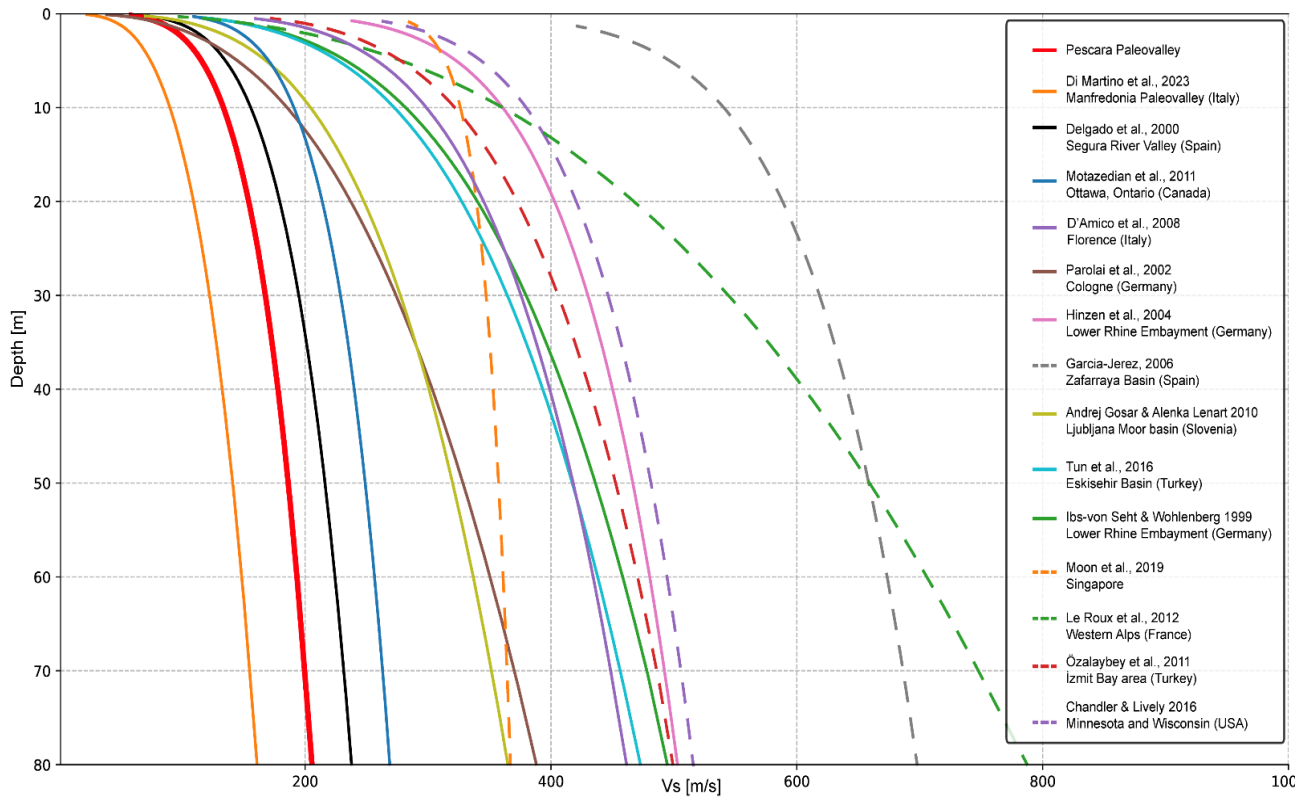


Fig. 7. Comparison of 15 Vs profiles from a variety of sedimentary basins and river valleys. The selected profiles are constrained with shallow points from 0 m to - 80 m.

Ground motion simulations that rely uniquely on the indirect estimation of velocity profiles can be unreliable in intricate geological contexts. Therefore, acquiring direct velocity measurements along the whole stratigraphic succession down to the bedrock is recommended and provides a clearer view of the actual layering in the study site.

With this purpose, we carried out a Down Hole test (DH) in the same location as the Marconi reference core described in Campo et al. (2022). Additional 5 DH tests (DH1, DH3, DH5, DH6, and DH7 in Fig. 8) were collected from seismic microzonation studies and tentatively re-interpreted.

We individually analyzed the DHs to characterize the velocity profiles beneath each measurement point. Furthermore, all the DHs were utilized to calculate the shear wave velocities, expressed in terms of mean and standard deviation, for the main stratigraphic layers identified in the study area (Fig. 8).

The velocity profiles from the 6 DHs show a clear seismic layering, and DHs 6, 7, and Marconi show a prominent velocity inversion that characterizes the uppermost 8 to 10 meters. This feature, caused by the local presence of a thick layer of fluvial and coastal sands, could not be detected by

equation 2. In all the DH profiles, a low-velocity layer can be identified, with a variable thickness ranging from 20 to 35 meters. This layer represents the soft fill of the paleovalley, with an average velocity of approximately 170 m/s. DHs 5, 1, and 3 were acquired in more proximal positions: they do not have sand on top, but show another distinguishable layer: the top 8 meters in DH 5, and stratigraphic intervals between -23 and -38 m in DH1, and between -23 and -32 in DH 3 are characterized by a slightly higher  $V_s$ , caused by the presence of a floodplain clay layer.

Down-Hole tests 1, 3, and 7 are deep enough to characterize the gravels at the paleovalley floor, denoting a  $V_s$  of 450 m/s, while only DH 1 reached the substrate, which shows the highest  $V_s$  of 700 m/s.

Velocity profiles from DHs and microtremor measurements did not differ significantly down to the valley floor (Fig. 8), confirming that the microtremor-based model is an adequate approximation of the  $V_s$  in the study area.

The  $V_{s30}$  values calculated based on the DH data are as follows: DH5 = 173 m/s, DH1 = 157 m/s, DH3 = 192 m/s, DH6 = 203 m/s, DH7 = 206 m/s, and DH Marconi = 212 m/s, with an average value of 190 m/s (Fig. 8). As a result, soil classification according to EC8 edges between categories C and D, falling into C for 4 out of 6 DH locations and into D for DH 5 and 1.

The thickness of the uppermost sandy layer strongly influences soil classification strictly based on the  $V_{s30}$  value. As this layer is laterally discontinuous, the  $V_{s30}$  value may fall above and below 180 m/s at different sites within the paleovalley.

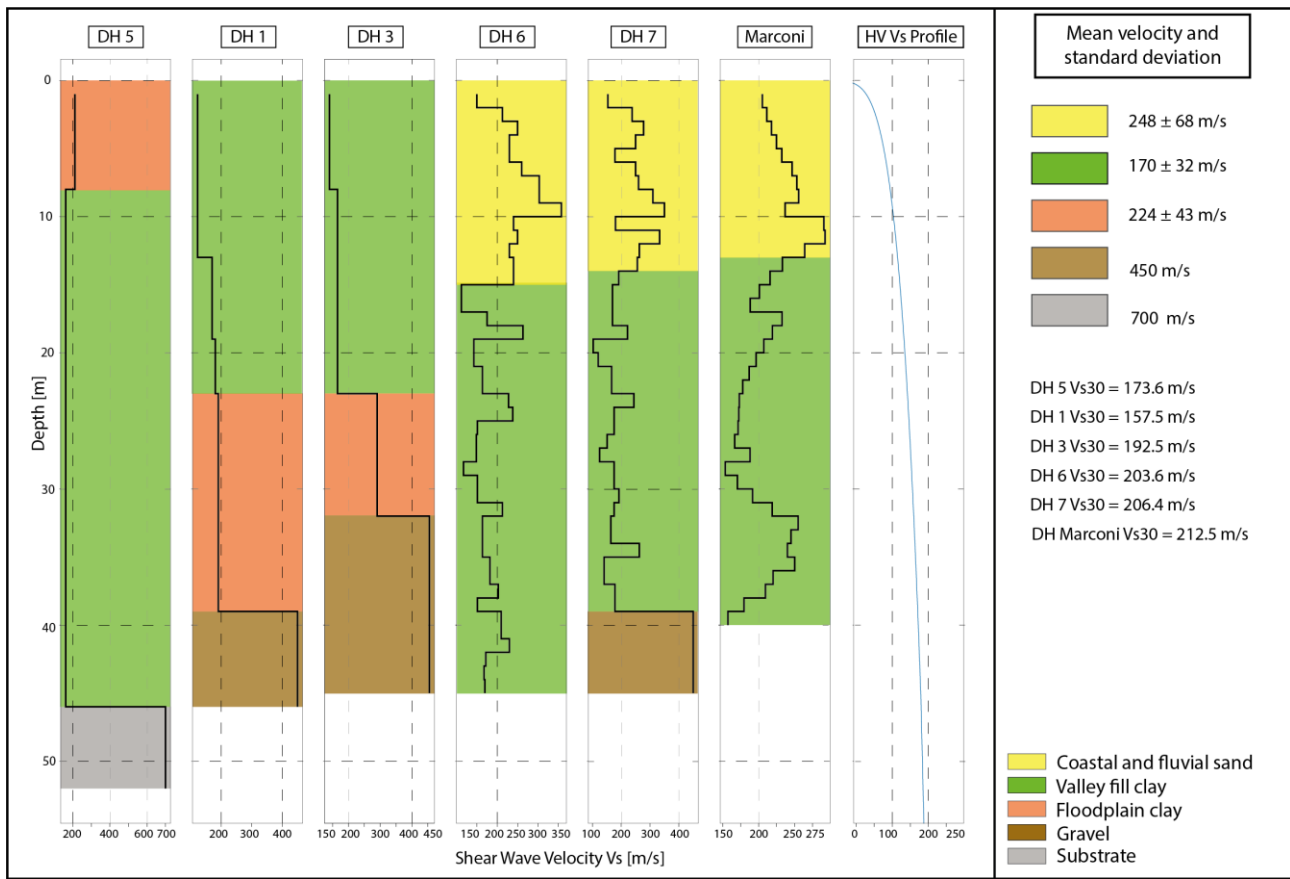


Fig. 8. Comparison between 6 Down Hole measurements and the microtremor-based velocity model derived from Equation 1. The DH measurements were individually analyzed to identify the primary subsurface layers. To the right, the average velocities of the layers and Vs30 values are indicated.

## 7.6 Seismic Response Analysis

### 7.6.1 Model parameters

To perform 1D-2D seismic response analysis, we utilized the LSR2D software (“Stacec LSR2D (Local Seismic Response 2D),” 2017) that relies on the Kelvin-Voigt model and employs a finite element approach under plain-strain conditions. In LSR2D, the wave equations are solved through direct integration in the time domain using the Newmark method; this method is known for its stability and a lack of numerical damping (Hudson et al., 1994).

The simulation was performed on a stratigraphic cross-section that runs transversal to the Pescara paleovalley, along its depocenter (Fig. 9). Cross-section geometries and layer thicknesses are based on the 3D geophysical depth model (red line in Fig. 9) and 22 core descriptions from the seismic microzonation project database ([https://ambiente.comune.pescara.it/?page\\_id=84](https://ambiente.comune.pescara.it/?page_id=84)) of the municipality of Pescara. The stratigraphic correlation was carried out based on sedimentological and geometric criteria.

In direct contact with the substrate (Mutignano Fm), a laterally extensive fluvial gravel body (brownish layer in Fig. 9) typifies the lower paleovalley fill, approximately between -40 and -50 meters above sea level. This gravel body is overlain by an up to 31-m-thick layer (green in Fig. 9), consisting of unconsolidated clays and representing the upper paleovalley fill. Modern alluvial and coastal sands (yellow layer in Fig. 9), up to 13 m thick, characterize the top of the succession, in lateral transition with floodplain deposits (orange layer in Fig 9).

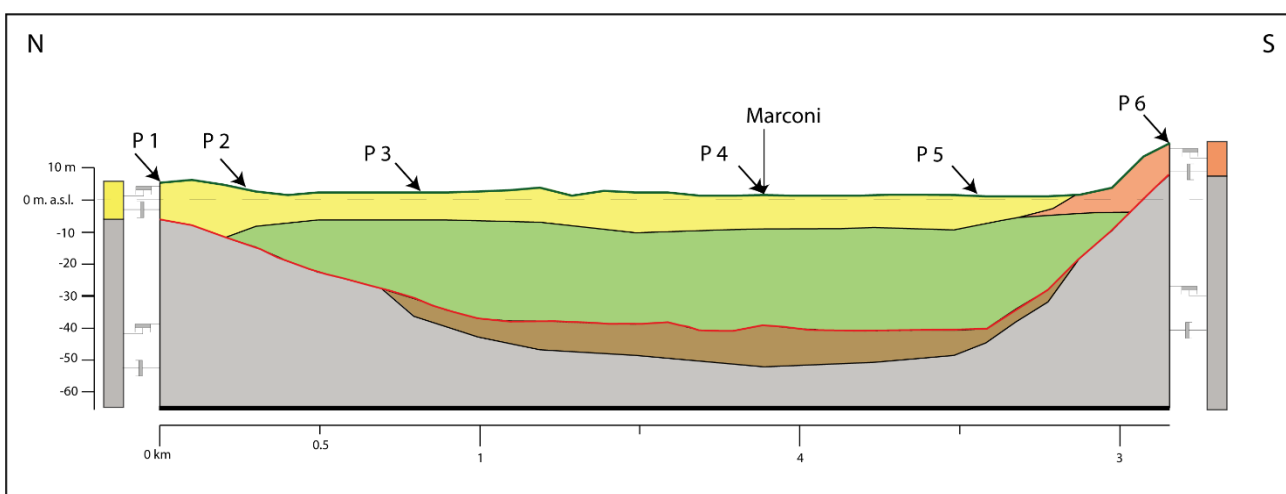


Fig. 9. Stratigraphic cross-section used for 2D-1D Seismic response modeling. The panel displays the five identified layers, and the output points used for the model output.

The subsurface model is approximated during the simulation using a mesh of interconnected quadrilateral elements with shared nodes. This approach enables the generation of a highly detailed mesh, representing a critical consideration in 2D modeling with a complex subsurface (Khan et al., 2017).

The output points utilized for the 2D seismic response model outputs are presented in Figure 9. Moreover, one-dimensional analysis was undertaken at these designated points, ensuring a comprehensive investigation through multiple analytical approaches.

The solution accuracy and the computational complexity strongly depend on the mesh characteristics. In this context, the subsurface model was discretized using quadrangular elements, following an adaptive approach based on the equation:  $D_{\max} = \frac{\lambda}{k} = \frac{TV}{k}$  (3), where  $D_{\max}$  is the maximum height of the quadrangular elements,  $V_s$  is the shear wave velocity,  $\lambda$  represents the wavelength, and  $T$  refers to the maximum period of interest. This adaptive approach discretized our cross-section into 115,044 elements.

To define the boundary conditions of the model, LSR2D provides a set of viscous dampers to replicate the characteristics of a deformable rock; we used this condition along the lower border of the mesh to avoid unrealistic seismic reflection. In addition, we incorporated free-field pillars along the section borders (Fig. 9) to absorb shear wave reflections originating from the rigid edges of the section (Zhang et al., 2003); the use of rigid boundaries is an inconsistent assumption, as the substrate and the overlying layers are laterally extensive.

We considered non-linear soil behavior in 1D and 2D simulations, including normalized shear modulus ( $G/G_0$ ) versus strain ( $\gamma$ ) and damping ratio ( $D$ ) versus ( $\gamma$ ) curves as input, with  $G$  being the shear module and  $D$  the damping ratio. To model the behavior of the paleovalley fill, we acquired two undisturbed samples from the clayey paleovalley fill and the coastal sand of the Marconi reference core through an Osterberg piston sampler. We performed the resonance column test to derive the constitutive law of soils (Fig. 10). The resulting  $G/G_0$  and  $D$  versus strain ( $\gamma$ ) curves (Fig. 10) were used to typify the valley fill and the top sandy layer. For the substrate, the fluvial gravel at the bottom, and the floodplain clays at the top of the paleovalley sedimentary succession, we used standard literature  $G/G_0$  and  $D$  versus strain ( $\gamma$ ) curves from (Seed et al., 1986).

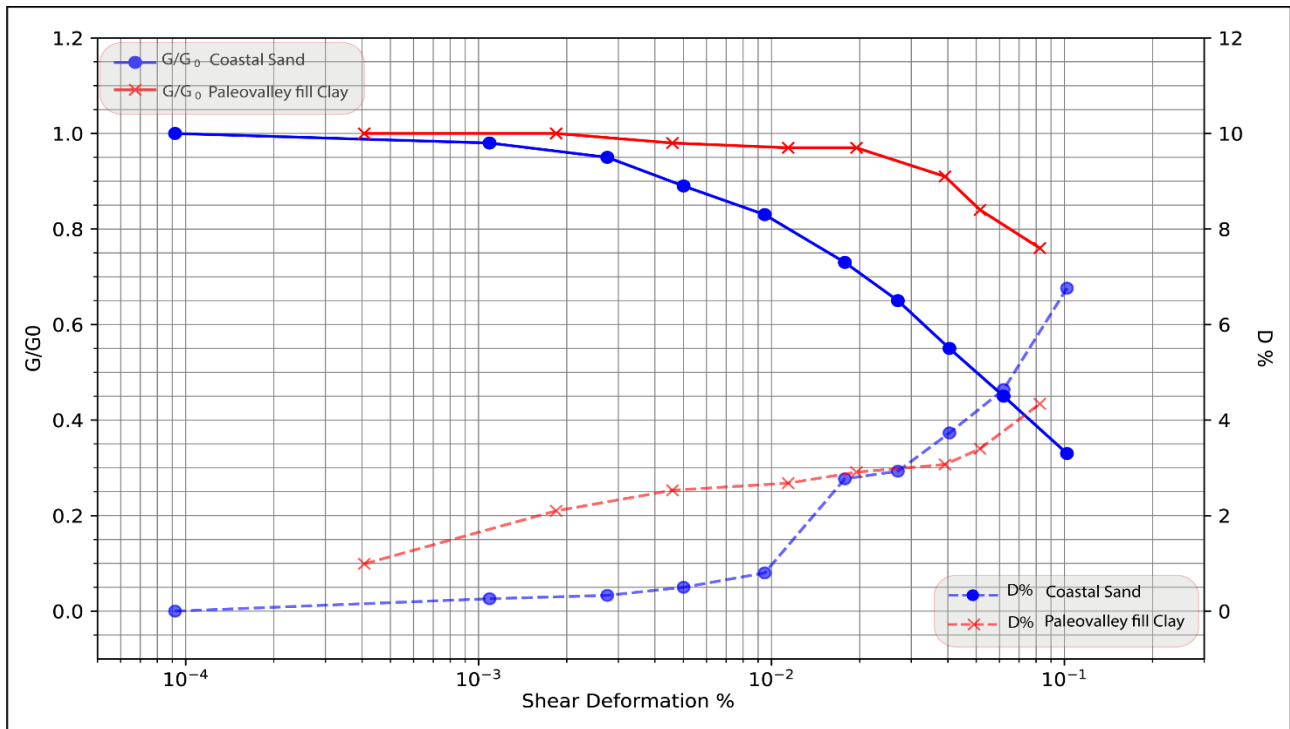


Figure 10. Constitutive law of coastal sand (blue line) and paleovalley fill clay (red line) from the Marconi reference core. Solid lines represent the  $G/G_0$  curves, dashed lines represent the  $D\%$  curves.

The LSR2D software requires discretizing the  $V_s$  for each layer. The velocity model utilized is based on the interpretation of the 6 DH tests within the study area, described in Section 3. The used values are the mean  $V_s$  for each stratigraphic layer, as shown in Figure 8.

To perform the local seismic response simulation, we utilized 9 different seismic inputs (Fig. 11) chosen from natural and artificial sources, following a widely adopted methodology in engineering practice and recommended by various international seismic codes, including NTC18 (“MIT (2018) NTC 2018 D.M. del Ministero delle Infrastrutture e dei trasporti del 17/01/2018. Aggiornamento delle Norme Tecniche per le Costruzioni (in Italian),” n.d.) and the (EUROPEAN COMMITTEE FOR STANDARDIZATION, 2004). Seismic inputs include two Ricker wavelets at 0.9 Hz and 3 Hz, used to simulate shear waves at the observed resonance frequencies in the center and along the flanks of the paleovalley. Additionally, we used 7 natural accelerograms (Bommer and Acevedo, 2004) recorded on rigid and flat soil (Soil type A and topography type T1 according to Eurocode 8 soil categories) derived from RexelWeb (Iervolino et al., 2011, 2010; Sgobba et al., 2021, 2019). All the

accelerograms (Luzi et al., 2020) are spectrum-compatible with the uniform hazard spectrum of Italian building code NTC18 in the Pescara area. Based on the Italian seismic hazard map, the Peak Ground Acceleration (PGA) estimate, calculated on rigid and flat ground, for a probability of exceedance of 10% in 50 years, which is the standard for ordinary buildings, is found to be 0.17 g. The selection accelerograms were constrained based on seismic disaggregation (Bazzurro and Allin Cornell, 1999; Pace, 2006), which relies on the parameters of magnitude and distance that most influence the Pescara area ( $M_w = 4.5-6.5$  and distance 0-30 km, (Stucchi et al., 2011)).

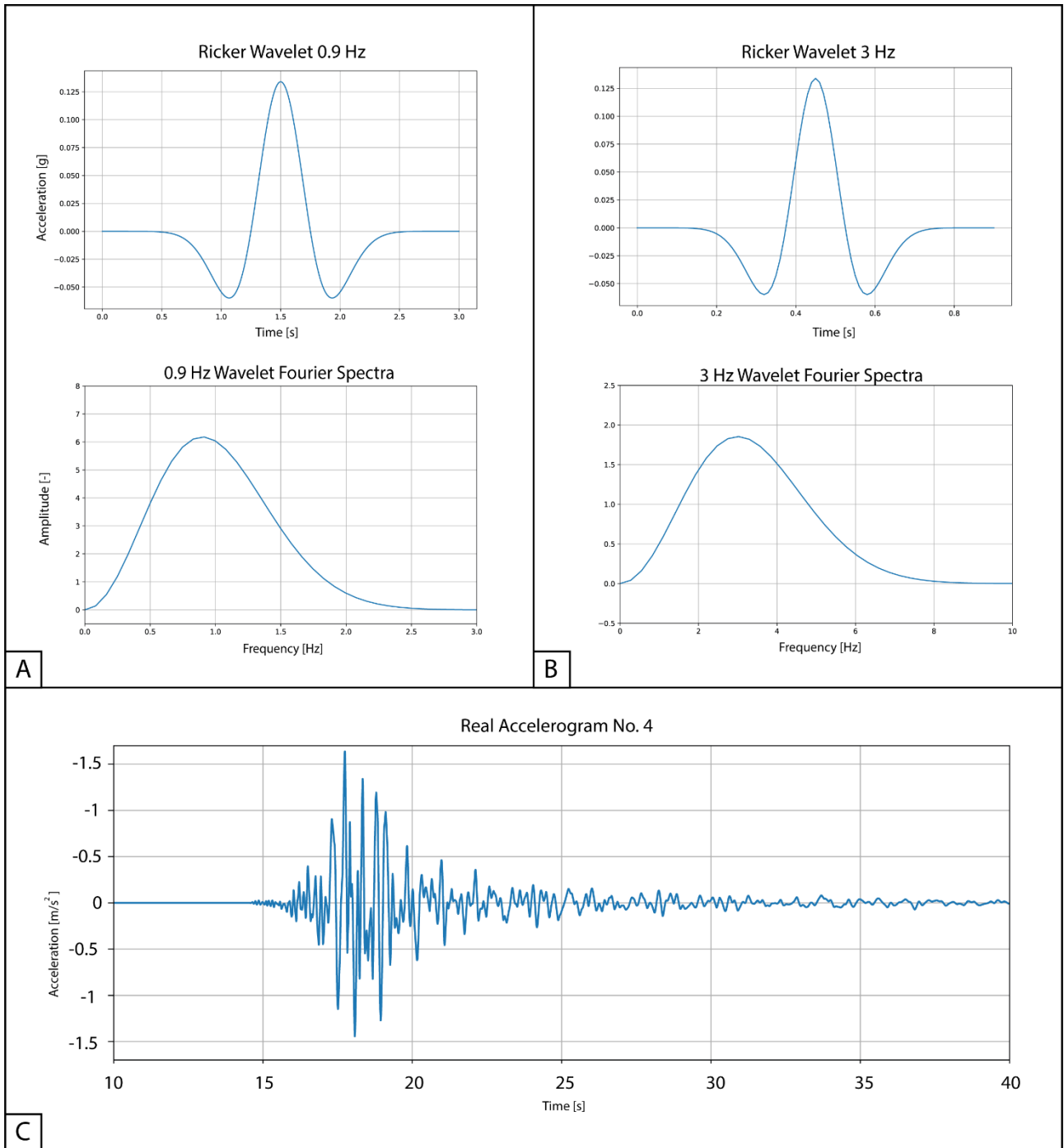


Figure 11. Input signals used for the 1D and 2D simulations. The top two subplots show Ricker wavelets centered at frequencies of 0.9 (A) and 3 Hz (B). Their respective Fourier spectra are presented below. The bottom subplot (C) shows an example of one out of seven real accelerograms used for the simulation.

## 7.6.2 Model Results

We analyzed the results obtained from the local seismic response modeling in terms of peak accelerations, transfer functions, amplification factors, and response spectra to provide a detailed insight into the seismic response of the Pescara paleovalley system.

The results obtained using both real and synthetic signals highlight the different behavior of the valley in response to the variations in the frequency content of the input signal. Figure 12 displays the peak acceleration values, expressed in  $\text{m/s}^2$ , calculated at every point on the mesh for Ricker Wavelets at 0.9 Hz and 3 Hz. Figure 12A, referring to the low-frequency signal, shows that the highest accelerations are located at the center of the valley, with a peak of  $1.9 \text{ m/s}^2$ , and that they tend to decrease towards the valley margins. The 3 Hz signal (Fig. 12B) exhibits an opposite trend, the highest accelerations ( $1.6 \text{ m/s}^2$ ) being recorded along the valley flanks. This result highlights the influence of the frequency content of the input signal on modeling the seismic response of the valley.

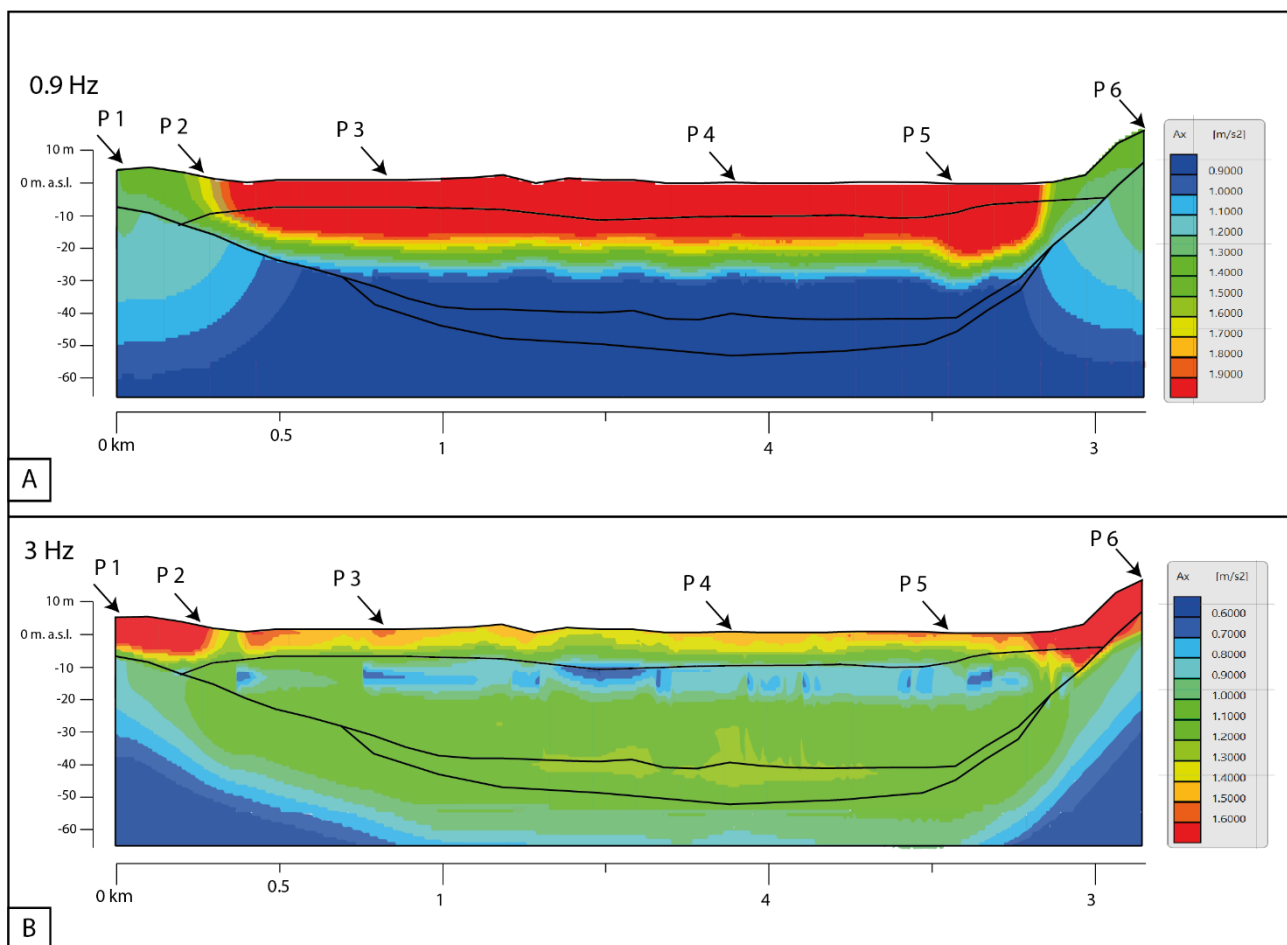


Figure 12.. Cross-section of peak accelerations (along the X direction) computed over the entire mesh. A) Valley response to the 0.9 Hz Ricker wavelet; B) valley response to the 3 Hz Ricker wavelet.

We calculated the transfer function, derived from the 2D seismic response model, at every output point (P1 to 6 of Fig. 9) to illustrate how the system amplifies or attenuates the seismic waves. The transfer function is defined as the ratio of the Fourier spectra of motion at the surface and at bedrock. The magnitude of this complex function is typically defined as the amplification function or transfer function and shows which components of the seismic motion, in terms of frequency, are amplified or attenuated compared to the reference motion at bedrock.

We computed the transfer functions using real and synthetic input signals (Fig.11) at every output point; the functions derived from synthetic signals are truncated according to their spectral content (Fig. 11). The results obtained from the synthetic and real signals are consistent (Fig. 13).

The transfer functions exhibit clear variations along the valley profile; at the northern and southern margins of the valley (output points P1 and P6 of Fig. 13), a distinct peak shows seismic amplifications of 2.3 at 5 Hz and 2.5 at 5.5 Hz, respectively. Along the valley flanks (P2, Fig. 13), high seismic amplification around 3 is observed at 3 Hz. The output points P3 and P5 (Fig. 13) are located in a middle position between the flanks and the depocenter (Fig. 9) and show higher seismic amplification of about 4 at 1.3 Hz and 1 Hz, respectively. In the valley center (output points P4, Fig. 13), the transfer functions display a clear peak with amplitudes of 4 and 4.5, respectively, at a frequency of 0.9Hz.

Secondary peaks with lower amplitudes and higher frequencies are also present along the valley flanks, in P2 (8.5 Hz), and in intermediate position, P5 (1.9 Hz, 3.4 Hz, and 4.8 Hz). Minor peaks in the valley center (P3 and P4) are observed at 2.8 Hz and 5 Hz.

At the same output points, 1D seismic response simulations showed comparable results (Fig. 14). The one-dimensional modeling reproduces the main amplification peaks at all output points, with minor differences observed only on the secondary peaks at output points P2 and P5 (Fig. 14).

The frequencies at which amplification occurs across the entire topographic profile of the valley are consistent with the resonance frequencies observed from the experimental data described in sub-section 3.2 (Fig. 4).

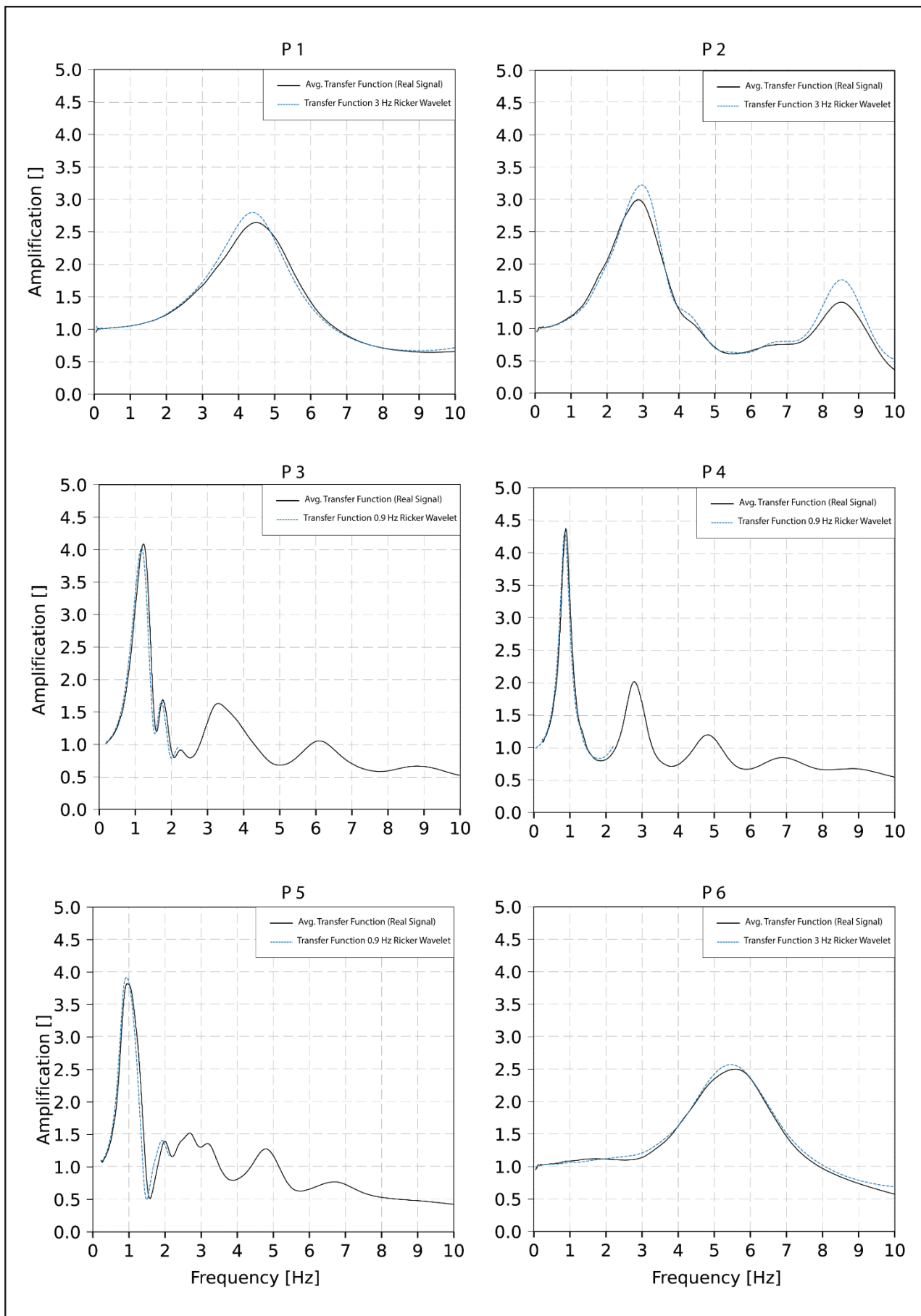


Figure 13. Transfer functions obtained from the 2D seismic response modeling and calculated at output points located at the surface, as shown in Fig. 9 (P1-2-3-4-5-6).

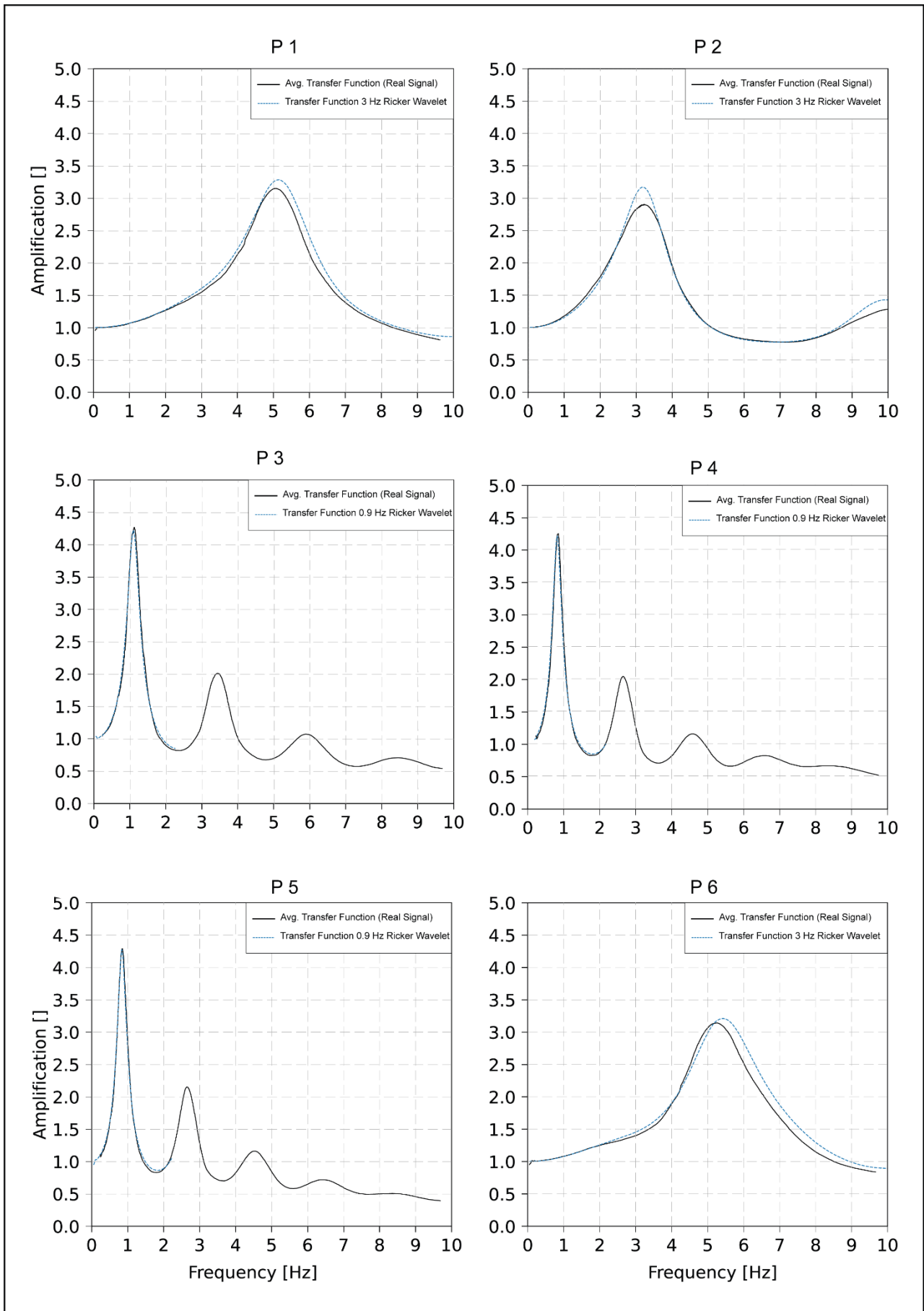


Figure 14. Transfer functions obtained from the 1D seismic response modeling, calculated at output points located at the surface, as shown in Fig. 9 (P1-2-3-4-5-6).

To evaluate the seismic amplification, we calculated the amplification factors along the transect in three distinct period ranges: 0.1-0.5 s, 0.4-0.8 s, and 0.7-1.8 s (Fig. 15). These values are typically employed in engineering practice, as they are likely to interact with different types of structures (Anand and Satish Kumar, 2018; Raheem, 2022). The blue curve (Fig. 15) represents the period range from 0.7 s to 1.8 s that was chosen to encompass the principal amplification peaks of the valley (occurring at frequencies between 0.5 and 1.5 Hz). It exhibits an average amplification of around 2.4 at the valley center within the portion of the valley with a nearly flat substrate, slightly increasing to 2.55 towards the northern and southern margins. The amplifications within this period range sharply decline on the northern and southern interflaves, reaching values close to 1.

The 0.4-0.8 s and 0.1-0.5 s curves, marked by green and red colors, respectively (Fig. 15), show the amplification factors at shorter periods (mid- to high frequencies). These two curves exhibit an opposite trend compared to the low-frequency amplifications, with lowest values close to 1 at the center of the valley and higher amplifications along the valley flanks; the 0.4-0.8 curve reaches 2.7 on the northern flank and 2.3 on the southern flank of the valley, while the 0.1-0.5 curve attains 1.95 on the north flank and 1.7 on the south flank.

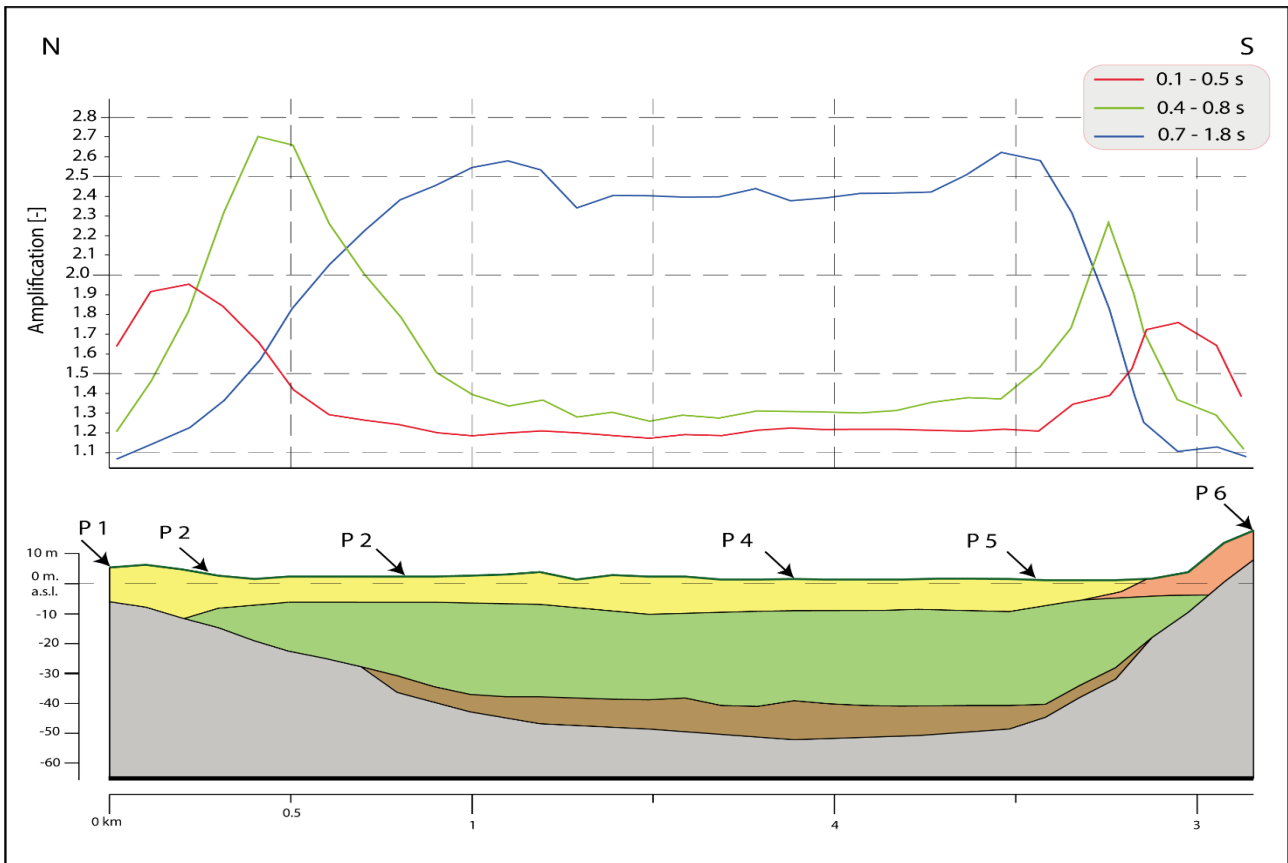


Figure 15. Profile of amplification factors within three different period ranges, calculated across the valley section.

We also conducted a comprehensive analysis of the horizontal acceleration response spectra calculated at all designated output points, which we compared with the design response spectra based on the Eurocode 8 guidelines (Fig. 16). The selected regulation response spectrum is based on the EC8 simplified approach for soil category C ( $V_{s30} > 180$  m/s). The selection of soil category C is based on the  $V_{s30}$  value calculated from the DH test closest to the analyzed valley cross-section, which is higher than 200 m/s. The comparison (Fig. 16) reveals that the EC8 spectrum significantly underestimates spectral accelerations at a period of around 1.0 s in the center of the valley and between 0.2 s and 0.6 s at the valley margins and flanks. We also calculated the response spectrum parameterized according to EC8 (dashed gray line in Figure 16) from the modeled response spectra at each output point. Compared with the soil C spectrum, the parameterized spectra also clearly underestimate spectral accelerations within periods ranging between 0.7 s and 4 s in the valley center and between 0.18 s to 0.35 s at its margins and flanks.

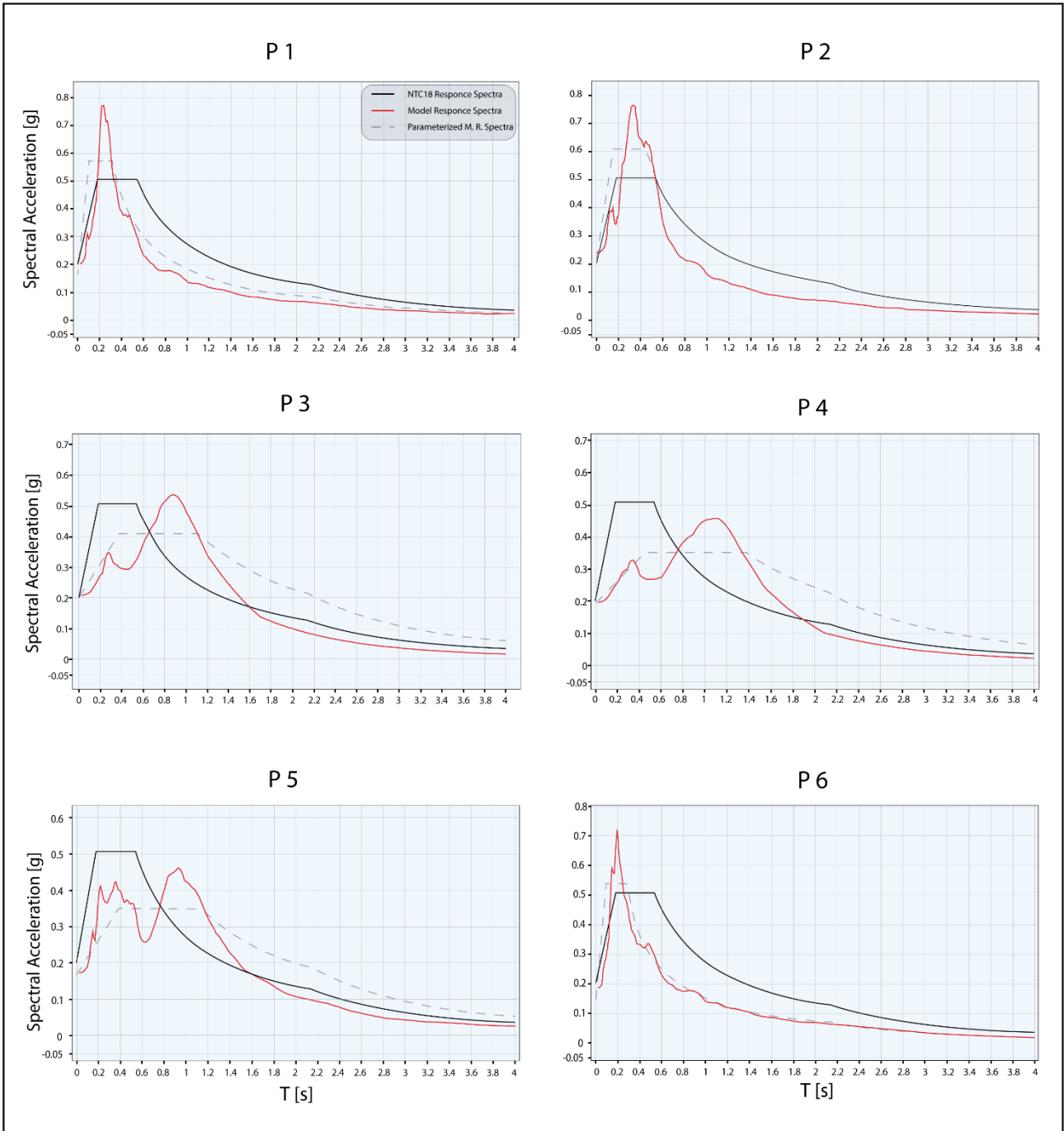


Figure 16. Horizontal acceleration response spectra obtained from the 2D seismic response simulation (red line) compared with response spectra based on the Eurocode 8 standards (black line). The figure also displays the parametrized response spectrum according to the Eurocode 8 guidelines (gray dashed line).

## 7.7 Discussion and Conclusions

Effective site characterization and seismic response studies require a comprehensive reconstruction of subsurface features, including variations in the geophysical properties of sediments and a detailed reconstruction of their geometry. Late Quaternary paleovalley systems represent a potential and usually underestimated seismic hazard, as they can modify ground motions due to their soft infill ( $V_s$  value  $< 200$  m/s) and the sharp contrast with the adjacent substrate.

Through geostatistical interpolation of 85 microtremor measurements (Fig. 1), we reconstructed a map of the resonance frequencies observed in the Pescara paleovalley area (Fig. 4), revealing abrupt frequency changes. This map also allowed us to delineate the boundaries of the paleovalley domain, which would have been otherwise difficult to define based uniquely on vertical, site-specific geological data.

Using high-resolution continuous core descriptions, we observed a strong correlation between resonance frequencies and subsurface stratigraphy that allowed us to estimate a frequency-depth model for the paleovalley infill (Fig. 5) and reconstruct a geophysical 3D depth model of the buried paleovalley morphology (Fig. 6). Moreover, leveraging six velocity profiles from down-hole tests, we reconstructed a detailed seismic layering of the valley infill, identifying five main seismic/stratigraphic layers (Fig. 8), with  $V_s$  values close to the average model derived from the frequency-depth regression.

To perform a 2D seismic response modeling, we built a stratigraphic cross-section running through the paleovalley depocenter that depicts facies architecture transversal to the paleovalley axis (Fig. 9). The stratigraphic cross-section provides a high-resolution framework for the seismic modeling that was conducted using synthetic and real seismic input along with  $V_s$ ,  $G/G_0$  and  $D\%$  curves directly measured on the paleovalley sediments.

Although the 2D model implemented for the seismic response simulation relied uniquely on stratigraphic data, the transfer functions computed at different output points on the surface revealed significant amplification factors peaking at frequencies that closely match the resonance frequencies obtained through geophysical investigation.

The main amplification in the center of the paleovalley is observed at frequencies between 0.9 and 1.3 Hz, with an amplification factor equal to 4. Towards the valley margins, the largest amplifications are observed at about 5 Hz and have smaller amplification factors, between 2.5 and 3. While at the valley flank, the main amplification is 3 at a frequency of 3 Hz. These factors reveal a

notable increase in the amplification amplitude compared to simpler geological contexts (Falcone et al., 2021) that lack paleovalley systems. Moreover, the amplifications are located in frequency ranges that can interact with a wide range of building types, including ordinary buildings (small and rigid or large and flexible structures), such as those that punctuate the Adriatic Sea coast (Fig. 15).

The comparison of the results obtained at the same output points with 1D e 2D modeling approaches revealed only slight differences between the two methods. The 2D modeling approach used, therefore, does not highlight clear 2D valley effects in the dynamic behavior of the paleovalley. This can be explained by the generally flat geometry of the valley fill, which is 3 km wide and less than 50 m thick. We note, however, that our 2D simulation only considers in-plane horizontal motion and, therefore, cannot consider the whole wavefield propagating within the mesh grid.

The results of our seismic response simulations clearly indicate that lateral changes in the seismic response of the valley strongly depend on the local subsurface stratigraphy. Therefore, detailed knowledge of subsurface layering and lateral changes of layer geometries is fundamental for a realistic estimate of the seismic response, especially where no surface morphological expression of the valley is observed. On the other hand, a 1D modeling approach appears a reasonable approximation of the seismic response at a specific point location, providing an adequate representation of the local stratigraphy.

Finally, we computed the response spectra based on 2D modeling and compared them with the response spectra proposed by the Eurocode 8 guideline for soil category C. Remarkably, the strong amplifications observed in the paleovalley system can lead to a significant underestimation of spectral accelerations when compared to EC8 regulations. In the study area, soil classification purely based on  $V_{s30}$  (as proposed by EC8) appears to be inadequate, as it is strongly influenced by the presence/absence of the topmost sand layer, which may result in classification under categories C and D, respectively (Fig. 8), leading to insufficiently restrictive guidelines. The outcomes of this study also imply that the presence of shallowly buried paleovalley systems should lead to classification in soil category D.

A reliable stratigraphic framework, combined with direct measurements of sediment properties such as shear wave velocity,  $G/G_0$ , and  $D\%$  curves, ensures the usage of robust parameters during the modeling phase. However, a limitation of this work lies in the inability to compare the results obtained with amplification values derived from real earthquakes recorded by a seismic station, since the city of Pescara currently does not host this instrument. Installing a seismic station might improve the understanding of paleovalleys amplification phenomena. This work only considered a

2D geometry of the paleovalley in its depocenter; detailed analysis on the influence of the entire 3D geometry will be carried out in future works.

This study highlighted the importance of combining geophysical and geological data, especially in complex geological settings. While the gentle geometry of paleovalleys does not seem to produce evident 2D effects, detailed reconstruction of paleovalley geometry is needed to correctly identify frequencies and amplification factors at every point on the surface.

## Acknowledgments

This research was supported by the Italian Ministry of University and Research under the PRIN 2017 program to Alessandro Amorosi, project number 2017ASZAKJ “*The Po-Adriatic Source-to-Sink system (PASS): from modern sedimentary processes to millennial-scale stratigraphic architecture*”.

## Data Availability

All data are available from the corresponding author upon reasonable request.

## Author Statement

ADM: Conceptualization, Data curation, Formal analysis, Investigation, Visualization, Writing – Original Draft

GS: Methodology, Supervision, Writing – Review & Editing

FP: investigation, Formal analysis

AM: Conceptualization, Funding acquisition, Project administration, Supervision, Writing – Review & Editing

## 8. Sediment core analysis using artificial intelligence

Andrea Di Martino<sup>1†</sup>, Gianluca Carlini<sup>2†</sup>, Gastone Castellani<sup>3</sup>, Daniel Remondini<sup>\*2‡</sup>, Alessandro Amorosi<sup>\*1‡</sup>

<sup>1</sup>Department of Biological, Geological and Environmental Sciences (BiGeA), University of Bologna.  
Piazza di Porta San Donato 1, 40126 Bologna, Italy

<sup>2</sup>Department of Physics and Astronomy, University of Bologna, 40127 Bologna, Italy

<sup>3</sup> Department of Medical and Surgical Sciences, University of Bologna, 40138 Bologna, Italy

<sup>†</sup> The authors contributed equally to the work.

<sup>‡</sup> The authors share the seniorship of the work.

<sup>\*</sup>Corresponding Author

## Abstract:

Subsurface stratigraphic modeling is crucial for a variety of environmental, societal, and economic challenges. However, the need for specific sedimentological skills in sediment core analysis may constitute a limitation. Methods based on Machine Learning and Deep Learning can play a central role in automatizing this time-consuming procedure. In this work, using a robust dataset of high-resolution digital images from continuous sediment cores of Holocene age that reflect a wide spectrum of continental to shallow-marine depositional environments, we outline a novel deep-learning-based approach to perform automatic semantic segmentation directly on core images, leveraging the power of convolutional neural networks. To optimize the interpretation process and maximize scientific value, we use six sedimentary facies associations as target classes *in lieu* of ineffective classification methods based uniquely on lithology. We propose an automated model that can rapidly characterize sediment cores, allowing immediate guidance for stratigraphic correlation and subsurface reconstructions.

## 8.1 Introduction

Understanding subsurface stratigraphy is essential for a wide range of industrial and societal applications, including studies of global climate change (Martinson et al., 1987; Mayewski et al., 2004), reservoir characterization (Mitchum et al., 1977; Neal and Abreu, 2009; Posamentier et al., 1988), land subsidence calculations (Teatini et al., 2006; Van Asselen et al., 2009), and engineering geology (Prins and Andresen, 2021). When approaching the investigation of the subsurface, by nature inaccessible to direct observation, sediment cores are the fundamental source of information. Sedimentary facies, in particular, i.e. sediment bodies or packages of strata formed in specific depositional environments, bear unique physical and mechanical properties (Campo et al., 2023) that can be used effectively for subsurface stratigraphic modeling.

Recent studies have shown that building a detailed model of the shallow subsurface based on sedimentary facies properties can be an effective tool to: (i) assess patterns of active tectonic deformation (Amorosi et al., 2021), (ii) define site response to earthquakes (Kruiver et al., 2015), and (iii) predict earthquake damage risk (Tanabe et al., 2021).

Sediment facies analysis is the first step in most Earth and environmental research studies; nevertheless, high-resolution facies reconstructions require specific sedimentological expertise and

training, usually involving a multidisciplinary research approach (Amorosi et al., 2023; Campo et al., 2023, 2022b).

Recent advances in Artificial Intelligence research are setting new standards for many research fields, with automated methods based on Machine Learning (ML) and Deep Learning (DL) achieving state-of-the-art performance in solving complex problems. Among the principal applications of AI methods, we find Natural Language Processing (NLP) (Devlin et al., 2019), Computer Vision (CV) (Redmon et al., 2016), synthetic data generation (Rombach et al., 2022), and more. In the last few years, AI methods have been increasingly applied to Earth and environmental research (Bolandi et al., 2017; Crnkovic-Friis and Erlandson, 2015; Hadler et al., 2021; Jacq et al., 2022; Kadow et al., 2020; Kuwatani et al., 2014; Wrona et al., 2018; Xiong et al., 2018). However, the proposed approaches did not fully exploit the potential of ML and DL systems and the usage of AI in geoscience. In a recent publication, Fleming et al., 2021 pointed out the necessity for a deeper understanding of AI and automated algorithms to strengthen geosciences research policies (Bergen et al., 2019; Goldstein et al., 2019; Karpatne et al., 2019).

An automatic approach was recently proposed to classify Holocene sediment facies using X-ray fluorescence (XRF) scanner data (Lee et al., 2022). This approach, however, although effective on a local scale, can hardly be exported outside the study area: XRF data rely mostly on sediment composition, which can vary greatly from site to site in the same depositional environment simply as a function of sediment dispersal.

In this context, we propose a novel approach leveraging DL to perform automatic semantic segmentation of sediment cores digital images directly acquired in the field. Semantic segmentation consists in classifying each image pixel according to a specific set of categories, and Convolutional Neural Networks (CNNs) usually achieve state-of-the-art performance (Guo et al., 2018; Li et al., 2022). CNNs are a particular class of networks primarily used to efficiently analyze image data. We identified six target Holocene sedimentary classes from the Po Plain and the Adriatic coastal plain of Marche, Abruzzo, and Apulia regions (Italy): Well-drained floodplain (WDF), Poorly-drained floodplain (PDF), Swamp (Sw), Peat layer (PL), Prodelta (P), and Fluvial sand (FS), deposits, with an additional background class. An expert sedimentologist manually annotated each core image, producing a final dataset of 82 non-overlapping, high-resolution digital images acquired from 32 continuous sediment cores with the associated segmentation masks. To perform the model validation, we divided the dataset into three mutually-exclusive subsets: training, validation, and test, containing 77%, 11%, and 12% of the data, respectively.

Our method can produce precise semantic segmentation and, thus, accurate facies interpretation, achieving high scores for the most used segmentation metrics. Our approach can drastically reduce the time and effort required to analyze core surveys; it can perform real-time predictions of high-resolution images on a regular computer and could be extended to mobile devices, making it suitable for on-field usage. This method does not need expensive data acquisition techniques or pre-processing, since it relies on images acquired with common digital cameras. Moreover, this approach is not necessarily limited to Holocene successions and could be adapted to different geologic conditions.

One of the major concerns with Deep Learning methods is the limited interpretability of model predictions. This is the reason why they are commonly called black-box methods (Ribeiro et al., 2016; Selvaraju et al., 2020; Vinogradova et al., 2020). In an attempt to better understand the results produced by our method, we visualize the regions of higher segmentation error and model prediction confidence, making the method more interpretable.

## 8.2 Results

### 8.2.1 Segmentation performance and visual evaluation

A deep CNN was trained to automatically produce the semantic segmentation masks of digital images acquired from continuous sedimentary cores. The images included six target classes corresponding to the observed sedimentary facies and a seventh background class. The model performance was evaluated on validation and test sets consisting of 11% and 12% of the total available data, respectively. We measured several standard segmentation metrics: the mean Intersection over Union (IoU), the F1-score, and the balanced accuracy. The results obtained for the validation and test data are shown in [Table 1](#). The performance achieved on the validation dataset tends to be positively biased due to the model being fine-tuned on it, whereas the test performances are more rigorous in evaluating the capabilities of the model. The scores obtained with both datasets show no remarkable differences.

	Mean IoU	F1-score	Balanced accuracy
Validation set	0.884	0.936	0.905
Test set	0.853	0.916	0.861

*Table 1: Model performance obtained on validation and test data, in terms of mean Intersection over Union, F1-score, and balanced accuracy.*

For a visual evaluation of the model performance, we produced the semantic segmentation mask of five full-resolution images from both the validation and test sets and compared them to the ground truths produced by the expert sedimentologist ([Fig. 1](#) and [Fig. 2](#)). The detailed quantitative presentation of the results and errors is covered in section 2.2 and showed in Fig.3. The five images were chosen as the most representative for the two datasets, showing all the target sedimentary facies. The visual performance on validation data shows high correlation between the model predictions and the ground truths. [Figure 1-A](#) is one of the most complex images in the whole dataset, containing four target classes: Well-drained floodplain (WDF), Poorly-drained floodplain (PDF), Swamp (Sw), and Peat layer (PL). The model prediction accurately reproduces the sedimentologist segmentation mask, correctly classifying most sedimentary facies. Minor errors are present, mainly localized at facies transitions (WDF–PDF, PDF–Sw, and Sw–PL). The transition between Swamp and Peat layer is also visible in [Fig. 1-B](#) and well classified by the model. In [Fig. 1-C](#), the model misclassified a portion of the Fluvial sand (FS) stratigraphic interval, while classifying the PDF correctly. [Figure 1-D](#) shows the high capability of the model in classifying the Prodelta (P) target class, whose identification commonly requires specific sedimentological training, with an impressive overlap between the model prediction and the reference segmentation. The model performs well in Fluvial sand classification in [Fig. 1-E](#), while only minor classification errors are present for Sw and PDF.

There are no noticeable visual performance differences between the validation and test images. Furthermore, four out of the five images shown in [Fig. 2](#) come from a set of sediment cores for which no images were present in the training set (red dots in Fig. 2). The usage of this set of images was intended to simulate the model application to external data acquired in the field, to validate its generalization capabilities. In [Fig. 2-A](#), WDF, PDF, and Sw are correctly classified, with satisfactory predictions also near facies transitions. Negligible errors are present, with a minor misclassification of PDF to Sw; [Fig. 2-\(B, C, D\)](#) shows an almost perfect model prediction for the four involved classes. The model confirms its robust prediction capabilities of sub-features in the sedimentary record, represented by PL. Consistent with the validation result, the Prodelta class is very well classified also in the test dataset. In [Fig. 2-E](#), WDF is correctly classified, while minor errors occur on Sw and PDF classification. However, in this case the model struggles to reproduce the sedimentologists sand classification.

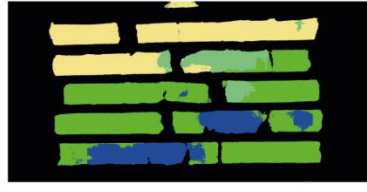
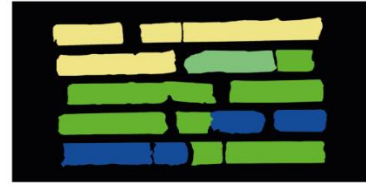
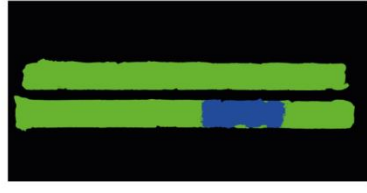
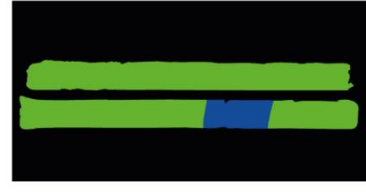
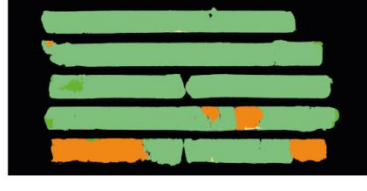
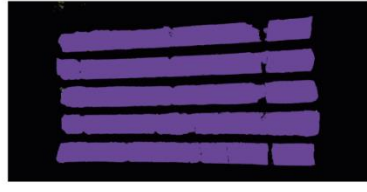
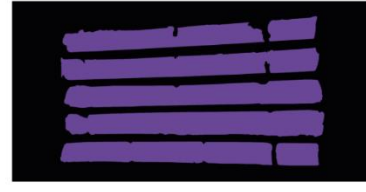
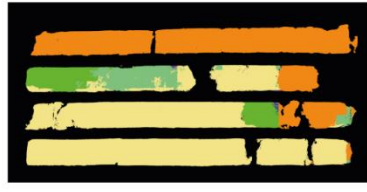
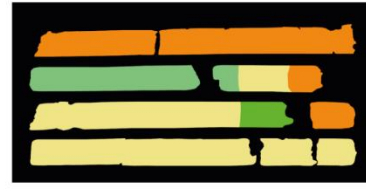
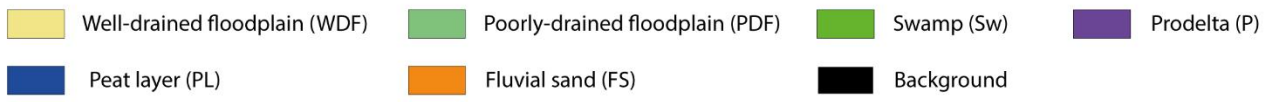
Visual Performance on Validation Data		
Original Image	Model Prediction	Ground Truth
		
A		
		
B		
		
C		
		
D		
		
E		
		

Fig. 6. Visual performance of the model on five representative images of the validation dataset. The original full-resolution digital images, the model-produced segmentation masks, and the corresponding ground truths are shown in the left, central, and right columns, respectively.

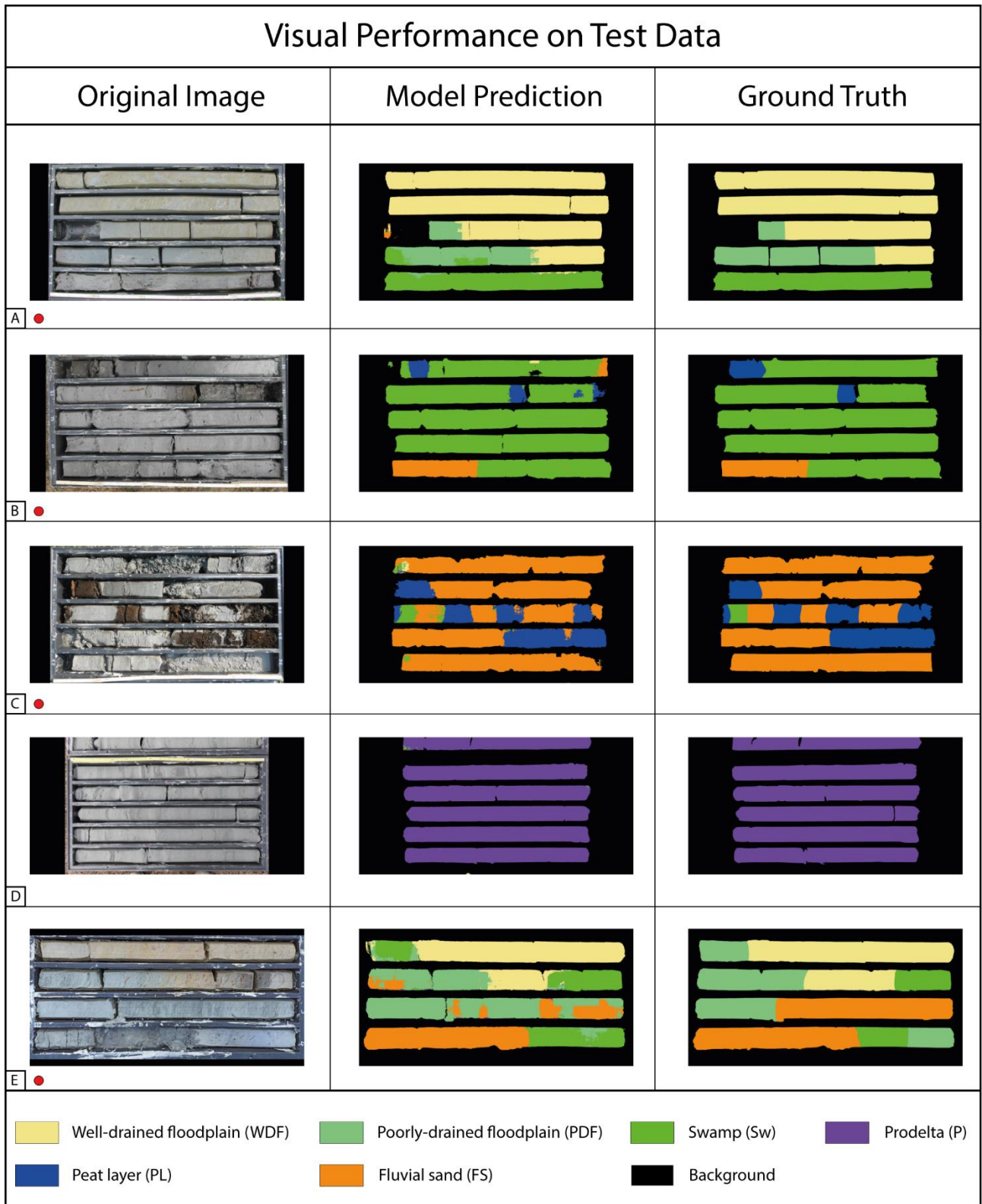


Fig. 7. Visual performance of the model on five representative images of the test dataset. The original full-resolution digital images, the model produced segmentation masks, and the corresponding ground truths are shown in the left, central, and right columns, respectively. The red dots mark the images coming from the external set of sediment cores.

## 8.2.2 Confusion Matrix and model misclassifications

For a deeper quantitative evaluation of the model performance, the confusion matrices for the validation and test sets were calculated ([Fig. 3 A-B](#)). The confusion matrix is a table layout in which each row represents the instances in a ground truth class, while each column represents the class instances predicted by the model. In a semantic segmentation context, the instances are the pixels associated with each class. This matrix shows which classes have been correctly classified and which were confused with other classes during the model test. It is a standard estimator used in machine learning and statistics, since it provides more information about model performance than the standard metrics (Susmaga, 2004). Most of the standard evaluation metrics can be derived from the confusion matrix, so it can be considered the most comprehensive method for performance evaluation in classification problems (Powers, 2020; Shaikh, 2011; Sokolova and Lapalme, 2009; Tharwat, 2020). However, the confusion matrix becomes more complex to read with the growing number of classes.

We normalized the confusion matrix with respect to the number of true instance classes, i.e., to the rows of the matrix. It follows that the resulting matrix values are between zero and one, with one representing a perfect classification; a colormap was used for a more intuitive visual evaluation.

The confusion matrix for the validation data ([Fig. 3-A](#)) shows good classification performance for all the classes. Excluding the background, the class with the highest classification accuracy is the Prodelta (0.963), followed by: Swamp (0.918), Well-drained floodplain (0.894), Poorly-drained floodplain (0.872), Fluvial sand (0.862), and Peat layer (0.838). The most significant classification errors occur for the PL, being misclassified as Sw (0.141), FS misclassified as PDF (0.080), PDF confused as Sw (0.068), and WDF confused as PDF (0.067).

The highest classification accuracy for the test data, excluding the background, is achieved again for Prodelta (0.973), followed by: Well-drained floodplain (0.905), Swamp (0.901), Fluvial sand (0.823), Peat layer (0.750), and Poorly-drained floodplain (0.699). On average, the classification accuracies are slightly lower than the validation ones, in agreement with the metrics reported in [Table 1](#). In this case, the most significant classification errors occur for the PDF being misclassified

as Sw (0.191), followed by: PL misclassified as Sw (0.127) and FS (0.081), and FS confused as Sw (0.063).

The results reported in [Table 1](#), the visual performance shown in Figs. 1 and 2, in combination with the confusion matrices of [Fig. 3](#), show a robust classification result for all the target classes with only minor errors.

To better understand the limitations of the proposed CNN and the possible sources of error, we produced the error maps between model predictions and ground truths, along with the model prediction confidence (Fig. 4), for two representative cores from the validation and test datasets. The sediment core, ground truth, segmentation mask, and prediction are shown in Fig .4-A-B-C-F-G-H, respectively. In Fig. 4-D-I, the model confidence is presented, with darker regions representing areas of lower confidence. Fig. 4-E-L reports the error between the prediction and the ground truth.

The validation core (Fig. 4-A) shows a prominent Peat layer as a sub-feature in the Swamp deposit, with no well-defined boundaries corresponding with the minimum confidence values, as shown in Fig. 4-D. The model error is restricted to a smaller portion of the image, while no major errors are noticeable from other areas of the sedimentary core.

The test image (Fig. 4-F) shows a possible real-case scenario with a poorly preserved core that was damaged during the drilling process. The high number of transition boundaries makes the prediction challenging; in Fig. 4-I, a generally lower model confidence is visible, with minima located in correspondence of facies transitions and on the damaged parts of the core.

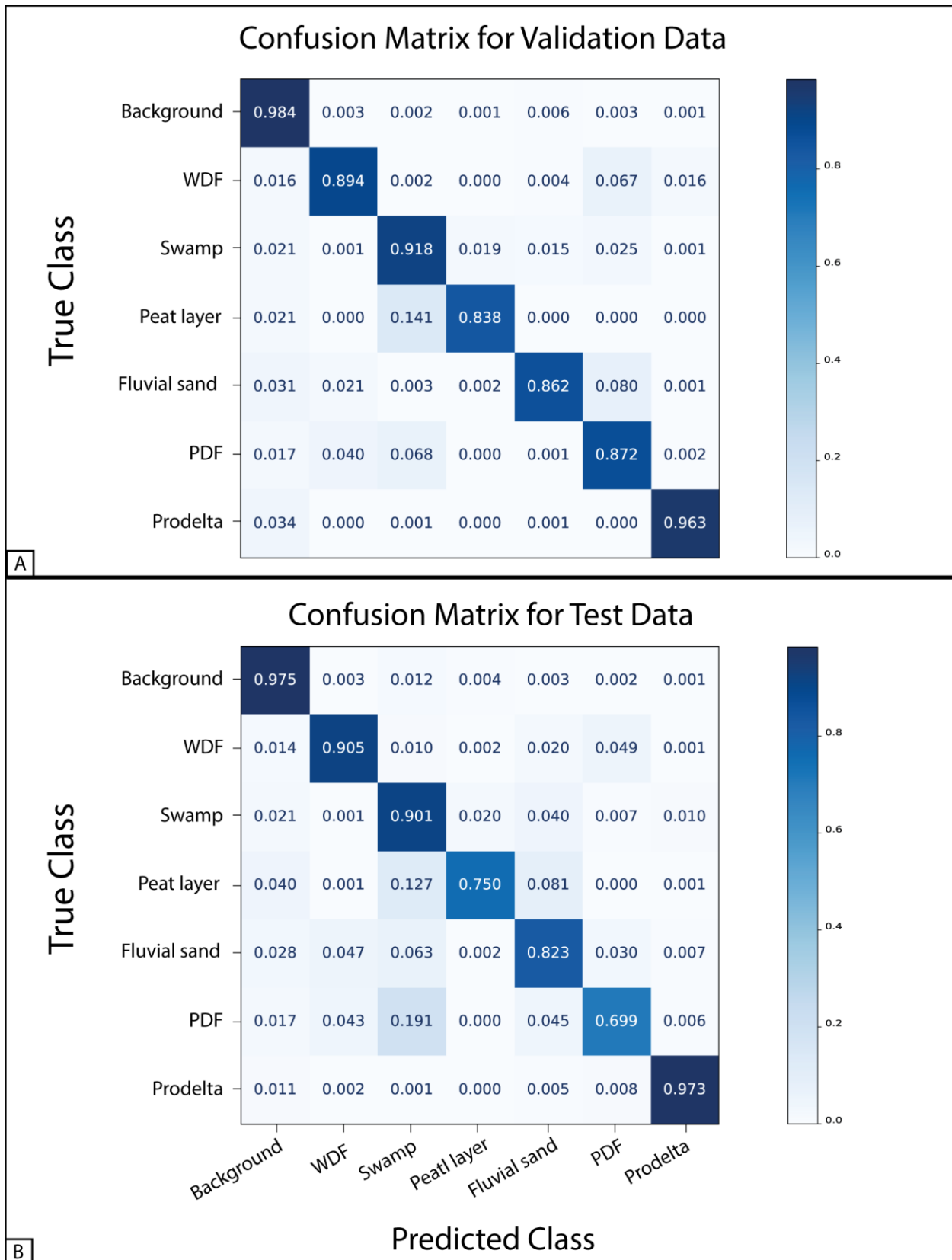


Fig. 8. Confusion matrices for validation data (A) and test data (B). Each row of the matrices represents the instances in a ground truth class, while each column represents the class instances predicted by the model. The values were normalized with respect to the number of ground truth instances for each class. A colormap visually highlights the higher values with darker shades of blue.

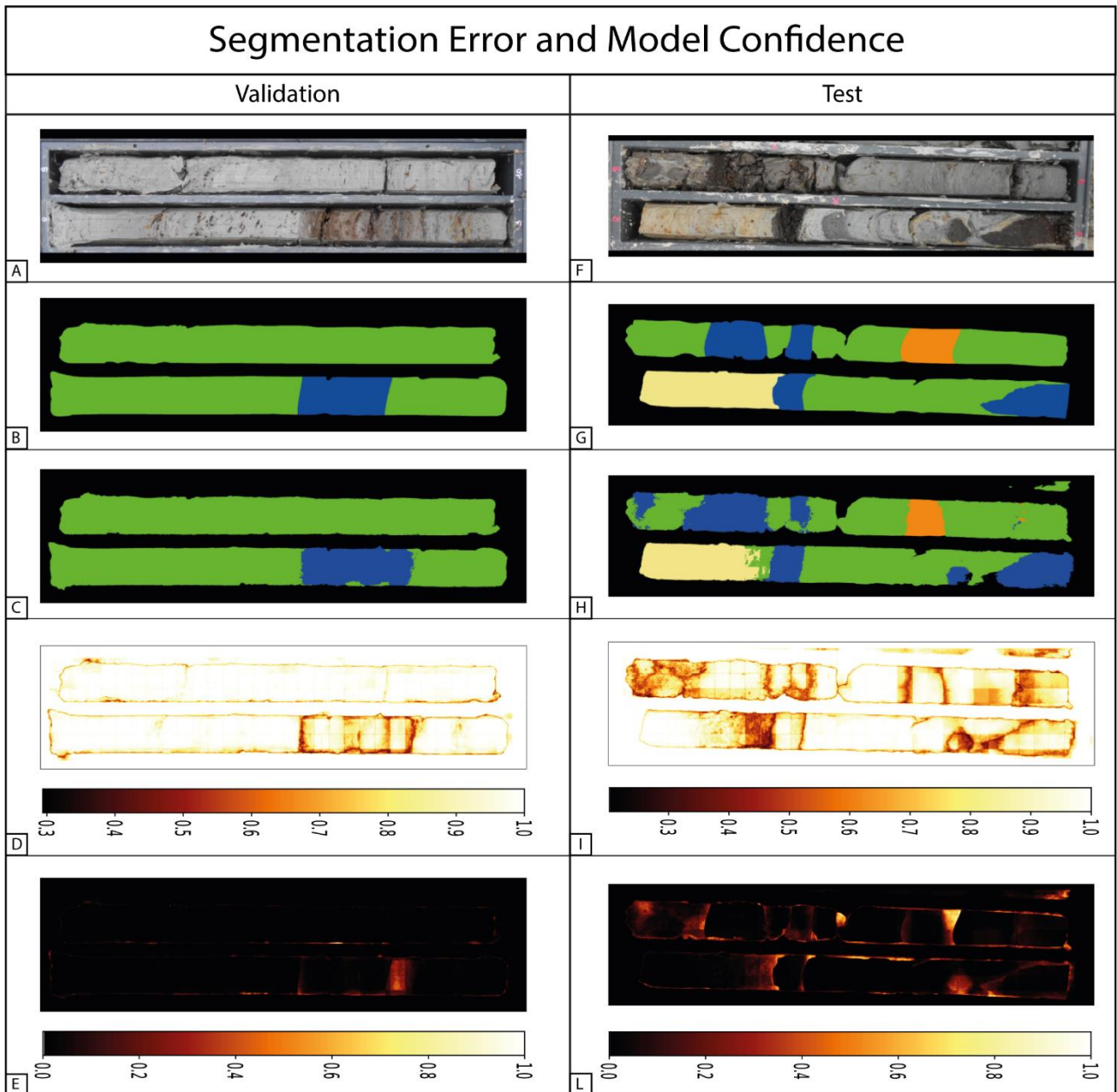


Fig. 9. Segmentation error and model confidence. Core images (A-F), ground truth segmentation masks (B-G), model predictions (C-H), model confidence (D-I), and segmentation error (E-L) are shown for two validation and test representative cores. The model confidence represents the prediction probability associated with the predicted class. The segmentation error is the normalized categorical cross-entropy calculated between the prediction and the ground truth.

## 8.3 Discussion

A powerful method leveraging DL and CNNs is proposed to produce accurate sedimentary facies interpretations starting from standard digital images. It constitutes a fast, precise, and easy-to-deploy tool that could largely improve subsurface stratigraphic modeling, making subsurface facies analysis more accessible to a wide range of scientists and professionals.

Using a convolutional neural network, we aimed to mimic the sedimentologist approach in facies classification; the model makes its prediction pixel-wise, but the decision process also considers local and global aspects of the image, such as the textural characteristics, color, and accessory materials, e.g., carbonate concretions, shells, and wood fragments (Gu et al., 2018; Li et al., 2022). The heterogeneity of the images used in the work and the data augmentation performed should make the model robust to different image lighting, contrast, orientation and quality.

The model performance obtained on the validation and test datasets shows robust generalization capabilities, with a strong agreement between the predicted classes and the ground truths identified by the sedimentologist. Furthermore, the scores obtained by the model in terms of mean IoU, F1-score, and balanced accuracy are notably high, considering the complexity of a multi-class semantic segmentation task. The numerical results are visually confirmed by the segmentation mask shown in [Figs. 1-2](#).

Swamp and Poorly-drained floodplain facies can have similar characteristics in terms of color and texture, thus can hardly be distinguished by visual inspection only. In such cases, the fossil content and geotechnical properties are fundamental tools for high-resolution facies analysis (Amorosi et al., 2014; Amorosi and Marchi, 1999; Campo et al., 2023; Scarponi et al., 2013). Our model generally performs well in discriminating these highly similar facies using visual information only, with minor errors. However, misclassification of Sw to PDF and vice-versa can hardly be considered real errors, because the distinction between these two classes is subtle and attributions could vary as a function of the sedimentologist expertise. Another typical misclassification error is due to the abundance of sand layers as sub-features within a clay deposit, such as in the case of WDF and PDF. These layers could be considered minor attributes by the sedimentologist, and thus ignored, or emphasized, and thus interpreted as a fluvial facies. A further source of error is transition between sedimentary facies, which makes precise identification of their boundary challenging. The definition of a sharp boundary is a consequence and limitation of the semantic segmentation tasks, but in some cases the transition between two facies is not an abrupt change and would be better characterized as a

zone of transition. In this case, the model is not capable of fully reproducing the sedimentologist interpretation, as it may become highly subjective.

Given the black-box nature of neural networks, the information arising from the confidence and error maps can be used to highlight the criticisms of the proposed segmentation task. From Fig. 4, we acknowledge that the model correctly reproduces the overall sedimentologist interpretation.

For the validation core, the model error is restricted to a smaller portion of the image, and the overall stratigraphic interpretation does not change; moreover, the misclassified region corresponds to facies transition, for which defining a sharp boundary is not straightforward even for a sedimentologist. The test image shows a complex case in which the core was damaged during the drilling process. Also in this case, segmentation errors do not significantly impact the global stratigraphic interpretation. The damaged portions of the core are also well classified, though with a lower model confidence.

In summary, the sources of error can be grouped into three main categories: (i) visual overlap of sedimentary facies, (ii) occurrence of transitional facies boundaries, and (iii) subjectivity in sedimentologist interpretations.

There is growing interest in the application of AI methods to environmental and Earth sciences (Bolandi et al., 2017; Wood, 2021; Wrona et al., 2018; Xiong et al., 2018). In this paper, we outline a novel approach to subsurface stratigraphy, performing semantic segmentation of Holocene sedimentary facies with convolutional neural networks. Previous subsurface studies have relied upon standard machine learning techniques, and for this reason they have been limited to simple data structures (Hadler et al., 2021; Jacq et al., 2022; Kuwatani et al., 2014; Lee et al., 2022; Rapuc et al., 2020). Our method leverages the power of deep learning models to produce accurate stratigraphic interpretations starting from digital images. This makes our approach easier to use and deploy in a wide range of geological applications.

During the last decades, a virtually continuous stratigraphic record of Holocene deposits in the Po Plain and beneath several coastal plains of Italy was acquired through core drilling. Robust high-resolution sequence-stratigraphic models that rely on information extracted from cores (Amorosi et al., 2017) demonstrated that the stratigraphic architecture of Holocene successions worldwide exhibits striking similarities in terms of sediment facies distribution. Sediment core analysis based on semantic segmentation of continuous core images, thus, represents a highly reproducible technique that is likely to be exported successfully to other coeval stratigraphic successions, constituting a reference framework for future CNN-based subsurface analysis. The research

approach presented in this paper is naturally suited for in-situ analysis and could substantially reduce the time and effort needed for detailed sediment facies interpretation, making it a valuable tool for large-scale exploration and for a broad range of industrial applications. The future integration of imaging data with other data sources, such as geotechnical and compositional data, and their incorporation in an automated method based on machine learning can make a substantial contribution to the progress of geological research below the ground surface.

## 8.4 Materials and Methods

### 8.4.1 Data acquisition and pre-processing

The dataset (Di Martino and Amorosi, 2023) used for this study consists of 82 digital images from 31 selected Holocene cored sedimentary successions of Italy (Po Plain and Adriatic coastal plains of Marche, Abruzzo, and Apulia regions), between December 2016 and July 2021 (Fig. 5-A). Given the remarkable length (30-50 m) of sediment cores, a series of non-overlapping digital images were acquired every 5 meters of recovered sediment, covering the whole core length. Digital images were obtained directly in the field using different devices, such as compact cameras and smartphones, with a broad range of resolutions, ranging from 1369×803 to 4605×2717 pixels. To make our method as general as possible, we did not enforce a strict image acquisition procedure in terms of camera settings and environmental conditions. Each image was resized to 3074 x 1538 pixels to obtain a homogeneous resolution. Whenever the aspect ratio of the target resolution was different from the aspect ratio of the image, this latter was padded with zero-valued pixels to maintain its original aspect ratio, i.e., to resize the image without distortions. No other pre-processing steps were carried out on the original images.

Using pre-existent, high-resolution stratigraphic reconstructions as a framework for facies interpretations (Amorosi et al., 2023, 2021; Campo et al., 2022b), we produced the ground truth segmentation mask for every image (Fig. 5-B), manually classifying the sediment core into seven classes: six target classes corresponding to the observed Holocene sedimentary facies, and a seventh background class. A segmentation mask is an image mapping each identified class to a corresponding unique RGB value. RGB masks are suited for visualization, but are not directly usable to train a segmentation model; thus, we quantized the original RGB masks, mapping each RGB triplet to a corresponding unique scalar value. There is a slight variation in the relative proportion of the six target classes, particularly for the Peat layer class, which is only locally observed, as it occurs at distinct stratigraphic intervals (Fig. 5).

The seven classes are as follows:

- i) Well-drained floodplain deposits (WDF), typical of subaerially exposed environments, consist of stiff, varicolored light grey to green silt and clay, with yellowish and orange

mottles due to Fe oxides. White carbonate concretions and other pedogenic features are common.

- ii) Poorly-drained floodplain deposits (PDF), characteristic of flood basins with fluctuating groundwater table, consist predominantly of soft, grey clay and silt, with scattered vegetal remains and a lack of body fossils.
- iii) Swamp deposits (Sw), typical of waterlogged environments, are dominated by grey to dark-grey clay, with abundant vegetal remains and wood fragments concentrated in discrete horizons or scattered along core sections.
- iv) Peat layers (PL) represent sub-features of swamp deposits, characterized by dark grey to black colors. They consist of wood fragments with subordinate clayey material and are typically organic-matter-rich.
- v) Prodelta deposits (P) consist of homogenous, light grey clay formed at fluvial mouths, with common silt and sand intercalations, interpreted to represent flood layers. Plant debris and other organic matter are locally observed, whereas salt-water mollusks are common.
- vi) Fluvial sand (FS) includes a wide range of grain size fractions, from silty sand to very coarse sand, formed in fluvial/distributary channels or in adjacent areas (levees and crevasse splays).
- vii) Background, corresponding to the grey box containing the sediment core.

The dataset was then divided into three, non-overlapping portions; 63 digital images were used for training, 9 for validations, and 10 for testing, corresponding to 76.83 %, 10.97%, and 12.20% of the total, respectively. The data were stratified, so that each class was equally represented in every subset. To further validate the generalization capabilities of the model, one image in the validation dataset and six images in the test dataset were taken from sediment cores that were not present in the training dataset.

Due to computational limitations, full-resolution images could not be used for model training. Thus, following data subdivision, the images and corresponding masks were subdivided into (i) 1609 non-overlapping patches of resolution 384x384 pixels for model training; (ii) 250 patches for model validation; and (iii) 265 patches for model testing. Patch subdivision is also useful for increasing the number of available samples. The padding with zero-valued pixels during the resize operation could lead to the generation of patches with mostly zero-valued pixels at image borders. For this reason,

patches with less than 5% non-zero pixels were automatically excluded from the data during the patch subdivision process.

#### 8.4. 2 Segmentation Model

The model used for the image segmentation was a U-Net (Ronneberger et al., 2015) with an EfficientNetB3 backbone (Tan and Le, 2020), with weights pre-trained on ImageNet (Russakovsky et al., 2015). We chose the EfficientNetB3 as the backbone for the segmentation model because EfficientNets can achieve better performance than other popular model architectures (Baheti et al., 2020), such as ResNets (He et al., 2015), while having a smaller number of parameters. Furthermore, to avoid overfitting, considering the limited number of training samples, we decided to employ a network with a relatively small number of parameters. Moreover, a lightweight model may also be used for real-time predictions without requiring a dedicated, powerful hardware.

The model was trained for 100 epochs using Adam (Kingma and Ba, 2017) as optimizer, with a starting learning rate of  $10^{-4}$  and a polynomial learning rate decay schedule. Data augmentation was used to improve the generalization capabilities of the model. The transformations used for data augmentation were: random rotation with a 360-degree range, random brightness variation, and random contrast variation. The loss function used for the model training was the categorical cross-entropy. During training, we monitored the mean Intersection over Union (IoU) as a measure of the model performance, and we saved the model weights achieving the highest mean IoU on the validation data. The IoU is a typical metric used in segmentation tasks; it measures the overlap between the predicted mask and the ground truth (Wang et al., 2020). The IoU is zero when there is no overlap between the prediction and the ground truth, while it is equal to one for a perfect overlap.

We used the trained model to predict the image patches in the validation and test sets, and we computed the mean IoU, the F1-score, the balanced accuracy, and the confusion matrix to measure the prediction performance (Goutte and Gaussier, 2005; Hay, 1988). The convolutional neural network was built using the Tensorflow (Martín Abadi et al., 2015) python library, while the metrics and confusion matrix were calculated with the Scikit-learn (Pedregosa et al., 2011) python library. In detail, the IoU, F1-score and accuracy are defined as follows:

$$F1 = \frac{2 \times \text{Precision} \times \text{Recall}}{\text{Precision} + \text{Recall}}$$

where

$$\text{Precision} = \frac{TP}{TP + FP}$$

$$\text{Recall} = \frac{TP}{TP + FN}$$

where TP is True Positive, FP is False positive, and FN is False Negative

$$\text{IoU} = \frac{TP}{TP + FP + FN}$$

$$\text{Accuracy} = \frac{TP + TN}{TP + TN + FP + FN}$$

where TN is True Negatives.

All the metrics were weighted with respect to the number of true instances for each class to take into account the classes unbalancing.

To predict a whole image, a sliding-window approach is used. A kernel of *patch-size* slides through the image with a stride of 96 pixels, corresponding to one-fourth of the patch dimension. The image portion identified by the kernel is given to the model to produce the prediction; then, the predicted regions are re-arranged to form the complete predicted image. With a stride smaller than the kernel dimension, the resulting predictions will overlap, with an overlapping portion depending on the stride size. The overlapping predictions are then averaged to produce the final predicted image, achieving a smoother result.

We produced visual maps for a thorough estimation of model errors and prediction confidence; we define as model prediction confidence the probability associated with the predicted class. The model confidence cannot be directly related to a measure of prediction uncertainty, since it could predict the wrong class, while being highly confident of its prediction. The error between the prediction and the ground truth is calculated as the normalized categorical cross-entropy, defined, for a single data point, as:

$$H(y, \hat{y}) = - \sum_{i=1}^C y_i \log(\hat{y}_i)$$

where C is the number of classes,  $y$  is the true probability distribution, and  $\hat{y}$  is the predicted probability distribution from the model.

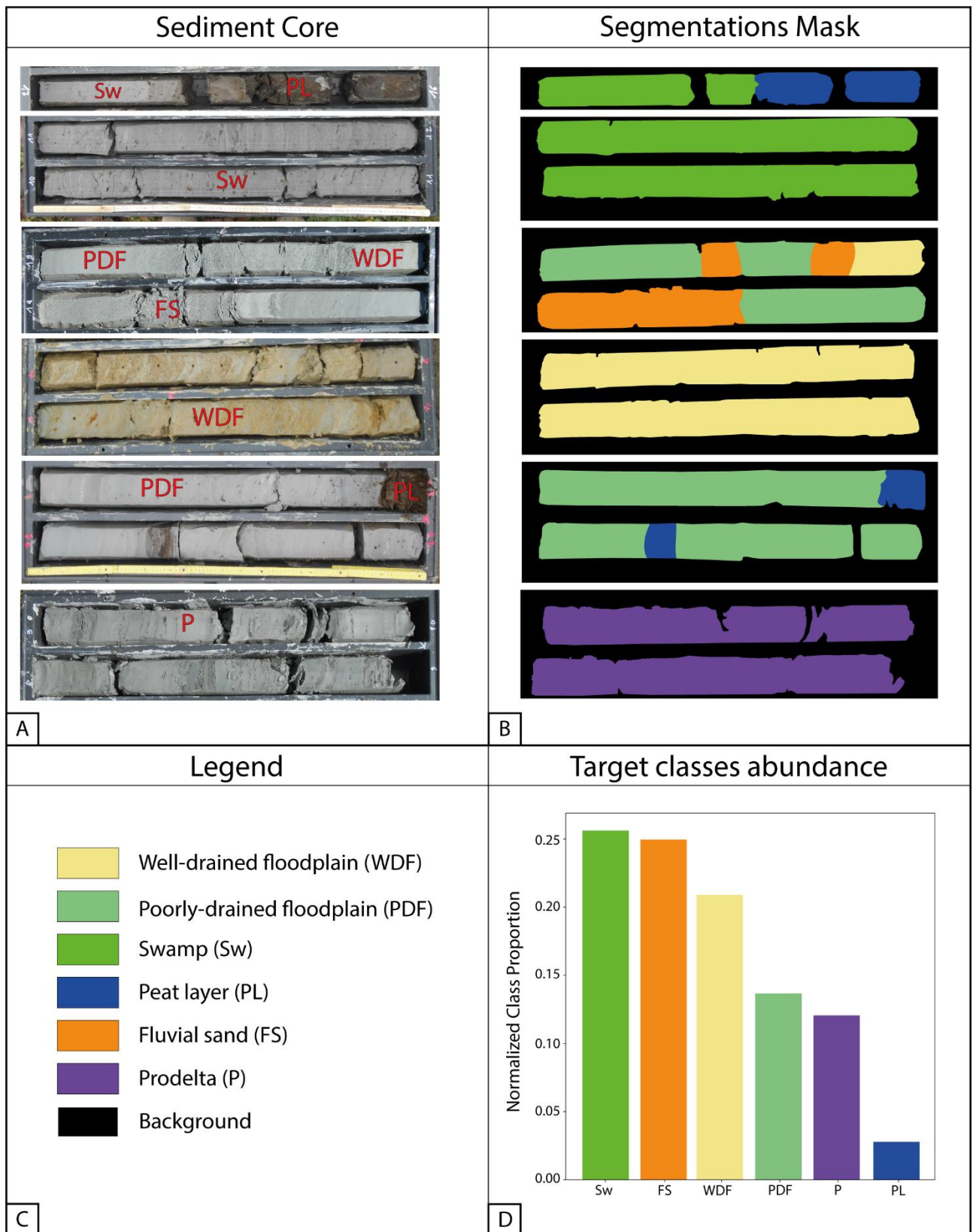


Fig. 10. A) Examples of digital images of continuous sediment cores with associated segmentation masks (B). C) Target classes and background colors. D) Relative target classes abundances.

## Data Availability

All the data used in this study can be found at <https://doi.org/10.6092/unibo/amsacta/7308> preserved in the repository AMSacta hosted by the University of Bologna and licensed under Creative Commons 4.0.

## Code availability

All the code developed for this study can be found at [GitHub - GianlucaCarlini/CoreNet: Semantic segmentation of continuous cores with CNNs](#)

## Competing Interest

The authors have no relevant financial or non-financial interest to disclose.

## Author contribution statement

A.D.M. and G. Carlini equally contributed to the conceptualization of the work, data curation, design of the methodology, and original writing.

A.A., G. Castellani, and D.R. jointly supervised the work contributing to funding acquisition, project administration, review, and editing of the original draft.

Throughout all stages, the authors engaged in discussions regarding results and implications.

## Acknowledgments

This research was supported by the Italian Ministry of University and Research under the PRIN 2017 program to Alessandro Amorosi, project number 2017ASZAKJ *“The Po-Adriatic Source-to-Sink system (PASS): from modern sedimentary processes to millennial-scale stratigraphic architecture”*.

## 9. Conclusions

In this work, we first reconstructed the depositional architecture of two Late Quaternary paleovalley systems located on the Adriatic coast of Italy, the Manfredonia paleovalley system and the Pescara paleovalley system.

In the Manfredonia area, we reconstructed a Late Pleistocene to Holocene history of valley formation and filling through a multidisciplinary approach using sedimentological, paleoecological, and geochemical analysis conducted on three sediment cores from onshore Apulia and their comparison with offshore seismic stratigraphy. The sequence stratigraphic interpretation was based on 25 radiocarbon dates to constrain the sedimentary succession chronologically, providing an integrated picture of multiple valley and interfluvial development in which stratigraphic architecture of paleovalley fills was largely driven by relative sea-level changes.

Above coarse-grained fluvial deposits that form the amalgamated lower paleovalley fill, the upper valley fill includes a vertical succession of mud-dominated inner- to outer-estuary deposits. These, in turn, are overlain by bay/open-marine clays and by a shallowing-upward succession of prodelta and delta front facies associations. The valley interfluvial is characterized by stratigraphic discontinuities, where Holocene transgressive deposits overlie indurated and pedogenized, pre-LGM deposits. Three stratigraphically significant surfaces were recognized: the sequence boundary and the transgressive surface have clear sedimentologic expression, whereas the maximum flooding surface demarcates subtle changes in paleoecological features and is marked by a condensed section.

Geochemical fingerprinting of inner-estuary deposits reveals enhanced sediment supply from Apulian river catchments in the early stages of paleovalley filling. The increasing contribution of material sourced from mafic/ultramafic rocks at the fluvial-marine transition is interpreted to reflect the influence of the SE-directed (longshore) Western Adriatic current, which carries the unique (Cr-rich) compositional signature of Po River sediments.

In the Pescara area, we recognized a buried paleovalley system, about 50 m deep and up to 2 km wide, through stratigraphic correlation based on sedimentological, paleontological (meiofauna and mollusks), chronological, and geotechnical (pocket penetrometer) data. Detailed facies analysis was conducted on a 52 m-long core specifically recovered in the valley depocenter.

Two NE-SE and SW-NE oriented stratigraphic cross-sections provided the 3D-facies architecture of the Late Pleistocene-Holocene paleovalley fill and allowed the reconstruction of the paleovalley profile. The stratigraphic architecture shows a lower paleovalley fill, made by up to 13-m-thick, amalgamated fluvial gravel bodies of Late Pleistocene age (30-pre-11.3 ka cal BP), interpreted as the lowstand systems tract (LST).

The mud-dominated, Holocene upper paleovalley fill is about 25 m-thick and consists mainly of non-marine, organic-rich deposits with low pocket penetrometer values (0.4-1.8 g/cm<sup>2</sup>). The vertical transition

from poorly-drained floodplain facies to swamp clays to lagoonal deposits reflects the progressive drowning of the valley and the formation of an estuary due to the Holocene transgression. During the last 8.0 ky, the estuary was progressively filled up to establish the modern wave-dominated delta plain environment.

These two studies demonstrate that a multidisciplinary approach based on stratigraphy, facies analysis, radiocarbon dating, and geochemical analysis may lead to a complete reconstruction of the high-resolution stratigraphy of paleovalley systems. Furthermore, an integrated paleoecological procedure encompassing data from mollusks, benthic foraminifers, and ostracods proved to be highly effective in assisting the paleoenvironmental interpretation of Late Quaternary paleovalley successions.

Late Quaternary paleovalley systems are typically buried beneath modern, densely populated coastal plains worldwide, but they do not have any geomorphological expression, and their recognition can be challenging when conducted exclusively through classic stratigraphic survey methods.

In this work, we employed the mHVSr technique as an exploration tool to map the buried body of the Pescara and Manfredonia area paleovalley systems. We acquired microtremor measurements in both study areas, staying as close as possible to the subsurface geological data. All measurements were analyzed using the microtremor-based horizontal-to-vertical spectral ratio technique to measure the main resonance frequencies.

The main resonance frequencies were identified as distinct peaks on the mHVSr curves as a function of the impedance contrasts below the measurement site. To obtain an accurate stratigraphic interpretation of the H/V curves, we correlated the geophysical and geological data by analyzing individual mHVSr curves in conjunction with the spectral components of motion, allowing the distinction between the stratigraphic vs. anthropic nature of mHVSr peaks. Furthermore, we laterally correlated the principal resonance peaks, distinguishing the characteristic U-shape that marks the buried geometry of the paleovalley in both study areas.

We mapped changes in resonance frequency within the paleovalley in the range of interactions with ordinary buildings. These phenomena become evident near the paleovalley flanks, where resonance frequencies may vary from 4 Hz to 0.9 Hz in only a few hundred meters, moving from the interfluvium to the depocenter.

Using high-resolution stratigraphic data, we carefully evaluated the link between geological and geophysical data to identify the stratigraphic surfaces responsible for the observed resonances. We pointed out how the impedance contrast between the soft, clayey valley-fill and fluvial gravels at the bottom of the paleovalley primarily generates the peaks in the H/V curves; however, pedogenized and overconsolidated horizons can locally account for this impedance contrast. Assuming a power-law relation for increasing  $V_s$  with depth, we transformed each mHVSr curve from the frequency to the spatial domain. We computed the equivalent shear wave velocity in the paleovalley depocenter, denoting a very low shear wave velocity.

By means of the two spatial domain equation models, we carried out a detailed depth reconstruction of the paleovalleys, showing overall good correlations with the a priori known stratigraphic architecture. Geophysical reconstructions proved to be crucial to map the geometries of the buried paleovalley systems, even where the lack of drilling data or poor-quality stratigraphic core descriptions did not provide sufficient information for conclusive geological reconstructions.

This study has shown that shallowly buried paleovalley systems can be easily identified in the subsurface through mHVSr, owing to their marked lithologic contrast with adjacent deposits, and that the mHVSr geophysical technique can be used as an exploration tool for mapping these buried paleovalley bodies while deriving crucial geophysical parameters, such as resonance frequency and shear wave velocity.

We addressed the importance of integrating geophysical data with accurate stratigraphic reconstructions when performing microzonation studies to ensure reliable geophysical modeling of the critical parameters that control seismic amplification. In paleovalley systems, the resonance frequencies exhibit rapid lateral variations in a range of interactions with standard buildings. Moreover, low S-wave velocities of paleovalley fills can cause longer shaking and seismic amplifications, making these sediment bodies a potential seismic hazard beneath modern coastal lowlands.

To conduct a detailed seismic response study of the Pescara paleovalley, we expanded the dataset of microtremor measurements acquired in the study area and integrated them with subsurface geological data derived from the seismic microzonation project of the municipality of Pescara.

We reconstructed the resonance frequency map of the area through geostatistical interpolation of 85 microtremor measurements. The map revealed abrupt frequency changes and allowed us to identify the boundaries of the paleovalley domain, which would otherwise be difficult to define based only on vertical, site-specific geological data.

We observed a strong correlation between resonance frequencies and subsurface stratigraphy from high-resolution continuous core stratigraphies that allowed us to estimate a frequency-depth model for the paleovalley infill (Fig. 5) and reconstruct a geophysical-based 3D depth model of the buried paleovalley morphology (Fig. 6). Moreover, leveraging six velocity profiles from down-hole tests, we reconstructed a detailed seismic layering of the valley infill, identifying five main seismic/stratigraphic layers (Fig. 8), with  $V_s$  values close to the average model derived by frequency-depth regression.

We leveraged the strong relationship between the measured resonance frequencies and the subsurface stratigraphy to construct a Frequency-Depth model, which enabled the conversion of all resonance frequencies into depth values, thereby reconstructing a geophysical-based 3D depth model of the buried paleovalley morphology. Moreover, exploiting six velocity profiles from down-hole tests, we reconstructed a detailed seismic layering of the valley infill, identifying five main seismic/stratigraphic layers.

To perform a 2D seismic response modeling, we constructed a stratigraphic cross-section running through the paleovalley depocenter. The cross-section was constrained using the geophysical 3D model and the

available geological data from the microdonations seismic project and thus constructed following geometric and sedimentological principles, faithfully reproducing the internal facies architecture and providing a high-resolution framework for the seismic modeling.

We computed the transfer functions at different output points on the surface, revealing significant amplification factors peaking at frequencies that closely match the resonance frequencies observed with the direct geophysical investigation. The main amplification at the center of the paleovalley was observed at frequencies between 0.9 and 1.2 Hz, with an amplification factor equal to 4. Towards the valley edges, the largest amplifications are observed at about 5 Hz and have smaller amplification factors, between 2.5 and 3. These factors reveal a notable increase in the amplification amplitude compared to less complex geological contexts. We point out how the seismic amplifications are in frequency ranges that can interact with a wide range of building types, including ordinary buildings (small and rigid or large and flexible structures), representing the most common type of buildings along the Adriatic coast.

We compared the results from the 2D and the 1D modeling approaches and revealed only slight differences between the two methods. The 2D modeling approach did not highlight clear 2D valley effects in the dynamic behavior of the paleovalley. The results of our seismic response simulations highlighted a few main observations. The lateral changes in the seismic response of the valley strongly depend on the local subsurface stratigraphy. Therefore, detailed knowledge of subsurface layering and lateral changes of layer geometries is fundamental for a realistic estimate of the seismic response, especially in a context where no surface morphological expression of the valley is observed. On the other hand, a 1D modeling approach appears to be a reasonable approximation of the seismic response at a specific point location, providing adequate knowledge of the local stratigraphy.

Furthermore, we computed the response spectra based on 2D modeling and compared them with the response spectra proposed by the Eurocode 8 guideline for soil category C. Remarkably, the strong amplifications observed in a paleovalley context lead to a significant underestimation of spectral accelerations according to the guideline. In the study area, soil classification purely based on  $V_{s30}$  (as proposed by Eurocode8) appears to be inadequate, as it is strongly influenced by the presence/absence of the topmost sand layer, which may alternatively result in classification under categories C and D, respectively.

These outcomes imply that soil classification based on  $V_{s30}$ , in this case, needs to be revised and can lead to insufficiently restrictive guidelines in seismic areas. This study highlighted the importance of combining geophysical and geological data, especially in a complex context. While the gentle geometry of the paleovalley does not produce evident 2D effects, detailed reconstruction of paleovalley geometry and facies architecture is necessary to correctly identify frequencies and amplification factors at every point on the surface.

Finally, we utilized our skills in sedimentary core interpretation to propose a powerful method, leveraging Deep Learning (DL) and Convolutional Neural Networks (CNNs) to produce accurate sedimentary facies interpretations starting from standard digital images.

Using a convolutional neural network, we aimed to mimic the sedimentologist approach in facies classification; the model makes its prediction pixel-wise, but the decision process also considers local and global aspects of the image, such as textural characteristics, color, and accessory materials.

We identified six target Holocene sedimentary classes from the Po Plain and the Adriatic coastal plain of Marche, Abruzzo, and Apulia regions (Italy): Well-drained floodplain (WDF), Poorly-drained floodplain (PDF), Prodelta (P), Peat layer (PL), Fluvial sand (FS), and Swamp (Sw) deposits, with an additional background class. The model performance obtained on the validation and test datasets shows robust generalization capabilities, with a significant correlation between the predicted classes and the ground truths identified by the sedimentologist. Furthermore, the scores obtained by the model in terms of mean IoU, F1-score, and balanced accuracy are significantly high, considering the complexity of a multi-class semantic segmentation task.

Given the black-box nature of neural networks, to better understand the limitations of the proposed CNN and the possible sources of error, we produced the error maps between model predictions and ground truths, along with the model prediction confidence. The sources of error can be summarized into three main categories: (i) visual overlap of sedimentary facies, (ii) occurrence of transitional facies boundaries, and (iii) subjectivity in sedimentologist interpretations.

This work outlines a novel approach to subsurface stratigraphy, performing semantic segmentation of Holocene sedimentary facies with convolutional neural networks. Robust high-resolution sequence-stratigraphic models that rely on information extracted from cores<sup>41</sup> demonstrated that the stratigraphic architecture of Holocene successions worldwide exhibits striking similarities regarding sediment facies distribution. Sediment core analysis based on semantic segmentation of continuous core images, thus, represents a highly reproducible technique likely to be exported successfully to other coeval stratigraphic successions.

## Reference

- Abdul, N.A., Mortlock, R.A., Wright, J.D., Fairbanks, R.G., (2016). Younger Dryas sea level and meltwater pulse 1B recorded in Barbados reef crest coral *Acropora palmata*. *Paleoceanography* 31, 330–344.
- Abdulah, K.C., Anderson, J.B., Snow, J.N., Holdford-Jack, L., (2004). The Late Quaternary Brazos and Colorado deltas, offshore Texas, USA—Their evolution and the factors that controlled their deposition, in: Anderson, J.B., Fillon, R.H. (Eds), *Late Quaternary Stratigraphic Evolution of the Northern Gulf of Mexico Margin*. SEPM Special Publication 79, 237–269.
- Afshari, K., & Stewart, J. P. (2019). Insights from California Vertical Arrays on the Effectiveness of Ground Response Analysis with Alternative Damping Models. *Bulletin of the Seismological Society of America*.  
<https://doi.org/10.1785/0120180292>
- Aguzzi, M., Amorosi, A., Colalongo, M.L., Lucchi, M.R., Rossi, V., Sarti, G., Vaiani, S.C., (2007). Late Quaternary climatic evolution of the Arno coastal plain (Western Tuscany, Italy) from subsurface data. *Sediment. Geol.* 202, 211–229.  
<https://doi.org/10.1016/j.sedgeo.2007.03.004>
- Aitken John F. & Flint Stephen S. (1996). Variable expressions of interfluvial sequence boundaries in the Breathitt Group (Pennsylvanian), eastern Kentucky, USA. *Geological Society, London, Special Publications*, 104(1), 193–206.  
<https://doi.org/10.1144/GSL.SP.1996.104.01.12>
- Aki, K. (1957). Space and time spectra of stationary stochastic waves, with special reference to microtremors. *Bulletin of the Earthquake Research Institute*, 35, 415–456.
- Allen, G. P., & Posamentier, H. W. (1993). Sequence Stratigraphy and Facies Model of an Incised Valley Fill: The Gironde Estuary, France. *Journal of Sedimentary Research*, 63, 378–391. <https://doi.org/10.1306/D4267B09-2B26-11D7-8648000102C1865D>
- Amorosi, A., (2012). Chromium and nickel as indicators of source-to-sink sediment transfer in a Holocene alluvial and coastal system (Po Plain, Italy). *Actual. Models Sediment Gener.* 280, 260–269. <https://doi.org/10.1016/j.sedgeo.2012.04.011>
- Amorosi, A., Bracone, V., Campo, B., D’Amico, C., Rossi, V., & Roskopf, C. M. (2016). A late Quaternary multiple paleovalley system from the Adriatic coastal plain (Biferno River, Southern Italy). *Geomorphology*, 254, 146–159.  
<https://doi.org/10.1016/j.geomorph.2015.11.023>
- Amorosi, A., Bracone, V., Di Donato, V., Roskopf, C. M., & Aucelli, P. P. (2009). The Plio-Pleistocene succession between Trigno and Fortore rivers (Molise and Apulia Apennines): Stratigraphy and facies characteristics. *GeoActa*, 8, 1–12.

- Amorosi, A., Bruno, L., Cacciari, M., Campo, B., Rossi, V., (2021). Tracing marine flooding surface equivalents across freshwater peats and other wetland deposits by integrated sedimentological and pollen data. *Int. J. Coal Geol.* 246, 103830. <https://doi.org/10.1016/j.coal.2021.103830>
- Amorosi, A., Bruno, L., Caldara, M., Campo, B., Cau, S., De Santis, V., Di Martino, A., Hong, W., Lucci, G., Pellegrini, C., Rossi, V., Sammartino, I., & Vaiani, S. C. (2023). Late Quaternary sedimentary record of estuarine incised-valley filling and interfluvial flooding: The Manfredonia paleovalley system (southern Italy). *Marine and Petroleum Geology*, 147, 105975. <https://doi.org/10.1016/j.marpetgeo.2022.105975>
- Amorosi, A., Bruno, L., Campo, B., & Morelli, A. (2015). The value of pocket penetration tests for the high-resolution palaeosol stratigraphy of late Quaternary deposits. *Geological Journal*, 50(5), 670–682. <https://doi.org/10.1002/gj.2585>
- Amorosi, A., Bruno, L., Campo, B., Di Martino, A., Sammartino, I., (2021). Patterns of geochemical variability across weakly developed paleosol profiles and their role as regional stratigraphic markers (Upper Pleistocene, Po Plain). *Palaeogeography, Palaeoclimatology, Palaeoecology* 574, 110413. <https://doi.org/10.1016/j.palaeo.2021.110413>
- Amorosi, A., Bruno, L., Campo, B., Morelli, A., Rossi, V., Scarponi, D., Hong, W., Bohacs, K. M., & Drexler, T. M. (2017). Global sea-level control on local parasequence architecture from the Holocene record of the Po Plain, Italy. *Sedimentology in Italy: Recent Advances and Insights*, 87, 99–111. <https://doi.org/10.1016/j.marpetgeo.2017.01.020>
- Amorosi, A., Dinelli, E., Rossi, V., Vaiani, S.C., Sacchetto, M., (2008). Late Quaternary palaeoenvironmental evolution of the Adriatic coastal plain and the onset of Po River Delta. *Palaeogeogr. Palaeoclimatol. Palaeoecol.* 268, 80–90. <https://doi.org/10.1016/j.palaeo.2008.07.009>
- Amorosi, A., Guermandi, M., Marchi, N., & Sammartino, I. (2014). Fingerprinting sedimentary and soil units by their natural metal contents: A new approach to assess metal contamination. *Science of The Total Environment*, 500–501, 361–372. <https://doi.org/10.1016/j.scitotenv.2014.08.078>
- Amorosi, A., Marchi, N., (1999). High-resolution sequence stratigraphy from piezocone tests: an example from the Late Quaternary deposits of the southeastern Po Plain. *Sedimentary Geology* 128, 67–81. [https://doi.org/10.1016/S0037-0738\(99\)00062-7](https://doi.org/10.1016/S0037-0738(99)00062-7)
- Amorosi, A., Pacifico, A., Rossi, V., & Ruberti, D. (2012). Late Quaternary incision and deposition in an active volcanic setting: The Volturno valley fill, southern Italy. *The (2011) Tohoku-Oki Tsunami*, 282, 307–320. <https://doi.org/10.1016/j.sedgeo.2012.10.003>

- Amorosi, A., Ricci Lucchi, M., Rossi, V., & Sarti, G. (2009). Climate change signature of small-scale parasequences from Lateglacial–Holocene transgressive deposits of the Arno valley fill. *Palaeogeography, Palaeoclimatology, Palaeoecology*, 273(1–2), 142–152. <https://doi.org/10.1016/j.palaeo.2008.12.010>
- Amorosi, A., Rossi, V., Sarti, G., & Mattei, R. (2013). Coalescent valley fills from the late Quaternary record of Tuscany (Italy). *Quaternary in Italy: Knowledge and Perspective*, 288, 129–138. <https://doi.org/10.1016/j.quaint.2011.10.015>
- Amorosi, A., Rossi, V., Scarponi, D., Vaiani, S.C., Ghosh, A., (2014). Biosedimentary record of postglacial coastal dynamics: High-resolution sequence stratigraphy from the northern Tuscan coast (Italy). *Boreas* 43, 939–954. <https://doi.org/10.1111/bor.12077>
- Amorosi, A., Sammartino, I., (2007). Influence of sediment provenance on background values of potentially toxic metals from near-surface sediments of Po coastal plain (Italy). *Int. J. Earth Sci.* 96, 389–396. <https://doi.org/10.1007/s00531-006-0104-8>
- Amorosi, A., Sarti, G., Rossi, V., Fontana, V., (2008). Anatomy and sequence stratigraphy of the late Quaternary Arno valley fill (Tuscany, Italy). *GeoActa* 117–128.
- Anand, V., & Satish Kumar, S. R. (2018). Seismic Soil-structure Interaction: A State-of-the-Art Review. *Structures*, 16, 317–326. <https://doi.org/10.1016/j.istruc.2018.10.009>
- Anderson, J. B., Rodriguez, A., Abdulah, K. C., Fillon, R. H., Banfield, L. A., McKeown, H. A., & Wellner, J. S. (2004). Late Quaternary Stratigraphic Evolution of the Northern Gulf of Mexico Margin: A Synthesis. In J. B. Anderson & R. H. Fillon (Eds.), *Late Quaternary Stratigraphic Evolution of the Northern Gulf of Mexico Margin* (Vol. 79). SEPM Society for Sedimentary Geology. <https://doi.org/10.2110/pec.04.79.0001>
- Anderson, J. B., Wallace, D. J., Simms, A. R., Rodriguez, A. B., Weight, R. W. R., & Taha, Z. P. (2016). Recycling sediments between source and sink during a eustatic cycle: Systems of late Quaternary northwestern Gulf of Mexico Basin. *Earth-Science Reviews*, 153, 111–138. <https://doi.org/10.1016/j.earscirev.2015.10.014>
- Antonioli, F., Ferranti, L., Fontana, A., Amorosi, A., Bondesan, A., Braitenberg, C., Dutton, A., (2009). Holocene relative sea-level changes and vertical movements along the Italian and Istrian coastlines. *Quat. Int.* 206, 102–133. <https://doi.org/10.1016/j.quaint.2008.11.008>
- Ascione, A., Cinque, A., Miccadei, E., Villani, F., Berti, C., (2008). The Plio-Quaternary uplift of the Apennine chain: new data from the analysis of topography and river valleys in Central Italy. *Geomorphology* 102, 105–118. <https://doi.org/10.1016/j.geomorph.2007.07.022>

- Asioli, A., (1996). High resolution foraminifera biostratigraphy in the Central Adriatic basin during the last deglaciation: a contribution to the PALICLAS Project. *Memorie-Istituto Ital. di Idrobiol.* 55, 197–218.
- Aslan, A., Autin, W.J., (1999). Evolution of the Holocene Mississippi River floodplain, Ferriday, Louisiana; insights on the origin of fine-grained floodplains. *J. Sediment. Res.* 69, 800–815. <https://doi.org/10.2110/jsr.69.800>
- Aslan, A., Autin, W.J., (1999). Evolution of the Holocene Mississippi River floodplain, Ferriday, Louisiana: insights on the origin of fine-grained floodplains. *J. Sediment. Res.* 69, 800-815.
- Aslan, A., Blum, M.D., (1999). Contrasting styles of Holocene avulsion, Texas Gulf Coastal Plain, in: Smith, N.D., Rogers, J.J. (Eds.), *Fluvial Sedimentology VI. IAS Special Publication*, 28, pp. 193-209.
- Athersuch, J., Horne, D.J., Whittaker, J.E., (1989). *Marine and Brackish Water Ostracods (Superfamilies Cypridacea and Cytheracea): Keys and Notes for the Identification of the Species, (New Series) 43.* ed. Brill E.J., Leiden.
- Athersuch, J., Horne, D.J., Whittaker, J.E., (1989). *Marine and brackish water ostracods (superfamilies Cypridacea and Cytheracea): keys and notes for the identification of the species.* Brill Archive, Leiden.
- Autin, W.J., Aslan, A., (2001). Alluvial pedogenesis in Pleistocene and Holocene Mississippi River deposits: Effects of relative sea-level change. *Geol. Soc. Am. Bull.* 113, 1456–1466.
- Azzarone, M., Pellegrini, C., Barbieri, G., Rossi, V., Gamberi, F., Trincardi, F., Scarponi, D., (2020). Linking benthic fauna and seismic facies to improve stratigraphic reconstructions: The case of the mid-adriatic deep since the late glacial period (central adriatic sea). *Boll. della Soc. Paleontol. Ital.* 59, 9–23. <https://doi.org/10.4435/BSPI.2020.03>
- Baheti, B., Innani, S., Gajre, S., Talbar, S., (2020). Eff-unet: A novel architecture for semantic segmentation in unstructured environment, in: *Proceedings of the IEEE/CVF Conference on Computer Vision and Pattern Recognition Workshops.* pp. 358–359.
- Barbieri, G., & Vaiani, S. C. (2018). Benthic foraminifera or Ostracoda? Comparing the accuracy of palaeoenvironmental indicators from a Pleistocene lagoon of the Romagna coastal plain (Italy). *Journal of Micropalaeontology*, 37(1), 203–230. <https://doi.org/10.5194/jm-37-203-2018>
- Barbieri, G., Amorosi, A., Vaiani, S.C., (2017). Benthic foraminifera as a key to delta evolution: A case study from the late Holocene succession of the Po River Delta. *Micropaleontology* 63, 27–41.
- Barbieri, G., Rossi, V., Vaiani, S.C., Dasgupta, U., Amorosi, A., (2021). Quantitative paleoecology in shallow-marine settings: The value of ostracods and foraminifers from the Holocene North Adriatic record. *Palaeogeogr. Palaeoclimatol. Palaeoecol.* 572, 110408. <https://doi.org/10.1016/j.palaeo.2021.110408>

- Bard, E., Hamelin, B., Delanghe-Sabatier, D., (2010). Deglacial meltwater pulse 1B and Younger Dryas sea levels revisited with boreholes at Tahiti. *Science* (80- ). 327, 1235–1237.
- Bard, E., Hamelin, B., Fairbanks, R.G., (1990). U-Th ages obtained by mass spectrometry in corals from Barbados: sea level during the past 130,000 years. *Nature* 346, 456–458.
- Bard, P.-Y., & Gariel, J.-C. (1986). The seismic response of two-dimensional sedimentary deposits with large vertical velocity gradients. *Bulletin of the Seismological Society of America*, 76(2), 343–366.
- Barnes, H., Hinojosa, J.R., Spinelli, G.A., Mozley, P.S., Koning, D., Sproule, T.G., Wilson, J.L., (2021). Detecting fault zone characteristics and paleovalley incision using electrical resistivity: Loma Blanca Fault, New Mexico. *Geophysics* 86, B209–B221.
- Bazzurro, P., & Allin Cornell, C. (1999). Disaggregation of seismic hazard. *Bulletin of the Seismological Society of America*, 89(2), 501–520.
- Bellotti, P., Caputo, C., Davoli, L., Evangelista, S., Garzanti, E., Pugliese, F., Valeri, P., (2004). Morpho-sedimentary characteristics and Holocene evolution of the emergent part of the Ombrone River delta (southern Tuscany). *Geomorphology* 61, 71–90. <https://doi.org/10.1016/j.geomorph.2003.11.007>
- Benito, G., Macklin, M.G., Panin, A., Rossato, S., Fontana, A., Jones, A.F., Machado, M.J., Matlakhova, E., Mozzi, P., Zielhofer, C., (2015). Recurring flood distribution patterns related to short-term Holocene climatic variability. *Sci. Rep.* 5, 1–8. <https://doi.org/10.1038/srep16398>
- Bergen, K.J., Johnson, P.A., De Hoop, M.V., Beroza, G.C., (2019). Machine learning for data-driven discovery in solid Earth geoscience. *Science* 363, eaau0323. <https://doi.org/10.1126/science.aau0323>
- Bhattacharya, J.P., (2006). Deltas, in: Posamentier, H.W., Walker, R.G. (Eds.), *Facies Models Revisited*. SEPM Society for Sedimentary Geology, pp. 237–292. <https://doi.org/10.2110/pec.06.84.0237>
- Bhattacharya, J.P., Copeland, P., Lawton, T.F., Holbrook, J., (2016). Estimation of source area, river paleo-discharge, paleoslope, and sediment budgets of linked deep-time depositional systems and implications for hydrocarbon potential. *Earth-Science Rev.* 153, 77–110.
- Bigi, S., Cantalamessa, G., Centamore, E., Didaskalu, P., Dramis, F., Farabollini, P., Gentili, B., Invernizzi, C., Micarelli, A., Nisio, S., Pambianchi, G., Potetti, M., (1995). La fascia periadriatica marchigiano-abruzzese dal Pliocene medio ai tempi attuali: evoluzione tettonico-sedimentaria e geomorfologica. *Studi Geologici Camerti Special volume*, 37-49.

- Bindi, D., Parolai, S., Cara, F., Di Giulio, G., Ferretti, G., Luzi, L., Monachesi, G., Pacor, F., & Rovelli, A. (2009). Site Amplifications Observed in the Gubbio Basin, Central Italy: Hints for Lateral Propagation Effects. *Bulletin of the Seismological Society of America*, 99(2A), 741–760. <https://doi.org/10.1785/0120080238>
- Bird, M.I., Fifield, L.K., Teh, T.S., Chang, C.H., Shirlaw, N., Lambeck, K., (2007). An inflection in the rate of early mid-Holocene eustatic sea-level rise: A new sea-level curve from Singapore. *Estuar. Coast. Shelf Sci.* 71, 523–536.
- Bishop, D., (2010). New approaches to understanding the structure and geotechnical characteristics of estuarine sediments. *Aust. Geomech.* 45, 111.
- Blanchon, P., Jones, B., Ford, D.C., (2002). Discovery of a submerged relic reef and shoreline off Grand Cayman: further support for an early Holocene jump in sea level. *Sediment. Geol.* 147, 253–270.
- Blockley, S. P. E., Lowe, J. J., Walker, M. J. C., Asioli, A., Trincardi, F., Coope, G. R., & Donahue, R. E. (2004). Bayesian analysis of radiocarbon chronologies: Examples from the European Late-glacial. *Journal of Quaternary Science*, 19(2), 159–175. <https://doi.org/10.1002/jqs.820>
- Blum, M. D., & Price, D. M. (1998). Quaternary alluvial plain construction in response to glacio-eustatic and climatic controls, Texas Gulf coastal plain.
- Blum, M. D., & Törnqvist, T. E. (2000). Fluvial responses to climate and sea-level change: A review and look forward: Fluvial responses to climate and sea-level change. *Sedimentology*, 47, 2–48. <https://doi.org/10.1046/j.1365-3091.2000.00008.x>
- Blum, M. D., & Törnqvist, T. E. (2000). Fluvial responses to climate and sea-level change: A review and look forward. *Sedimentology*, 47, 2–48. <https://doi.org/10.1046/j.1365-3091.2000.00008.x>
- Blum, M. D., Tomkin, J. H., Purcell, A., & Lancaster, R. R. (2008). Ups and downs of the Mississippi Delta. *Geology*, 36(9), 675–678. <https://doi.org/10.1130/G24728A.1>
- Blum, M.D., Aslan, A., (2006). Signatures of climate vs. sea-level change within incised valley-fill successions: Quaternary examples from the Texas GULF Coast. *Sediment. Geol.* 190, 177–211. <https://doi.org/10.1016/j.sedgeo.2006.05.024>
- Blum, M.D., Martin, J., Milliken, K., Garvin, M., (2013). Paleovalley systems: Insights from Quaternary analogs and experiments. *Earth-Science Rev.* 116, 128–169. <https://doi.org/10.1016/j.earscirev.2012.09.003>
- Blum, M.D., Morton, R.A., Durbin, J.M., (1995). Deweyville” terraces and deposits of the Texas Gulf coastal plain. *Gulf Coast Assoc. Geol. Soc. Trans.* 45, 53–60.

- Blum, M.D., Price, D.M., (1998). Quaternary alluvial plain construction in response to glacio-eustatic and climatic controls, Texas Gulf coastal plain, in: Shanley, K.W., McCabe, P.J. (Eds.), *Relative Role of Eustacy, Climate, and Tectonism in Continental Rocks*. SEPM Special Publication 59, pp. 31–48.
- Blum, M.D., Womack, J.H., (2009). Climate change, sea-level change, and fluvial sediment supply to deepwater systems, in: Kneller, B., Martinsen, O.J., McCaffrey, B. (Eds.), *External Controls on Deep Water Depositional Systems: Climate, Sea-Level, and Sediment Flux*. SEPM Special Publication, 92, pp. 15-39.
- Boenzi, F., Caldara, M., Pennetta, L., (1991). Stratigraphic and geomorphological observations in the southern part of the Tavoliere coastal plain, Apulia. *Geogr. Fis. e Din. Quat.* 14, 23–31.
- Bolandi, V., Kadkhodaie, A., & Farzi, R. (2017). Analyzing organic richness of source rocks from well log data by using SVM and ANN classifiers: A case study from the Kazhdumi formation, the Persian Gulf basin, offshore Iran. *Journal of Petroleum Science and Engineering*, 151, 224–234. <https://doi.org/10.1016/j.petrol.2017.01.003>
- Boore, D. M. (2004). Can site response be predicted? *Journal of Earthquake Engineering*, 8(spec01), 1–41.
- Boyd, R., Dalrymple, R. W., & Zaitlin, B. A. (2006). Estuarine and Incised-Valley Facies Models. In H. W. Posamentier & R. G. Walker (Eds.), *Facies Models Revisited* (Vol. 84, p. 0). SEPM Society for Sedimentary Geology. <https://doi.org/10.2110/pec.06.84.0171>
- Boyd, R., Dalrymple, R.W., Zaitlin, B.A., (2006). Estuarine and incised-valley facies models, in: Posamentier, H.W., Walker, R.G. (Eds.), *Facies Models Revisited*. SEPM Special Publication 84, pp. 171-235.
- Boyd, R., Suter, J., Penland, S., (1989). Relation of sequence stratigraphy to modern sedimentary environments. *Geology* 17, 926–929. [https://doi.org/10.1130/0091-7613\(1989\)017<0926:ROSSTM>2.3.CO;2](https://doi.org/10.1130/0091-7613(1989)017<0926:ROSSTM>2.3.CO;2)
- Breda, A., Amorosi, A., Rossi, V., Fusco, F., (2016). Late-glacial to holocene depositional architecture of the ombrone palaeovalley system (Southern Tuscany, Italy): Sealevel, climate and local control in valley-fill variability. *Sedimentology* 63, 1124–1148. <https://doi.org/10.1111/sed.12253>
- Bridge, J.S., (2006). Fluvial facies models: recent developments, in: Posamentier, H., Walker, R.G. (Eds.), *Facies Models Revisited*. SEPM Special Publication 84, pp. 85–170.
- Bronk Ramsey, C. (2009). Bayesian Analysis of Radiocarbon Dates. *Radiocarbon*, 51(1), 337–360. Cambridge Core. <https://doi.org/10.1017/S0033822200033865>
- Browne, G. H., & Naish, T. R. (2003). Facies development and sequence architecture of a late Quaternary fluvial-marine transition, Canterbury Plains and shelf, New Zealand: Implications for forced regressive deposits. *Sedimentary Geology*, 158(1), 57–86. [https://doi.org/10.1016/S0037-0738\(02\)00258-0](https://doi.org/10.1016/S0037-0738(02)00258-0)

- Bruno, L., Bohacs, K.M., Campo, B., Drexler, T.M., Rossi, V., Sammartino, I., Scarponi, D., Hong, W., Amorosi, A., (2017). Early Holocene transgressive palaeogeography in the Po coastal plain (northern Italy). *Sedimentology* 64, 1792–1816. <https://doi.org/10.1111/sed.12374>
- Bruno, L., Campo, B., Di Martino, A., Hong, W., Amorosi, A., (2019). Peat layer accumulation and post-burial deformation during the mid-late Holocene in the Po coastal plain (Northern Italy). *Basin Res.* 31, 621–639. <https://doi.org/10.1111/bre.12339>
- Buck, C. E., Kenworthy, J. B., Litton, C. D., & Smith, A. F. M. (1991). Combining archaeological and radiocarbon information: A Bayesian approach to calibration. *Antiquity*, 65(249), 808–821. <https://doi.org/10.1017/S0003598X00080534>
- Buck, C. E., Litton, C. D., & Smith, A. F. M. (1992). Calibration of radiocarbon results pertaining to related archaeological events. *Journal of Archaeological Science*, 19(5), 497–512. [https://doi.org/10.1016/0305-4403\(92\)90025-X](https://doi.org/10.1016/0305-4403(92)90025-X)
- Busschers, F. S., Kasse, C., van Balen, R. T., Vandenberghe, J., Cohen, K. M., Weerts, H. J. T., Wallinga, J., Johns, C., Cleveringa, P., & Bunnik, F. P. M. (2007). Late Pleistocene evolution of the Rhine-Meuse system in the southern North Sea basin: Imprints of climate change, sea-level oscillation and glacio-isostasy. *Quaternary Science Reviews*, 26(25), (3216)–3248. <https://doi.org/10.1016/j.quascirev.2007.07.013>
- Busschers, F.S., Weerts, H.J.T., Wallinga, J., Cleveringa, P., Kasse, C., de Wolf, H., Cohen, K.M., (2005). Sedimentary architecture and optical dating of Middle and Late Pleistocene Rhine-Meuse deposits — fluvial response to climate change, sea-level fluctuation and glaciation. *Netherlands Journal of Geosciences* 84, 25-41.
- Caldara, M., Pennetta, L., (1991). Pleistocenic buried abrasion platforms in Southeastern "Tavoliere" (Apulia, South Italy). *Alp. Mediterr. Quat.* 4, 303–309.
- Caldara, M., Pennetta, L., (1993). Nuovi dati per la conoscenza geologica e morfologica del Tavoliere di Puglia. *Bonifica* 8, 25–42.
- Campo, B., Amorosi, A., Bruno, L., (2016). Contrasting alluvial architecture of Late Pleistocene and Holocene deposits along a 120-km transect from the central Po Plain (northern Italy). *Sediment. Geol.* 341, 265–275.
- Campo, B., Amorosi, A., Vaiani, S.C., (2017). Sequence stratigraphy and late Quaternary paleoenvironmental evolution of the Northern Adriatic coastal plain (Italy). *Palaeogeogr. Palaeoclimatol. Palaeoecol.* 466, 265-278.
- Campo, B., Barbieri, G., Di Martino, A., Hong, W., Scarponi, D., Vaiani, S. C., & Amorosi, A. (2022). Late Pleistocene to Holocene glacio-eustatic history as recorded in the Pescara paleovalley system (Central Italy, Adriatic basin). *Marine and Petroleum Geology*, 145, 105908. <https://doi.org/10.1016/j.marpetgeo.2022.105908>

- Campo, B., Bruno, L., Amorosi, A., (2023). Sedimentary facies characterization through CPTU profiles: An effective tool for subsurface investigation of modern alluvial and coastal plains. *Sedimentology* n/a. <https://doi.org/10.1111/sed.13079>
- Carruba, S., Casnedi, R., Perotti, C.R., Tornaghi, M., Bolis, G., (2006). Tectonic and sedimentary evolution of the lower Pliocene Periadriatic foredeep in Central Italy. *Int. J. Earth Sci.* 95, 665–683. <https://doi.org/10.1007/s00531-005-0056-4>
- Castellaro, S. (2016). The complementarity of H/V and dispersion curves. *Geophysics*, 81(6), T323–T338. <https://doi.org/10.1190/geo2015-0399.1>
- Castellaro, S., & Mulargia, F. (2009). VS30 Estimates Using Constrained H/V Measurements. *Bulletin of the Seismological Society of America*, 99(2A), 761–773. <https://doi.org/10.1785/0120080179>
- Castellaro, S., & Mulargia, F. (2010). How Far from a Building Does the Ground-Motion Free-Field Start? The Cases of Three Famous Towers and a Modern Building. *Bulletin of the Seismological Society of America*, 100(5A), (2080)–2094. <https://doi.org/10.1785/0120090188>
- Cattaneo, A., Correggiari, A., Langone, L., Trincardi, F., (2003). The late-Holocene Gargano subaqueous delta, Adriatic shelf: Sediment pathways and supply fluctuations. *Mar. Geol.* 193, 61–91. [https://doi.org/10.1016/S0025-3227\(02\)00614-X](https://doi.org/10.1016/S0025-3227(02)00614-X)
- Cattaneo, A., Steel, R.J., (2003). Transgressive deposits: an overview of their variability. *Earth—Science Reviews* 62, 187–228.
- Cattaneo, A., Trincardi, F., (1999). The Late-Quaternary transgressive record in the Adriatic epicontinental sea: basin widening and facies partitioning. In: Bergman, K.M., Snedden, J.W., (Eds.), *Isolated Shallow Marine Sand Bodies: Sequence Stratigraphic Analysis and Sedimentologic Interpretation*. SEPM Special Publication 64, pp. 127–146.
- Cattaneo, A., Trincardi, F., Asioli, A., Correggiari, A., (2007). The Western Adriatic shelf clinof orm: energy-limited bottomset. *Cont. Shelf Res.* 27, 506–525. <https://doi.org/10.1016/j.csr.2006.11.013>
- Catuneanu, O., (2006). *Principles of sequence stratigraphy*, Elsevier, Amsterdam, 386 pp. <https://doi.org/10.5860/choice.44-4462>
- Catuneanu, O., (2017). Chapter One - Sequence Stratigraphy: Guidelines for a Standard Methodology, in: Montenari, M. (Ed.), *Stratigraphy & Timescales*. Academic Press, pp. 1–57. <https://doi.org/10.1016/bs.sats.2017.07.003>
- Catuneanu, O., (2019). Scale in sequence stratigraphy. *Mar. Pet. Geol.* 106, 128–159. <https://doi.org/10.1016/j.marpetgeo.2019.04.026>
- Catuneanu, O., Abreu, V., Bhattacharya, J. P., Blum, M. D., Dalrymple, R. W., Eriksson, P. G., Fielding, C. R., Fisher, W. L., Galloway, W. E., Gibling, M. R., Giles, K. A., Holbrook, J. M., Jordan, R., Kendall, C. G. St. C., Macurda, B., Martinsen, O. J.,

- Miall, A. D., Neal, J. E., Nummedal, D., ... Winker, C. (2009). Towards the standardization of sequence stratigraphy. *Earth-Science Reviews*, 92(1), 1–33. <https://doi.org/10.1016/j.earscirev.2008.10.003>
- Cau, S., Laini, A., Monegatti, P., Roveri, M., Scarponi, D., Taviani, M., (2019). Palaeoecological anatomy of shallow-water Plio-Pleistocene biocalcarenites (northern Apennines, Italy). *Palaeogeogr. Palaeoclimatol. Palaeoecol.* 514, 838–851. <https://doi.org/10.1016/j.palaeo.2018.08.011>
- Chandler, A. M., Lam, N. T. K., & Tsang, H. H. (2006). Near-surface attenuation modelling based on rock shear-wave velocity profile. *Soil Dynamics and Earthquake Engineering*, 26(11), (1004)–1014. <https://doi.org/10.1016/j.soildyn.2006.02.010>
- Chandler, V. W., & Lively, R. S. (2016). Utility of the horizontal-to-vertical spectral ratio passive seismic method for estimating thickness of Quaternary sediments in Minnesota and adjacent parts of Wisconsin. *Interpretation*, 4(3), SH71–SH90. <https://doi.org/10.1190/INT-2015-0212.1>
- Chatelain, J.-L., Guillier, B., Cara, F., Duval, A.-M., Atakan, K., Bard, P.-Y., & The WPO2 SESAME team. (2008). Evaluation of the influence of experimental conditions on H/V results from ambient noise recordings. *Bulletin of Earthquake Engineering*, 6(1), 33–74. <https://doi.org/10.1007/s10518-007-9040-7>
- Chaumillon, E., Tessier, B., Reynaud, J.Y., (2010). Stratigraphic records and variability of Incised valleys and estuaries along French coasts. *Bull. la Soc. Geol. Fr.* 181, 75–85. <https://doi.org/10.2113/gssgfbull.181.2.75>
- Cheng, H., Zhang, H., Spötl, C., Baker, J., Sinha, A., Li, H., Bartolomé, M., Moreno, A., Kathayat, G., Zhao, J., Dong, X., Li, Y., Ning, Y., Jia, X., Zong, B., Brahim, Y.A., Pérez-Mejías, C., Cai, Y., Novello, V.F., Cruz, F.W., Severinghaus, J.P., An, Z., Edwards, R.L., (2020). Timing and structure of the Younger Dryas event and its underlying climate dynamics. *Proc. Natl. Acad. Sci. U. S. A.* 117, 23408–23417. <https://doi.org/10.1073/pnas.2007869117>
- Chua, S., Switzer, A.D., Kearsley, T.I., Bird, M.I., Rowe, C., Chiam, K., Horton, B.P., (2020). A new Quaternary stratigraphy of the Kallang River Basin, Singapore: Implications for urban development and geotechnical engineering in Singapore. *J. Asian Earth Sci.* 200, 104430.
- Ciaranfi, N., Loiacono, F., Moretti, M., (2011). Note illustrative della Carta Geologica d'Italia alla scala 1: 50.000, Foglio 408 'Foggia.' *Litografia Artist. Cartogr. Ed. Firenze.*
- Cilumbriello, A., Sabato, L., Tropeano, M., Gallicchio, S., Grippa, A., Maiorano, P., Mateu-Vicens, G., Rossi, C.A., Spilotro, G., Calcagnile, L., Quarta, G., (2010). Sedimentology, stratigraphic architecture and preliminary hydrostratigraphy of the Metaponto coastal-plain subsurface (Southern Italy), in: Bersezio, R., Amanti, M. (Eds.), *Proceedings of the National Workshop "Multidisciplinary Approach for Porous Aquifer Characterization"*. *Mem. Descr. Carta Geol. d'It.*, pp. 75–92.

- Cimerman, F., Langer, M., (1991). Mediterranean foraminifera: Slovenska akademija znanosti in umetnosti. Acad. Sci. Artium Slov. Ljubl. 30, 118.
- Clark, P.U., Dyke, A.S., Shakun, J.D., Carlson, A.E., Clark, J., Wohlfarth, B., Mitrovica, J.X., Hostetler, S.W., McCabe, A.M., (2009). The Last Glacial Maximum. *Science* 325, 710–714. <https://doi.org/10.1126/science.1172873>
- Coccioni, R., (2000). Benthic foraminifera as bioindicators of heavy metal pollution—A case study from the Goro Lagoon (Italy), in: Martin, R.E., (Ed.), *Environmental Micropaleontology: The Application of Microfossils to Environmental Geology*, Kluwer Academic/Plenum Publishers, New York, pp. 71–103.
- Correggiari, A., Roveri, M., Trincardi, F., (1996). Late pleistocene and holocene evolution of the North Adriatic Sea. *Alp. Mediterr. Quat.* 9, 697–704.
- Cox, B. R., Bachhuber, J., Rathje, E., Wood, C. M., Dulberg, R., Kottke, A., Green, R. A., & Olson, S. M. (2011). Shear Wave Velocity- and Geology-Based Seismic Microzonation of Port-au-Prince, Haiti. *Earthquake Spectra*, 27(1\_suppl1), 67–92. <https://doi.org/10.1193/1.3630226>
- Crescenti, U., D'amato, C., (1980). Il Plio-Pleistocene del sottosuolo abruzzese-marchigiano tra Ascoli Piceno e Pescara.
- Crippa, G., Azzarone, M., Bottini, C., Crespi, S., Felletti, F., Marini, M., Petrizzo, M.R., Scarponi, D., Raffi, S., Raineri, G., (2019). Bio- and lithostratigraphy of lower Pleistocene marine successions in western Emilia (Italy) and their implications for the first occurrence of *Arctica islandica* in the Mediterranean Sea. *Quat. Res.* 92, 549–569. <https://doi.org/10.1017/qua.2019.20>
- Crnčević, M., Peharda, M., Ezgeta-Balić, D., Pećarević, M., (2013). Reproductive cycle of *Glycymeris nummaria* (Mollusca: Bivalvia) from Mali Ston Bay, Adriatic Sea, Croatia. *Sci. Mar.* 77, 293–300.
- Crnkovic-Friis, L., Erlandson, M., (2015). Geology Driven EUR Prediction Using Deep Learning. Presented at the SPE Annual Technical Conference and Exhibition, OnePetro. <https://doi.org/10.2118/174799-MS>
- Cross, T.A., Baker, M.R., Chapin, M.A., Clark, M.S., Gardner, M.H., Hanson, M.S., Lessenger, M.A., Little, L.D., McDonough, K.J., Sonnenfield, M.D., Valasek, D.W., Williams, M.R., Witter, D.N., (1993). Applications of high-resolution sequence stratigraphy to reservoir analysis, in: Eschard, R., Doligez, B. (Eds.), *Subsurface Reservoir Characterization from Outcrop Observations*. Proceedings 7th IFP Exploration and Production Conference, pp. 11-33.
- Csato, I., Catuneanu, O., Granjeon, D., (2014). Millennial-scale sequence stratigraphy: Numerical simulation with dionisos. *J. Sediment. Res.* 84, 394–406.
- D'Alessandro, L., Genevois, R., Marino, A., (2001). Dinamica recente della costa alta tra Ortona e Vasto (Abruzzo centro meridionale). *Mem. della Soc. Geol. Ital.* 56, 53–60.

- D'Alessandro, L., Miccadei, E., Piacentini, T., (2003). Morphostructural elements of central-eastern Abruzzi: Contributions to the study of the role of tectonics on the morphogenesis of the Apennine chain. *Quat. Int.* 101–102, 115–124. [https://doi.org/10.1016/S1040-6182\(02\)00094-0](https://doi.org/10.1016/S1040-6182(02)00094-0)
- D'Alessandro, L., Miccadei, E., Piacentini, T., (2008). Morphotectonic study of the lower Sangro River valley (Abruzzi, Central Italy). *Geomorphology* 102, 145–158. <https://doi.org/10.1016/j.geomorph.2007.06.019>
- D'Amico, C., Aiello, G., Barra, D., Bracone, V., Di Bella, L., Esu, D., Frezza, V., Roskopf, C.M., (2013). Late quaternary foraminiferal, molluscan and ostracod assemblages from a core succession in the Trigno River mouth area (Central Adriatic sea, Italy). *Boll. della Soc. Paleontol. Ital.* 52, 197–205. <https://doi.org/10.4435/BSPI.2013.23>
- D'Amico, V., Picozzi, M., Baliva, F., & Albarello, D. (2008). Ambient Noise Measurements for Preliminary Site-Effects Characterization in the Urban Area of Florence, Italy. *Bulletin of the Seismological Society of America*, 98(3), (1373)–1388. <https://doi.org/10.1785/0120070231>
- Dabrio, C.J., Zazo, C., Goy, J.L., Sierro, F.J., Borja, F., Lario, J., Gonzalez, J.A., Flores, J.A., (2000). Depositional history of estuarine infill during the last postglacial transgression (Gulf of Cadiz, Southern Spain). *Mar. Geol.* 162, 381–404.
- Dalla, S., Harby, H., Serazzi, M., (1997). Hydrocarbon exploration in a complex incised valley fill: an example from the late Messinian Abu Madi Formation (Nile Delta Basin, Egypt). *Lead. Edge* 16, 1819–1826.
- Dalrymple, R. W., Boyd, R., & Zaitlin, B. A. (1994). History of Research, Types and Internal Organisation of Incised-Valley Systems: Introduction to the Volume. In R. W. Dalrymple, R. Boyd, & B. A. Zaitlin (Eds.), *Incised-Valley Systems: Origin and Sedimentary Sequences* (Vol. 51, p. 0). SEPM Society for Sedimentary Geology. <https://doi.org/10.2110/pec.94.12.0003>
- Dalrymple, R.W., Boyd, R., Zaitlin, B.A., (1994). *Incised-Valley Systems: Origin and Sedimentary Sequences*. SEPM Special Publication 51, pp. 1-391.
- Dalrymple, R.W., Leckie, D.A., Tillman, R.W., (2006). *Incised Valleys in Time and Space: SEPM Special Publication*, 85.
- Dalrymple, R.W., Zaitlin, B.A., Boyd, R., (1992). Estuarine facies models: conceptual basis and stratigraphic implications. *J. Sediment. Petrol.* 62, 1130-1146.
- De Santis, V., & Caldara, M. (2016). Evolution of an incised valley system in the southern Adriatic Sea (Apulian margin): An onshore–offshore correlation. *Geological Journal*, 51(2), 263–284. <https://doi.org/10.1002/gj.2628>
- De Santis, V., Caldara, M., de Torres, T., Ortiz, J.E., (2010). Stratigraphic units of the Apulian Tavoliere plain (Southern Italy): Chronology, correlation with marine isotope stages and implications regarding vertical movements. *Sediment. Geol.* 228, 255–270. <https://doi.org/10.1016/j.sedgeo.2010.05.001>

- De Santis, V., Caldara, M., Pennetta, L., (2013). The marine and alluvial terraces of Tavoliere di Puglia plain (southern Italy). *J. Maps* 10, 114–125. <https://doi.org/10.1080/17445647.2013.861366>
- De Santis, V., Caldara, M., Torres, T., & Ortiz, J. E. (2014). Two middle Pleistocene warm stages in the terrace deposits of the Apulia region (southern Italy). *Relative Sea Level Changes: Signature on Continental Shelves, Changing Coastlines, and Implications for Coastal Morphodynamics*, 332, 2–18. <https://doi.org/10.1016/j.quaint.2013.10.009>
- De Stigter, H.C., Jorissen, F.J., van der Zwaan, G.J., (1998). Bathymetric distribution and microhabitat partitioning of live (Rose Bengal stained) benthic Foraminifera along a shelf to bathyal transect in the southern Adriatic Sea. *J. Foraminifer. Res.* 28, 40–65.
- Debenay, J.-P., Guillou, J.-J., Redois, F., & Geslin, E. (2000). Distribution Trends of Foraminiferal Assemblages in Paralic Environments. In R. E. Martin (Ed.), *Environmental Micropaleontology: The Application of Microfossils to Environmental Geology* (pp. 39–67). Springer US. [https://doi.org/10.1007/978-1-4615-4167-7\\_3](https://doi.org/10.1007/978-1-4615-4167-7_3)
- Debenay, J.-P., Guillou, J.-J., Redois, F., Geslin, E., (2000). Distribution Trends of Foraminiferal Assemblages in Paralic Environments, in: Martin, R.E. (Ed.), *Environmental Micropaleontology: The Application of Microfossils to Environmental Geology, Topics in Geobiology*. Springer US, Boston, MA, pp. 39–67. [https://doi.org/10.1007/978-1-4615-4167-7\\_3](https://doi.org/10.1007/978-1-4615-4167-7_3)
- Debenay, J.P., Guillou, J.J., Redois, F., Geslin, E., (2000). Distribution trends of foraminiferal assemblages in paralic environments: a base for using foraminifera as bioindicators, in: Martin, R.E., (Ed.), *Environmental Micropaleontology: The Application of Microfossils to Environmental Geology*, Kluwer Academic/Plenum Publishers, New York, pp. 39–67.
- Del Gaudio, V., Muscillo, S., & Wasowski, J. (2014). What we can learn about slope response to earthquakes from ambient noise analysis: An overview. *Engineering Geology*, 182, 182–200. <https://doi.org/10.1016/j.enggeo.2014.05.010>
- Del Monaco, F., Tallini, M., De Rose, C., & Durante, F. (2013). HVNSR survey in historical downtown L'Aquila (central Italy): Site resonance properties vs. Subsoil model. *Engineering Geology*, 158, 34–47. <https://doi.org/10.1016/j.enggeo.2013.03.008>
- Delgado, J., López Casado, C., Estévez, A., Giner, J., Cuenca, A., & Molina, S. (2000). Mapping soft soils in the Segura river valley (SE Spain): A case study of microtremors as an exploration tool. *Journal of Applied Geophysics*, 45(1), 19–32. [https://doi.org/10.1016/S0926-9851\(00\)00016-1](https://doi.org/10.1016/S0926-9851(00)00016-1)
- Della Seta, M., Del Monte, M., Fredi, P., Miccadei, E., Nesci, O., Pambianchi, G., Piacentini, T., Troiani, F., (2008). Morphotectonic evolution of the Adriatic piedmont of the Apennines: An advancement in the knowledge of the Marche-Abruzzo border area. *Geomorphology* 102, 119–129. <https://doi.org/10.1016/j.geomorph.2007.06.018>

- Denton, G.H., Anderson, R.F., Toggweiler, J.R., Edwards, R.L., Schaefer, J.M., Putnam, A.E., (2010). The last glacial termination. *Science* 328, 1652–1656. <https://doi.org/10.1126/science.1184119>
- Desiderio, G., Ferracuti, L., & Rusi, S. (2007). Structural-stratigraphic setting of middle Adriatic alluvial plains and its control on quantitative and qualitative groundwater circulation. *Memorie Descrittive Della Carta Geologica d'Italia*, 76, 147–162.
- Desiderio, G., Ferracuti, L., Rusi, S., (2007). Structural-stratigraphic setting of middle Adriatic alluvial plains and its control on quantitative and qualitative groundwater circulation, in: *Mem. Descr. Carta Geol. d'It.*, pp. 147–162.
- Devlin, J., Chang, M.-W., Lee, K., & Toutanova, K. (2019). BERT: Pre-training of Deep Bidirectional Transformers for Language Understanding (arXiv:(1810).04805). arXiv. <http://arxiv.org/abs/1810.04805>
- Devlin, J., Chang, M.-W., Lee, K., Toutanova, K., (2019). BERT: Pre-training of Deep Bidirectional Transformers for Language Understanding.
- Di Giulio, G., de Nardis, R., Boncio, P., Milana, G., Rosatelli, G., Stoppa, F., & Lavecchia, G. (2016). Seismic response of a deep continental basin including velocity inversion: The Sulmona intramontane basin (Central Apennines, Italy). *Geophysical Journal International*, 204(1), 418–439. <https://doi.org/10.1093/gji/ggv444>
- Di Martino, A., Amorosi, A., (2023). Sedimentary Facies Analysis and Segmentation.
- Doglioni, C., (1991). A proposal for the kinematic modelling of W-dipping subductions - possible applications to the Tyrrhenian-Apennines system. *Terra Nova* 3, 423–434. <https://doi.org/10.1111/j.1365-3121.1991.tb00172.x>
- Doglioni, C., Harabaglia, P., Martinelli, G., Mongelli, F., Zito, G., (1996). A geodynamic model of the Southern Apennines accretionary prism. *Terra Nova* 8, 540–547. <https://doi.org/10.1111/j.1365-3121.1996.tb00783.x>
- Doglioni, C., Mongelli, F., Pieri, P., (1994). The Puglia uplift (SE Italy): An anomaly in the foreland of the Apenninic subduction due to buckling of a thick continental lithosphere. *Tectonics* 13, 1309–1321. <https://doi.org/10.1029/94TC01501>
- Drago, T., Freitas, C., Rocha, F., Moreno, J., Cachão, M., Naughton, F., Fradique, C., Araújo, F., Silveira, T., & Oliveira, A. (2006). Paleoenvironmental evolution of estuarine systems during the last 14000 years-the case of Douro estuary (NW Portugal). *Journal of Coastal Research*, 186–192.
- Durand, M., Mojtahid, M., Maillet, G. M., Baltzer, A., Schmidt, S., Blet, S., Marchès, E., & Howa, H. (2018). Late Holocene record from a Loire River incised paleovalley (French inner continental shelf): Insights into regional and global forcing factors. *Palaeogeography, Palaeoclimatology, Palaeoecology*, 511, 12–28. <https://doi.org/10.1016/j.palaeo.2018.06.035>
- Ellis, B.F. & Messina, A.R. (1940). *Catalogue of Foraminifera*. The American Museum of Natural History, New York.

- Ellis, B.F., Messina, A.R., (1940). *Catalogue of Foraminifera*; Micropaleontology Press, New York, NY, USA.
- Ellis, B.F., Messina, A.R., (1952). *Catalogue of Ostracoda*. The American Museum of Natural History, New York.
- EUROPEAN COMMITTEE FOR STANDARDIZATION. (2004). Eurocode 8, Design of structures for earthquake resistance—Part 1: General rules, seismic actions and rules for buildings.
- Fairbanks, R.G., (1989). A 17,000-year glacio-eustatic sea level record: influence of glacial melting rates on the Younger Dryas event and deep-ocean circulation. *Nature* 342, 637–642.
- Falcone, G., Acunzo, G., Mendicelli, A., Mori, F., Naso, G., Peronace, E., Porchia, A., Romagnoli, G., Tarquini, E., & Moscatelli, M. (2021). Seismic amplification maps of Italy based on site-specific microzonation dataset and one-dimensional numerical approach. *Engineering Geology*, 289, 106170. <https://doi.org/10.1016/j.enggeo.2021.106170>
- Fan, D., Shang, S., Burr, G., (2019). Sea level implications from late quaternary/holocene paleosols from the Oujiang Delta, China. *Radiocarbon* 61, 83–99.
- Fiorentino, G., Forte, A., Pagano, E., Sabetta, F., Baggio, C., Lavorato, D., Nuti, C., & Santini, S. (2018). Damage patterns in the town of Amatrice after August 24th (2016) Central Italy earthquakes. *Bulletin of Earthquake Engineering*, 16(3), 1399–1423. <https://doi.org/10.1007/s10518-017-0254-z>
- Fleming, S.W., Watson, J.R., Ellenson, A., Cannon, A.J., Vesselinov, V.C., (2021). Machine learning in Earth and environmental science requires education and research policy reforms. *Nat. Geosci.* 14, 878–880. <https://doi.org/10.1038/s41561-021-00865-3>
- Fontana, A., Mozzi, P., & Bondesan, A. (2008). Alluvial megafans in the Venetian–Friulian Plain (north-eastern Italy): Evidence of sedimentary and erosive phases during Late Pleistocene and Holocene. *Fluvial Architecture and Dynamics in Rising Mountain Chains and Related Basins: Tectonic and Climatic Influences and Human Impacts*, 189(1), 71–90. <https://doi.org/10.1016/j.quaint.2007.08.044>
- Forzoni, A., Storms, J.E.A., Reimann, T., Moreau, J., Jouet, G., (2015). Non-linear response of the Golo River system, Corsica, France, to Late Quaternary climatic and sea level variations. *Quat. Sci. Rev.* 121, 11–27. <https://doi.org/10.1016/j.quascirev.2015.04.021>
- Frezza, V., & Carboni, M. G. (2009). Distribution of recent foraminiferal assemblages near the Ombrone River mouth (Northern Tyrrhenian Sea, Italy). *Revue de Micropaléontologie*, 52(1), 43–66. <https://doi.org/10.1016/j.revmic.2007.08.007>

- Gamberi, F., Pellegrini, C., Dalla Valle, G., Scarponi, D., Bohacs, K., Trincardi, F., (2020). Compound and hybrid clinothems of the last lowstand Mid-Adriatic Deep: Processes, depositional environments, controls and implications for stratigraphic analysis of prograding systems. *Basin Res.* 32, 363–377. <https://doi.org/10.1111/bre.12417>
- Garcia-Jerez, A. (2006). Characterization of the Sedimentary Cover of the Zafarraya Basin, Southern Spain, by Means of Ambient Noise. *Bulletin of the Seismological Society of America*, 96(3), 957–967. <https://doi.org/10.1785/0120050061>
- Garzanti, E., (2016). From static to dynamic provenance analysis—Sedimentary petrology upgraded. *Sediment. Geol.* 336, 3–13. <https://doi.org/10.1016/j.sedgeo.2015.07.010>
- Garzanti, E., Andò, S., Vezzoli, G., (2009). Grain-size dependence of sediment composition and environmental bias in provenance studies. *Earth Planet. Sci. Lett.* 277, 422–432. <https://doi.org/10.1016/j.epsl.2008.11.007>
- Gibling, M. R., Fielding, C. R., & Sinha, R. (2011). Alluvial Valleys and Alluvial Sequences: Towards a Geomorphic Assessment. In S. K. Davidson, S. Leleu, & C. P. North (Eds.), *From River to Rock Record: The preservation of fluvial sediments and their subsequent interpretation* (Vol. 97, p. 0). SEPM Society for Sedimentary Geology. <https://doi.org/10.2110/sepmsp.097.423>
- Gibling, M.R., Bird, D.J., (1994). Late Carboniferous cyclothems and alluvial paleovalleys in the Sydney Basin, Nova Scotia. *Geol. Soc. Am Bull.* 106(1), 105-117.
- Gibling, M.R., Fielding, C.R., Sinha, R., (2011). Alluvial valleys and alluvial sequences. Towards a geomorphic assessment, in: Davidson, S.K., Leleu, S., North, C. (Eds.), *From River to Rock Record: The Preservation of Fluvial Sediments and Their Subsequent Interpretation*. SEPM Special Publication 97, pp. 423–447.
- Girotti, O., & Mancini, M. (2003). Plio-Pleistocene stratigraphy and relations between marine and non-marine successions in the Middle Valley of the Tiber River (Latium, Umbria). *Alpine and Mediterranean Quaternary*, 16(1 bis), 89–106.
- Goetz, A.M., Beckie, R.D., Cahill, A.G., (2021). Groundwater recharge in a confined paleovalley setting, Northeast British Columbia, Canada. *Hydrogeol. J.* 29, 1797–1812.
- Goldstein, E.B., Coco, G., Plant, N.G., (2019). A review of machine learning applications to coastal sediment transport and morphodynamics. *Earth-Science Reviews* 194, 97–108. <https://doi.org/10.1016/j.earscirev.2019.04.022>
- Gosar, A., & Lenart, A. (2010). Mapping the thickness of sediments in the Ljubljana Moor basin (Slovenia) using microtremors. *Bulletin of Earthquake Engineering*, 8(3), 501–518. <https://doi.org/10.1007/s10518-009-9115-8>
- Goudeau, M.-L.S., Grauel, A.-L., Bernasconi, S.M., de Lange, G.J., (2013). Provenance of surface sediments along the southeastern Adriatic coast off Italy: An overview. *Estuar. Coast. Shelf Sci.* 134, 45–56. <https://doi.org/10.1016/j.ecss.2013.09.009>

- Goutte, C., & Gaussier, E. (2005). A Probabilistic Interpretation of Precision, Recall and F-Score, with Implication for Evaluation. In D. E. Losada & J. M. Fernández-Luna (Eds.), *Advances in Information Retrieval* (pp. 345–359). Springer. [https://doi.org/10.1007/978-3-540-31865-1\\_25](https://doi.org/10.1007/978-3-540-31865-1_25)
- Goutte, C., Gaussier, E., (2005). A Probabilistic Interpretation of Precision, Recall and F-Score, with Implication for Evaluation, in: Losada, D.E., Fernández-Luna, J.M. (Eds.), *Advances in Information Retrieval, Lecture Notes in Computer Science*. Springer, Berlin, Heidelberg, pp. 345–359. [https://doi.org/10.1007/978-3-540-31865-1\\_25](https://doi.org/10.1007/978-3-540-31865-1_25)
- Grano, M., Di Giuseppe, R., (2021). I molluschi terrestri e dulciacquicoli ( Mollusca : Gastropoda , Bivalvia ) di Castel di Guido ( Lazio , Italia centrale ). *Boll. Mus. reg. Sci. nat. Torino* 38, 149–168.
- Grano, M., Giuseppe, R.D., (2021). I molluschi terrestri e dulciacquicoli (Mollusca: Gastropoda, Bivalvia) di Castel di Guido (Lazio, Italia centrale) Checklist preliminare. *Boll. Mus. Reg. Sci. Nat. Torino* 38, 149–168.
- Grippa, A., Bianca, M., Tropeano, M., Cilumbriello, A., Gallipoli, M.R., Mucciarelli, M., Sabato, L., (2011). Use of the HVSR method to detect buried paleomorphologies (filled incised-valleys) below a coastal plain: The case of the metaponto plain (Basilicata, Southern Italy). *Boll. di Geofis. Teor. ed Appl.* 52, 1–16. <https://doi.org/10.4430/bgta0011>
- Gu, J., Wang, Z., Kuen, J., Ma, L., Shahroudy, A., Shuai, B., Liu, T., Wang, X., Wang, G., Cai, J., Chen, T., (2018). Recent advances in convolutional neural networks. *Pattern Recognition* 77, 354–377. <https://doi.org/10.1016/j.patcog.2017.10.013>
- Guijia, Z. and Congxian, L., (1996). The fills and stratigraphic sequences in the Qiantangjiang incised paleovalley, China. *J. Sediment. Res.* 66(2), 406–414.
- Guo, Y., Liu, Y., Georgiou, T., & Lew, M. S. (2018). A review of semantic segmentation using deep neural networks. *International Journal of Multimedia Information Retrieval*, 7(2), 87–93. <https://doi.org/10.1007/s13735-017-0141-z>
- Hadler, H., Vött, A., Willershäuser, T., Wilken, D., Blankenfeldt, R., von Carnap-Bornheim, C., Emde, K., Fischer, P., Ickerdt, U., Klooß, S., Majchczack, B., Obrocki, L., Rabbel, W., (2021). Automated facies identification by Direct Push-based sensing methods (CPT, HPT) and multivariate linear discriminant analysis to decipher geomorphological changes and storm surge impact on a medieval coastal landscape. *Earth Surface Processes and Landforms* 46, 3228–3251. <https://doi.org/10.1002/esp.5232>
- Hallal, M. M., & Cox, B. R. (2023). What Spatial Area Influences Seismic Site Response: Insights Gained from Multiazimuthal 2D Ground Response Analyses at the Treasure Island Downhole Array. *Journal of Geotechnical and Geoenvironmental Engineering*, 149(1), 04022124.

- Hampson, G., Stollhofen, H., Flint, S., (1999). A sequence stratigraphic model for the Lower Coal Measures (Upper Carboniferous) of the Ruhr district, north-west Germany. *Sedimentology* 46, 1199–1231. <https://doi.org/10.1046/j.1365-3091.1999.00273.x>
- Hanebuth, T.J.J., Stattegger, K., (2004). Depositional sequences on a late Pleistocene–Holocene tropical siliciclastic shelf (Sunda Shelf, southeast Asia). *J. Asian Earth Sci.* 23, 113–126.
- Harms, J.C., (1966). Stratigraphic Traps in a Valley Fill, Western Nebraska: ABSTRACT. *Am. Assoc. Pet. Geol. Bull.* 50, 2119–2149. <https://doi.org/10.1306/a663379c-16c0-11d7-8645000102c1865d>
- Harrison, S., Smith, D.E., Glasser, N.F., (2019). Late Quaternary meltwater pulses and sea level change. *J. Quat. Sci.* 34, 1–15.
- Hay, A. M. (1988). The derivation of global estimates from a confusion matrix. *International Journal of Remote Sensing*, 9(8), (1395)–1398. <https://doi.org/10.1080/01431168808954945>
- Hayes, M.O., (1975). Morphology of sand accumulation in estuaries: an introduction to the symposium, in: Cronin, L.E. (Ed.), *Geology and Engineering*. Academic Press. Academic Press, pp. 3–22. <https://doi.org/10.1016/B978-0-12-197502-9.50006-X>
- He, K., Zhang, X., Ren, S., Sun, J., (2015). Deep Residual Learning for Image Recognition. <https://doi.org/10.48550/arXiv.1512.03385>
- Henderson, P.A., (1990). Freshwater Ostracods, in: Kermack, D.M., Barnes, R.S.K., (Eds.), *Synopses of the British Fauna (New Series)*, Leiden, The Netherlands, 228 p.
- Henderson, P.A., (1990). *Freshwater Ostracods: Keys and Notes for the Identification of the Species*, New Series 42. ed. Linnean Society of London and the Estuarine and Coastal Sciences Association, Leiden.
- Hickin, A.S., Best, M.E., (2013). Mapping the geometry and lithostratigraphy of a paleovalley with a time-domain electromagnetic technique in an area with small resistivity contrasts, Groundbirch, British Columbia, Canada. *J. Environ. Eng. Geophys.* 18, 119–135.
- Hijma, M.P., Cohen, K.M., Hoffmann, G., Van der Spek, A.J.F., Stouthamer, E., (2009). From river valley to estuary: the evolution of the Rhine river mouth in the early to middle Holocene (western Netherlands, Rhine-Meuse delta). *Neth. J. Geosci.* 88, 13-53.
- Hinzen, K.-G., Weber, B., & Scherbaum, F. (2004). On the resolution of H/V measurements to determine sediment thickness, a case study across a normal fault in the Lower Rhine Embayment, Germany. *Journal of Earthquake Engineering*, 8(06), 909–926.

- Holbrook, J. M., & Bhattacharya, J. P. (2012). Reappraisal of the sequence boundary in time and space: Case and considerations for an SU (subaerial unconformity) that is not a sediment bypass surface, a time barrier, or an unconformity. *Earth-Science Reviews*, 113(3), 271–302. <https://doi.org/10.1016/j.earscirev.2012.03.006>
- Hori, K., Saito, Y., Zhao, Q., Wang, P., (2002). Evolution of the coastal depositional systems of the Changjiang (Yangtze) in response to late Pleistocene-Holocene sea-level changes. *J. Sediment. Res.* 72, 884-897.
- Hori, K., Tanabe, S., & Urabe, A. (2023). Accumulation of thick fluvial sediments in the Shinano River incised-valley fills: Implications for sequence stratigraphy and alluvial architecture. *Journal of Sedimentary Research*, 93(7), 453–462. <https://doi.org/10.2110/jsr.2022.049>
- Hori, K., Tanabe, S., Saito, Y., Haruyama, S., Nguyen, V., Kitamura, A., (2004). Delta initiation and Holocene sea-level change: example from the Song Hong (Red River) delta, Vietnam. *Sedimentary Geology*, 164, 237–249.
- Horike, M. (1985). Inversion of phase velocity of long-period microtremors to the S-wave-velocity structure down to the basement in urbanized areas. *Journal of Physics of the Earth*, 33(2), 59–96. <https://doi.org/10.4294/jpe.1952.33.59>
- Horozal, S., Chae, S., Seo, J. M., Lee, S. M., Han, H. S., Cukur, D., Kim, E. D., & Son, J. H. (2021). Quaternary evolution of the southeastern Korean continental shelf, East Sea: Paleo-incised valley and channel systems. *Marine and Petroleum Geology*, 128, 105011. <https://doi.org/10.1016/j.marpetgeo.2021.105011>
- Hudson, M., Idriss, I. M., & Beikae, M. (1994). QUAD4M: a computer program to evaluate the seismic response of soil structures using finite element procedures and incorporating a compliant base. Center for Geotechnical Modeling, Department of Civil and Environmental ....
- Ibs-von Seht, M., & Wohlenberg, J. (1999). Microtremor measurements used to map thickness of soft sediments. *Bulletin of the Seismological Society of America*, 89(1), 250–259. <https://doi.org/10.1785/BSSA0890010250>
- Imbrie, J., & Imbrie, K. P. (1986). *Ice ages: Solving the mystery*. Harvard University Press.
- Ishihara, T., & Sugai, T. (2017). Eustatic and regional tectonic controls on late Pleistocene paleovalley morphology in the central Kanto Plain, Japan. *Quaternary International*, 456, 69–84. <https://doi.org/10.1016/j.quaint.2017.06.029>
- Ishihara, Y., Miyazaki, Y., Eto, C., Fukuoka, S., & Kimura, K. (2013). Shallow subsurface three-dimensional geological model using borehole logs in Tokyo Bay area, central Japan. *J Geol Soc Japan*, 119(8), 554–566. <https://doi.org/10.5575/geosoc.2013.0019>
- Iyengar, R. N., & Ghosh, S. (2004). Microzonation of earthquake hazard in greater Delhi area. *Current Science*, 87(9), (1193)–1202.

- J. C. Harms. (1965). Stratigraphic Traps in a Valley Fill, Western Nebraska: ABSTRACT. AAPG Bulletin, 49. <https://doi.org/10.1306/A663379C-16C0-11D7-8645000102C1865D>
- Jacq, K., Rapuc, W., Benoit, A., Coquin, D., Fanget, B., Perrette, Y., Sabatier, P., Wilhelm, B., Debret, M., Arnaud, F., (2022). Sedimentary structure discrimination with hyperspectral imaging in sediment cores. *Science of The Total Environment* 817, 152018. <https://doi.org/10.1016/j.scitotenv.2021.152018>
- Jennette, D. C., Jones, C. R., Van Wagoner, J. C., & Larsen, J. E. (1991). High-resolution sequence stratigraphy of the Upper Cretaceous Tociito Sandstone: The relationship between incised valleys and hydrocarbon accumulation, San Juan Basin, New Mexico.
- Jennette, D.C., Jones, C.R., Van Wagoner, J.C., Larsen, J.E., (1991). High-resolution sequence stratigraphy of the Upper Cretaceous Tociito Sandstone: the relationship between incised valleys and hydrocarbon accumulation, San Juan Basin, New Mexico, in: J.C. Van Wagoner, C.R. Jones, D.R. Taylor, D. Nummedal, D.C. Jennette, G.W. Riley (Eds.), *Sequence stratigraphy applications to shelf sandstone reservoirs, outcrop to subsurface examples*, 24-62.
- Jessen, S., Larsen, F., Postma, D., Viet, P.H., Ha, N.T., Nhan, P.Q., Nhan, D.D., Duc, M.T., Hue, N.T.M., Huy, T.D., (2008). Palaeo-hydrogeological control on groundwater As levels in Red River delta, Vietnam. *Appl. Geochemistry* 23, 3116–3126.
- Jorissen, F., Nardelli, M.P., Almogi-Labin, A., Barras, C., Bergamin, L., Bicchi, E., El Kateb, A., Ferraro, L., McGann, M., Morigi, C., Romano, E., Sabbatini, A., Schweizer, M., Spezzaferri, S., (2018). Developing Foram-AMBI for biomonitoring in the Mediterranean: Species assignments to ecological categories. *Mar. Micropaleontol.* 140, 33–45. <https://doi.org/10.1016/j.marmicro.2017.12.006>
- Jorissen, F.J., (1988). Benthic foraminifera from the Adriatic Sea : principles of phenotypic variation. *Utrecht Micropaleontol. Bull.* 37, 176.
- Jorissen, F.J., Barmawidjaja, D.M., Puskaric, S., Van der Zwaan, G.J., (1992). Vertical distribution of benthic foraminifera in the northern Adriatic Sea: the relation with the organic flux. *Marine Micropaleontol.* 19, 131-146.
- Kadow, C., Hall, D.M., Ulbrich, U., (2020). Artificial intelligence reconstructs missing climate information. *Nat. Geosci.* 13, 408–413. <https://doi.org/10.1038/s41561-020-0582-5>
- Karimzadeh, S., & Mastuoka, M. (2017). Building Damage Assessment Using Multisensor Dual-Polarized Synthetic Aperture Radar Data for the (2016) M 6.2 Amatrice Earthquake, Italy. *Remote Sensing*, 9(4), 330. <https://doi.org/10.3390/rs9040330>
- Karpatne, A., Ebert-Uphoff, I., Ravela, S., Babaie, H.A., Kumar, V., (2019). Machine Learning for the Geosciences: Challenges and Opportunities. *IEEE Trans. Knowl. Data Eng.* 31, 1544–1554. <https://doi.org/10.1109/TKDE.2018.2861006>

- Kasse, C., Bohncke, S.J.P., Vandenberghe, J., Gábris, G., (2010). Fluvial style changes during the last glacial–interglacial transition in the middle Tisza valley (Hungary). *Fluv. Rec. Arch. Hum. Act. Environ. Change* 121, 180–194. <https://doi.org/10.1016/j.pgeola.2010.02.005>
- Kawase, H. (1996). The Cause of the Damage Belt in Kobe: “The Basin-Edge Effect,” Constructive Interference of the Direct S-Wave with the Basin-Induced Diffracted/Rayleigh Waves. *Seismological Research Letters*, 67(5), 25–34. <https://doi.org/10.1785/gssrl.67.5.25>
- Kettner, A.J., Syvitski, J.P.M., (2008). Predicting discharge and sediment flux of the Po River, Italy since the Last Glacial Maximum. In: de Boer, P.L. (Ed.), *Analogue and Numerical Forward Modeling of Sedimentary Systems; From Understanding to Prediction: IAS Special Publication*, 40, pp. 171–190.
- Khan, S., Van Der Meijde, M., Van Der Werff, H., & Shafique, M. (2017). Impact of Mesh and DEM Resolutions in SEM Simulation of 3D Seismic Response. *Bulletin of the Seismological Society of America*, 107(5), (2151)–2159. <https://doi.org/10.1785/0120160213>
- Kingma, D.P., Ba, J., (2017). Adam: A Method for Stochastic Optimization. <https://doi.org/10.48550/arXiv.1412.6980>
- Kiureghian, A. D., & Neuenhofer, A. (1992). Response spectrum method for multi-support seismic excitations. *Earthquake Engineering & Structural Dynamics*, 21(8), 713–740. <https://doi.org/10.1002/eqe.4290210805>
- Köhler, A., Ohrnberger, M., Scherbaum, F., Wathelet, M., & Cornou, C. (2007). Assessing the reliability of the modified three-component spatial autocorrelation technique. *Geophysical Journal International*, 168(2), 779–796. <https://doi.org/10.1111/j.1365-246X.2006.03253.x>
- Kowalewski, M., Wittmer, J.M., Dexter, T.A., Amorosi, A., Scarponi, D., (2015). Differential responses of marine communities to natural and anthropogenic changes. *Proc. R. Soc. B Biol. Sci.* 282, 20142990. <https://doi.org/10.1098/rspb.2014.2990>
- Kroonenberg, S.B., Alekseevski, N.I., Aliyeva, E., Allen, M.B., Aybulatov, D.N., Baba-Zadeh, A., Badyukova, E.N., Davies, C.E., Hinds, D.J., Hoogendoorn, R.M., Huseynov, D., Ibrahimov, B., Mamedov, P., Overeem, I., Rusakov, G. V, Suleymanova, S., Svitoch, A.A., Vincent, S.J., (2005). Two Deltas, Two Basins, One River, One Sea: The Modern Volga Delta as an Analogue of the Neogene Productive Series, South Caspian Basin, in: Giosan, L., Bhattacharya, J.P. (Eds.), *River Deltas—Concepts, Models, and Examples*. SEPM Society for Sedimentary Geology, pp. 231–256. <https://doi.org/10.2110/pec.05.83.0231>
- Kruiver, P.P., de Lange, G., Wiersma, A., Meijers, P., Korff, M., Peeters, J., Stafleu, J., Harting, R., Dambrink, R., Busschers, F., (2015). Geological schematisation of the shallow subsurface of Groningen—for site response to earthquakes for the Groningen gas field. *Deltares report*.

- Kuwatani, T., Nagata, K., Okada, M., Watanabe, T., Ogawa, Y., Komai, T., & Tsuchiya, N. (2014). Machine-learning techniques for geochemical discrimination of (2011) Tohoku tsunami deposits. *Scientific Reports*, 4(1), Article 1. <https://doi.org/10.1038/srep07077>
- Labaune, C., Tesson, M., Gensous, B., Parize, O., Imbert, P., Delhaye-Prat, V., (2010). Detailed architecture of a compound incised valley system and correlation with forced regressive wedges: Example of Late Quaternary Têt and Agly rivers, western Gulf of Lions, Mediterranean Sea, France. *Sediment. Geol.* 223, 360–379.
- Labourdette, R., Jones, R.R., (2007). Characterization of fluvial architectural elements using a three-dimensional outcrop data set: Escanilla braided system, South-Central Pyrenees, Spain. *Geosphere* 3, 422–434. <https://doi.org/10.1130/GES00087.1>
- Lagomarsino, S. (2012). Damage assessment of churches after L'Aquila earthquake (2009). *Bulletin of Earthquake Engineering*, 10(1), 73–92. <https://doi.org/10.1007/s10518-011-9307-x>
- Lambeck, K., Antonioli, F., Anzidei, M., Ferranti, L., Leoni, G., Scicchitano, G., Silenzi, S., (2011). Sea level change along the Italian coast during the Holocene and projections for the future. *Quat. Int.* 232, 250–257. <https://doi.org/10.1016/j.quaint.2010.04.026>
- Lambeck, K., Rouby, H., Purcell, A., Sun, Y., & Sambridge, M. (2014). Sea level and global ice volumes from the Last Glacial Maximum to the Holocene. *Proceedings of the National Academy of Sciences*, 111(43), 15296–15303. <https://doi.org/10.1073/pnas.1411762111>
- Laurendeau, A., Bard, P.-Y., Hollender, F., Perron, V., Foundotos, L., Ktenidou, O.-J., & Hernandez, B. (2018). Derivation of consistent hard rock (1000 < VS < (3000) m/s) GMPs from surface and down-hole recordings: Analysis of KiK-net data. *Bulletin of Earthquake Engineering*, 16(6), 2253–2284. <https://doi.org/10.1007/s10518-017-0142-6>
- Le Roux, O., Cornou, C., Jongmans, D., & Schwartz, S. (2012). 1-D and 2-D resonances in an Alpine valley identified from ambient noise measurements and 3-D modelling: 1-D and 2-D resonances in an Alpine valley. *Geophysical Journal International*, 191(2), 579–590. <https://doi.org/10.1111/j.1365-246X.2012.05635.x>
- Lee, A.-S., Enters, D., Huang, J.-J.S., Liou, S.Y.H., Zolitschka, B., (2022). An automatic sediment-facies classification approach using machine learning and feature engineering. *Commun Earth Environ* 3, 1–9. <https://doi.org/10.1038/s43247-022-00631-2>
- Legarreta, L., & Uliana, M. A. (1998). Anatomy of Hinterland Depositional Sequences: Upper Cretaceous Fluvial Strata, Neuquen Basin, West-Central Argentina. In G. Kocurek (Ed.), *Relative Role of Eustacy, Climate, and Tectonism in Continental Rocks* (Vol. 59, p. 0). SEPM Society for Sedimentary Geology. <https://doi.org/10.2110/pec.98.59.0083>

- Legarreta, L., Uliana, M.A., (1998). Anatomy of hinterland depositional sequences: Upper Cretaceous fluvial strata, Neuquen Basin, west-central Argentina, in: Shanley, K.W., McCabe, P.J. (Eds.), *Relative Role of Eustasy, Climate and Tectonism in Continental Rocks*. SEPM Special Publication, pp. 83–92.
- Leithold, E.L., Blair, N.E., Wegmann, K.W., (2016). Source-to-sink sedimentary systems and global carbon burial: A river runs through it. *Earth-Science Rev.* 153, 30–42.
- Li, C., Chen, Q., Zhang, J., Yang, S., & Fan, D. (2000). Stratigraphy and paleoenvironmental changes in the Yangtze Delta during the Late Quaternary. *Journal of Asian Earth Sciences*, 18(4), 453–469. [https://doi.org/10.1016/S1367-9120\(99\)00078-4](https://doi.org/10.1016/S1367-9120(99)00078-4)
- Li, W., Bhattacharya, J.P., Campbell, C., (2010). Temporal Evolution of Fluvial Style in a Compound Incised-Valley Fill, Ferron “Notom Delta”, Henry Mountains Region, Utah (U.S.A.). *J. Sed. Res.* 80, 529–549.
- Li, Z., Liu, F., Yang, W., Peng, S., & Zhou, J. (2022). A Survey of Convolutional Neural Networks: Analysis, Applications, and Prospects. *IEEE Transactions on Neural Networks and Learning Systems*, 33(12), Article 12. <https://doi.org/10.1109/TNNLS.2021.3084827>
- Lisiecki, L. E., & Raymo, M. E. (2007). Plio–Pleistocene climate evolution: Trends and transitions in glacial cycle dynamics. *Quaternary Science Reviews*, 26(1), 56–69. <https://doi.org/10.1016/j.quascirev.2006.09.005>
- Liu, H., Meng, J., Zhang, Y., Yang, L., (2019). Pliocene seismic stratigraphy and deep-water sedimentation in the Qiongdongnan Basin, South China Sea: Source-to-sink systems and hydrocarbon accumulation significance. *Geol. J.* 54, 392–408.
- Liu, J.P., Milliman, J.D., (2004). Reconsidering melt-water pulses 1A and 1B: Global impacts of rapid sea-level rise. *J. Ocean Univ. China* 3, 183–190. <https://doi.org/10.1007/s11802-004-0033-8>
- Liu, J.P., Milliman, J.D., Gao, S., Cheng, P., (2004). Holocene development of the Yellow River’s subaqueous delta, north Yellow Sea. *Mar. Geol.* 209, 45–67.
- Lopes-Rocha, M., Langone, L., Miserocchi, S., Giordano, P., Guerra, R., (2017). Spatial patterns and temporal trends of trace metal mass budgets in the western Adriatic sediments (Mediterranean Sea). *Sci. Total Environ.* 599–600, 1022–1033. <https://doi.org/10.1016/j.scitotenv.2017.04.114>
- Lowe, J. J., Blockley, S., Trincardi, F., Asioli, A., Cattaneo, A., Matthews, I. P., Pollard, M., & Wulf, S. (2007). Age modelling of late Quaternary marine sequences in the Adriatic: Towards improved precision and accuracy using volcanic event stratigraphy. *Continental Shelf Research*, 27(3–4), 560–582. <https://doi.org/10.1016/j.csr.2005.12.017>

- Luzi, L., Lanzano, G., Felicetta, C., D'Amico, M. C., Russo, E., Sgobba, S., Pacor, F., & ORFEUS Working Group 5. (2020). Engineering Strong Motion Database (ESM), version 2.0 [Text/html,application/json,image/jpeg,application/vnd.fdsn.mseed,text/plain,application/zip,text/plain,text/xml,application/xml]. <https://doi.org/10.13127/ESM.2>
- Macerola, L., Tallini, M., Di Giulio, G., Nocentini, M., & Milana, G. (2019). The 1-D and 2-D Seismic modeling of deep quaternary basin (Downtown L'Aquila, Central Italy). *Earthquake Spectra*, 35(4), (1689)–1710.
- Macklin, M.G., Fuller, I.C., Lewin, J., Maas, G.S., Passmore, D.J., Rose, J., Woodward, J.C., Black, S., Hamlin, R.H.B., Rowan, J.S., (2002). Correlation of fluvial sequences in the Mediterranean basin over the last 200 ka and their relationship to climate change. *Quat. Sci. Rev.* 21, 1633-1641.
- Malinverno, A., Ryan, W.B.F., (1986). Extension in the Tyrrhenian Sea and shortening in the Apennines as result of arc migration driven by sinking of the lithosphere. *Tectonics* 5, 227–245. <https://doi.org/10.1029/TC005i002p00227>
- Mantovani, A., Valkaniotis, S., Rapti, D., & Caputo, R. (2018). Mapping the Palaeo-Piniada Valley, Central Greece, Based on Systematic Microtremor Analyses. *Pure and Applied Geophysics*, 175(3), 865–881. <https://doi.org/10.1007/s00024-017-1731-7>
- Martín Abadi, Ashish Agarwal, Paul Barham, Eugene Brevdo, Zhifeng Chen, Craig Citro, Greg S. Corrado, Andy Davis, Jeffrey Dean, Matthieu Devin, Sanjay Ghemawat, Ian Goodfellow, Andrew Harp, Geoffrey Irving, Michael Isard, Jia, Y., Rafal Jozefowicz, Lukasz Kaiser, Manjunath Kudlur, Josh Levenberg, Dandelion Mané, Rajat Monga, Sherry Moore, Derek Murray, Chris Olah, Mike Schuster, Jonathon Shlens, Benoit Steiner, Ilya Sutskever, Kunal Talwar, Paul Tucker, Vincent Vanhoucke, Vijay Vasudevan, Fernanda Viégas, Oriol Vinyals, Pete Warden, Martin Wattenberg, Martin Wicke, Yuan Yu, Xiaoqiang Zheng, (2015). TensorFlow: Large-Scale Machine Learning on Heterogeneous Systems.
- Martinson, D. G., Pisias, N. G., Hays, J. D., Imbrie, J., Moore, T. C., & Shackleton, N. J. (1987). Age Dating and the Orbital Theory of the Ice Ages: Development of a High-Resolution 0 to 300,000-Year Chronostratigraphy. *Quaternary Research*, 27(1), 1–29. Cambridge Core. [https://doi.org/10.1016/0033-5894\(87\)90046-9](https://doi.org/10.1016/0033-5894(87)90046-9)
- Maselli, V., & Trincardi, F. (2013). Large-scale single incised valley from a small catchment basin on the western Adriatic margin (central Mediterranean Sea). *Global and Planetary Change*, 100, 245–262. <https://doi.org/10.1016/j.gloplacha.2012.10.008>
- Maselli, V., Hutton, E.W., Kettner, A.J., Syvitski, J.P.M., Trincardi, F., (2011). High-frequency sea level and sediment supply fluctuations during Termination I: An integrated sequence-stratigraphy and modeling approach from the Adriatic Sea (Central Mediterranean). *Mar. Geol.* 287, 54–70. <https://doi.org/10.1016/j.margeo.2011.06.012>

- Maselli, V., Trincardi, F., Asioli, A., Ceregato, A., Rizzetto, F., & Taviani, M. (2014). Delta growth and river valleys: The influence of climate and sea level changes on the South Adriatic shelf (Mediterranean Sea). *Quaternary Science Reviews*, 99, 146–163. <https://doi.org/10.1016/j.quascirev.2014.06.014>
- Maselli, V., Trincardi, F., Cattaneo, A., Ridente, D., Asioli, A., (2010). Subsidence pattern in the central Adriatic and its influence on sediment architecture during the last 400 kyr. *J. Geophys. Res. Solid Earth* 115, 1–23. <https://doi.org/10.1029/2010JB007687>
- Mattheus, C.R., Ramsey, K.W., Tomlinson, J.L., (2020). The evolution of coastal-plain incised valleys over multiple glacio-eustatic cycles: Insights from the inner continental shelf of Delaware, USA. *J. Sediment. Res.* 90, 1510–1526. <https://doi.org/10.2110/jsr.2020.69>
- Mattheus, C.R., Rodriguez, A.B., (2014). Controls on lower-coastal-plain valley morphology and fill architecture. *J. Sediment. Res.* 84, 314–325. <https://doi.org/10.2110/jsr.2014.30>
- Mayewski, P.A., Rohling, E.E., Curt Stager, J., Karlén, W., Maasch, K.A., Meeker, L.D., Meyerson, E.A., Gasse, F., Van Kreveld, S., Holmgren, K., Lee-Thorp, J., Rosqvist, G., Rack, F., Staubwasser, M., Schneider, R.R., Steig, E.J., (2004). Holocene climate variability. *Quat. res.* 62, 243–255. <https://doi.org/10.1016/j.yqres.2004.07.001>
- Mazzini, I., Aiello, G., Frenzel, P., & Pint, A. (2022). Marine and marginal marine Ostracoda as proxies in geoarchaeology. *Marine Micropaleontology*, 174, 102054. <https://doi.org/10.1016/j.marmicro.2021.102054>
- Mazzini, I., Marrone, F., Arculeo, M., Rossetti, G., (2017). Revision of Recent and fossil *Mixtacandona Klie 1938* (Ostracoda, Candonidae) from Italy, with description of a new species. *Zootaxa* 4221, zootaxa.4221.3.3. <https://doi.org/10.11646/zootaxa.4221.3.3>
- McCarthy, P.J., Plint, G.A., (1998). Recognition of interfluvial sequence boundaries: Integrating paleopedology and sequence stratigraphy. *Geology* 26, 387–390. [https://doi.org/10.1130/0091-7613\(1998\)026<0387:ROISBI>2.3.CO;2](https://doi.org/10.1130/0091-7613(1998)026<0387:ROISBI>2.3.CO;2)
- McGhee, C., Muhammed, D., Simon, N., Acikalin, S., Utley, J. E. P., Griffiths, J., Wooldridge, L., Verhagen, I. T. E., Land, C., & Worden, R. H. (2022). Stratigraphy and sedimentary evolution of a modern macro-tidal incised valley: An analogue for reservoir facies and architecture. *Sedimentology*, 69(2), 696–723. <https://doi.org/10.1111/sed.12922>
- McGhee, C., Muhammed, D., Simon, N., Acikalin, S., Utley, J.E.P., Griffiths, J., Wooldridge, L., Verhagen, I.T.E., van der Land, C., Worden, R.H., (2022). Stratigraphy and sedimentary evolution of a modern macro-tidal incised valley: An analogue for reservoir facies and architecture. *Sedimentology* 69, 696–723. <https://doi.org/10.1111/sed.12922>
- Meisch, C., (2000). *Freshwater Ostracoda of Western and Central Europe*, Heidelberg, Spektrum, 522 p.

- Mele, M., Bersezio, R., Bini, A., Bruno, M., Giudici, M., & Tantardini, D. (2021). Subsurface profiling of buried valleys in central alps (northern Italy) using HVSR single-station passive seismic. *Journal of Applied Geophysics*, 193, 104407. <https://doi.org/10.1016/j.jappgeo.2021.104407>
- Miall, A.D., (1992). Alluvial deposits, in: Walker, R.G., James, N.P. (Eds.), *Facies Models: Response to Sea Level Change*. Geological Association of Canada, Waterloo, Ontario, pp. 119-139.
- Miall, A.D., (1992). Facies models, response to sea level change. *Geol. Assoc. Can.*, 119–142.
- Milker, Y., Schmiedl, G., (2012). A taxonomic guide to modern benthic shelf foraminifera of the western Mediterranean Sea. *Palaeontol. Electron.* 15, 2;16A,134p. <https://doi.org/10.26879/271>
- Milker, Y., Schmiedl, G., (2012). A taxonomic guide to modern benthic shelf foraminifera of the western Mediterranean Sea, *Palaeontologia Electronica* 15 (2), 16A, 134 p.
- Milli, S., D'Ambrogio, C., Bellotti, P., Calderoni, G., Carboni, M. G., Celant, A., Di Bella, L., Di Rita, F., Frezza, V., Magri, D., Pichezzi, R. M., & Ricci, V. (2013). The transition from wave-dominated estuary to wave-dominated delta: The Late Quaternary stratigraphic architecture of Tiber River deltaic succession (Italy). *Sedimentary Geology*, 284–285, 159–180. <https://doi.org/10.1016/j.sedgeo.2012.12.003>
- Milli, S., Mancini, M., Moscatelli, M., Stigliano, F., Marini, M., & Cavinato, G. P. (2016). From river to shelf, anatomy of a high-frequency depositional sequence: The Late Pleistocene to Holocene Tiber depositional sequence. *Sedimentology*, 63(7), (1886)–1928. <https://doi.org/10.1111/sed.12277>
- Mitchum, R.M., Jr., Vail, P.R., Sangree, J.B., (1977). *Seismic Stratigraphy and Global Changes of Sea Level, Part 6: Stratigraphic Interpretation of Seismic Reflection Patterns in Depositional Sequences. Section 2. Application of seismic reflection configuration to stratigraphic interpretation*, in: Payton, C.E. (Ed.), *Seismic Stratigraphy — Applications to Hydrocarbon Exploration*. Am. Ass. Petrol. Geol. Memoir 26, pp. 117–133. <https://doi.org/10.1306/M26490C8>
- Mitchum, R.M., Jr., Vail, P.R., Thompson, S., III, (1977). *Seismic Stratigraphy and Global Changes of Sea Level, Part 2: The Depositional Sequence as a Basic Unit for Stratigraphic Analysis*, in: Payton, C.E. (Ed.), *Seismic Stratigraphy — Applications to Hydrocarbon Exploration*. American Association of Petroleum Geologists. <https://doi.org/10.1306/M26490C4>
- Moon, S.-W., Subramaniam, P., Zhang, Y., Vinoth, G., & Ku, T. (2019). Bedrock depth evaluation using microtremor measurement: Empirical guidelines at weathered granite formation in Singapore. *Journal of Applied Geophysics*, 171, 103866. <https://doi.org/10.1016/j.jappgeo.2019.103866>

- Morelli, A., Bruno, L., Cleveland, D. M., Drexler, T. M., & Amorosi, A. (2017). Reconstructing Last Glacial Maximum and Younger Dryas paleolandscapes through subsurface paleosol stratigraphy: An example from the Po coastal plain, Italy. *Geomorphology*, 295, 790–800. <https://doi.org/10.1016/j.geomorph.2017.08.013>
- Moscattelli, M., Albarello, D., Scarascia Mugnozza, G., & Dolce, M. (2020). The Italian approach to seismic microzonation. *Bulletin of Earthquake Engineering*, 18(12), (5425)–5440. <https://doi.org/10.1007/s10518-020-00856-6>
- Motazedian, D., Hunter, J. A., Pugin, A., & Crow, H. (2011). Development of a Vs 30 (NEHRP) map for the city of Ottawa, Ontario, Canada. *Canadian Geotechnical Journal*, 48(3), 458–472. <https://doi.org/10.1139/T10-081>
- Mozzi, P., Ferrarese, F., & Fontana, A. (2013). Integrating digital elevation models and stratigraphic data for the reconstruction of the post-LGM unconformity in the Brenta alluvial megafan (North-Eastern Italy). *Alpine and Mediterranean Quaternary*, 26(1), 41–54.
- Murray, J.W., (2006). *Ecology and Applications of Benthic Foraminifera*. Cambridge University Press, Cambridge.
- Nakamura, Y. (1989). A method for dynamic characteristics estimation of subsurface using microtremor on the ground surface. *Railway Technical Research Institute, Quarterly Reports*, 30(1), 25–33.
- Nakamura, Y. (2000). Clear identification of fundamental idea of Nakamura's technique and its applications. *Proceedings of the 12th World Conference on Earthquake Engineering*, (2656), 1–8. [https://scholar.google.com/scholar?hl=it&as\\_sdt=0%2C5&q=Clear+identification+of+fundamental+idea+of+Nakamura+%E2%80%99s+technique+and+its+applications&btnG=](https://scholar.google.com/scholar?hl=it&as_sdt=0%2C5&q=Clear+identification+of+fundamental+idea+of+Nakamura+%E2%80%99s+technique+and+its+applications&btnG=)
- Neal, J. E., Abreu, V., Bohacs, K. M., Feldman, H. R., & Pederson, K. H. (2016). Accommodation succession ( $\delta A/\delta S$ ) sequence stratigraphy: Observational method, utility and insights into sequence boundary formation. *Journal of the Geological Society*, 173(5), 803–816. <https://doi.org/10.1144/jgs2015-165>
- Neal, J., Abreu, V., (2009). Sequence stratigraphy hierarchy and the accommodation succession method. *Geology* 37, 779–782. <https://doi.org/10.1130/G25722A.1>
- Nogoshi, M., & Igarashi, T. (1971). On the amplitude characteristics of microtremor, Part II. *Journal of the Seismological Society of Japan*, 24, 26–40.
- Ockelmann, K.W., Muss, K., (1978). The biology, ecology and behaviour of the bivalve *Mysella bidentata* (Montagu). *Ophelia* 17), 1–93.
- Ohori, M., Nobata, A., & Wakamatsu, K. (2002). A comparison of ESAC and FK methods of estimating phase velocity using arbitrarily shaped microtremor arrays. *Bulletin of the Seismological Society of America*, 92(6), (2323)–2332. <https://doi.org/10.1785/0119980109>

- Okada, H., & Suto, K. (2003). The microtremor survey method. Geophysical Monograph Series. Society of Exploration Geophysicists (S.E.G.). <https://doi.org/10.1190/1.9781560801740.ch3>
- Oliver, P. G., Holmes, A. M., Killeen, I. J., Turner, J. A. (2016). Marine Bivalve Shells of the British Isles. Amgueddfa Cymru - National Museum Wales. Available from: <http://naturalhistory.museumwales.ac.uk/britishbivalves>
- Ori, G.G., Roveri, M., Vannoni, F., (1986). Plio-Pleistocene sedimentation in the Apenninic foredeep (Central Adriatic Sea, Italy), in: Allen, P.A., Homewood, P. (Eds.), Foreland Basins. IAS Special Publication 8, pp. 183-198.
- Ori, G.G., Serafini, G., Visentin, F., Ricci Lucchi, F., Casnedi, R., Colalongo, M.L., Mosna, S., (1991). The Pliocene end Pleistocene Adriatic foredeep (Marche and Abruzzo, Italy): an integrated approach to surface and subsurface geology, in: Third Conference of the European Association of Petroleum Geology, May 1991, Adriatic Foredeep Field Trip Guide Book, 85, Florence, Italy.
- Özalaybey, S., Zor, E., Ergintav, S., & Tapırdamaz, M. C. (2011). Investigation of 3-D basin structures in the İzmit Bay area (Turkey) by single-station microtremor and gravimetric methods. *Geophysical Journal International*, 186(2), 883–894. <https://doi.org/10.1111/j.1365-246X.2011.05085.x>
- Özalaybey, S., Zor, E., Ergintav, S., & Tapırdamaz, M. C. (2011). Investigation of 3-D basin structures in the İzmit Bay area (Turkey) by single-station microtremor and gravimetric methods: 3-D basin structures of the İzmit Bay area. *Geophysical Journal International*, 186(2), 883–894. <https://doi.org/10.1111/j.1365-246X.2011.05085.x>
- Pace, B. (2006). Layered Seismogenic Source Model and Probabilistic Seismic-Hazard Analyses in Central Italy. *Bulletin of the Seismological Society of America*, 96(1), 107–132. <https://doi.org/10.1785/0120040231>
- Paolucci, E., Albarello, D., D'Amico, S., Lunedei, E., Martelli, L., Mucciarelli, M., & Pileggi, D. (2015). A large scale ambient vibration survey in the area damaged by May–June (2012) seismic sequence in Emilia Romagna, Italy. *Bulletin of Earthquake Engineering*, 13(11), 3187–3206. <https://doi.org/10.1007/s10518-015-9767-5>
- Parlagreco, L., Mascioli, F., Miccadei, E., Antonioli, F., Gianolla, D., Devoti, S., Leoni, G., Silenzi, S., (2011). New data on Holocene relative sea level along the Abruzzo coast (central Adriatic, Italy). *Quat. Int.* 232, 179–186. <https://doi.org/10.1016/j.quaint.2010.07.021>
- Parolai, S., Bormann, P., & Milkereit, C. (2001). Assessment of the natural frequency of the sedimentary cover in the Cologne area (Germany) using noise measurements. *Journal of Earthquake Engineering*, 05(04), 541–564. <https://doi.org/10.1142/S1363246901000558>

- Parolai, S., Picozzi, M., Richwalski, S. M., & Milkereit, C. (2005). Joint inversion of phase velocity dispersion and H/V ratio curves from seismic noise recordings using a genetic algorithm, considering higher modes. *Geophysical Research Letters*, 32(1). <https://doi.org/10.1029/2004GL021115>
- Pasini, G., Colalongo, M., (1996). The Pliocene–Pleistocene boundary-stratotype at Vrica, Italy, in: Couvering, J., (Ed.), *The Pleistocene Boundary and the Beginning of the Quaternary, World and Regional Geology*, Cambridge: Cambridge University Press. pp. 15-45. doi:10.1017/CBO9780511585760.004
- Patacca, E., Scandone, P., (1989). Post-Tortonian mountain building in the Apennines. The role of the passive sinking of a relic lithospheric slab. *Accad. Naz. Dei Lincei, Atti dei Convegni Lincei* 80, 157–176.
- Patacca, E., Scandone, P., (2001). Late thrust propagation and sedimentary response in the thrust-belt—foredeep system of the Southern Apennines (Pliocene-Pleistocene), in: Vai, G.B., Martini, I.P. (Eds.), *Anatomy of an Orogen: The Apennines and Adjacent Mediterranean Basins*. Springer Netherlands, Dordrecht, pp. 401–440. [https://doi.org/10.1007/978-94-015-9829-3\\_23](https://doi.org/10.1007/978-94-015-9829-3_23)
- Payenberg, T. H., Boyd, R., Beaudoin, J., Ruming, K., Davies, S., Roberts, J., & Lang, S. C. (2006). The filling of an incised valley by shelf dunes—An example from Hervey Bay, east coast of Australia.
- Payenberg, T.H.D., Boyd, R., Beaudoin, J., Ruming, K., Davies, S., Roberts, J., Lang, S.C., (2006). The Filling of an Incised Valley by Shelf Dunes—an example from Hervey Bay, East Coast OF Australia, in: Dalrymple, R.W., Leckie, D.A., Tillman, R. (Eds.), *Incised Valleys in Time and Space*. SEPM Special Publication, pp. 87–98. <https://doi.org/10.2110/pec.06.85.0087>
- Pedregosa, F., Varoquaux, G., Gramfort, A., Michel, V., Thirion, B., Grisel, O., Blondel, M., Prettenhofer, P., Weiss, R., Dubourg, V., Vanderplas, J., Passos, A., Cournapeau, D., Brucher, M., Perrot, M., Duchesnay, É., (2011). Scikit-learn: Machine Learning in Python. *Journal of Machine Learning Research* 12, 2825–2830.
- Peeters, J., Busschers, F.S., Stouthamer, E., (2015). Fluvial evolution of the Rhine during the last interglacial-glacial cycle in the southern North Sea basin: A review and look forward. *Quat. Int.* 357, 176–188. <https://doi.org/10.1016/j.quaint.2014.03.024>
- Pellegrini, C., Asioli, A., Bohacs, K.M., Drexler, T.M., Feldman, H.R., Sweet, M.L., Maselli, V., Rovere, M., Gamberi, F., Valle, G.D., Trincardi, F., (2018). The late Pleistocene Po River lowstand wedge in the Adriatic Sea: Controls on architecture variability and sediment partitioning. *Mar. Pet. Geol.* 96, 16–50. <https://doi.org/10.1016/j.marpetgeo.2018.03.002>
- Pellegrini, C., Maselli, V., Cattaneo, A., Piva, A., Ceregato, A., Trincardi, F., (2015). Anatomy of a compound delta from the post-glacial transgressive record in the Adriatic Sea. *Mar. Geol.* 362, 43–59. <https://doi.org/10.1016/j.margeo.2015.01.010>

- Pellegrini, C., Maselli, V., Gamberi, F., Asioli, A., Bohacs, K.M., Drexler, T.M., Trincardi, F., (2017). How to make a 350-m-thick lowstand systems tract in 17,000 years: The Late Pleistocene Po River (Italy) lowstand wedge. *Geology* 45, 327–330. <https://doi.org/10.1130/G38848.1>
- Pellegrini, C., Patruno, S., Helland-Hansen, W., Steel, R.J., Trincardi, F., (2020). Clinofolds and clinothems: Fundamental elements of basin infill. *Basin Res.* 32, 187–205. <https://doi.org/10.1111/bre.12446>
- Pellegrini, C., Tesi, T., Schieber, J., Bohacs, K.M., Rovere, M., Asioli, A., Nogarotto, A., Trincardi, F., (2021). Fate of terrigenous organic carbon in muddy clinothems on continental shelves revealed by stratal geometries: Insight from the Adriatic sedimentary archive. *Glob. Planet. Change* 203, 103539. <https://doi.org/10.1016/j.gloplacha.2021.103539>
- Pérès, J.M., Picard, J., (1964). Nouveau manuel de bionomie benthique. *Recueil des Travaux de la Station marine d'Endoume* 31.47, 1–137.
- Pergalani, F., Pagliaroli, A., Bourdeau, C., Compagnoni, M., Lenti, L., Lualdi, M., Madiari, C., Martino, S., Razzano, R., Varone, C., & Verrubbi, V. (2020). Seismic microzoning map: Approaches, results and applications after the (2016)–2017 Central Italy seismic sequence. *Bulletin of Earthquake Engineering*, 18(12), 5595–5629. <https://doi.org/10.1007/s10518->
- Phillips, J.D., Slattery, M.C., Musselman, Z.A., (2004). Dam-to-delta sediment inputs and storage in the lower trinity river, Texas. *Geomorphology* 62, 17–34. <https://doi.org/10.1016/j.geomorph.2004.02.004>
- Pillans, B., Gibbard, P., (2012). The quaternary period, in: *The Geologic Time Scale 2012*. Elsevier.
- Pilz, M., & Cotton, F. (2019). Does the One-Dimensional Assumption Hold for Site Response Analysis? A Study of Seismic Site Responses and Implication for Ground Motion Assessment Using KiK-Net Strong-Motion Data. *Earthquake Spectra*, 35(2), 883–905. <https://doi.org/10.1193/050718EQS113M>
- Pint, A., Frenzel, P., (2017). Ostracod Fauna Associated with *Cyprideis torosa* - An Overview. *J. Micropalaeontol.*, 36, pp. 113–119.
- Plint, A.G., Nummedal, D., (2000). The falling stage systems tract: recognition and importance in sequence stratigraphic analysis, in: Hunt, D., Gawthorpe, R.L., (Eds.), *Sedimentary Responses to Forced Regressions: Geol. Soc. London Special Publications*, 172, pp. 1-17.
- Poggi, V., Ermert, L., Burjanek, J., Michel, C., & Fäh, D. (2014). Modal analysis of 2-D sedimentary basin from frequency domain decomposition of ambient vibration array recordings. *Geophysical Journal International*, 200(1), 615–626. <https://doi.org/10.1093/gji/ggu420>

- Posamentier, H. W., & Vail, P. R. (1988). Eustatic Controls on Clastic Deposition II—Sequence and Systems Tract Models. In C. K. Wilgus, B. S. Hastings, H. Posamentier, J. V. Wagoner, C. A. Ross, & C. G. St. C. Kendall (Eds.), *Sea-Level Changes: An Integrated Approach* (Vol. 42). SEPM Special Publication. <https://doi.org/10.2110/pec.88.01.0125>
- Posamentier, H. W., Jervey, M. T., & Vail, P. R. (1988). Eustatic Controls on Clastic Deposition I—Conceptual Framework. In C. K. Wilgus, B. S. Hastings, H. Posamentier, J. V. Wagoner, C. A. Ross, & C. G. St. C. Kendall (Eds.), *Sea-Level Changes: An Integrated Approach* (Vol. 42). SEPM Special Publication. <https://doi.org/10.2110/pec.88.01.0109>
- Posamentier, H.W., Jervey, M.T., Vail, P.R., (1988). Eustatic controls on clastic deposition I—conceptual framework, in: Wilgus, C.K., Hastings, B.S., Kendal, C.G.C., Posamentier, H.W., Ross, C.A., Van Wagoner, J.C. (Eds.), *Sea-Level Changes: An Integrated Approach*. SEPM Special Publication, 42, pp. 109–124.
- Posamentier, H.W., Vail, P.R., (1988). Eustatic Controls on Clastic Deposition II—Sequence and Systems Tract Models, in: Wilgus, C.K., Hastings, B.S., Kendall, C.G.St.C., Posamentier, H.W., Ross, C.A., Van Wagoner, J.C. (Eds.), *Sea-Level Changes: An Integrated Approach*. SEPM Special Publication 42, pp. 125–154. <https://doi.org/10.2110/pec.88.01.0125>
- Potter, P.E., (1967). Sand bodies and sedimentary environments: a review. *Am. Ass. Petrol. Geol. Bull.* 51, 337–365.
- Powers, D.M.W., (2020). Evaluation: from precision, recall and F-measure to ROC, informedness, markedness and correlation. <https://doi.org/10.48550/arXiv.2010.16061>
- Prell, W. L., & Kutzbach, J. E. (1992). Sensitivity of the Indian monsoon to forcing parameters and implications for its evolution. *Nature*, 360(6405), 647–652. <https://doi.org/10.1038/360647a0>
- Prins, L.T., Andresen, K.J., (2021). A geotechnical stratigraphy for the shallow subsurface in the Southern Central Graben, North Sea. *Engineering Geology* 286, 106089. <https://doi.org/10.1016/j.enggeo.2021.106089>
- Quarta, G., Fago, P., Calcagnile, L., Cipriano, G., D’Elia, M., Moretti, M., Scardino, G., Valenzano, E., Mastronuzzi, G., (2019). 14C Age offset in the Mar Piccolo Sea basin in Taranto (Southern Italy) estimated on *Cerastoderma glaucum* (Poiret, 1789). *Radiocarbon* 61, 1387–1401. <https://doi.org/10.1017/RDC.2019.38>
- Raheem, S. E. A. (2022). Soil–structure interaction for seismic analysis and design of bridges. In *Innovative Bridge Design Handbook* (pp. 229–263). Elsevier. <https://doi.org/10.1016/B978-0-12-823550-8.00024-X>
- Ramsey, C.B., (1995). Radiocarbon Calibration and Analysis of Stratigraphy: The OxCal Program. *Radiocarbon* 37, 425–430. <https://doi.org/10.1017/S0033822200030903>
- Ramsey, C.B., Lee, S., (2013). Recent and Planned Developments of the Program OxCal. *Radiocarbon* 55, 720–730. <https://doi.org/10.1017/s0033822200057878>

- Rapuc, W., Jacq, K., Develle, A.-L., Sabatier, P., Fanget, B., Perrette, Y., Coquin, D., Debret, M., Wilhelm, B., Arnaud, F., (2020). XRF and hyperspectral analyses as an automatic way to detect flood events in sediment cores. *Sedimentary Geology* 409, 105776. <https://doi.org/10.1016/j.sedgeo.2020.105776>
- Rasmussen, T.L., (2005). Systematic paleontology and ecology of benthic foraminifera from the Plio-Pleistocene Kallithea Bay Section, Rhodes, Greece, in: Rasmussen, T.L., Hastrup, A., Thomsen, E., (Eds.), *Lagoon to Deep-water Foraminifera and Ostracods From the Plio-Pleistocene Kallithea Bay Section, Rhodes, Greece Special Publication 39*. Cushman Foundation, Fredericksburg, Virginia, pp. 53–157.
- Ravaioli, M., Alvisi, F., Vitturi, L.M., (2003). Dolomite as a tracer for sediment transport and deposition on the northwestern Adriatic continental shelf (Adriatic Sea, Italy). *Cont. Shelf Res.* 23, 1359–1377. [https://doi.org/10.1016/S0278-4343\(03\)00121-3](https://doi.org/10.1016/S0278-4343(03)00121-3)
- Redmon, J., Divvala, S., Girshick, R., Farhadi, A., (2016). *You Only Look Once: Unified, Real-Time Object Detection*.
- Reimer, P. J., Bard, E., Bayliss, A., Beck, J. W., Blackwell, P. G., Ramsey, C. B., Buck, C. E., Cheng, H., Edwards, R. L., Friedrich, M., Grootes, P. M., Guilderson, T. P., Haflidason, H., Hajdas, I., Hatté, C., Heaton, T. J., Hoffmann, D. L., Hogg, A. G., Hughen, K. A., ... van der Plicht, J. (2013). *IntCal13 and Marine13 Radiocarbon Age Calibration Curves 0–50,000 Years cal BP*. *Radiocarbon*, 55(4), (1869)–1887. Cambridge Core. [https://doi.org/10.2458/azu\\_js\\_rc.55.16947](https://doi.org/10.2458/azu_js_rc.55.16947)
- Reimer, P.J., Austin, W.E.N., Bard, E., Bayliss, A., Blackwell, P.G., Bronk Ramsey, C., Butzin, M., Cheng, H., Edwards, R.L., Friedrich, M., Grootes, P.M., Guilderson, T.P., Hajdas, I., Heaton, T.J., Hogg, A.G., Hughen, K.A., Kromer, B., Manning, S.W., Muscheler, R., Palmer, J.G., Pearson, C., Van Der Plicht, J., Reimer, R.W., Richards, D.A., Scott, E.M., Southon, J.R., Turney, C.S.M., Wacker, L., Adolphi, F., Büntgen, U., Capano, M., Fahrni, S.M., Fogtmann-Schulz, A., Friedrich, R., Köhler, P., Kudsk, S., Miyake, F., Olsen, J., Reinig, F., Sakamoto, M., Sookdeo, A., Talamo, S., (2020). *The IntCal20 Northern Hemisphere Radiocarbon Age Calibration Curve (0-55 cal kBP)*. *Radiocarbon* 62, 725–757. <https://doi.org/10.1017/RDC.2020.41>
- Ribeiro, M.T., Singh, S., Guestrin, C., (2016). “Why Should I Trust You?”: Explaining the Predictions of Any Classifier.
- Ricchetti, G., Ciaranfi, N., Luperto Sinni, E., Mongelli, F., Pieri, P., (1992). *Geodinamica ed evoluzione sedimentaria e tettonica dell'avampese apulo*. *Mem. Soc. Geol. Ital.* 41, 57–82.
- Ridente, D., Trincardi, F., Piva, A., Asioli, A., Cattaneo, A., (2008). Sedimentary response to climate and sea level changes during the past ~400 ka from borehole PRAD1-2 (Adriatic margin). *Geochemistry, Geophys. Geosystems* 9. <https://doi.org/10.1029/2007GC001783>

- Rittenour, T.M., Blum, M.D., Goble, R.J., (2007). Fluvial evolution of the lower Mississippi River valley during the last 100 k.y. glacial cycle: Response to glaciation and sea-level change. *Bull. Geol. Soc. Am.* 119, 586–608. <https://doi.org/10.1130/B25934.1>
- Rittenour, T.M., Goble, R.J., Blum, M.D., (2005). Development of an OSL chronology for Late Pleistocene channel belts in the lower Mississippi valley, USA. *Quat. Sci. Rev.* 24, 2539–2554.
- Rodriguez, A.B., Anderson, J.B., Bradford, J., (1998). Holocene tidal deltas of the Trinity incised valley: analogs for exploration and production.
- Rombach, R., Blattmann, A., Lorenz, D., Esser, P., Ommer, B., (2022). High-Resolution Image Synthesis with Latent Diffusion Models.
- Ronchi, L., Fontana, A., Cohen, K. M., & Stouthamer, E. (2021). Late Quaternary landscape evolution of the buried incised valley of Concordia Sagittaria (Tagliamento River, NE Italy): A reconstruction of incision and transgression. *Geomorphology*, 373, 107509. <https://doi.org/10.1016/j.geomorph.2020.107509>
- Ronchi, L., Fontana, A., Correggiari, A., Asioli, A., (2018). Late Quaternary incised and infilled landforms in the shelf of the northern Adriatic Sea (Italy). *Mar. Geol.* 405, 47–67. <https://doi.org/10.1016/j.margeo.2018.08.004>
- Ronneberger, O., Fischer, P., Brox, T., (2015). U-Net: Convolutional Networks for Biomedical Image Segmentation, in: Navab, N., Hornegger, J., Wells, W.M., Frangi, A.F. (Eds.), *Medical Image Computing and Computer-Assisted Intervention – MICCAI 2015, Lecture Notes in Computer Science*. Springer International Publishing, Cham, pp. 234–241. [https://doi.org/10.1007/978-3-319-24574-4\\_28](https://doi.org/10.1007/978-3-319-24574-4_28)
- Rossi, V., & Vaiani, S. C. (2008). Benthic foraminiferal evidence of sediment supply changes and fluvial drainage reorganization in Holocene deposits of the Po Delta, Italy. *Marine Micropaleontology*, 69(2), 106–118. <https://doi.org/10.1016/j.marmicro.2008.07.001>
- Rossi, V., Amorosi, A., Sarti, G., & Mariotti, S. (2017). Late Quaternary multiple incised valley systems: An unusually well-preserved stratigraphic record of two interglacial valley-fill successions from the Arno Plain (northern Tuscany, Italy). *Sedimentology*, 64(7), (1901)–1928. <https://doi.org/10.1111/sed.12379>
- Rossi, V., Amorosi, A., Sarti, G., & Romagnoli, R. (2012). New stratigraphic evidence for the mid-late Holocene fluvial evolution of the Arno coastal plain (Tuscany, Italy). *Géomorphologie: Relief, Processus, Environnement*, 18(2), 201–214.
- Rossi, V., Amorosi, A., Sarti, G., Potenza, M., (2011). Influence of inherited topography on the Holocene sedimentary evolution of coastal systems: an example from Arno coastal plain (Tuscany, Italy). *Geomorphology* 135, 117–128.

- Rossi, V., Barbieri, G., Vaiani, S.C., Amorosi, A., (2021). Benthic foraminifers from Holocene subaqueous deltas of the Western Mediterranean: Stratigraphic implications and palaeoenvironmental significance of the biofacies. *Mar. Geol.* 442, 106632. <https://doi.org/10.1016/j.margeo.2021.106632>
- Rossi, V., Barbieri, G., Vaiani, S.C., Cacciari, M., Bruno, L., Campo, B., Marchesini, M., Marvelli, S., Amorosi, A., (2021). Millennial-scale shifts in microtidal ecosystems during the Holocene: dynamics and drivers of change from the Po Plain coastal record (NE Italy). *J. Quat. Sci.* 36, 961–979. <https://doi.org/10.1002/jqs.3322>
- Rovere, M., Pellegrini, C., Chiggiato, J., Campiani, E., Trincardi, F., (2019). Impact of dense bottom water on a continental shelf: An example from the SW Adriatic margin. *Mar. Geol.* 408, 123–143. <https://doi.org/10.1016/j.margeo.2018.12.002>
- Royden, L., Patacca, E., Scandone, P., (1987). Segmentation and configuration of subducted lithosphere in Italy: An important control on thrust-belt and foredeep-basin evolution. *Geology* 15, 714–717. [https://doi.org/10.1130/0091-7613\(1987\)15<714:SACOSL>2.0.CO;2](https://doi.org/10.1130/0091-7613(1987)15<714:SACOSL>2.0.CO;2)
- Ruberti, D., Sacchi, M., Pepe, F., Vigliotti, M., (2018). LGM incised valley in a volcanic setting. The northern Campania Plain (Southern Italy). *Alp. Mediterr. Quat.* 31, 35–38.
- Russakovsky, O., Deng, J., Su, H., Krause, J., Satheesh, S., Ma, S., Huang, Z., Karpathy, A., Khosla, A., Bernstein, M., Berg, A.C., Fei-Fei, L., (2015). ImageNet Large Scale Visual Recognition Challenge. *Int J Comput Vis* 115, 211–252. <https://doi.org/10.1007/s11263-015-0816-y>
- Saganeiti, L., Amato, F., Nolè, G., Vona, M., & Murgante, B. (2020). Early estimation of ground displacements and building damage after seismic events using SAR and LiDAR data: The case of the Amatrice earthquake in central Italy, on 24th August (2016). *International Journal of Disaster Risk Reduction*, 51, 101924. <https://doi.org/10.1016/j.ijdr.2020.101924>
- Salel, T., Bruneton, H., & Lefèvre, D. (2016). Ostracods and environmental variability in lagoons and deltas along the north-western Mediterranean coast (Gulf of Lions, France and Ebro delta, Spain). *Revue de Micropaléontologie*, 59(4), 425–444. <https://doi.org/10.1016/j.revmic.2016.09.001>
- Salem, A. M., Ketzer, J. M., Morad, S., Rizk, R. R., & Al-Aasm, I. S. (2005). Diagenesis and Reservoir-Quality Evolution of Incised-Valley Sandstones: Evidence from the Abu Madi Gas Reservoirs (Upper Miocene), the Nile Delta Basin, Egypt. *Journal of Sedimentary Research*, 75(4), 572–584. <https://doi.org/10.2110/jsr.2005.047>
- Salem, A.M., Ketzer, J.M., Morad, S., Rizk, R.R., Al-Aasm, I.S., (2005). Diagenesis and reservoir-quality evolution of incised-valley sandstone: Evidence from the Abu Madi gas reservoirs (upper Miocene), the Nile Delta Basin, Egypt. *J. Sediment. Res.* 75, 572–584. <https://doi.org/10.2110/jsr.2005.047>

- Sangree, J.B., Widmier, J.M., (1977). Seismic stratigraphy and global changes of sea level, part 9: Seismic interpretation of clastic depositional facies. Section 2. Application of seismic reflection configuration to stratigraphic interpretation, in: Payton, C.E. (Ed.), *Seismic Stratigraphy — Applications to Hydrocarbon Exploration*. Am. Ass. Petrol. Geol. Memoir 26, pp. 165–184. <https://doi.org/10.1306/M26490C11>
- Sarti, G., Sammartino, I., Amorosi, A., (2020). Geochemical anomalies of potentially hazardous elements reflect catchment geology: An example from the Tyrrhenian coast of Italy. *Sci. Total Environ.* 714, 136870. <https://doi.org/10.1016/j.scitotenv.2020.136870>
- Scarponi, D., & Kowalewski, M. (2004). Stratigraphic paleoecology: Bathymetric signatures and sequence overprint of mollusk associations from upper Quaternary sequences of the Po Plain, Italy. *Geology*, 32(11), 989–992. <https://doi.org/10.1130/G20808.1>
- Scarponi, D., Angeletti, L., (2008). Integration of palaeontological patterns in the sequence stratigraphy paradigm: a case study from Holocene deposits of the Po Plain (Italy). *GeoActa* 7, 1–13.
- Scarponi, D., Azzarone, M., Kowalewski, M., Huntley, J.W., (2017). Surges in trematode prevalence linked to centennial-scale flooding events in the Adriatic. *Sci. Rep.* 7, 6–11. <https://doi.org/10.1038/s41598-017-05979-6>
- Scarponi, D., Azzarone, M., Kusnerik, K., Amorosi, A., Bohacs, K.M., Drexler, T.M., Kowalewski, M., (2017). Systematic vertical and lateral changes in quality and time resolution of the macrofossil record: Insights from Holocene transgressive deposits, Po coastal plain, Italy. *Mar. Petrol. Geol.* 87, 128–136. <https://doi.org/10.1016/j.marpetgeo.2017.03.031>
- Scarponi, D., Huntley, J.W., Capraro, L., Raffi, S., (2014). Stratigraphic paleoecology of the Valle di Manche section (Crotona Basin, Italy): A candidate GSSP of the Middle Pleistocene. *Palaeogeogr. Palaeoclimatol. Palaeoecol.* 402, 30–43. <https://doi.org/10.1016/j.palaeo.2014.02.032>
- Scarponi, D., Kaufman, D., Amorosi, A., Kowalewski, M., (2013). Sequence stratigraphy and the resolution of the fossil record. *Geology* 41, 239–242. <https://doi.org/10.1130/G33849.1>
- Scarponi, D., Nawrot, R., Azzarone, M., Pellegrini, C., Gamberi, F., Trincardi, F., & Kowalewski, M. (2022). Resilient biotic response to long-term climate change in the Adriatic Sea. *Global Change Biology*, 28(13), (4041)–4053. <https://doi.org/10.1111/gcb.16168>
- Scheib, A., Morris, P., Murdie, R., & Delle Piane, C. (2016). A passive seismic approach to estimating the thickness of sedimentary cover on the Nullarbor Plain, Western Australia. *Australian Journal of Earth Sciences*, 63(5), 583–598. <https://doi.org/10.1080/08120099.2016.1233455>

- Seifert, D., Sonnenborg, T.O., Scharling, P., Hinsby, K., (2008). Use of alternative conceptual models to assess the impact of a buried valley on groundwater vulnerability. *Hydrogeol. J.* 16, 659–674.
- Selvaraju, R.R., Cogswell, M., Das, A., Vedantam, R., Parikh, D., Batra, D., (2020). Grad-CAM: Visual Explanations from Deep Networks via Gradient-based Localization. *Int J Comput Vis* 128, 336–359. <https://doi.org/10.1007/s11263-019-01228-7>
- Semblat, J. F., Kham, M., Parara, E., Bard, P. Y., Pitilakis, K., Makra, K., & Raptakis, D. (2005). Seismic wave amplification: Basin geometry vs soil layering. *Soil Dynamics and Earthquake Engineering*, 25(7–10), 529–538. <https://doi.org/10.1016/j.soildyn.2004.11.003>
- Sgarrella, F., Moncharmont Zei, M., (1993). Benthic foraminifera of the Gulf of Naples (Italy): systematics and autoecology. *Boll. Soc. Paleontol. Ital.* 32, 145–264.
- Sgattoni, G., & Castellaro, S. (2020). Detecting 1-D and 2-D ground resonances with a single-station approach. *Geophysical Journal International*, 223(1), 471–487. <https://doi.org/10.1093/gji/ggaa325>
- Sgattoni, G., & Castellaro, S. (2021). Combining single-station microtremor and gravity surveys for deep stratigraphic mapping. *Geophysics*, 86(5), G77–G88. <https://doi.org/10.1190/geo2020-0757.1>
- Shackleton, N. J., & Opdyke, N. D. (1973). Oxygen Isotope and Palaeomagnetic Stratigraphy of Equatorial Pacific Core V28-238: Oxygen Isotope Temperatures and Ice Volumes on a 105 Year and 106 Year Scale. *Quaternary Research*, 3(1), 39–55. Cambridge Core. [https://doi.org/10.1016/0033-5894\(73\)90052-5](https://doi.org/10.1016/0033-5894(73)90052-5)
- Shaikh, S.A., (2011). Measures Derived from a 2 x 2 Table for an Accuracy of a Diagnostic Test. *J Biomet Biostat* 02. <https://doi.org/10.4172/2155-6180.1000128>
- Shanley, K. W., & McCabe, P. J. (1992). Alluvial architecture in a sequence stratigraphic framework: A case history from the Upper Cretaceous of southern Utah, USA. *The Geological Modelling of Hydrocarbon Reservoirs and Outcrop Analogues*, 21–55.
- Shanley, K.W., McCabe, P.J., (1991). Predicting facies architecture through sequence stratigraphy—An example from the Kaiparowits Plateau, Utah. *Geology* 19, 742–745. [https://doi.org/10.1130/0091-7613\(1991\)019<0742:PFATSS>2.3.CO;2](https://doi.org/10.1130/0091-7613(1991)019<0742:PFATSS>2.3.CO;2)
- Shanley, K.W., McCabe, P.J., (1991). Predicting facies architecture through sequence stratigraphy - an example from the Kaiparowits Plateau, Utah. *Geology* 19, 742–745. [https://doi.org/10.1130/0091-7613\(1991\)019<0742:PFATSS>2.3.CO;2](https://doi.org/10.1130/0091-7613(1991)019<0742:PFATSS>2.3.CO;2)
- Shanley, K.W., McCabe, P.J., (1994). Perspectives on the sequence stratigraphy of continental strata: report of a working group at the 1991 NUNA Conference on High Resolution Sequence Stratigraphy. *AAPG Bull.* 78, 544-568. <https://doi.org/10.1306/bdff9258-1718-11d7-8645000102c1865d>

- Shanley, K.W., McCabe, P.J., (1994). Perspectives on the Sequence Stratigraphy of Continental Strata. *Am. Ass. Petrol. Geol. Bull.* 78, 544–568. <https://doi.org/10.1306/BDF9258-1718-11D7-8645000102C1865D>
- Shanley, K.W., McCabe, P.J., Flint, S.S., Bryant, I.D., (1993). Alluvial architecture in a sequence stratigraphic framework: a case history from the Upper Cretaceous of southern Utah, USA, in: *The Geological Modelling of Hydrocarbon Reservoirs and Outcrop Analogues*. IAS Special Publication 15, pp. 21–55.
- Shaver, R.B., Pusc, S.W., (1992). Hydraulic barriers in Pleistocene buried-valley aquifers. *Groundwater* 30, 21–28.
- Simms, A. R., Aryal, N., Miller, L., & Yokoyama, Y. (2010). The incised valley of Baffin Bay, Texas: A tale of two climates. *Sedimentology*, 57(2), 642–669. <https://doi.org/10.1111/j.1365-3091.2009.01111.x>
- Sloss, C.R., Jones, B.J., Murray-Wallace, C.V., McClennen, C.E., (2005). Holocene Sea Level Fluctuations and the Sedimentary Evolution of a Barrier Estuary: Lake Illawarra, New South Wales, Australia. *J. Coastal Res.* 215, 943–959.
- Smith, D.E., Harrison, S., Firth, C.R., Jordan, J.T., (2011). The early Holocene sea level rise. *Quat. Sci. Rev.* 30, 1846–1860. <https://doi.org/10.1016/j.quascirev.2011.04.019>
- Sokolova, M., Lapalme, G., (2009). A systematic analysis of performance measures for classification tasks. *Information Processing & Management* 45, 427–437. <https://doi.org/10.1016/j.ipm.2009.03.002>
- Sømme, T.O., Piper, D.J.W., Deptuck, M.E., Helland-Hansen, W., (2011). Linking onshore-offshore sediment dispersal in the golo source-to-sink system (Corsica, France) during the late quaternary. *J. Sediment. Res.* 81, 118–137. <https://doi.org/10.2110/jsr.2011.11>
- Song, B., Yi, S., Yu, S.-Y., Nahm, W.-H., Lee, J.-Y., Lim, J., Kim, J.-C., Yang, Z., Han, M., Jo, K., (2018). Holocene relative sea-level changes inferred from multiple proxies on the west coast of South Korea. *Palaeogeogr. Palaeoclimatol. Palaeoecol.* 496, 268–281.
- Soupios, P. M., Georgakopoulos, P., Papadopoulos, N., Saltas, V., Andreadakis, A., Vallianatos, F., Sarris, A., & Makris, J. P. (2007). Use of engineering geophysics to investigate a site for a building foundation. *Journal of Geophysics and Engineering*, 4(1), 94–103. <https://doi.org/10.1088/1742-2132/4/1/011>
- Spagnoli, F., Bartholini, G., Dinelli, E., Giordano, P., (2008). Geochemistry and particle size of surface sediments of Gulf of Manfredonia (Southern Adriatic sea). *Estuar. Coast. Shelf Sci.* 80, 21–30. <https://doi.org/10.1016/j.ecss.2008.07.008>
- Spagnoli, F., De Marco, R., Dinelli, E., Frapiccini, E., Frontalini, F., Giordano, P., (2021). Sources and metal pollution of sediments from a coastal area of the Central Western Adriatic Sea (southern Marche Region, Italy). *Appl. Sci.* 11. <https://doi.org/10.3390/app11031118>

- Spagnoli, F., Dinelli, E., Giordano, P., Marcaccio, M., Zaffagnini, F., Frascari, F., (2014). Sedimentological, biogeochemical and mineralogical facies of Northern and Central Western Adriatic Sea. *J. Mar. Syst.* 139, 183–203. <https://doi.org/10.1016/j.jmarsys.2014.05.021>
- Stacec LSR2D. (2013). [Computer software]. available at [http://www.stacec.com/lsr-2d\\_pp92.aspx](http://www.stacec.com/lsr-2d_pp92.aspx)
- Storms, J.E.A., Weltje, G.J., Terra, G.J., Cattaneo, A., Trincardi, F., (2008). Coastal dynamics under conditions of rapid sea-level rise: Late Pleistocene to Early Holocene evolution of barrier–lagoon systems on the northern Adriatic shelf (Italy). *Quat. Sci. Rev.* 27, 1107–1123.
- Strong, N., & Paola, C. (2008). Valleys That Never Were: Time Surfaces Versus Stratigraphic Surfaces. *Journal of Sedimentary Research*, 78(8), 579–593. <https://doi.org/10.2110/jsr.2008.059>
- Stucchi, M., Meletti, C., Montaldo, V., Crowley, H., Calvi, G. M., & Boschi, E. (2011). Seismic Hazard Assessment (2003-2009) for the Italian Building Code. *Bulletin of the Seismological Society of America*, 101(4), (1885)–1911. <https://doi.org/10.1785/0120100130>
- Susmaga, R., (2004). Confusion Matrix Visualization, in: Kłopotek, M.A., Wierchoń, S.T., Trojanowski, K. (Eds.), *Intelligent Information Processing and Web Mining, Advances in Soft Computing*. Springer, Berlin, Heidelberg, pp. 107–116. [https://doi.org/10.1007/978-3-540-39985-8\\_12](https://doi.org/10.1007/978-3-540-39985-8_12)
- Sweet, M.L., Gaillot, G.T., Jouet, G., Rittenour, T.M., Toucanne, S., Marsset, T., Blum, M.D., (2020). Sediment routing from shelf to basin floor in the Quaternary Golo System of Eastern Corsica, France, western Mediterranean Sea. *Bull. Geol. Soc. Am.* 132, 1217–1234. <https://doi.org/10.1130/B35181.1>
- Syvitski, J.P.M., Kettner, A.J., (2007). On the flux of water and sediment into the Northern Adriatic Sea. *Cont. Shelf Res.* 27, 296–308.
- Ta, T.K.O., Nguyen, V.L., Saito, Y., Gugliotta, M., Tamura, T., Nguyen, T.M.L., Truong, M.H., Bui, T.L., (2021). Latest Pleistocene to Holocene stratigraphic record and evolution of the Paleo-Mekong incised valley, Vietnam. *Mar. Geol.* 433, 106406. <https://doi.org/10.1016/j.margeo.2020.106406>
- Tan, M., & Le, Q. V. (2020). EfficientNet: Rethinking Model Scaling for Convolutional Neural Networks (arXiv:(1905).11946; Issue arXiv:1905.11946). arXiv. <https://doi.org/10.48550/arXiv.1905.11946>
- Tan, M., Le, Q.V., (2020). EfficientNet: Rethinking Model Scaling for Convolutional Neural Networks. <https://doi.org/10.48550/arXiv.1905.11946>
- Tanabe, S., (2020). Stepwise accelerations in the rate of sea-level rise in the area north of Tokyo Bay during the Early Holocene. *Quat. Sci. Rev.* 248, 106575. <https://doi.org/10.1016/j.quascirev.2020.106575>

- Tanabe, S., Ishihara, Y., Nakanishi, T., Stafleu, J., & Busschers, F. S. (2021). Distribution of Holocene Marine Mud and Its Relation to Damage from the (1923) Earthquake Disaster in the Tokyo Metropolitan Area, Japan. *Geosciences*, 11(7), 272. <https://doi.org/10.3390/geosciences11070272>
- Tanabe, S., Nakanishi, T., Ishihara, Y., & Nakashima, R. (2015). Millennial-scale stratigraphy of a tide-dominated incised valley during the last 14 kyr: Spatial and quantitative reconstruction in the Tokyo Lowland, central Japan. *Sedimentology*, 62(7), (1837)–1872. <https://doi.org/10.1111/sed.12204>
- Tanabe, S., Nakashima, R., Ishihara, Y., (2022). Transition from a transgressive to a regressive river-mouth sediment body in Tokyo Bay during the early Holocene: Sedimentary facies, geometry, and stacking pattern. *Sediment. Geol.* 428, 106059. <https://doi.org/10.1016/j.sedgeo.2021.106059>
- Tanabe, S., Saito, Y., Vu, Q.L., Hanebuth, T.J.J., Ngo, Q.L., Kitamura, A., (2006). Holocene evolution of the Song Hong (Red River) delta system, northern Vietnam. *Sediment. Geol.* 187, 29-61.
- Tao, Y., & Rathje, E. (2020). Taxonomy for evaluating the site-specific applicability of one-dimensional ground response analysis. *Soil Dynamics and Earthquake Engineering*, 128, 105865. <https://doi.org/10.1016/j.soildyn.2019.105865>
- Teatini, P., Ferronato, M., Gambolati, G., Gonella, M., (2006). Groundwater pumping and land subsidence in the Emilia-Romagna coastland, Italy: Modeling the past occurrence and the future trend: MODELING LAND SUBSIDENCE. *Water Resour. Res.* 42. <https://doi.org/10.1029/2005WR004242>
- Tesi, T., Asioli, A., Minisini, D., Maselli, V., Valle, G.D., Gamberi, F., Langone, L., Cattaneo, A., Montagna, P., Trincardi, F., (2017). Large-scale response of the Eastern Mediterranean thermohaline circulation to African monsoon intensification during sapropel S1 formation. *Quat. Sci. Rev.* 159, 139–154. <https://doi.org/10.1016/j.quascirev.2017.01.020>
- Tharwat, A., (2020). Classification assessment methods. *Applied Computing and Informatics* 17, 168–192. <https://doi.org/10.1016/j.aci.2018.08.003>
- Thomas, M. A., & Anderson, J. B. (1994). Sea-Level Controls on the Facies Architecture of the Trinity/Sabine Incised-Valley System, Texas Continental Shelf. In R. W. Dalrymple, R. Boyd, & B. A. Zaitlin, *Incised-Valley Systems: Origin and Sedimentary Sequences*. SEPM Society for Sedimentary Geology. <https://doi.org/10.2110/pec.94.12.0063>
- Thomas, M.A., Anderson, J.B., (1994). Sea-level controls on the facies architecture of the Trinity/Sabine incised-valley system, Texas continental shelf, in: Dalrymple, R.W., Boyd, R., Zaitlin, B.A. (Eds.), *Incised-Valley Systems: Origin and Sedimentary Sequences*, SEPM Special Publication 51, 63–82. <https://doi.org/10.2110/pec.94.12.0063>

- Thompson, E. M., Baise, L. G., Kayen, R. E., & Guzina, B. B. (2009). Impediments to Predicting Site Response: Seismic Property Estimation and Modeling Simplifications. *Bulletin of the Seismological Society of America*, 99(5), (2927)–2949. <https://doi.org/10.1785/0120080224>
- Thompson, E. M., Baise, L. G., Tanaka, Y., & Kayen, R. E. (2012). A taxonomy of site response complexity. *Soil Dynamics and Earthquake Engineering*, 41, 32–43. <https://doi.org/10.1016/j.soildyn.2012.04.005>
- Tian, S.Y., Yasuhara, M., Hong, Y., Huang, H.-H.M., Iwatani, H., Chiu, W.-T.R., Mamo, B., Okahashi, H., Rasmussen, T.L., (2020). Deglacial–Holocene Svalbard paleoceanography and evidence of meltwater pulse 1B. *Quat. Sci. Rev.* 233, 106237.
- Tomašových, A., Gallmetzer, I., Haselmair, A., Kaufman, D.S., Mavrič, B., Zuschin, M., (2019). A decline in molluscan carbonate production driven by the loss of vegetated habitats encoded in the Holocene sedimentary record of the Gulf of Trieste. *Sedimentology* 66, 781–807. <https://doi.org/10.1111/sed.12516>
- Trincardi, F., Amorosi, A., Bosman, A., Correggiari, A., Madricardo, F. & Pellegrini, C., (2020). Ephemeral rollover points and clinothem evolution in the modern Po Delta based on repeated bathymetric surveys. *Basin Res.* 32, 402–418.
- Trincardi, F., Cattaneo, A., Asioli, A., Correggiari, A., Langone, L., (1996). Stratigraphy of the late-Quaternary deposits in the central Adriatic basin and the record of short-term climatic events. *Mem. Ist. Ital. di Idrobiol.* 55, 39–70.
- Trincardi, F., Correggiari, A., Ridente, D., Verdicchio, G., Cattaneo, A., Minisini, D., Remia, A., Taviani, M., Asioli, A., & Piva, A. (2011). *Carta Geologica dei Mari Italiani. Foglio NK33-8/9 Bari.*
- Trincardi, F., Correggiari, A., Roveri, M., (1994). Late Quaternary transgressive erosion and deposition in a modern epicontinental shelf: The Adriatic semienclosed basin. *Geo-Marine Lett.* 14, 41–51. <https://doi.org/10.1007/BF01204470>
- Tropeano, M., Cilumbriello, A., Grippa, A., Sabato, L., Bianca, M., Gallicchio, S., Gallipoli, M. R., & Mucciarelli, M. (2011). Stratigraphy of the subsurface of the Metaponto Plain vs a geophysical 3D view of the late Pleistocene incised-valleys (Basilicata, Southern Italy). *Rend. Online Soc. Geol. Ital*, 17, 187–193. <https://doi.org/10.3301/ROL.2011.54>
- Tropeano, M., Cilumbriello, A., Sabato, L., Gallicchio, S., Grippa, A., Longhitano, S. G., Bianca, M., Gallipoli, M. R., Mucciarelli, M., & Spilotro, G. (2013). Surface and subsurface of the Metaponto Coastal Plain (Gulf of Taranto—Southern Italy): Present-day- vs LGM-landscape. *Continental Shelf Drowned Landscapes (INQUA-CMP and IGCP-526)*, 203, 115–131. <https://doi.org/10.1016/j.geomorph.2013.07.017>
- Truong, M.H., Nguyen, V.L., Ta, T.K.O., Takemura, J., (2011). Changes in late Pleistocene–Holocene sedimentary facies of the Mekong River Delta and the influence of sedimentary environment on geotechnical engineering properties. *Eng. Geol.* 122, 146–159.

- Tün, M., Pekkan, E., Özel, O., & Guneş, Y. (2016). An investigation into the bedrock depth in the Eskisehir Quaternary Basin (Turkey) using the microtremor method. *Geophysical Journal International*, 207(1), 589–607. <https://doi.org/10.1093/gji/ggw294>
- Urbano, T., Piacentini, T., & Buccolini, M. (2017). Morphotectonics of the Pescara River basin (Central Italy). *Journal of Maps*, 13(2), 511–520. <https://doi.org/10.1080/17445647.2017.1338204>
- Vacchi, M., Marriner, N., Morhange, C., Spada, G., Fontana, A., Rovere, A., (2016). Earth-Science Reviews Multiproxy assessment of Holocene relative sea-level changes in the western Mediterranean: Sea-level variability and improvements in the definition of the isostatic signal. *Earth Sci. Rev.* 155, 172–197. <https://doi.org/10.1016/j.earscirev.2016.02.002>
- Van Asselen, S., Stouthamer, E., Van Asch, Th.W.J., (2009). Effects of peat compaction on delta evolution: A review on processes, responses, measuring and modeling. *Earth-Science Reviews* 92, 35–51. <https://doi.org/10.1016/j.earscirev.2008.11.001>
- Van Wagoner, J.C., (1995). Sequence stratigraphy and marine to nonmarine facies architecture of foreland basin strata, Book Cliffs, Utah, U.S.A, in: Van Wagoner, J.C., Bertram, G.T., (Eds.), *Sequence Stratigraphy of Foreland Basin Deposits: AAPG Memoir*, 64, pp. 137-223.
- Van Wagoner, J.C., Mitchum, R.M., Campion, K.M., Rahmanian, V.D., (1990). Siliciclastic sequence stratigraphy in well logs, cores, and outcrops: Concepts for high-resolution correlation of time and facies. *Am. Ass. Petrol. Geol. Methods Explor.* 7, 3–55.
- Van Wagoner, J.C., Posamentier, H.W., Mitchum, R.M., Vail, P.R., Sarg, J.F., Loutit, T.S., Hardenbol, J., (1988). An Overview of the Fundamentals of Sequence Stratigraphy and Key Definitions, in: Wilgus, C.K., Hastings, B.S., Kendall, C.G.C., H.W., P., Ross, C.A., Van Wagoner, J.C. (Eds.), *Sea-Level Changes: An Integrated Approach*. SEPM Special Publication, 42, pp. 39–45. <https://doi.org/10.2110/pec.88.01.0039>
- Verma, M., Singh, R. J., & Bansal, B. K. (2014). Soft sediments and damage pattern: A few case studies from large Indian earthquakes vis-a-vis seismic risk evaluation. *Natural Hazards*, 74(3), (1829)–1851. <https://doi.org/10.1007/s11069-014-1283-4>
- Vinogradova, K., Dibrov, A., Myers, G., (2020). Towards Interpretable Semantic Segmentation via Gradient-Weighted Class Activation Mapping (Student Abstract). *AAAI* 34, 13943–13944. <https://doi.org/10.1609/aaai.v34i10.7244>
- von Eynatten, H., Barceló-Vidal, C., Pawlowsky-Glahn, V., (2003). Composition and discrimination of sandstones: A statistical evaluation of different analytical methods. *J. Sediment. Res.* 73, 47–57. <https://doi.org/10.1306/070102730047>

- Walker, R.G., (1995). An Incised Valley in the Cardium Formation at Ricinus, Alberta: Reinterpretation as an Estuary Fill., in: Plint, A.G. (Ed.), *Sedimentary Facies Analysis*. Wiley Online Library, pp. 47–74. <https://doi.org/https://doi.org/10.1002/9781444304091.ch3>
- Wang, R., Colombera, L., & Mountney, N. P. (2020). Quantitative analysis of the stratigraphic architecture of incised-valley fills: A global comparison of Quaternary systems. *Earth-Science Reviews*, 200, 102988. <https://doi.org/10.1016/j.earscirev.2019.102988>
- Wang, R., Colombera, L., Mountney, N.P., (2019). Geological controls on the geometry of incised-valley fills: Insights from a global dataset of late-Quaternary examples. *Sedimentology* 2134–2168. <https://doi.org/10.1111/sed.12596>
- Wang, Z., Wang, E., Zhu, Y., (2020). Image segmentation evaluation: a survey of methods. *Artif Intell Rev* 53, 5637–5674. <https://doi.org/10.1007/s10462-020-09830-9>
- Weltje, G.J., Brommer, M.B., (2011). Sediment-budget modelling of multi-sourced basin fills: application to recent deposits of the western Adriatic mud wedge (Italy). *Basin Res.* 23, 291–308.
- Wilgus, C. K., Hastings, B. S., Posamentier, H., Van Wagoner, J., Ross, C. A., & Kendall, C. G. St. C. (Eds.). (1988). *Sea-Level Changes: An Integrated Approach*. SEPM (Society for Sedimentary Geology). <https://doi.org/10.2110/pec.88.42>
- Wittmer, J. M., Dexter, T. A., Scarponi, D., Amorosi, A., & Kowalewski, M. (2014). Quantitative Bathymetric Models for Late Quaternary Transgressive-Regressive Cycles of the Po Plain, Italy. *The Journal of Geology*, 122(6), 649–670. <https://doi.org/10.1086/677901>
- Wood, D.A., (2021). Enhancing lithofacies machine learning predictions with gamma-ray attributes for boreholes with limited diversity of recorded well logs. *Artificial Intelligence in Geosciences* 2, 148–164. <https://doi.org/10.1016/j.aiig.2022.02.007>
- Wright, V. P., & Marriott, S. B. (1993). The sequence stratigraphy of fluvial depositional systems: The role of floodplain sediment storage. *Sedimentary Geology*, 86(3–4), 203–210.
- Wrona, T., Pan, I., Gawthorpe, R.L., Fossen, H., (2018). Seismic facies analysis using machine learning. *GEOPHYSICS* 83, O83–O95. <https://doi.org/10.1190/geo2017-0595.1>
- Wu, C., Ye, G., Zhang, L., Bishop, D., Wang, J., (2015). Depositional environment and geotechnical properties of Shanghai clay: a comparison with Ariake and Bangkok clays. *Bull. Eng. Geol. Environ.* 74, 717–732.
- Xiong, Y., Zuo, R., Carranza, E.J.M., (2018). Mapping mineral prospectivity through big data analytics and a deep learning algorithm. *Ore Geology Reviews* 102, 811–817. <https://doi.org/10.1016/j.oregeorev.2018.10.006>

- Yanbin, G., Tongyu, W., (2016). Discussion on the engineering geological stratification of the soft soil deposited in deep-incised valley in Qiantang River of Hangzhou Bay. *J. Eng. Geol.* 24, 933–939. <https://doi.org/10.13544/j.cnki.jeg.2016.s1.135>
- Yu, S.-Y., Berglund, B.E., Sandgren, P., Lambeck, K., (2007). Evidence for a rapid sea-level rise 7600 yr ago. *Geology* 35, 891–894.
- Zaitlin, B. A., Dalrymple, R. W., & Boyd, R. (1994). The Stratigraphic Organization of Incised-Valley Systems Associated with Relative Sea-Level Change. In R. W. Dalrymple, R. Boyd, & B. A. Zaitlin (Eds.), *Incised-Valley Systems: Origin and Sedimentary Sequences* (Vol. 51, p. 0). SEPM Society for Sedimentary Geology. <https://doi.org/10.2110/pec.94.12.0045>
- Zaitlin, B.A., Dalrymple, R.W., Boyd, R., (1994). The Stratigraphic Organization of Incised-Valley Systems Associated with Relative Sea-Level Change, in: Dalrymple, R.W., Boyd, R., Zaitlin, B.A. (Eds.), *Incised-Valley Systems: Origin and Sedimentary Sequences*, SEPM Special Publication 51, pp. 45–60. <https://doi.org/10.2110/pec.94.12.0045>
- Zaitlin, B.A., Dalrymple, R.W., Boyd, R., (1994). The stratigraphic organization of incised valley systems associated with relative sea-level change, in: Dalrymple, R.W., Boyd, R., Zaitlin, B.A., (Eds.), *Incised-Valley Systems: Origin and Sedimentary Sequences*. SEPM Special Publication 51, pp. 45-60.
- Zecchin, M., Caffau, M., Catuneanu, O., (2021). Recognizing maximum flooding surfaces in shallow-water deposits: An integrated sedimentological and micropaleontological approach (Croton Basin, southern Italy). *Mar. Petrol. Geol.* 133, 105225.
- Zecchin, M., Ceramicola, S., Lodolo, E., Casalbore, D., Chiocci, F.L., (2015). Episodic, rapid sea-level rises on the central Mediterranean shelves after the Last Glacial Maximum: A review. *Mar. Geol.* 369, 212–223.
- Zeng, Z., Zhu, H., Mei, L., Du, J., Zeng, H., Xu, X., Dong, X., (2019). Multilevel source-to-sink (S2S) subdivision and application of an ancient uplift system in South China Sea: Implications for further hydrocarbon exploration. *J. Pet. Sci. Eng.* 181, 106220.
- Zhang, X., Li, X. long, Garzanti, E., Lin, C. ming, Deng, K., (2021). Sedimentary geochemistry response to climate change on a millennial timescale in the Qiantang River incised-valley system, eastern China. *Chem. Geol.* 586, 120587. <https://doi.org/10.1016/j.chemgeo.2021.120587>
- Zhang, Y., Yang, Z., Bielak, J., Conte, J. P., & Elgamal, A. (2003). Treatment of seismic input and boundary conditions in nonlinear seismic analysis of a bridge ground system. 16th ASCE Engineering Mechanics Conference, 16–18.

Zong, Y., Yim, W.-S., Yu, F., Huang, G., (2009). Late Quaternary environmental changes in the Pearl River mouth region, China. *Quat. Int.* 206, 35–45.

## Supplementary Material

### Supplementary Material- Chapter 4

#### taxonomic reference list (MOLLUSKS)

This list includes genus and species of mollusks cited in the text. Taxonomic classification and references according to WoRMS Editorial Board (2022) and MolluscaBase (2022).

- Abra nitida* - *Mya nitida* O. F. Müller, 1776, p. 245.  
*Abra prismatica* - *Ligula prismatica* Montagu, 1808, p. 183.  
*Abra segmentum* - *Syndosmya segmentum* Récluz, 1843, p. 359.  
*Acanthocardia tuberculata* – *Cardium tuberculatum* Linnaeus, 1758, p. 695.  
*Antalis cf. dentalis* - *Dentalium dentalis* Linnaeus, 1758, p. 785.  
*Antalis inaequicostatum* - *Dentalium inaequicostatum* Dautzenberg, 1891, p. 53.  
*Antalis* – *Antalis* H. Adams & A. Adams, 1854.  
*Arca noae* – *Arca noae* Linnaeus, 1758, p. 693.  
*Sorgenfreispira brachystoma* – *Pleurotoma brachystoma* Philippi, 1844, p. 169, pl. 26, fig. 10.  
*Bittium reticulatum* - *Strombiformis reticulatus* da Costa, 1778, p. 117-118, pl. 8, fig. 13.  
*Bittium* - *Bittium* Gray, 1847, p. 270.  
*Cerastoderma glaucum* - *Cardium glaucum* Bruguière, 1789, p. 221-222.  
*Cerithidium submammillatum* - *Cerithium submammillatum* de Rayneval & Ponzi, 1854, p. 19.  
*Cernuella* - *Cernuella* Schlüter, 1838, p. 6.  
*Cochlicella* - *Cochlicella* A. Férussac, 1821, p.773.  
*Donax semistriatus* - *Donax semistriatus* Poli, 1795, p. 79-80, pl. 19, fig. 17.  
*Donax* – *Donax* Linnaeus, 1758, p. 682.  
*Donax trunculus* - *Donax trunculus* Linnaeus, 1758, p. 682.  
*Dosinia lupines* - *Venus lupinus* Linnaeus, 1758, p. 689.  
*Glycymeris nummaria* – *Arca mummaria* Linnaeus, 1758, p. 695.  
*Gouldia minima* - *Venus minima* Montagu, 1803, p. 121.  
*Kurtiella bidentata* - *Mya bidentata* Montagu, 1803, p. 44-45.  
*Lembulus pella* - *Arca pella* Linnaeus, 1758, p. 693.  
*Loripes orbiculatus* - *Loripes orbiculatus* Poli, 1795, p. 253.  
*Lucinella divaricata* - *Tellina divaricata* Linnaeus, 1758, p. 677.  
*Moerella distorta* - *Tellina distorta* Poli 1791, p. 39, pl. 15, fig. 11.  
*Nucula nitidosa* - *Nucula nitidosa* Winckworth, 1930, p. 14.  
*Ostrea edulis* - *Ostrea edulis* Linnaeus, 1758, p. 699.  
*Pitar rudis* - *Venus rudis* Poli, 1795, p.94.  
*Tritia* - *Tritia* Risso, 1826, p. 172.  
*Turritellinella tricarinata* - *Turbo tricarinatus* Brocchi, 1814 †, p. 374.  
*Varicorbula gibba* - *Tellina gibba* Olivi, 1792, p. 101.

## References

- MolluscaBase eds. (2022). MolluscaBase. Accessed at <https://www.molluscabase.org/doi:10.14284/448>
- WoRMS Editorial Board (2022). World Register of Marine Species. Available from <https://www.marinespecies.org/doi:10.14284/170>

### Supplementary N- taxonomic reference list (MEIOFAUNA)

This list includes genus and species of foraminifera and ostracoda cited in the text. Taxonomic classification and references according to Ellis and Messina (1940, 1952), Brandão et al. (2022) and Hayward et al. (2022).

- Adelosina - *Adelosina* d'Orbigny, 1826, p. 303
- Ammonia - *Ammonia* Brünnich, 1771, p. 232.
- Ammonia beccarii* - *Nautilus beccarii* Linnaeus 1758, p. 710.
- Ammonia parkinsoniana* - *Rosalina parkinsoniana* d'Orbigny, 1839a, p. 99, pl. 4, figs. 25-27.
- Ammonia tepida* - *Rotalia beccarii* (Linnaeus) var. *tepida* Cushman, 1926, p. 79, pl. 1.
- Aubignyna perlucida* - *Rotalia perlucida* Heron-Allen & Earland, 1913, p. 139, pl. 13, figs. 7-9.
- Bulimina - *Bulimina* d'Orbigny, 1826, p. 269.
- Criboelphidium* - *Criboelphidium* Cushman & Brönnimann, 1948, p. 18.
- Criboelphidium gunteri* - *Elphidium gunteri* Cole, 1931, p. 34, pl. 4, figs. 9-10.
- Cyprideis torosa* - *Candona torosa* Jones, 1850, p. 27, pl. 3, figs. 6a-e.
- Elphidium* - *Elphidium* Montfort, 1808, p. 15.
- Elphidium fichtelianum* - *Polystomella fichtelliana* d'Orbigny, 1846, p. 125, Pl.6, figs. 7-8.
- Elphidium oceanense* - *Polystomella oceanensis* d'Orbigny in Fornasini, 1904, p. 13 pl. 3 figs. 10, 10a.
- Globigerina* - *Globigerina* d'Orbigny, 1826, p. 277.
- Globigerinoides* - *Globigerinoides* Cushman, 1927, p. 87.
- Gyroidina* - *Gyroidina* d'Orbigny, 1826, p. 278.
- Haynesina germanica* - *Nonionina germanica* Ehrenberg, 1840, p. 23, pl. 2, figs. 1a-g.
- Miliolinella* - *Miliolinella* Wiesner, 1931, pp. 63, 65, 107.
- Porosonion* - *Porosonion* Putrya in Voloshinova, 1958, p. 135.
- Porosonion granosum* - *Nonionina granosa* d'Orbigny, 1846, p. 110, Pl. 5, figs. 19-20.
- Porosonion lidoense* - *Elphidium lidoense* Cushman, 1936, p. 86, pl. 15, figs. 6a-b.
- Pseudocandona* - *Pseudocandona* Kaufmann, 1900, p. 375.
- Quinqueloculina* - *Quinqueloculina* d'Orbigny, 1826, p. 301.
- Quinqueloculina seminulum* - *Serpula seminulum* Linnaeus, 1758, p. 786.

Rosalina bradyi - Discorbis globularis var. bradyi Cushman, 1915, p. 12, pl. 8, figs. 1a-c.  
Triloculina - Triloculina d'Orbigny, 1826, p. 299.  
Triloculina inflata - Triloculina inflata d'Orbigny, 1826, p. 278, pl. 17, figs. 13-15.  
Triloculina trigonula - Miliolites trigonula Lamarck, 1804, p. 351; Lamarck, 1807, pl. 17, figs. 4a-c.  
Triloculina affinis - Triloculina affinis d'Orbigny, 1852, p. 161; Fornasini (1905), pl. 1, figs. 1, 1a-b.

## References cited

Brandão, S.N.; Antonietto, L.S; Nery, D.G.; Karanovic, I. (2022). World Ostracoda Database. Accessed through: World Register of Marine Species at: <https://www.marinespecies.org>

Ellis, B.F., Messina, A.R., 1940 (with suppl.). Catalogue of Foraminifera, Spec. Publ., The American Museum of Natural History, New York.

Ellis, B.F., Messina, A.R., 1952 (with suppl.). Catalogue of Ostracoda, Spec. Publ., The American Museum of Natural History, New York.

Hayward, B.W.; Le Coze, F.; Vachard, D.; Gross, O. (2022). World Foraminifera Database. Accessed through: World Register of Marine Species at: <https://www.marinespecies.org>

Sample	Cr (ppm)	V (ppm)	Cr/V
<b>Apulia Rivers</b>			
CE03	97	115	0.85
CE04	94	118	0.80
CE05	78	95	0.82
CN03	104	146	0.71
CN04	100	121	0.83
CN05	98	115	0.85
CR04	103	131	0.79
CR05	93	110	0.85
OF02	85	101	0.84
OF04	90	116	0.78
OF05	94	114	0.83
<b>Inner estuary</b>			
MAN 30.50	111	128	0.86
MAN 31.20	88	111	0.79
MAN 31.80	86	103	0.83
MAN 32.10	109	127	0.86
MAN 33.70	103	124	0.83
MAN 34.40	111	131	0.85
MAN 35.30	117	138	0.85
MAN 36.20	107	122	0.88
MAN 36.40	72	90	0.80
MAN 36.90	77	86	0.89
MAN 37.70	71	86	0.83
MAN 38.20	72	88	0.82
MAN 38.90	98	113	0.87
MAN 39.50	116	133	0.88
MAN 41.90	130	150	0.86
MAN 43.10	123	154	0.80
<b>Outer estuary/bay</b>			
MAN 8.70	77	81	0.94
MAN 13.30	68	74	0.91
MAN 14.70	87	103	0.85
MAN 16.30	93	101	0.92
MAN 17.50	93	105	0.88
MAN 18.70	79	90	0.87
MAN 19.90	87	100	0.88
MAN 20.80	92	112	0.82
MAN 21.80	90	114	0.79
MAN 22.80	91	113	0.80
MAN 23.80	97	112	0.86
MAN 24.80	97	102	0.95
MAN 25.70	92	108	0.85
MAN 26.60	96	102	0.94
MAN 27,70	95	105	0.90
MAN 28.70	112	125	0.90
MAN 29.70	111	125	0.89

Samples list

## Supplementary Material- Chapter 5

### 1.1 Bayesian Analysis of AMS dates in Table 1

In this section, an age-depth model of the stratigraphic interval including parasequences 1-5 is provided. This model has been developed using the OxCal 4.4 (<https://c14.arch.ox.ac.uk/oxcal/OxCal.html>) Bayesian analysis tool (Ramsey 2008, 2009), and allows for random fluctuations in sediment deposition (P\_sequence). The main goal of this analysis is to test the reliability of the available radiocarbon chronology available for this study (Table 1 of main text), and resolve potential issues of age-depth inversions. The measurement of the coherence between the observational data (likelihood; Fig. S1) and the model (prior; Fig. S2) is provided by the agreement index. The prior probability was fixed to 0.05 to weigh down the radiocarbon measurements that have statistical probability of more than 5% of being outliers. The age model turned out having an excellent agreement index between calibrated and modelled ages. As shown in Fig. S3, none of the AMS dates can be considered an outlier and all have to be retained. As a result, the chronological framework and the age model can be regarded as reliable for the high-resolution stratigraphic purposes of this study.

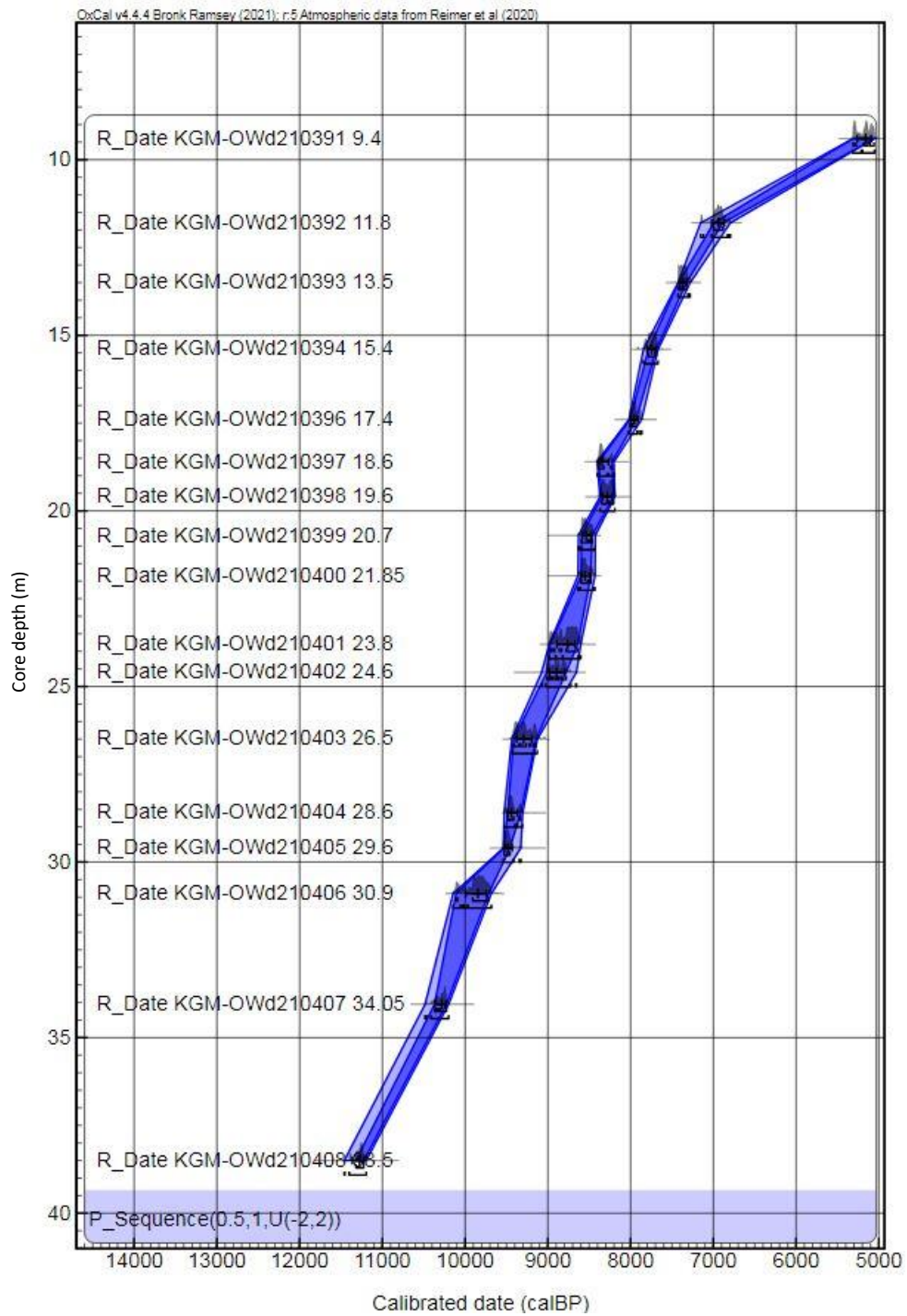


Fig. S1 – Likelihood probability distributions of calibrated radiocarbon dates. Light blue: 16; dark blue: 26.

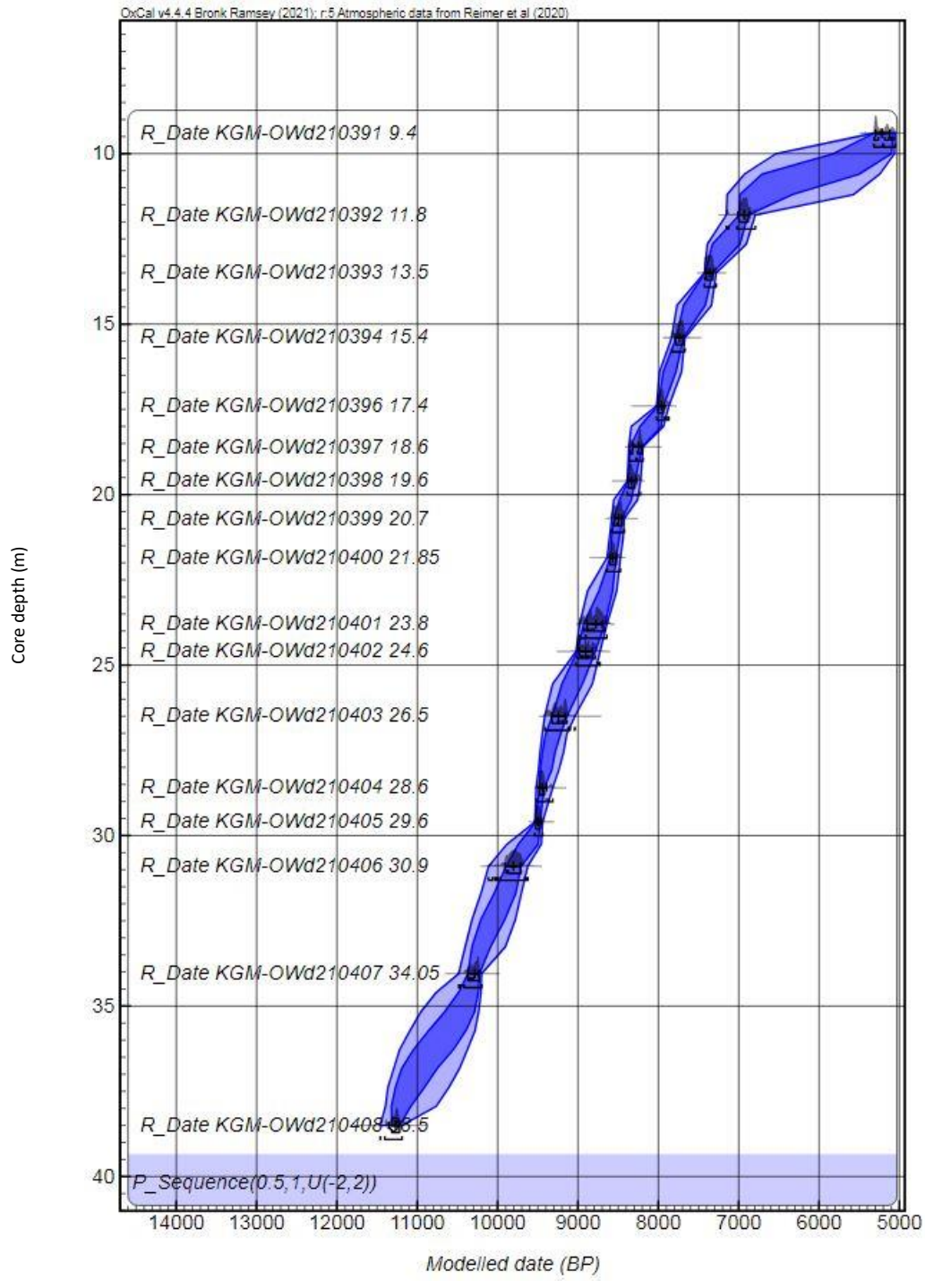


Fig. S2 – Posterior probability distributions of modelled radiocarbon dates. Light blue: 16; dark blue: 26.

Element	Ok 	Outlier 	Prior	Posterior	Model	Type
KGM-OWd210408 38.5			5	4	General	t
KGM-OWd210407 34.05			5	4	General	t
KGM-OWd210406 30.9			5	4	General	t
KGM-OWd210405 29.6			5	4	General	t
KGM-OWd210404 28.6			5	3	General	t
KGM-OWd210403 26.5			5	4	General	t
KGM-OWd210402 24.6			5	4	General	t
KGM-OWd210401 23.8			5	4	General	t
KGM-OWd210400 21.85			5	3	General	t
KGM-OWd210399 20.7			5	4	General	t
KGM-OWd210398 19.6			5	4	General	t
KGM-OWd210397 18.6			5	4	General	t
KGM-OWd210396 17.4			5	4	General	t
KGM-OWd210394 15.4			5	4	General	t
KGM-OWd210393 13.5			5	4	General	t
KGM-OWd210392 11.8			5	4	General	t
KGM-OWd210391 9.4			5	4	General	t

Fig. S3 – View of the potential outliers: all the analyzed dates can be retained in the study.

## Oxcal Script

The OxCal script used to generate the model is reported below.

```
Plot()
{
  Curve("IntCal20","intcal20.14c");
  Outlier_Model("General",T(5),U(0,4),"t");
  P_Sequence("",0.5,1,U(-2,2))
  {
    Boundary();
    R_Date("KGM-OWd210408 38.5", 9874,48)
    {
      Outlier(0.05);
      z=38.5;
    };
    R_Date("KGM-OWd210407 34.05", 9123,48)
    {
      Outlier(0.05);
      z=34.05;
    };
    R_Date("KGM-OWd210406 30.9", 8812,39)
    {
      Outlier(0.05);
      z=30.9;
    };
    R_Date("KGM-OWd210405 29.6", 8458,47)
    {
      Outlier(0.05);
      z=29.6;
    };
  }
}
```

```

R_Date("KGM-OWd210404 28.6", 8405,40)
{
  Outlier(0.05);
  z=28.6;
};
R_Date("KGM-OWd210403 26.5", 8288,44)
{
  Outlier(0.05);
  z=26.5;
};
R_Date("KGM-OWd210402 24.6", 8035,43)
{
  Outlier(0.05);
  z=24.6;
};
R_Date("KGM-OWd210401 23.8", 7925,40)
{
  Outlier(0.05);
  z=23.8;
};
R_Date("KGM-OWd210400 21.85",7778,43)
{
  Outlier(0.05);
  z=21.85;
};
R_Date("KGM-OWd210399 20.7",7766,42)
{
  Outlier(0.05);
  z=20.7;
};
R_Date("KGM-OWd210398 19.6",7473,44)
{
  Outlier(0.05);
  z=19.6;
};
R_Date("KGM-OWd210397 18.6",7522,40)
{
  Outlier(0.05);
  z=18.6;
};
R_Date("KGM-OWd210396 17.4",7134,39)
{
  Outlier(0.05);
  z=17.4;
};
R_Date("KGM-OWd210394 15.4",6919,41)
{
  Outlier(0.05);
  z=15.4;
};
R_Date("KGM-OWd210393 13.5",6444,37)
{

```

```

Outlier(0.05);
z=13.5;
};
R_Date("KGM-OWd210392 11.8",6079,37)
{
  Outlier(0.05);
  z=11.8;
};
R_Date("KGM-OWd210391 9.4",4535,33)
{
  Outlier(0.05);
  z=9.4;
};
Boundary();
};
};

```

### Bayesian analysis reference list

Ramsey, C.B., 2008. Deposition models for chronological records. *Quat. Sci. Rev.* 27, 42–60.

Ramsey, C.B., 2009. Dealing with outliers and offsets in radiocarbon dating. *Radiocarbon* 51, 1023–1045.  
<https://doi.org/10.1017/s0033822200034093>

### Taxonomic reference list

This list includes foraminifera and ostracoda cited in the text. Taxonomic classification according to Loeblich and Tappan (1988), Ellis and Messina (1940, 1952), Meisch (2000) and "www.marinespecies.org/"

*Ammonia parkinsoniana* - *Rosalina parkinsoniana* d'Orbigny, 1839a, p. 99, pl. 4, figs. 25-27.

*Ammonia tepida* - *Rotalia beccarii* (Linnaeus) var. *tepida* Cushman, 1926, p. 79, pl. 1.

*Bolivina* - *Bolivina* d'Orbigny, 1839b, p. 60.

*Bolivina seminuda* - *Bolivina seminuda* Cushman, 1911, p. 34, fig. 55.

*Bulimina etnea* - *Bulimina etnea* Seguenza, 1862, pp. 108, 125, pl. 1, fig. 9.

*Bulimina marginata* - *Bulimina marginata* d'Orbigny, 1826, p. 269, pl. 12, figs. 10-12.

*Cassidulina carinata* - *Cassidulina laevigata* var. *carinata* Silvestri, 1896, p. 104, pl. 2, figs. 10a-c.

*Criboelphidium oceanensis* - *Polystomella oceanensis* d'Orbigny, 1826 in Fornasini, 1904, pl. 3, figs. 10-10a.

*Globobulimina affinis* - *Bulimina affinis* d'Orbigny, 1839a, p. 105, pl. 2, figs. 25-26.

*Globobulimina pyrula* - *Bulimina pyrula* d'Orbigny, 1846, p. 184, pl. 11, figs. 9-10.

*Haynesina germanica* - *Nonionina germanica* Ehrenberg, 1840, p. 23, pl. 2, figs. 1a-g.

*Sigmoilopsis schlumbergeri* - *Sigmoilina schlumbergeri* Silvestri, 1904, pp. 267, 269, illustrated in Schlumberger, 1887, pl. 7, figs. 12-14, tfigs. 6-7.

*Candona neglecta* - *Candona neglecta* Sars, 1887, pp. 279-288, pl. 15, figs. 5-7; pl. 19, figs. 1-21.

*Cyclocypris* - *Cyclocypris* Brady & Norman, 1889, p. 70.

*Cypria ophtalmica* - *Monoculus ophtalmicus* Jurine, 1820, p. 178, pl. 19, figs. 16-17.

*Cyprideis torosa* - *Candona torosa* Jones, 1850, p. 27, pl. 3, figs. 6a-e.

*Fabaeformiscandona* - *Fabaeformiscandona* Krstic, 1972, p. 92.

*Ilyocypris* - *Ilyocypris* Brady & Norman, 1889, p. 106.

*Loxoconcha elliptica* - *Loxoconcha elliptica* Brady, 1868, p. 435, pl 27, figs. 38-39; 45-48; pl. 40, fig. 3.

*Pseudocandona albicans* - *Candona albicans* Brady, 1864, p. 61, pl. 4, figs. 6-10.

*Xestoleberis aurantia* - *Cythere aurantia* Baird, 1838, p. 143, pl. 5, fig. 26.

Baird, W. (1838). The natural history of the British Entomostraca. *Magazine of Zoology and Botany*, 2: 132-144.

Brady, G S. (1864). On species of Ostracoda new to Britain. *Annals and Magazine of Natural History*, 13(3), 59-64.

Brady, G. S. (1868). A monograph of the recent British Ostracoda. *Transactions of the Linnean Society of London*. 26: 353-495.

Brady, G. S., Norman, A. M. (1889). A Monograph of the Marine and Freshwater Ostracoda of the North Atlantic and of North Western Europe. Sect I. Podocopa. *Scientific Transactions of the Royal Dublin Society* (2) iv, pp. 63-270.

Cushman, J. A. (1911). A monograph of the Foraminifera of the North Pacific Ocean. Part II. Textulariidae. *Bulletin of the United States National Museum*. 71(2): 1-108.

Cushman, J.A. 1926. Recent foraminifera from Porto Rico. Publications of the Carnegie Institution of Washington 342: 73-84.

Ellis, B. F., Messina, A. R. (1940). Catalogue of Foraminifera. *Micropaleontology Press, American Museum of Natural History, New York*.

Ellis, B. F., Messina, A. R. (1952). Catalogue of Ostracoda. *Micropaleontology Press, American Museum of Natural History, New York*.

Ehrenberg, C. G. (1840). Eine weitere Erläuterung des Organismus mehrerer in Berlin lebend beobachteter Polythalamien der Nordsee. *Bericht über die zur Bekanntmachung geeigneten Verhandlungen der Königlich-Preussischen Akademie der Wissenschaften zu Berlin*. 1840: 18-23.

Fornasini, C. (1904). Illustrazione di specie orbignyane di foraminiferi istituite nel 1826. *Memorie della Reale Accademia delle Scienze dell'Istituto di Bologna, Classe di Scienze Fisiche*. ser. 6 t. 1, 3-17.

Jones, T.R. (1850). Description of the Entomostraca of the Pleistocene Beds of Newbury Copford, Clacton and Grays. *The Annals and magazine of natural history*. 6(2): 25-28.

Jurine, L. (1820). Histoire des Monocles, qui se trouvent aux environs de Genève. Genève, *J.J. Paschoud*, 258 p.

Krstic, N., 1972. Rod Candona (Ostracoda) iz kongerijskikh slojeva juzhnog dela Panonskog basena. Monographs of the Serbian Academie of Sciences and Arts, Section of Natural and Mathematical Sciences 39 (I–VII), 145 p.

Loeblich, A. R., Tappan, H. (1988). Foraminiferal Genera and their Classification. Van Nostrand Reinhold Company, New York. 970 p.

Meisch, C. (2000) Freshwater Ostracoda of Western and Central Europe; Süßwasserfauna von Mitteleuropa; Spektrum Akademischer Verlag: Heidelberg/Berlin, 513 p.

Orbigny, A. D. d'. (1826). Tableau méthodique de la classe des Céphalopodes. *Annales des Sciences Naturelles*. vol. 7: 96-169, 245-314.

Orbigny, A. D. d'. (1839a). Foraminifères, in de la Sagra R., Histoire physique, politique et naturelle de l'île de Cuba. A. Bertrand. 1-224.

Orbigny, A. D. d'. (1839b). Voyage dans l'Amérique Méridionale. Foraminifères. t. 5 pt. 5: 1-86.

Orbigny, A. D. d'. (1846). Die fossilen Foraminiferen des tertiären Beckens von Wien. Foraminifères fossiles du bassin tertiaire de Vienne. 312 p.

Sars, G.O. (1887). Nye Bidrag til Kundskaben om Middelhavets Invertebratfauna 4: Ostracoda Mediterranea (Sydeuropaeiske Ostracoder). *Archiv for Mathematik og Naturvidenskab* 12, 173–324.

Seguenza, G. (1862). Prime ricerche intorno ai rizopodi fossili delle argille pleistoceniche dei dintorni di Catania. *Atti della Accademia gioenia di scienze naturali in Catania*. ser. 2 vol. 18: 85-125.

Silvestri, A. (1896). Foraminiferi pliocenici della provincia di Siena. Part I. Memorie dell'Accademia Pontificia dei Nuovi Lincei 12: 1-224.

Silvestri, A. (1904). Ricerche strutturali su alcune forme dei Trubi dei Bonfornello (Palermo). *Memorie dell'Accademia Pontificia dei Nuovi Lincei*. 22: 235-276.

Schlumberger, C. (1887). Note sur le genre Planispirina. *Bulletin de la Société Zoologique de France*. 12: 475-488.